Nonlinear Control of Co-operating Hydraulic Manipulators

By

Hairong Zeng

A thesis presented to the University of Manitoba
in fulfillment of the thesis requirement
for the degree of Doctor of Philosophy
in Mechanical and Manufacturing Engineering
Winnipeg, Manitoba, Canada 2007

Abstract

This thesis presents the design, analysis, and numerical and experimental evaluation of nonlinear controllers for co-operation among several hydraulic robots operating in the presence of significant system uncertainties, non-linearities and friction. The designed controllers allow hydraulically driven manipulators to (i) co-operatively handle a rigid object (payload) following a given trajectory, (ii) share the payload and (iii) maintain an acceptable internal force on the object.

A general description of the kinematic and dynamic relations for a hydraulically actuated multi-manipulator system is presented first. The entire mathematical model incorporates object dynamics, robot dynamics, hydraulic actuator functions and friction dynamics. For the purpose of simulations, a detailed numerical simulation program of such a system is also developed, in which two three-link planar robot manipulators resembling the Magnum hydraulic manipulators manufactured by ISE, interact with each other through manipulating a common object.

The regulating control problem is studied next, in which the desired position of the object and the corresponding desired link displacement change step-wise. Initially, a controller is designed based on a backstepping technique, assuming that full knowledge of the dynamics and kinematics of the system is available. The assumption is then relaxed and the control system is analyzed. Based on the analysis, the controller is then modified to account for the uncertainty of the payload, robot dynamic parameters and hydraulic functions.

Next, the regulating controller is extended to a tracking controller, which allows the object to follow a given trajectory and is robust against parameter uncertainties. Additionally, an observer is added to the controller to avoid the need of acceleration feedback.

To investigate the effect of friction force, the above controllers are examined by introducing the most recent and complete LuGre friction model into the system dynamics. The tracking controller is then redesigned to compensate the effect of friction. Observers are designed to observe the immeasurable friction states. Based on the observed friction

states and estimated friction parameters, an appropriate friction compensation scheme is designed which does not directly use velocity in order to avoid the need of acceleration feedback by the controller.

Finally, the problem of “explosion of terms” coming from the backstepping method is solved by using the concept of dynamic surface control in which a low pass filter is integrated to avoid model differentiation.

Simulations are carried out for analysis of the control system and verification of the developed controllers. Experimental examinations are performed on an available hydraulic system consisting of two single-axis hydraulic actuators.

Acknowledgment

I would like to thank all of those who have supported me throughout the course of this project. Without their time and effort, this endeavor would not have been possible.

First and foremost, I would like to express my gratitude to Dr. Nariman Sepehri for invaluable guidance, advice and encouragement throughout the research of this project as well as the writing of this thesis, and for ensuring financial support throughout my studies.

I would also like to thank other members of my Ph.D. committee: Dr. Steve Onyshko, Dr. Greg E. Bridges, Dr. Christine Q. Wu, and Dr. Tim Salcudean (external, University of British Columbia) for their invaluable comments. Additionally, particular gratitude is also owed to Dr. Wu, for her relevant advice and steady discussions on the theory including non-smooth systems.

I am grateful to all fellows in the Experimental Robotics and Tele-operation Laboratory for their help, advice and company; with a particular gratitude owed to Mark Karpenko for his substantial assistance in the experiments. In addition, I would like to thank Leslie Foreman and Keith Hanson for proofreading this manuscript.

The grant provided by the Natural Sciences and Engineering Research Council of Canada (NSERC) and the fellowship awarded by the University of Manitoba were instrumental in the success of my studies.

A great debt of gratitude is owed to my family for their love and support. No words can express the patience that my dearest wife Jun Chen has offered me. My final appreciation goes to my daughter Wendy, for being in my life and helping me to relax after work. Her laughter was essential and supportive.

Contents

List of Figures

List of Tables

Nomenclature

$A^i_{I,j}$, $A^i_{O,j}$	Piston effective areas (m^2)
$\boldsymbol{A}_I$, $\boldsymbol{A}_O$	Diagonal matrices of piston effective areas
b^i	Weight coefficient appearing in matrix $\boldsymbol{V}$
$\boldsymbol{C}_m$	Matrix related to the Coriolis and centrifugal effects in the robots dynamics
c_d	Servovalve coefficient of discharge
D	Matrix related to the Coriolis and centrifugal effects in the robots-object dynamics
D_o	Matrix related to the Coriolis and centrifugal effects in the object dynamics
e	Vector of the position errors of the object
E	Matrix relating v and $\dot{X}$
$\boldsymbol{F}$	Vector of the total forces from actuators
$\boldsymbol{F}^d$	Virtual force or desired force for $\boldsymbol{F}$
F^i_j	Net force provided by the actuator (N)
$F^i_{fr,j}$	Actuator friction force (N)
$\boldsymbol{F}_{fr}$	Vector of actuator friction forces
$\boldsymbol{F}_c$	Vector of contact forces/moments on the object
F_{ext}	Vector of external (resultant) force /moment on the object
F_{int}	Vector of internal force/moment on the object
F^d_{int}	Vector of desired internal force/moment on the object
$F^i_{sl,j}$	Actuator slip friction (N)
$f^i_{sl,j}$	Actuator normalized slip friction (m/s)
$f_{sl,L}$	Lower bound of the norm of the vector of normalized slip frictions (m/s)
$F^i_{st,j}$	Actuator stiction force (N)
$f^i_{st,j}$	Actuator normalized stiction force (m/s)
$\boldsymbol{G}_m$	Vector of gravitational terms in the robots dynamics
G_o	Vector of gravitational terms in the object dynamics
G	Vector of gravitational terms in the robots-object dynamics
$\boldsymbol{H}_m$	Inertia matrix in the robots' dynamics

$\boldsymbol{J}$	Jacobian matrix from the joint space to the Cartisan reference frame
$\bar{J}^i_j(q^i_j)$	Jacobian from link joint space to the linear actuator coordinate (m/rad)
$\bar{\boldsymbol{J}}$	Jacobian matrix (diagonal) from link joint space to the linear actuator coordinate
$\boldsymbol{J}_a$	Matrix relating $\dot{\boldsymbol{x}}$ and $\dot{X}$
K^i_j	Flow gain ($\sqrt{m^5/kg}$)
$\boldsymbol{K}$	Diagonal matrix of Flow gains
$K^i_{sp,j}$	Valve constant (m/V)
$\boldsymbol{K}_{sp}$	Diagonal matrix of valve constants
M	Inertia matrix of the robots-object system
M_o	Inertia matrix of the object
$P^i_{I,j}, P^i_{O,j}$	Line pressures (Pa)
$\boldsymbol{P}_I$, $\boldsymbol{P}_O$	Vector of line pressures
P_e	Return pressure (Pa)
P_s	Supply pressure (Pa)
q^i_j	Link angular position (rad)
$\boldsymbol{q}$	Vector of link angular positions
$\boldsymbol{q}^d$	Vector of desired link angular positions
$q^i_{I,j}, q^i_{O,j}$	Control flows (m^3/s)
$r(t)$	Vector of states of the control system
$\boldsymbol{T}_m$	Vector of net torques from actuators
T	Vector of generalized forces/torques in the robots-object dynamics
u^i_j	Input signal to servovalve (V)
$\boldsymbol{U}$	Vector of input signals to servovalves
v	Vector of linear and angular velocities of the object
$\boldsymbol{V}$	A full-column-rank matrix satisfying $\boldsymbol{WV}$=0
V_2	Lyapunov-like scalar function
$\bar{V}^i_{I,j}$, $\bar{V}^i_{O,j}$	Initial fluid volumes at the sides of actuator (m^3) when $x^i_j = 0$
$V^i_{I,j}$, $V^i_{O,j}$	Trapped fluid volumes at the sides of actuator (m^3)
$\boldsymbol{W}$	Grasp matrix
$\boldsymbol{W}^\dagger$	General inverse of $\boldsymbol{W}$; $\boldsymbol{WW}^\dagger=\boldsymbol{I}$
w^i_j	Servovalve orifice area gradient (m^2/m)
X	Vector of object position and orientation

X^d	Vector of desired object position and orientation
$\hat{X}$	Vector of estimated X
x_j^i	Piston position (m)
$\boldsymbol{x}$	Vector of cylinder/piston positions (m)
$x_{sp,j}^i$	Servovalve spool displacement (m)
$\dot{x}_{s,j}^i$	Stribeck velocity (m/s)
z_j^i	Friction internal state (m)
$\boldsymbol{z}$	Vector of friction internal states
$\hat{\boldsymbol{z}}_0, \hat{\boldsymbol{z}}_1$	Vectors of estimates of friction internal states
α^i	Weight coefficient appearing in matrix $\boldsymbol{W}^\dagger$
β_j^i	Effective bulk modulus (Pa)
$\Delta(x_{sp,j}^i)$	Servovalve orifice area (m^2)
φ	Vector of unknown parameters in the hydraulic functions
$\hat{\varphi}$	Vector of estimates of unknown parameters in the hydraulic functions
Φ	Regressive matrix for the hydraulic functions
θ	Vector of unknown parameters in the robots-object dynamics
$\hat{\theta}$	Vector of estimates of unknown parameters in the robots-object dynamics
Θ	Regressive matrix for the robots-object dynamics
ρ	Hydraulic fluid density (kg/m^3)
$\sigma_{0,j}^i$	Friction force parameter (stiffness of the bristles between two contact surfaces) (N/m)
$\boldsymbol{\sigma}_0$	Vector containing friction force parameters $\sigma_{0,j}^i$
$[\boldsymbol{\sigma}_0]$	Diagonal matrix of $\boldsymbol{\sigma}_0$
$\sigma_{1,j}^i$	Friction force parameters (damping coefficient) (Ns/m)
$\boldsymbol{\sigma}_1$	Vector containing friction force parameters $\sigma_{1,j}^i$
$[\boldsymbol{\sigma}_1]$	Diagonal matrix of $\boldsymbol{\sigma}_1$
$\sigma_{2,j}^i$	Viscous friction coefficient (Ns/m)
$\boldsymbol{\sigma}_2$	Vector containing viscous friction force parameters $\sigma_{2,j}^i$
$[\boldsymbol{\sigma}_2]$	Diagonal matrix of $\boldsymbol{\sigma}_2$
$\sigma_{12,j}^i$	$\sigma_{1,j}^i + \sigma_{2,j}^i$
$\boldsymbol{\sigma}_{12}$	$\boldsymbol{\sigma}_1 + \boldsymbol{\sigma}_2$
$[\boldsymbol{\sigma}_{12}]$	$[\boldsymbol{\sigma}_1] + [\boldsymbol{\sigma}_2]$

$\underline{\sigma}(.)$	Minimum singular value of its matrix argument
$\overline{\sigma}(.)$	Maximum singular value of its matrix argument

Chapter 1 Introduction

1.1 Problem Statement

In recent years, co-operative robots have continued to receive a great deal of attention from both the robotics research community (Vukobratovic, 1998) and the robotics industry.

It has been recognized that many tasks are difficult or impossible to execute by a single robot. It is more manageable when two or more manipulators are employed in a co-operative manner. Typically a single manipulator cannot handle an object because it is either beyond the manipulator's load capacity or the geometry of the object makes it difficult to manipulate. Among various types of actuators to drive manipulators; hydraulic actuators are prevailing in many industrial applications due to their high load capability and reliable performance. Their application scope ranges from heavy-duty robots in mining and forestry, to fine machine tools and underwater exploration. An example is that of two hydraulic manipulators installed in an underwater vehicle; named Magnum and manufactured by International Submarine Engineering Ltd. (ISE) in BC, Canada. The control of co-operating hydraulic robots to perform tasks such as handling a common object presents many difficulties which are outlined in the following.

The addition of a second manipulator or several manipulators, leads to a complex system since the motion of multiple manipulators must be both kinematically and dynamically coordinated. In addition, for an object being rigidly grasped (i.e. no relative motion among grippers and the object) and manipulated by multiple robots, the problem of internal loading, which does not contribute to the object's motion, must also be addressed (Walker *et al.*, 1991). Due to the kinematic and dynamic interaction imposed in co-operative robots and the nonlinear dynamics of the hydraulic actuators, a global description of the kinematic and dynamic relations for a multi-manipulator system is needed for controller development.

Hydraulic actuators are highly nonlinear, resulting from servovalve flow-pressure characteristics, unequal piston cross sectional areas, orifice area openings and in part also, to the variations of fluid volume under compression (Merritt, 1967).

Aside from the nonlinear nature of the hydraulic dynamics, hydraulic systems also contain to a large extent, uncertainties. The uncertainties can be classified into two categories: parametric uncertainties and un-modeled nonlinearities. Examples of parametric uncertainties are large changes in the load seen by the system and/or large variations in the hydraulic parameters due to the change of temperature (e.g., bulk modulus) and component wear (Watton, 1989). Other general uncertainties, such as external disturbances and leakage cannot be modeled exactly and the nonlinear functions that describe them are unknown. These types of uncertainties are called un-modeled nonlinearities, which may cause the control system designed on the nominal model, to become unstable or have a much-degraded performance (Yao *et al*. 2000).

In practical applications, friction compensation is particularly important for hydraulic manipulators. Due to high supply pressure, tight sealing is required to prevent the actuators from significant internal and external leaks. This in turn generates very high joint friction that can reach up to 30% of the nominal actuator torque (Lischinsky *et al*., 1997). Because friction is a very complicated phenomenon that relies on the material properties of the contact surfaces, relative velocity and lubrication conditions, a good friction model is important.

Unlike electrical actuators, force and position control of hydraulic manipulators is a difficult problem. In a hydraulic actuator, the control signal activates the spool valve that controls the flow of hydraulic fluid into and out of, the actuator. This flow, in turn causes a pressure differential buildup that is proportional to the actuator force. Even if the spool valve dynamics are ignored, the control signal fundamentally controls the derivative of the actuator force and not the force itself (Heinrichs *et al*. 1997).

Finally, most existing control methods for hydraulic systems deal with only one hydraulic actuator (see references by Alleyne, 1996; Niksefat, *et al*. 2000; Yao *et al*. 2000; Duraiswamy and Chiu, 2003; Sekhavat *et al*. 2004). Certain assumptions held in these control methods do not apply to a system of multiple hydraulic manipulators designed to co-operatively handle an object. This includes control of the internal force exerted on the manipulated object.

1.2 General Background

Prior to the work reported here, a number of control methods have been proposed for rigid body dynamics of closed-loop kinematic chains for electrically driven manipulators. To name a few, Khatib (1988) developed a coordinated control scheme for non-redundant arms based on the dynamic model in the operational space. Liu and Arimoto (1996) developed a distributed controller, which needs knowledge of the payload, although the internal force can be regulated by feed-forward of the desired forces. Caccavale *et al*. (1999) provided a stability analysis for a joint space control law in which asymptotic stability of a set of equilibrium points was demonstrated. The problem of steady-state error was noted for the case of imperfect gravity compensation while its solution is not recommended.

Other studies on this topic include the work by Alford and Belyeu (1984) who provided a master-slave control scheme for a two-robot system. Zheng and Luh (1986) assigned one robot to carry the major part of the task with its motion planned accordingly, and the second robot to follow the first one with the corresponding variables determined through the constrained relations. Tarn *et al.* (1987) established a formulation describing two co-operative electric robots handling a common object by considering the whole system as a closed kinematic chain. Giving a symmetric role to the manipulators in the coordination, Uchiyama and Dauchez (1988) redefined the task and the joint space coordinates to formulate the kinematics and dynamics for two co-operating robots. A controller was then developed to regulate the motion of an object as well as the internal forces applied to it.

The methods outlined above all require the exact dynamic model of the robots as well as the payload. To overcome the effects of the uncertainties, a few control laws have been developed (Hu and Goldenberg, 1989; Walker *et al*., 1989; Zribi and Ahmad, 1991). These methods are based on the fact that the dynamics of a robot can be represented as a linear combination of its physical parameters. A few other research studies focused on the communication among the robots. For example, Sugar *et al*. (1999) proposed a decentralized control approach for multiple robots in which the robots do not exchange information at servo-rates; they are weakly coupled to exchange motion plans. Built upon such work, a design for tightly coupled multi-robot co-operation was developed by

Chaimowicz *et al*. (2001) focusing on the use of communication in conjunction with simple control algorithms.

Within the context of hydraulic manipulators, most existing control methods are designed for a single hydraulic actuator. There are only a few papers that address the control of manipulators driven by hydraulic actuators. d'Andrea-Novel et. al. (1994) established a simplified model for the hydraulic actuator and applied singular perturbation methods to position control. No experimental or numerical results were presented in their work. Sirouspour and Salcudean (2001) developed a nonlinear position tracking controller, in which the effect of friction (both viscous and Coulomb) in the hydraulic actuators or external disturbances, were not considered in their controller development. In their paper, they briefly discussed the effect of Coulomb friction and noted that the proposed controller could only guarantee the "boundedness" of the tracking error. Bu and Yao (2000, 2001) proposed a Lyapunov-based adaptive controller for a hydraulic arm driven by single-rod hydraulic actuators. The effects of uncompensated friction forces were lumped together with external disturbances as disturbance torques. Or, friction was modeled as a static map between velocity and friction force/torque that depended on the sign of velocity. Dynamics of the friction were not explicitly considered in their controller design and stability analysis. However, there are several interesting properties in systems with friction that cannot be explained by static models alone. This is due to the fact that friction does not have an instantaneous response on a change of velocity, i.e., it has internal dynamics (Lin and Chen, 2006).

In applications with high precision positioning and low velocity tracking; it is more desirable to develop a strategy during the controller design, for on-line estimation and compensation of frictional forces, than to use the static friction model or to consider friction as simply being part of the external disturbance to be identified.

It has been shown by Tafazoli *et al*. (1998) that friction can lead to tracking errors, limit cycle oscillations and undesirable stick-slip motion. They discussed the importance of modeling friction and compensation for its effects and proposed an adaptive technique for tracking control in a single horizontal hydraulic actuator with friction being the only disturbance in the system. No stability analysis was reported in their work. Bonchis et al. (2002) evaluated ten previously developed methods on low-level positioning control of the pitch axis of an instrumented four-degree-of-freedom hydraulic manipulator, resembling a heavy-duty mining machine. Using a low bandwidth, proportional directional valve, the performances of the controllers in terms of tracking accuracy, robustness and control effort were compared. The importance of friction compensation and the difficulty in its experimental identification was emphasized in their work.

Friction is an important issue that needs to be considered in the controller design of multiple co-operating robots. As a complex, natural phenomenon, friction is present in virtually all mechanical control systems. It poses a serious challenge towards achieving good performance. In particular, friction plays an important albeit damaging role in hydraulic control systems (Merritt, 1967). Friction should be considered early in the system design by reducing it as much as possible through good hardware design. Recent advances in computer control have also shown the possibility to reduce the effects of friction by estimation and control. Modeling friction and compensation for its effects have received considerable attention (Armstrong-H´elouvry, 1991 and 1994; Friedland and Park, 1992; Mentzelopoulou and Friedland, 1994; and Amin *et al*., 1997). Recently, a dynamic friction model, named the LuGre model, has been presented (Canudas de Wit *et al*., 1995), which relates to the bristle interpretation of friction (Haessig and Friedland, 1991). The LuGre friction model includes the phenomenon that the surfaces are pushed apart by the lubricant, and models the Stribeck effect. The model also includes rate dependent friction phenomena such as varying breakaway force and frictional lag. Applications of the LuGre friction model can be found in Vedagarbha *et al*. (1999), Gafvert (1999), Tan *et al*. (2003), and Lin and Chen (2006).

As far as previous work on controller design for co-operative hydraulic manipulators is concerned, the existing literature is very limited. Sun and Chiu (2002) investigated the problem of load-lifting synchronization of two vertical single hydraulic linear actuators coupled by an unknown payload. Internal force regulation was not considered in their study. Karpenko et. al. (2006) applied a reinforced learning scheme to coordinate in a decentralized fashion, the motions of a pair of horizontal hydraulic actuators whose task was to move an object along a specified trajectory under conventional control. The learning goal was to reduce the internal force acting on the object that may arise due to positioning errors resulting from the imperfect closed-loop actuator dynamics. Friction compensation was not considered in these papers.

1.3 Objective of this Research

The objective of this research is to develop and evaluate appropriate controllers for co-operating hydraulic manipulators, handling rigid objects. An example of such a system is the HYSUB, one type of Remotely Operated Vehicles by ISE. HYSUB is generally equipped with two hydraulic manipulators named MAGNUM. With individual joystick control for each manipulator, the handling of a common object could cause serious damage to both the load and the manipulators even with very experienced operators. Thus, a controller needs to take into account the internal forces on the object and the coordination between the manipulators. Other applications may be found in mining and construction. The demanding performance specifications for these applications have motivated researchers to examine how to develop controllers applied to co-operating hydraulic actuators within the robot-object systems defined here.

In this research, the Lyapunov-based controller design method is utilized to construct appropriate controllers that:

- (i) incorporate the nonlinear dynamics of hydraulic actuators and dynamic friction model
- (ii) deal with parametric uncertainties
- (iii) do not need measurement of acceleration
- (iv) compensate for friction
- (v) are capable of tracking desired position and regulating internal force acting on the manipulated object.

1.4 Thesis Outline

The thesis consists of nine chapters and four appendices. The outline of the thesis is given as follows:

In Chapter 2, a global description of the kinematic and dynamic relations for a hydraulically actuated multi-manipulator system is presented. The whole system includes object dynamics, robot dynamics, hydraulic actuator functions and friction dynamic model. For the purpose of simulations, a detailed numerical model of such a system is created in which the three-link planar robot manipulator resembles the real hydraulic manipulator manufactured by ISE. This model is substantially used for simulations conducted in the following chapters to evaluate the developed control laws.

Chapter 3 starts from the regulating control problem, in which the desired position of the object and the corresponding desired link displacement change step-wise. Initially, a controller is designed assuming that full knowledge of the dynamics and kinematics of the system is available. The purpose is to introduce a controller for an ideal case to establish a ground for future work. The assumption is then relaxed and the control system is analyzed. Based on the analysis, the controller is then modified to account for the uncertainty of the payload, robot dynamic parameters and hydraulic functions. Using the detailed numerical model, simulations are carried out to investigate the controllers developed in this chapter.

In Chapter 4, the regulating controller is extended to a tracking controller which enables the manipulated object to follow a given trajectory and is robust against parameter uncertainties of the system. An observer is associated with the controller to avoid the need of acceleration feedback. Stability with final zero errors of position and velocity tracking is achieved and the error of internal force can be made arbitrarily small. Simulations are carried out to verify the developed controller.

Chapter 5 investigates the effects of friction. The above controllers are examined by introducing the well-known LuGre friction model into the actuator dynamics. Theoretical analysis is given. Same or similar simulations are carried out, but with the introduction of friction into the model, to investigate the previously developed controllers. The simulation results validate the theoretical findings, which substantiate the importance of modeling friction and compensation for its effects.

The tracking controller is redesigned in Chapter 6 to accommodate the introduction of the most recent and sophisticated friction dynamic model. The friction parameters are to be taken care of. Observers have to be designed to observe the immeasurable friction states. Based on the estimated friction parameters and observed friction states, an appropriate friction compensation scheme is designed which does not directly use velocity in order to avoid the need of acceleration feedback. Simulations are carried out to evaluate the performance of the developed controller.

The problem of “explosion of terms” stemming from the traditional backstepping controller design method is addressed by employing the concept of dynamic surface control (Swaroop et al., 1997); in which a low pass filter is integrated to avoid model differentiation. The adaptation law and friction compensation scheme is redesigned in Chapter 7. Simulations then test the developed controller, using the same numerical model.

Experimental examinations are shown in Chapter 8 on an available system consisting of two single-axis hydraulic actuators. The goal is to test the final controller developed in Chapter 7 in a real hydraulic system. The experimental results further validate the developed controller which:

(i) is capable of tracking a reference position of the common object and regulating a reference internal force
(ii) is robust against uncertainties and nonlinearities presented in hydraulic power systems
(iii) does not require measurements of accelerations, only needs to measure line pressures, position and velocity.
(iv) guarantees stability

The contributions of this thesis along with suggestions for future research are summarized in Chapter 9.

Four appendices are provided in the thesis. The issue of degree of freedom of a multi-end-effector/object system is reviewed in Appendix A. Appendix B proves some properties regarding those matrices appearing in the dynamic equation of motion for the entire robots-object system. The backstepping controller design method is reviewed in Appendix C. A detailed dynamic model of a three-degree-of-freedom manipulator used for simulation is presented in Appendix D.

Chapter 2 Development of a Complete Model of Co-operating Hydraulic Manipulators

Consider the problem of manipulating a rigid object with *n* hydraulic robots as shown in Figure 2.1. All the robots are considered non-redundant and the end-effectors of all robots are rigidly connected to the object, i.e., there is no relative motion between the object and the end-effectors (Khatib, 1988; Liu and Arimoto, 1996).

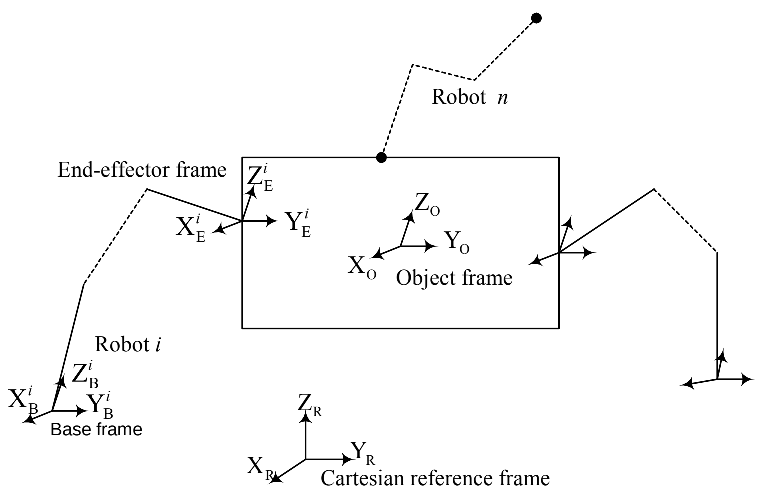

Figure 2.1: Coordinate systems for co-operating manipulators and object.

2.1 Kinematics

The position/orientation of the object frame $\{X_o, Y_o, Z_o\}$ with respect to the Cartesian reference frame $\{X_R, Y_R, Z_R\}$ is described by $X = [x_o\ y_o\ z_o\ \psi_o\ \theta_o\ \varphi_o]^T \in R^{6\times 1}$, where $\psi_o, \theta_o, \varphi_o$ are the Euler angles. The Euler angles can be defined using the following sequence: first a rotation ψ_o about the *z* axis, then a rotation θ_o about the new *x* axis and finally, a rotation about the new *z* axis, of φ_o. Let $X_e^i = [x_e^i\ y_e^i\ z_e^i\ \psi_e^i\ \theta_e^i\ \varphi_e^i]^T \in R^{6\times 1}$ be the position/orientation of the i^{th} end-effector frame $\{X_E^i, Y_E^i, Z_E^i\}$ with respect to the

Cartesian reference frame. q_j^i is the joint variable of the j^{th} link of the i^{th} manipulator; thus, $q^i = [q_1^i q_2^i ... q_6^i]^T \in R^{6\times1}$, and $\boldsymbol{q} = [q^{1T} q^{2T} ... q^{nT}]^T \in R^{6n\times1}$. The relation between X and X_e^i can be expressed as (Sun and Mills, 2002):

$$X_e^i = X + \begin{bmatrix} R_o(\psi_o, \theta_o, \varphi_o) r_e^i \\ \phi_e^i \end{bmatrix} \tag{2.1}$$

where r_e^i and ϕ_e^i are the position and orientation vectors of the i^{th} end-effector frame $\{X_E^i, Y_E^i, Z_E^i\}$ with respect to the origin of the object body frame $\{X_o, Y_o, Z_o\}$ and expressed in the object frame, respectively. They correspond to the configuration of the grasp and are constant due to the rigid grasp assumption. $R_o(\psi_o, \theta_o, \varphi_o)$ is the rotation matrix of the object frame $\{X_o, Y_o, Z_o\}$ relative to the Cartesian reference frame $\{X_R, Y_R, Z_R\}$. Corresponding to the series of rotation defined here, the rotation matrix is given by Thornton and Marion (2004) as

$$R_o(\psi_o, \theta_o, \varphi_o) =$$
$$\begin{bmatrix} \cos\psi_o \cos\varphi_o - \cos\theta_o \sin\psi_o \sin\varphi_o & -\cos\psi_o \sin\varphi_o - \cos\theta_o \sin\psi_o \cos\varphi_o & \sin\psi_o \sin\theta_o \\ \sin\psi_o \cos\varphi_o + \cos\theta_o \cos\psi_o \sin\varphi_o & -\sin\psi_o \sin\varphi_o + \cos\theta_o \cos\psi_o \cos\varphi_o & -\cos\psi_o \sin\theta_o \\ \sin\theta_o \sin\varphi_o & \sin\theta_o \cos\varphi_o & \cos\theta_o \end{bmatrix}$$

Let $v \in R^{6\times1}$ and $v_e^i \in R^{6\times1}$ be the vectors of linear and angular velocities of the object and the i^{th} end-effector expressed in Cartesian reference frame $\{X_R, Y_R, Z_R\}$, respectively. $\boldsymbol{v}_e = [v_e^{1T} v_e^{2T} ... v_e^{nT}]^T \in R^{6n\times1}$. The relation between v and the derivatives of the position/orientation of the object $\dot{X}$, is given by Khatib (1988) as

$$v = E\dot{X} \tag{2.2}$$

where $E = \begin{bmatrix} I & 0 \\ 0 & E_r \end{bmatrix}$ and $E_r = \begin{bmatrix} 0 & \cos\psi_o & \sin\psi_o \sin\theta_o \\ 0 & \sin\psi_o & -\cos\psi_o \sin\theta_o \\ 1 & 0 & \cos\theta_o \end{bmatrix}$.

The following relation holds between the motion velocities:

$$v_e^i = W^{iT} v, \quad i = 1,2,...,n \tag{2.3}$$

where

$$W^i = \begin{bmatrix} I & 0 \\ R^i & I \end{bmatrix} \tag{2.4}$$

and

$$R^i = \begin{bmatrix} 0 & -(z_e^i - z_o) & (y_e^i - y_o) \\ (z_e^i - z_o) & 0 & -(x_e^i - x_o) \\ -(y_e^i - y_o) & (x_e^i - x_o) & 0 \end{bmatrix} \tag{2.5}$$

v_e^i is related to $\dot{q}^i$ by the following relation:

$$v_e^i = J^i \dot{q}^i \tag{2.6}$$

where J^i is the (6×6) Jacobian matrix from the joint space to the Cartesian reference frame, which is assumed to be nonsingular. Combining equations (2.2), (2.3) and (2.6), leads to

$$\dot{q}^i = \{J^i\}^{-1} W^{iT} E\dot{X} \tag{2.7}$$

or

$$\dot{\boldsymbol{q}} = \boldsymbol{J}^{-1} \boldsymbol{W}^T E\dot{X} \tag{2.8}$$

where $\boldsymbol{J} = diag[J^1, J^2, ..., J^n] \in R^{6n \times 6n}$ and $\boldsymbol{W} = [W^1\ W^2 ... W^n] \in R^{6 \times 6n}$. $\boldsymbol{W}$ is called the grasp matrix (Uchiyama and Dauchez, 1988; Zribi Ahmad, 1992; Caccavale *et al.*, 1999). From equation (2.8), one can arrive at the following kinematic relation:

$$\ddot{\boldsymbol{q}} = \boldsymbol{J}^{-1}(\boldsymbol{W}^T E\ddot{X} + \boldsymbol{W}^T \dot{E}\dot{X} + \dot{\boldsymbol{W}}^T E\dot{X}) - \dot{\boldsymbol{J}}\boldsymbol{J}^{-1}\boldsymbol{W}^T E\dot{X} \tag{2.9}$$

2.2 Dynamics

2.2.1 Manipulator and Object Dynamics

The dynamic equation of *n* co-operating robots with respect to joint coordinates is given below (Caccavale *et al.*, 1999):

$$\boldsymbol{H}_m(\boldsymbol{q})\ddot{\boldsymbol{q}} + \boldsymbol{C}_m(\boldsymbol{q}, \dot{\boldsymbol{q}})\dot{\boldsymbol{q}} + \boldsymbol{G}_m(\boldsymbol{q}) = \boldsymbol{T}_m - \boldsymbol{J}^T \boldsymbol{F}_c \tag{2.10}$$

where, $\boldsymbol{H}_m = diag[H^1, H^2, ..., H^n] \in R^{6n \times 6n}$, $\boldsymbol{C}_m = diag[C^1, C^2, ..., C^n] \in R^{6n \times 6n}$, $\boldsymbol{G}_m = [G^{1T}\ G^{2T} ... G^{nT}]^T \in R^{6n \times 1}$, $\boldsymbol{T}_m = [T^{1T}\ T^{2T} ... T^{nT}]^T \in R^{6n \times 1}$ and $\boldsymbol{F}_c = [F_c^{1T}\ F_c^{2T} ... F_c^{nT}]^T \in R^{6n \times 1}$. For the i^{th} manipulator, H^i denotes the robot inertia matrix, C^i denotes the Coriolis and centrifugal effects, G^i is the gravitational term and,

$T^i = [T_1^i \; T_2^i \ldots T_6^i]^T \in R^{6\times 1}$ where T_j^i is the generalized joint torque originating from the j^{th} hydraulic actuator of the i^{th} manipulator. F_c^i is the vector of contact force/moment on the object exerted by the end-effector of the i^{th} robot, also called end-effector force.

The matrices describing the robot dynamics in equation (2.10) satisfy the following properties (Slotine and Li, 1991):

Property 2.1: $\boldsymbol{H}_m$ is a symmetric positive definite matrix,

Property 2.2: $(\dot{\boldsymbol{H}}_m - 2\boldsymbol{C}_m)$ is a skew-symmetric matrix, i.e.,

$$x^T(\dot{\boldsymbol{H}}_m - 2\boldsymbol{C}_m)x = 0; \forall x \in R^{6n\times 1},$$

Property 2.3: $\boldsymbol{C}_m(\boldsymbol{q}, x)y = \boldsymbol{C}_m(\boldsymbol{q}, y)x \quad \forall \boldsymbol{q}, x, y \in R^{6n\times 1}$ and,

Property 2.4: $\boldsymbol{H}_m(\boldsymbol{q})$ and $\boldsymbol{C}_m(\boldsymbol{q}, \dot{\boldsymbol{q}})$ are bounded, i.e., $0 < \boldsymbol{H}_L \le \|\boldsymbol{H}_m(\boldsymbol{q})\| \le \boldsymbol{H}_U$

$$\forall \boldsymbol{q} \in R^{6n\times 1} \text{ and } \|\boldsymbol{C}_m(\boldsymbol{q}, x)\| \le \boldsymbol{C}_U \|x\| \quad \forall \boldsymbol{q}, x \in R^{6n\times 1}.$$

The degree of freedom of the co-operating system is discussed in Appendix A. The object dynamics expressed in Cartesian space can be obtained using Lagrange formulation or from the literature (Caccavale, et. al., 1999; Khatib, 1988; Kawasaki, et. al., 2000):

$$M_o(X)\ddot{X} + D_o(X, \dot{X})\dot{X} + G_o(X) = E^T \boldsymbol{W}\boldsymbol{F}_c \tag{2.11}$$

where $M_o(X) \in R^{6\times 6}$ is the inertia matrix of the object, $D_o(X, \dot{X})\dot{X} \in R^{6\times 1}$ is the vector of Coriolis and centrifugal effects, $G_o(X) \in R^{6\times 1}$ is the vector of gravity effects, and $E^T \boldsymbol{W}\boldsymbol{F}_c$ is the generalized force corresponding to the vector of position/orientation of the object, X. Similarly, matrices describing the object dynamics in equation (2.11) have the following properties:

Property 2.5: $M_o(X)$ is a symmetric positive definite matrix,

Property 2.6: $(\dot{M}_o(X) - 2D_o(X, \dot{X}))$ is a skew-symmetric matrix,

Property 2.7: $D_o(x, y)z = D_o(x, z)y \quad \forall x, y, z \in R^{6n\times 1}$ and,

Property 2.8: $M_o(X)$ and $D_o(X, \dot{X})$ are bounded, i.e., $0 < M_{o,L} \le \|M_o(x)\| \le M_{o,U}$

$$\forall x \in R^{6n\times 1} \text{ and } \|D_o(x, y)\| \le D_{o,U}\|y\| \qquad \forall x, y \in R^{6n\times 1}.$$

The effects of each end-effector force F_c^i can be transformed to their equivalent effects at the object coordinates. This will produce a resultant motion force applied on the object at the object coordinates. The resultant force generates the object motion. The contact forces (a set of end-effect forces) could also produce another type of force on the object: internal loading. The internal loading represents the elements of force vectors applied to an object, which are canceled within the object and therefore do not influence the object motion (Vukobratovic and Tuneski, 1998). Let the resultant external force vector be, F_{ext}, and the internal loading force vector be, F_{int}. The mapping of the contact force vector, $\boldsymbol{F}_c$, onto F_{ext} is unique and is expressed as (Khatib, 1988; Walker et al., 1991; Caccavale et al.,1999):

$$F_{ext} = \boldsymbol{W}\boldsymbol{F}_c \tag{2.12}$$

On the other hand, the reverse mapping is not unique and should take the internal force F_{int} into account (Caccavale *et al*., 1999):

$$\boldsymbol{F}_c = \boldsymbol{W}^{\dagger} F_{ext} + \boldsymbol{V} F_{\text{int}} \tag{2.13}$$

where $\boldsymbol{W}^{\dagger}$ is a generalized inverse, or pseudo-inverse (Noble and Daniel, 1977) of $\boldsymbol{W}$, such that $\boldsymbol{W}\boldsymbol{W}^{\dagger} = \boldsymbol{I}$. $\boldsymbol{V}$ is a full-column-rank matrix spanning the null space of $\boldsymbol{W}$ such that $\boldsymbol{W}\boldsymbol{V} = 0$. The matrix $\boldsymbol{W}^{\dagger}$ specifies the contribution of each robot in generating the external force applied to the object. It may be defined in general by $\boldsymbol{W}^{\dagger} = A\boldsymbol{W}^{\mathrm{T}}(\boldsymbol{W}A\boldsymbol{W}^{\mathrm{T}})^{-1}$ for some positive-definite A. In fact, there are an infinite number of possible pseudo-inverses $\boldsymbol{W}^{\dagger}$ to choose from. Thus, there are multiple solutions in general for the contact forces, $\boldsymbol{F}_c$, given the desired object motion represented by F_{ext}. However, it has been discussed (Walker et al., 1991) that $\boldsymbol{W}^{\dagger}$ must be properly chosen; otherwise, internal forces may arise even given the desired internal force represented by F_{int} as zero. To better understand this, consider a one-dimensional problem: given $F_{ext} = 100$ N, $F_{\text{int}} = 0$ N, and $\boldsymbol{W} = \begin{bmatrix} 1 & 1 \end{bmatrix}$, choosing $\boldsymbol{W}^{\dagger} = \begin{bmatrix} 2 \\ -1 \end{bmatrix}$ which meets $\boldsymbol{W}\boldsymbol{W}^{\dagger} = \boldsymbol{I}$, equation (2.13) gives $\boldsymbol{F}_c = \begin{bmatrix} 200 \\ -100 \end{bmatrix}$. Such a set of contact forces results in an internal force of 100N, though given $F_{\text{int}} = 0$. This is a case shown in Figure 2.2(a). Now choose $\boldsymbol{W}^{\dagger} = \begin{bmatrix} 0.5 \\ 0.5 \end{bmatrix}$ ($\boldsymbol{W}\boldsymbol{W}^{\dagger} = \boldsymbol{I}$ is satisfied). Distinctly, it gives $\boldsymbol{F}_c = \begin{bmatrix} 50 \\ 50 \end{bmatrix}$ which results in the given external force and produces no internal force, as shown in Figure 2.2(b).

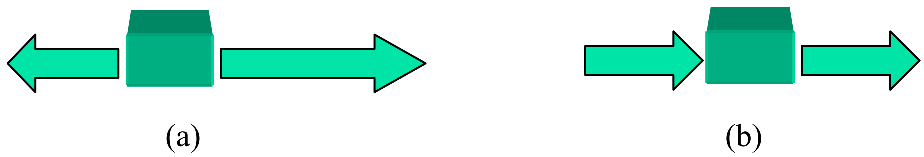

Figure 2.2: (a) Object experiencing internal force, (b) Object under no internal force.

As illustrated above, by choosing an appropriate $\boldsymbol{W}^{\dagger}$ so that the first term in equation (2.13) contributes no internal force effects, the contact force is completely decoupled into two components that contribute to the object motion and internal force respectively. Importantly, this also makes it feasible to regulate the internal force. An acceptable form for $\boldsymbol{W}^{\dagger}$ is given below:

$$\boldsymbol{W}^{\dagger} = \begin{bmatrix} \alpha^1 I & 0 \\ -\alpha^1 R^1 & \alpha^1 I \\ \vdots & \vdots \\ \alpha^n I & 0 \\ -\alpha^n R^n & \alpha^n I \end{bmatrix} \tag{2.14}$$

where $\sum_{i=1}^{n} \alpha^i = 1$ with $\alpha^i > 0$. This choice of $\boldsymbol{W}^{\dagger}$ guarantees that the first term in equation (2.13), $\boldsymbol{W}^{\dagger} F_{ext}$, contributes no internal force effects. The proof is given below:

Recalling that $\boldsymbol{W} = [W^1\, W^2 ... W^n]$ and $W^i = \begin{bmatrix} I & 0 \\ R^i & I \end{bmatrix}$, it is easy to show that

$$\boldsymbol{W}\boldsymbol{W}^{\dagger} = \begin{bmatrix} I & 0 & \cdots & I & 0 \\ R^1 & I & \cdots & R^n & I \end{bmatrix} \begin{bmatrix} \alpha^1 I & 0 \\ -\alpha^1 R^1 & \alpha^1 I \\ \vdots & \vdots \\ \alpha^n I & 0 \\ -\alpha^n R^n & \alpha^n I \end{bmatrix} = \boldsymbol{I}^{6n \times 6n}.$$

Furthermore, assuming $F_{ext} = \begin{bmatrix} f \\ \tau \end{bmatrix}$, where f and τ represent vectors of forces and moments, respectively, the following is obtained

$$\boldsymbol{W}^{\dagger} F_{ext} = \begin{bmatrix} \alpha^1 f \\ \alpha^1 \tau - \alpha^1 R^1 f \\ \vdots \\ \alpha^n f \\ \alpha^n \tau - \alpha^n R^n f \end{bmatrix}$$

where, the i^{th} component corresponding to the i^{th} end-effector is $\left[\alpha^i f^T \quad (\alpha^i \tau - \alpha^i R^i f)^T\right]^T$. Pre-multiplying it by W^i, gives its equivalent force at the object coordinates which is $\left[\alpha^i f^T \quad \alpha^i \tau^T\right]^T$. Since $\alpha^i > 0$ no forces or moments will be canceled by each other at the object coordinates. Thus, according to the work by Walker et al. (1991), the first term in equation (2.13), $\boldsymbol{W}^{\dagger} F_{ext}$, contributes no internal force effects given the choice of $\boldsymbol{W}^{\dagger}$ in equation (2.14).

Remarks:

By setting different values for α^i, the shared payload for each robot will be different. This allows the stronger robot to share more of the payload. In a particular case where $\alpha^i = 1/n$, equation (2.14) becomes the same solution as given by Walker *et al*. (1991) which allows the manipulators to equally share the load.

The matrix, ***V***, in equation (2.13) indicates the contribution of each robot in generating the internal force applied on the object. Here, the following form for ***V*** is adopted:

$$\boldsymbol{V} = \begin{bmatrix} b^1 I & 0 \\ -b^1 R^1 & b^1 I \\ \vdots & \vdots \\ b^n I & 0 \\ -b^n R^n & b^n I \end{bmatrix} \tag{2.15}$$

Where $b^i, i = 1,2,...n$ are constants satisfying $\sum_{i=1}^{n} b^i = 0$. For a case where manipulators equally contribute to the internal loading, one possible solution for the weight coefficient b^i is

$$b^i = \frac{2(-1)^i}{n-(-1)^i(1-(-1)^n)/2}, \quad i = 1,...,n \tag{2.16}$$

or

$$b^i = \frac{2(-1)^i}{n}, \quad i = 1,...,n, \quad \text{when } n \text{ is even}$$

$$b^i = \frac{2(-1)^i}{n-(-1)^i}, \quad i = 1,...,n, \quad \text{when } n \text{ is odd}$$

For example, when an object is manipulated by two manipulators, coefficients b^1 and b^2 become -1 and 1, respectively. When an object is manipulated by an odd number of manipulators, for instance, five robots; coefficients b^1, b^2, b^3, b^4, and b^5 become -1/3, 1/2, -1/3, 1/2 and -1/3, respectively. In this case, two of the five robots will be contributing half of the internal force against the three other robots, evenly sharing an opposite force.

2.2.2 Hydraulic Actuator Dynamics

With reference to Figure 2.3, for the j^{th} cylinder of the i^{th} manipulator, the governing equations that describe the nonlinear valve flow characteristics can be written as (Niksefat and Sepehri, 2000):

extension ($x^i_{sp,j} \geq 0$)

$$q^i_{I,j} = C_d \Delta(x^i_{sp,j}) \sqrt{\frac{2}{\rho}(P_s - P^i_{I,j})} \tag{2.17a}$$

$$q^i_{O,j} = C_d \Delta(x^i_{sp,j}) \sqrt{\frac{2}{\rho}(P^i_{O,j} - P_e)} \tag{2.17b}$$

retraction ($x^i_{sp,j} < 0$)

$$q^i_{I,j} = C_d \Delta(x^i_{sp,j}) \sqrt{\frac{2}{\rho}(P^i_{I,j} - P_e)} \tag{2.17c}$$

$$q^i_{O,j} = C_d \Delta(x^i_{sp,j}) \sqrt{\frac{2}{\rho}(P_s - P^i_{O,j})} \tag{2.17d}$$

where $q^i_{I,j}$ and $q^i_{O,j}$ represent fluid flows into and out of the valve, respectively. C_d and ρ are the orifice coefficients of the discharge and the mass density of the fluid, respectively. $x^i_{sp,j}$ represents the spool displacement. $P^i_{I,j}$ and $P^i_{O,j}$ are the input and output line pressures, respectively. P_s and P_e are the pump and the return (exit) pressures. $\Delta(x^i_{sp,j})$ represents a function that relates the spool displacement, $x^i_{sp,j}$, to the valve orifice area. Here it is assumed that (Niksefat and Sepehri, 2000; Bu and Yao, 2001)

$$\Delta(x^i_{sp,j}) = w^i_j x^i_{sp,j} \tag{2.18}$$

where, w^i_j is the orifice area gradient.

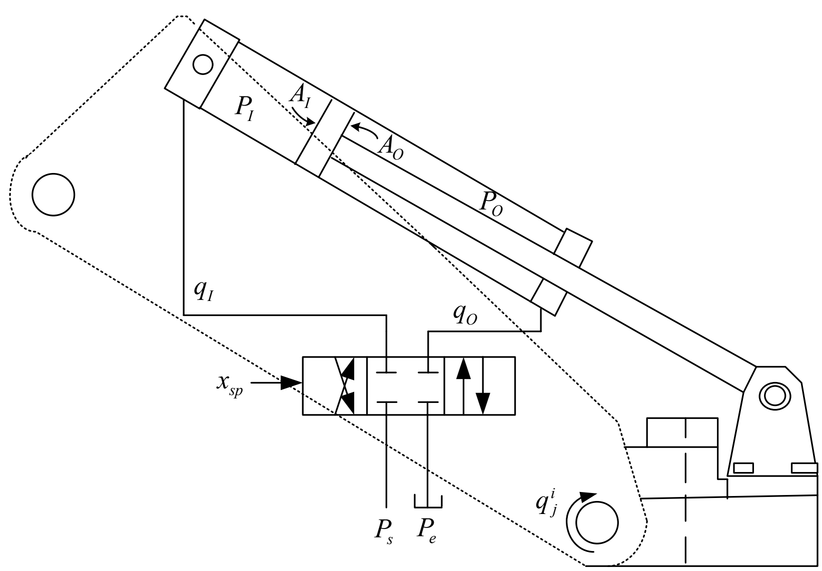

Figure 2.3: Diagram of hydraulic actuator with its driven link.

Equations (2.17) and (2.18) are now rewritten in compact forms as

$$q^i_{I,j} = K^i_j x^i_{sp,j} Q^i_{I,j} \tag{2.19}$$

$$q^i_{O,j} = K^i_j x^i_{sp,j} Q^i_{O,j} \tag{2.20}$$

where

$$K_j^i = C_d \sqrt{\frac{2}{\rho}} w_j^i \tag{2.21}$$

$$Q_{I,j}^i = \sqrt{(P_s - P_e)/2 + \text{sgn}(x_{sp,j}^i)((P_s + P_e)/2 - P_{I,j}^i)} \tag{2.22}$$

$$Q_{O,j}^i = \sqrt{(P_s - P_e)/2 + \text{sgn}(x_{sp,j}^i)(P_{O,j}^i - (P_s + P_e)/2)} \tag{2.23}$$

and

$$\text{sgn}(x_{sp,j}^i) = \begin{cases} 1 & \text{when } x_{sp,j}^i > 0 \\ 0 & \text{when } x_{sp,j}^i = 0 \\ -1 & \text{when } x_{sp,j}^i < 0 \end{cases} \tag{2.24}$$

Continuity equations for fluid flow through the cylinder are (Niksefat and Sepehri, 2000)

$$q_{I,j}^i = A_{I,j}^i \dot{x}_j^i + \frac{V_{I,j}^i(x_j^i)}{\beta_j^i} \dot{P}_{I,j}^i \tag{2.25a}$$

$$q_{O,j}^i = A_{O,j}^i \dot{x}_j^i - \frac{V_{O,j}^i(x_j^i)}{\beta_j^i} \dot{P}_{O,j}^i \tag{2.25b}$$

where β_j^i is the effective bulk modulus of the hydraulic fluids. x_j^i is the cylinder position and $\dot{x}_j^i$ is the actuator cylinder speed. Volumes $V_{I,j}^i$ and $V_{O,j}^i$ are the fluid volumes trapped in the blind and the rod sides of the actuator, respectively. They are expressed as

$$V_{I,j}^i(x_j^i) = \overline{V}_{I,j}^i + x_j^i A_{I,j}^i \tag{2.26a}$$

$$V_{O,j}^i(x_j^i) = \overline{V}_{O,j}^i - x_j^i A_{O,j}^i \tag{2.26b}$$

where $\overline{V}_{I,j}^i$ and $\overline{V}_{O,j}^i$ are the volumes of the two chambers when $x_j^i = 0$.

Assuming a very small rise time, the relation between the spool displacement $x_{sp,j}^i$ and the input voltage u_j^i to the proportional valve is simply expressed as

$$K_{sp,j}^i u_j^i = x_{sp,j}^i \tag{2.27}$$

where $K_{sp,j}^i$ is a gain. The net force from hydraulic actuator F_j^i is

$$F_j^i = A_{I,j}^i P_{I,j}^i - A_{O,j}^i P_{O,j}^i - F_{fr,j}^i \tag{2.28}$$

$F^i_{fr,j}$ is the friction that is further described in Section 2.3. The cylinder speed is related to the joint angular velocity as

$$\dot{x}^i_j = \bar{J}^i_j(q^i_j)\dot{q}^i_j \tag{2.29}$$

where $\bar{J}^i_j(q^i_j)$ is the Jacobian from link joint space to the linear actuator coordinate and assumed nonsingular. Using virtual work principle, the net torque originating from the actuator T^i_j is

$$T^i_j = \bar{J}^i_j(q^i_j)F^i_j \tag{2.30}$$

2.2.3 Friction Model

The friction force $F^i_{fr,j}$ appearing in equation (2.28) is modeled by the LuGre friction model with friction force variations

$$F^i_{fr,j} = \sigma^i_{0,j} z^i_j + \sigma^i_{1,j}\dot{z}^i_j + \sigma^i_{2,j}\dot{x}^i_j \tag{2.31}$$

$$\dot{z}^i_j = \dot{x}^i_j - \frac{\left|\dot{x}^i_j\right|}{g(\dot{x}^i_j)} z^i_j \tag{2.32}$$

where z^i_j is the friction internal state that describes the average deflections of the bristles between each pair of contact surfaces. This state is not measurable, but finite (Canudas de Wit *et al*., 1995). The nonlinear function $g(\dot{x}^i_j)$ is used to describe different friction effects and can be parameterized to characterize the Stribeck effect (Canudas de Wit *et al*., 1995)

$$\sigma^i_{0,j} g(\dot{x}^i_j) = F^i_{sl,j} + (F^i_{st,j} - F_{sl,j})e^{-(\dot{x}^i_j / \dot{x}^i_{s,j})^2} \tag{2.33a}$$

or

$$g(\dot{x}^i_j) = f^i_{sl,j} + (f^i_{st,j} - f_{sl,j})e^{-(\dot{x}^i_j / \dot{x}^i_{s,j})^2} \tag{2.33b}$$

where $F^i_{sl,j}$ and $F^i_{st,j}$ represent the levels of the slip friction and the stiction force, respectively. Consequently, $f^i_{sl,j}$ and $f^i_{st,j}$ represent the levels of the normalized slip friction and the normalized stiction force (Tan et al., 2003), respectively. $\dot{x}^i_{s,j}$ is the Stribeck velocity. Variables $\sigma^i_{0,j}$, $\sigma^i_{1,j}$, and $\sigma^i_{2,j}$ are the friction force parameters physically interpreted as the stiffness of the bristles between two contact surfaces, damping coefficient, and viscous friction coefficient. These friction force parameters $\sigma^i_{0,j}$, $\sigma^i_{1,j}$, and $\sigma^i_{2,j}$ can be calibrated through systematic experiments, which may involve considerable work (Canuds de Wit et. al., 1995). Also, they may vary slowly but significantly in real applications due to temperature changes, material wear, lubrication condition, and the nominal acting forces between contact surfaces (Tan, *et al*., 2003). Therefore, as will be described in the next chapters, these three parameters are considered unknown. The friction force/torque is assumed to follow the dynamics in equation (2.31) and (2.32), but each friction state z^i_j, referred to as the internal state, is finite but unknown and not measurable. Hence, each friction state z^i_j needs to be observed by the controller.

Note that the remaining parameters in equation (2.33a) or (2.33b) are normally estimated by the construction of static friction-velocity map measured during constant velocity motions (Lischinsky, 1999).

2.3 Model of the Entire System

From equations (2.28) and (2.30) one arrives at:

$$\boldsymbol{T_m} = \boldsymbol{\bar{J}}(\boldsymbol{F} - \boldsymbol{F_{fr}}) \tag{2.34}$$

where

$$\boldsymbol{F} = \boldsymbol{A_I}\boldsymbol{P_I} - \boldsymbol{A_O}\boldsymbol{P_O} \tag{2.35}$$

and

$$\boldsymbol{\bar{J}} = diag[\bar{J}^1\bar{J}^2\cdots\bar{J}^n];\ \bar{J}^i = [\bar{J}^i_1\bar{J}^i_2\cdots\bar{J}^i_6];$$

$$\boldsymbol{P_I} = [P_I^{1T}P_I^{2T}\cdots P_I^{nT}]^T;\ P_I^i = [P^i_{I,1}P^i_{I,2}\cdots P^i_{I,6}]^T;$$

$$\boldsymbol{P_O} = [P_O^{1T}P_O^{2T}\cdots P_O^{nT}]^T;\ P_O^i = [P^i_{O,1}P^i_{O,2}\cdots P^i_{O,6}]^T;$$

$$\boldsymbol{F_{fr}} = [F_{fr}^{1T}F_{fr}^{2T}\cdots F_{fr}^{nT}]^T;\ F_{fr}^i = [F^i_{fr,1}F^i_{fr,2}\cdots F^i_{fr,6}]^T;$$

$$\boldsymbol{A_I} = diag[A^i_{I,j}];\ \boldsymbol{A_O} = diag[A^i_{O,j}];\quad i = 1,\dots,n;\ j = 1,\dots,6.$$

Combining equations (2.8), (2.9), (2.10) and (2.34) one arrives at the following equation:

$$\Lambda\ddot{X} + B\dot{X} + E^T\boldsymbol{W}\boldsymbol{J}^{-T}\boldsymbol{G_m} = E^T\boldsymbol{W}\boldsymbol{J}^{-T}\boldsymbol{\bar{J}}(\boldsymbol{F} - \boldsymbol{F_{fr}}) - E^T\boldsymbol{W}\boldsymbol{F_c} \tag{2.36}$$

where

$$\Lambda = E^T \boldsymbol{W}\boldsymbol{J}^{-T}\boldsymbol{H}_{\boldsymbol{m}}\boldsymbol{J}^{-1}\boldsymbol{W}^T E \tag{2.37}$$

and

$$B = E^T \boldsymbol{W}\boldsymbol{J}^{-T}[\boldsymbol{C}_{\boldsymbol{m}}\boldsymbol{J}^{-1}\boldsymbol{W}^T E + \boldsymbol{H}_{\boldsymbol{m}}\boldsymbol{J}^{-1}(\dot{\boldsymbol{W}}^T E + \boldsymbol{W}^T \dot{E} - \dot{\boldsymbol{J}}\boldsymbol{J}^{-1}\boldsymbol{W}^T E)] \tag{2.38}$$

Combining equations (2.11) and (2.36) together, will cancel the term "$E^T \boldsymbol{W}\boldsymbol{F}_c$" and lead to the dynamic equation of motion for the entire robots-object system:

$$M(X)\ddot{X} + D(X,\dot{X})\dot{X} + G(X) = T \tag{2.39}$$

where

$$M(X) = \Lambda(X) + M_o(X) \tag{2.40}$$

$$D(X,\dot{X}) = B(X,\dot{X}) + D_o(X,\dot{X}) \tag{2.41}$$

$$G(X) = E^T \boldsymbol{W}\boldsymbol{J}^{\boldsymbol{-T}}\boldsymbol{G}_{\boldsymbol{m}} + G_o(X) \tag{2.42}$$

$$T = E^T \boldsymbol{W}\boldsymbol{J}^{\boldsymbol{-T}}\bar{\boldsymbol{J}}(\boldsymbol{F} - \boldsymbol{F}_{\boldsymbol{fr}}) \tag{2.43}$$

It can be shown (see Appendix B) that the following properties hold:

Property 2.9: $M(X)$ is a symmetric positive definite matrix,

Property 2.10: $\dot{M} - 2D$ is a skew-symmetric matrix,

Property 2.11: $D(x,y)z = D(x,z)y \quad \forall x,y,z \in R^{6n\times1}$, and

Property 2.12: $M(X)$ and $D(X,\dot{X})$ are bounded as follows:

$$0 < M_L \le \|M(x)\| \le M_U \quad \forall x \in R^{6n\times1}$$

$$\|D(x,y)\| \le D_U\|y\| \qquad \forall x,y \in R^{6n\times1}$$

Note that $\boldsymbol{H}_{\boldsymbol{m}}(\boldsymbol{q})$, $\boldsymbol{C}_{\boldsymbol{m}}(\boldsymbol{q},\dot{\boldsymbol{q}})$, and $\boldsymbol{G}_{\boldsymbol{m}}(\boldsymbol{q})$ are linear in terms of the combined manipulator parameters (Slotine and Li, 1991). Also, $M_o(X)$, $D_o(X,\dot{X})$, and $G_o(X)$ are linear in terms of the payload parameters. Thus, M, D and G are linear with respect to the manipulators and object dynamic parameters, and the following relation can be written:

$$M(X)\ddot{X} + D(X,\dot{X})\dot{X} + G(X) = \Theta(X,\dot{X},\ddot{X})\theta \tag{2.44}$$

where θ is a vector of individual or combined unknown parameters of the system and $\Theta(\cdot)$ is a regressive matrix.

From equations (2.19), (2.20), (2.25), (2.26) and (2.27), one arrives at

$$\dot{\boldsymbol{P}}_I = \boldsymbol{C}_I[\boldsymbol{K}\boldsymbol{K}_{sp}\boldsymbol{Q}_I\boldsymbol{U} - \boldsymbol{A}_I\bar{\boldsymbol{J}}(\boldsymbol{q})\dot{\boldsymbol{q}}] \quad (2.45)$$

$$\dot{\boldsymbol{P}}_O = \boldsymbol{C}_O[-\boldsymbol{K}\boldsymbol{K}_{sp}\boldsymbol{Q}_O\boldsymbol{U} + \boldsymbol{A}_O\bar{\boldsymbol{J}}(\boldsymbol{q})\dot{\boldsymbol{q}}] \quad (2.46)$$

where

$$\boldsymbol{C}_I = diag(C^i_{I,j}); C^i_{I,j} = \frac{\beta^i_j}{V^i_{I,j} + A^i_{I,j}x^i_j};$$

$$\boldsymbol{C}_O = diag(C^i_{O,j}); C^i_{O,j} = \frac{\beta^i_j}{V^i_{O,j} - A^i_{O,j}x^i_j};$$

$$\boldsymbol{K} = diag(K^i_j);\ \boldsymbol{K}_{sp} = diag(K^i_{sp,j});$$

$$\boldsymbol{Q}_I = diag(Q^i_{I,j}); \boldsymbol{Q}_O = diag(Q^i_{O,j});$$

$$\boldsymbol{U} = [u^{1T}\ u^{2T} \ldots u^{nT}]^T;\ u^i = [u^i_1\ u^i_2 \ldots u^i_6]^T;\ \ i = 1,\ldots,n; j = 1,\ldots,6.$$

Differentiating equation (2.35) and using equations (2.45) and (2.46), result in

$$\dot{\boldsymbol{F}} = \boldsymbol{A}_{cq}(\boldsymbol{q})\boldsymbol{U} - \boldsymbol{A}_{ca}(\boldsymbol{q}, \dot{\boldsymbol{q}}) \quad (2.47)$$

where

$$\boldsymbol{A}_{cq}(\boldsymbol{q}) = (\boldsymbol{A}_I\boldsymbol{C}_I\boldsymbol{Q}_I + \boldsymbol{A}_O\boldsymbol{C}_O\boldsymbol{Q}_O)\boldsymbol{K}\boldsymbol{K}_{sp} \quad (2.48)$$

$$\boldsymbol{A}_{ca}(\boldsymbol{q}, \dot{\boldsymbol{q}}) = (\boldsymbol{A}^2_I\boldsymbol{C}_I + \boldsymbol{A}^2_O\boldsymbol{C}_O)\bar{\boldsymbol{J}}\dot{\boldsymbol{q}} \quad (2.49)$$

Similarly, the right-hand side of the hydraulic dynamics (2.47) can be linearly parameterized as

$$\boldsymbol{A}_{cq}(\boldsymbol{q})\boldsymbol{U} - \boldsymbol{A}_{ca}(\boldsymbol{q}, \dot{\boldsymbol{q}}) = \Phi(\boldsymbol{q}, \dot{\boldsymbol{q}}, \boldsymbol{U})\varphi \quad (2.50)$$

where φ is the vector of unknown parameters of the hydraulic function and $\Phi(\cdot)$ represents a regressive matrix.

Equations (2.39) and (2.47) describe the dynamics of a complete system of n hydraulic robots carrying a common rigid object.

Chapter 3 Regulating Control of Co-operating Hydraulic Manipulators

In this chapter, a nonlinear stable control scheme is developed to allow two or more hydraulic robots to coordinately regulate an object's position, while maintaining desired internal forces on the object and sharing the load.

The design is based on the backstepping technique (Khalil, 2002), which is a recursive procedure that interlaces the choice of a Lyapunov function with the design of feedback control. A review about this technique is presented in Appendix C. The controller is augmented by an on-line updating law to eliminate the steady-state errors, due to the lack of knowledge about the weight of the object. Furthermore, the requirement about the knowledge of robot dynamics and hydraulic functions are relaxed and the controller is redesigned. Friction is not considered at this stage. The stability of the system is guaranteed by constructing a smooth Lyapunov function. For the purpose of simulations, a detailed numerical simulation program is also developed. Two three-link planar robot manipulators resembling Magnum hydraulic manipulators manufactured by ISE, interact with each other through manipulating a common object. Simulation results are presented to substantiate the developed controller.

3.1 Controller Design with Full Knowledge of Physical Parameters

3.1.1 Controller Design

Using equation (2.2), one can write equation (2.8) as

$$\dot{\boldsymbol{q}} = \boldsymbol{J}^{-1}\boldsymbol{W}^{T} v \tag{3.1}$$

and the following is further obtained

$$\ddot{\boldsymbol{q}} = \boldsymbol{J}^{-1}(\boldsymbol{W}^{T}\dot{v} + \dot{\boldsymbol{W}}^{T} v - \dot{\boldsymbol{J}}\dot{\boldsymbol{q}}) \tag{3.2}$$

The dynamic equation (2.10) can also be expressed in terms of the object velocity, v

$$\Lambda_v \dot{v} + B_v v + \boldsymbol{W}\boldsymbol{J}^{-T}\boldsymbol{G}_m = \boldsymbol{W}\boldsymbol{J}^{-T}\boldsymbol{T}_m - \boldsymbol{W}\boldsymbol{F}_c \tag{3.3}$$

where

$$\Lambda_v = \boldsymbol{W}\boldsymbol{J}^{-T}\boldsymbol{H}_m\boldsymbol{J}^{-1}\boldsymbol{W}^{T} \tag{3.4}$$

and

$$B_v = \boldsymbol{W}\boldsymbol{J}^{-T}\boldsymbol{H}_m\boldsymbol{J}^{-1}(\dot{\boldsymbol{W}}^T - \dot{\boldsymbol{J}}\boldsymbol{J}^{-1}\boldsymbol{W}^T) + \boldsymbol{W}\boldsymbol{J}^{-T}\boldsymbol{C}_m\boldsymbol{J}^{-1}\boldsymbol{W}^T \tag{3.5}$$

Dry friction is neglected at this stage and only viscous force is taken into account. Thus equation (2.28) becomes

$$F_j^i = A_{I,j}^i P_{I,j}^i - A_{O,j}^i P_{O,j}^i - K_{damp,j}^i \dot{x}_j^i \tag{3.6}$$

where $K_{damp,j}^i$ is a viscous coefficient. Accordingly, equation (2.34) becomes

$$\boldsymbol{T}_m = \bar{\boldsymbol{J}}\boldsymbol{F} - \boldsymbol{K}_{damp}\bar{\boldsymbol{J}}^2\dot{\boldsymbol{q}} \tag{3.7}$$

where $\boldsymbol{K}_{damp} = diag(K_{damp,j}^i)$, $i = 1,...,n; j = 1,...,6$. The object dynamics expressed in Cartesian space can be expressed in term of its velocity, and is given below (Caccavale *et al*., 1999):

$$\Lambda_o(X)v + B_o(X, v_o)v + g_o(X) = F_{ext} \tag{3.8}$$

where $\Lambda_o(X) \in R^{6\times6}$ is the symmetric and positive definite inertia matrix of the object, $B_o(X, v)v \in R^{6\times1}$ is the vector of Coriolis and centrifugal forces, $g_o(X) \in R^{6\times1}$ is the vector of gravity forces, and $F_{ext} \in R^{6\times1}$ is the vector of resulting forces acting at the origin of the object frame expressed in the Cartesian reference frame, and is given by equation (2.12). Note $\dot{\Lambda}_o(X) - 2B_o(X, v)$ is a skew-symmetric matrix.

Combining equations (3.3), (3.8) and (2.12) together will cancel the term "$\boldsymbol{W}\boldsymbol{F}_c$" and lead to the dynamic equation of motion for the robots-object system:

$$(\Lambda_o + \Lambda_v)\dot{v} + (B_o + B_v)v + g_o + \boldsymbol{W}\boldsymbol{J}^{-T}\boldsymbol{G}_m = \boldsymbol{W}\boldsymbol{J}^{-T}\boldsymbol{T}_m \tag{3.9}$$

Note that equation (3.9) is another form of equation (2.39) representing the overall system dynamics. The regulating controller design will be based on equation (3.9).

The following positive definite quadratic form is now chosen as the initial Lyapunov function candidate:

$$\mathrm{V}_1 = \tfrac{1}{2}\dot{\boldsymbol{q}}^T\boldsymbol{H}_m\dot{\boldsymbol{q}} + \tfrac{1}{2}v^T\Lambda_o v + \tfrac{1}{2}\tilde{\boldsymbol{q}}^T\boldsymbol{K}_p\tilde{\boldsymbol{q}} \tag{3.10}$$

where $\tilde{\boldsymbol{q}} = \boldsymbol{q} - \boldsymbol{q}^d$ and $\boldsymbol{q}^d$ denotes the vector of the desired link angular positions corresponding to the desired position/orientation of the object. Since the desired position/orientation of the object is related to each robot end-effector's desired position/orientation given by equation (2.1); $\boldsymbol{q}^d$ can then be derived from the manipulators' desired end-effector positions/orientations by the inverse kinematic solution of the robots (Paul, 1981). Note, $\dot{\tilde{\boldsymbol{q}}} = \dot{\boldsymbol{q}}$ since $\dot{\boldsymbol{q}}^d = 0$ for regulation problem. $\boldsymbol{K}_p \in R^{6n \times 6n}$ is a positive definite diagonal matrix.

Noting that $\dot{\Lambda}_o(X) - 2B_o(X, v)$ is a skew-symmetric matrix, and using properties 2.1 and 2.2, stated in Section 2.2, it can be shown that the time derivative of V_1 is

$$\dot{\mathrm{V}}_1 = -\dot{\boldsymbol{q}}^T \boldsymbol{K}_{damp} \bar{\boldsymbol{J}}^2(\boldsymbol{q})\dot{\boldsymbol{q}} + \dot{\boldsymbol{q}}^T(\bar{\boldsymbol{J}}(\boldsymbol{q})\boldsymbol{F} - \boldsymbol{G}_m(\boldsymbol{q}) + \boldsymbol{K}_p\tilde{\boldsymbol{q}}) - v^T g_o \tag{3.11}$$

Let the virtual controller for $\boldsymbol{F}$ be

$$\boldsymbol{F}^d = \bar{\boldsymbol{J}}^{-1}(-\boldsymbol{J}^T \boldsymbol{W}^\dagger \boldsymbol{W} \boldsymbol{J}^{-T} \boldsymbol{K}_p \tilde{\boldsymbol{q}} + \boldsymbol{G}_m(\boldsymbol{q}) + \boldsymbol{J}^T \boldsymbol{W}^\dagger g_o + \boldsymbol{J}^T \boldsymbol{V} F_{\mathrm{int}}^d) \tag{3.12}$$

where F_{int}^d is the desired internal force. Define

$$\tilde{\boldsymbol{F}} = \boldsymbol{F} - \boldsymbol{F}^d \tag{3.13}$$

Replacing $\boldsymbol{F}$ with $\tilde{\boldsymbol{F}} + \boldsymbol{F}^d$, equation (3.11) can be rewritten as

$$\dot{\mathrm{V}}_1 = -\dot{\boldsymbol{q}}^T \boldsymbol{K}_{damp} \bar{\boldsymbol{J}}^2(\boldsymbol{q})\dot{\boldsymbol{q}} + \dot{\boldsymbol{q}}^T \bar{\boldsymbol{J}}(\boldsymbol{q})\tilde{\boldsymbol{F}} + \dot{\boldsymbol{q}}^T(I - \boldsymbol{J}\boldsymbol{W}^\dagger \boldsymbol{W} \boldsymbol{J}^{-T})\boldsymbol{K}_p\tilde{\boldsymbol{q}} + (\dot{\boldsymbol{q}}^T \boldsymbol{J}^T \boldsymbol{W}^\dagger - v^T)g_o + \dot{\boldsymbol{q}}^T \boldsymbol{J}^T \boldsymbol{V} F_{\mathrm{int}}^d \tag{3.14}$$

Terms 3, 4 and 5 on the right side of equation (3.14) are now proven to be zero. Any vector of $\boldsymbol{F}_c$ can be written as follows:

$$\boldsymbol{F}_c = \boldsymbol{W}^\dagger \boldsymbol{W} \boldsymbol{F}_c + (\boldsymbol{I} - \boldsymbol{W}^\dagger \boldsymbol{W})\boldsymbol{F}_c \tag{3.15}$$

The first term of equation (3.15), $\boldsymbol{W}^\dagger \boldsymbol{W} \boldsymbol{F}_c$, represents the part that leads to a resultant/ external force on the object since $\boldsymbol{W}(\boldsymbol{W}^\dagger \boldsymbol{W} \boldsymbol{F}_c) = \boldsymbol{F}_{ext}$. Thus, $\boldsymbol{W}^\dagger \boldsymbol{W}$ acts as a filter to remove those force components leading to internal forces. In particular, the internal force related components could be completely removed with the choice of $\boldsymbol{W}^\dagger$ in equation (2.14). The second term, $(\boldsymbol{I} - \boldsymbol{W}^\dagger \boldsymbol{W})\boldsymbol{F}_c$, represents the part of the contact forces that produce internal forces, since

$$\boldsymbol{W}(\boldsymbol{I} - \boldsymbol{W}^\dagger \boldsymbol{W})\boldsymbol{F}_c = 0 \tag{3.16}$$

Vector $\boldsymbol{F}_c$ can be related to $\boldsymbol{T}_c$, the part of the generalized forces/torques, corresponding to the contact forces. The relation can be expressed by

$$\boldsymbol{F}_c = \boldsymbol{J}^{-T} \boldsymbol{T}_c \tag{3.17}$$

Substituting equation (3.17) into equation (3.15) leads to

$$\boldsymbol{T}_c = \boldsymbol{J}^T \boldsymbol{W}^{\dagger} \boldsymbol{W} \boldsymbol{T}_c + \boldsymbol{J}^T (I - \boldsymbol{W}^{\dagger} \boldsymbol{W}) \boldsymbol{T}_c \tag{3.18}$$

Similar to terms in equation (3.15); $\boldsymbol{J}^T \boldsymbol{W}^{\dagger} \boldsymbol{W} \boldsymbol{J}^{-T}$ acts as a filter to remove those torques corresponding to the internal forces. Equation (3.15) indicates that any set of contact forces can always be divided into two parts: one part contributes to the motion of the object; the other makes no contribution to the motion of the object. Similarly, any set of torques which produce contact forces, can be decoupled as described by equation (3.18). For a rigid object, the second term on the right side of equation (3.18) only corresponds to producing the internal forces, meaning that this part of the torque makes no work. Thus, the following relation holds:

$$\dot{\boldsymbol{q}}^T \boldsymbol{J}^T (I - \boldsymbol{W}^{\dagger} \boldsymbol{W}) \boldsymbol{T}_c = 0 \tag{3.19}$$

Since $\boldsymbol{T}_c$ can be any value, one has

$$\dot{\boldsymbol{q}}^T \boldsymbol{J}^T (I - \boldsymbol{W}^{\dagger} \boldsymbol{W}) = 0 \tag{3.20}$$

Alternatively, equations (3.19) and (3.20) can be explained in terms of relative velocity (Caccavale *et al*., 1999). The left side of equation (3.20) can be actually treated as the relative velocity due to the internal force, and then the left side of equation (3.19) is the work corresponding to deformation. For a rigid body, there is no deformation and no relative velocity due to internal force. This helps to explain equations (3.19) and (3.20).

It is easy to verify that term 3 on the right side of equation (3.14) is zero using equation (3.20). Also, terms 4 and 5 on the right side of equation (3.14), are zero by substituting equation (3.1) into these terms and using the fact that $\boldsymbol{W}\boldsymbol{V} = 0$.

Equation (3.14) then becomes

$$\dot{\mathrm{V}}_1 = -\dot{\boldsymbol{q}}^T \boldsymbol{K}_{damp} \overline{\boldsymbol{J}}^2 (\boldsymbol{q}) \dot{\boldsymbol{q}} + \dot{\boldsymbol{q}}^T \overline{\boldsymbol{J}} (\boldsymbol{q}) \widetilde{\boldsymbol{F}} \tag{3.21}$$

The Lyapunov candidate function of the entire closed-loop system is now defined as

$$\mathrm{V}_2 = \mathrm{V}_1 + \tfrac{1}{2} \widetilde{\boldsymbol{F}}^T \boldsymbol{\Gamma} \widetilde{\boldsymbol{F}} \tag{3.22}$$

where $\boldsymbol{\Gamma}$ is a positive definite diagonal matrix. The time derivative of V_2 is

$$\dot{\mathrm{V}}_2 = -\dot{\boldsymbol{q}}^T \boldsymbol{K}_{damp} \overline{\boldsymbol{J}}^2 (\boldsymbol{q}) \dot{\boldsymbol{q}} + \widetilde{\boldsymbol{F}}^T \overline{\boldsymbol{J}} (\boldsymbol{q}) \dot{\boldsymbol{q}} + \widetilde{\boldsymbol{F}}^T \boldsymbol{\Gamma} (\dot{\boldsymbol{F}} - \dot{\boldsymbol{F}}^d) \tag{3.23}$$

Using equation (2.47) to replace $\dot{\boldsymbol{F}}$ results in

$$\dot{\mathrm{V}}_2 = -\dot{\boldsymbol{q}}^T \boldsymbol{K}_{damp} \overline{\boldsymbol{J}}^2(\boldsymbol{q})\dot{\boldsymbol{q}} + \widetilde{\boldsymbol{F}}^T \overline{\boldsymbol{J}}(\boldsymbol{q})\dot{\boldsymbol{q}} + \widetilde{\boldsymbol{F}}^T \boldsymbol{\Gamma}[\boldsymbol{A}_{cq}(\boldsymbol{q})\boldsymbol{U} - \boldsymbol{A}_{ca}(\boldsymbol{q},\dot{\boldsymbol{q}}) - \dot{\boldsymbol{F}}^d] \tag{3.24}$$

Equation (3.24) suggests the controller to be

$$\boldsymbol{U} = \boldsymbol{A}_{cq}^{-1}(\boldsymbol{q})(\boldsymbol{A}_{ca}(\boldsymbol{q},\dot{\boldsymbol{q}}) - \boldsymbol{\Gamma}^{-1}\overline{\boldsymbol{J}}(\boldsymbol{q})\dot{\boldsymbol{q}} + \dot{\boldsymbol{F}}^d - \boldsymbol{K}_F \widetilde{\boldsymbol{F}}) \tag{3.25}$$

where $\boldsymbol{K}_F$ is a positive definite diagonal matrix.

The derivative of V_2 then becomes

$$\dot{\mathrm{V}}_2 = -\dot{\boldsymbol{q}}^T \boldsymbol{K}_{damp} \overline{\boldsymbol{J}}^2(\boldsymbol{q})\dot{\boldsymbol{q}} - \widetilde{\boldsymbol{F}}^T \boldsymbol{\Gamma} \boldsymbol{K}_F \widetilde{\boldsymbol{F}} \tag{3.26}$$

It is easy to see that $\dot{\mathrm{V}}_2$ is continuous, negative and semi-definite. Therefore, the control system, given the controller (3.25), is stable in the sense of Lyapunov.

3.1.2 Equilibrium of the Control System

For a set point $\boldsymbol{q}^d$ corresponding to the desired set-position of the object, the equilibrium of system (3.9), under controller (3.25), satisfies the following relations:

$$\boldsymbol{U}^{ss} = 0 \tag{3.27}$$

$$\widetilde{\boldsymbol{F}}^{ss} = 0 \tag{3.28}$$

$$\boldsymbol{W}\boldsymbol{J}^{-T}\boldsymbol{K}_p \widetilde{q}^{ss} = 0 \tag{3.29}$$

$$\boldsymbol{F}_c^{ss} = \boldsymbol{W}^{\dagger} g_o + \boldsymbol{V} F_{\mathrm{int}}^d \tag{3.30}$$

where the superscript "ss" represents steady-state. Variables with superscripts are the corresponding variables at the steady-state phase. For example, $\boldsymbol{U}^{ss}$ is the steady-state input voltage. Equation (3.27) indicates the hydraulic control valves are closed when the system is at the steady-state phase. If $\boldsymbol{K}_p \widetilde{\boldsymbol{q}}^{ss}$ is treated as the joint-error related torques, terms $\boldsymbol{J}^{-T}\boldsymbol{K}_p \widetilde{\boldsymbol{q}}^{ss}$ and $\boldsymbol{W}\boldsymbol{J}^{-T}\boldsymbol{K}_p \widetilde{\boldsymbol{q}}^{ss}$ become the joint-error related contact forces and external forces, respectively. Thus, equation (3.29) implies that the steady-state joint-error related external forces are zero and a set of solution points exist. It can be shown in a way similar to the work by Caccavale *et al* (1999) that there actually exists a domain of attraction for the equilibrium point with $\widetilde{\boldsymbol{q}}^{ss} = 0$. Because V_2 is quadratic, there always exists a positive l and a bounded region R_l such that R_l includes the point with $\widetilde{\boldsymbol{q}}^{ss} = 0$ and

$$\begin{cases} \mathrm{V}_2(x) < l \\ \dot{\mathrm{V}}_2(x) \le 0 \end{cases} \qquad \forall x \in R_l$$

By employing the local invariant set theorem, it follows that R_l is a domain of attraction for the equilibrium point with $\tilde{\boldsymbol{q}}^{ss} = 0$. Equation (3.30) leads to the desired internal forces at the steady-state phase. By applying equations (2.12), (2.13) and (3.30), it can be proven that:

$$\boldsymbol{F}_{ext}^{ss} = \boldsymbol{W}\boldsymbol{F}_c^{ss} = g_o \tag{3.31}$$

and

$$\boldsymbol{V}F_{\text{int}}^{ss} = \boldsymbol{F}_c^{ss} - \boldsymbol{W}^{\dagger} F_{ext}^{ss} = \boldsymbol{V}F_{\text{int}}^{d} \tag{3.32}$$

where F_{ext}^{ss} and F_{int}^{ss} are steady-state external and internal forces, respectively. Since matrix $\boldsymbol{V}$ is full-column-rank, it can be concluded that

$$F_{\text{int}}^{ss} = F_{\text{int}}^{d} \tag{3.33}$$

3.1.3 Comments on the Control Law

With respect to controller (3.25), the hydraulic system parameters needed by the controller are the effective piston areas $\boldsymbol{A}_I$ and $\boldsymbol{A}_O$, and the effective bulk modulus of the hydraulic fluid, β. Measurements of line pressures are required for feedback. Mass, length and position of the center of mass for each link of the robots are also required, since the Jacobian and compensation of link gravity appear in the controller. To calculate $\dot{\boldsymbol{F}}^d$, measurements of robot joint positions and velocities are required. Finally, the mass of the object is also required for the control law.

Usually, only rough estimates of some of those parameters are available. Thus, stability and equilibrium of the control system need to be studied under different cases.

Assuming that only a rough estimate of the load weight $\hat{g}_o$, is available, the desired force vector needed by the actuators and determined in equation (3.12) becomes

$$\boldsymbol{F}^d = \bar{\boldsymbol{J}}^{-1}(-\boldsymbol{J}^T\boldsymbol{W}^{\dagger}\boldsymbol{W}\boldsymbol{J}^{-T}\boldsymbol{K}_p\tilde{\boldsymbol{q}} + \boldsymbol{G}_m(\boldsymbol{q}) + \boldsymbol{J}^T\boldsymbol{W}^{\dagger}\hat{g}_o + \boldsymbol{J}^T\boldsymbol{V}F_{\text{int}}^d) \tag{3.34}$$

The equilibrium of the system under the controller (3.25) and (3.34), will then be

$$\boldsymbol{U}^{ss} = 0 \tag{3.35}$$

$$\tilde{\boldsymbol{F}}^{ss} = 0 \tag{3.36}$$

$$\boldsymbol{W}\boldsymbol{J}^{-T}\boldsymbol{K}_p\tilde{\boldsymbol{q}}^{ss} = \hat{g}_o - g_o \tag{3.37}$$

$$\boldsymbol{F}_c^{ss} = \boldsymbol{W}^{\dagger}\hat{g}_o + \boldsymbol{V}F_{\text{int}}^{d} \tag{3.38}$$

As seen, the uncertainty in the estimation of the payload leads to a new equilibrium configuration set, indicated by equations (3.35) to (3.38). Note that although the contact forces are different due to the inaccurate estimation of the payload, the internal forces remain at the desired steady-state level. This can be shown by equations (2.12), (2.13) and (3.38):

$$F_{ext}^{ss} = \boldsymbol{W}\boldsymbol{F}_c^{ss} = \hat{g}_o \tag{3.39}$$

$$F_{\text{int}}^{ss} = F_{\text{int}}^{d} \tag{3.40}$$

With respect to stability, considering a gravity energy function $E(\boldsymbol{q})$, such that it is positive semi-definite and $\frac{\partial E(\boldsymbol{q})}{\partial \boldsymbol{q}} = \boldsymbol{J}^T\boldsymbol{W}^{\dagger}(g_o - \hat{g}_o)$, let the Lyapunov candidate be

$$\mathrm{V}_2 = \tfrac{1}{2}\dot{\boldsymbol{q}}^T\boldsymbol{H}_m\dot{\boldsymbol{q}} + \tfrac{1}{2}v^T\Lambda_o v + \tfrac{1}{2}\tilde{\boldsymbol{q}}^T\boldsymbol{K}_p\tilde{\boldsymbol{q}} + \tfrac{1}{2}\tilde{\boldsymbol{F}}^T\boldsymbol{\Gamma}\tilde{\boldsymbol{F}} + E(\boldsymbol{q}) \tag{3.41}$$

It can be then shown that

$$\dot{\mathrm{V}}_2 = -\dot{\boldsymbol{q}}^T\boldsymbol{K}_{damp}\bar{\boldsymbol{J}}^2(\boldsymbol{q})\dot{\boldsymbol{q}} - \tilde{\boldsymbol{F}}^T\boldsymbol{\Gamma}\boldsymbol{K}_F\tilde{\boldsymbol{F}} \tag{3.42}$$

which is negative semi-definite. Thus, the stability is still guaranteed in spite of the imperfect gravity compensation.

3.2 Modification to the Controller to Account for the Uncertainty of Payload

Previous analysis shows that there exist position errors in the case of unknown payload. The controller is now modified to cope with the uncertainty of the payload.

3.2.1 Controller Design

To avoid leading to a different equilibrium configuration due to the uncertainty of the payload; it is proposed to add an integral-like adaptive scheme to the controller (3.25), which updates the estimate $\hat{g}_o$. Let

$$\dot{\hat{g}}_o = -K_I\boldsymbol{W}\boldsymbol{J}^{-T}\boldsymbol{K}_p\tilde{\boldsymbol{q}} \tag{3.43}$$

where K_I is a positive diagonal matrix. The equilibrium of equation (3.43) is

$$\boldsymbol{W}\boldsymbol{J}^{-T}\boldsymbol{K}_p\tilde{\boldsymbol{q}}^{ss} = 0 \tag{3.44}$$

which is the same as equation (3.29). By updating the estimate of the payload using equation (3.43); the steady-state error of the system, due to imperfect object gravity compensation, can be eliminated.

To prove the stability of the entire system given the modified controller, consider a gravity energy function $E(\boldsymbol{q}, \tilde{g}_o)$, where $\tilde{g}_o = \hat{g}_o - g_o$, such that it is positive semi-definite, $\frac{\partial E(\boldsymbol{q}, \tilde{g}_o)}{\partial \boldsymbol{q}} = -\boldsymbol{J}^T \boldsymbol{W}^{\dagger} \tilde{g}_o$, and $\frac{\partial E(\boldsymbol{q}, \tilde{g}_o)}{\partial \tilde{g}_o} = -\zeta \tilde{g}_o$, where ζ is a constant. Let the Lyapunov candidate be

$$\mathrm{V}_2 = \tfrac{1}{2}\dot{\boldsymbol{q}}^T \boldsymbol{H}_m \dot{\boldsymbol{q}} + \tfrac{1}{2}\nu^T \Lambda_o \nu + \tfrac{1}{2}\tilde{\boldsymbol{q}}^T \boldsymbol{K}_p \tilde{\boldsymbol{q}} + \tfrac{1}{2}\tilde{\boldsymbol{F}}^T \boldsymbol{\Gamma} \tilde{\boldsymbol{F}} + \tfrac{1}{2}\tilde{g}_o^T \zeta \tilde{g}_o + E(\boldsymbol{q}, \tilde{g}_o) \tag{3.45}$$

It can be easily shown that

$$\dot{\mathrm{V}}_2 = -\dot{\boldsymbol{q}}^T \boldsymbol{K}_{damp} \bar{\boldsymbol{J}}^2(\boldsymbol{q})\dot{\boldsymbol{q}} - \tilde{\boldsymbol{F}}^T \boldsymbol{\Gamma} \boldsymbol{K}_F \tilde{\boldsymbol{F}} \tag{3.46}$$

which is negative semi-definite. Thus, the stability is guaranteed for the system with the on-line payload updating scheme (3.43).

3.2.2 Simulation Studies

Numerical simulations have tested the nonlinear controller presented in Section 3.2.1. With reference to Figure 3.1, two three-degree-of-freedom manipulators (see Appendix D for single manipulator's dynamics) held an object, which was initially rested on the ground. Parameters of the robots used in simulations were chosen to closely resemble the MAGNUM 7-function hydraulic manipulators manufactured by International Submarine Engineering Ltd. (ISE), Canada, with some joints fixed. These parameters, adopted from AutoCAD drawings provided by ISE, are given in Table 3.1 and Table 3.2. Each actuator has the same parameters, with the exception of a different stroke. The load distribution between the two robots needs to be even, as defined by $\alpha^1 = \alpha^2 = 0.5$. The controller gains were chosen as $K_{p,j}^i = 8\mathrm{Nm}$, $\Gamma_j^i = 0.01\mathrm{mN}^{-1}$, $K_{F,j}^i = 40\ \mathrm{s}^{-1}$, and $K_{I,j}^i = 5\mathrm{s}^{-1}$.

Table 3.1: Link parameters.

Link	Length (m)	Mass (kg)	Inertia ($\mathrm{kg\,m^2}$)	Range
1	0.537	22.5	0.5407	$90°$
2	0.336	15.7	0.1477	$130°$
3	0.606	22.5	0.6886	$115°$

Table 3.2: Hydraulic actuator parameters.

Parameter	Symbol	Value
Pump pressure	P_s	6.895 MPa
Exit(tank) pressure	P_e	0 MPa
Valve constant	$K^i_{sp,j}$	4.064×10^{-5} m/V
Orifice area gradient	w^i_j	1.01×10^{-2} m
Flow gain	$K^i_j = C_d w^i_j \sqrt{\dfrac{2}{\rho}}$	$2.94415\times10^{-4}\sqrt{\dfrac{\mathrm{m}^5}{\mathrm{kg}}}$
Bulk modulus of the hydraulic fluid	β^i_j	689 MPa
Piston area (blind side)	$A^i_{I,j}$	3.167×10^{-3} m^2
Piston area (rod side)	$A^i_{O,j}$	2.6603×10^{-3} m^2
Stroke of cylinder 1	l_{stroke1}	0.26416 m
Stroke of cylinder 2	l_{stroke2}	0.15875 m
Stroke of cylinder 3	l_{stroke3}	0.1016 m
Initial fluid volume (blind side)	$\bar{V}^i_{I,j}$	2.14×10^{-5} m^3
Initial fluid volume (rod side), cylinder 1	$\bar{V}^i_{o,1}$	72.4144×10^{-5} m^3
Initial fluid volume (rod side), cylinder 2	$\bar{V}^i_{o,2}$	44.37×10^{-5} m^3
Initial fluid volume (rod side), cylinder 3	$\bar{V}^i_{o,3}$	29.17×10^{-5} m^3

As shown in Figure 3.1, a payload of 80 kg sat on the ground with both robots holding it rigidly. At this point, the loads experienced by the robots were only due to their own arms. A command was given to the robots to lift the object 0.2-meter above the ground, while maintaining a horizontal internal force of zero on the payload. At the moment the command was issued, the object weight was unknown and estimated as zero.

Figure 3.2 shows that the object was moved to the desired position. Control signals to the actuators for one of the manipulators are shown in Figure 3.3. Control signals for the other manipulator were very much the same and are therefore not shown here. Note that the control signals at the beginning of the task were small. This was due to the object's weight being estimated as zero at the beginning of the task. The controller initially produced small signals. As the true value of the load was identified, the controller adjusted its signals to compensate for the load. The lifting forces by the two manipulators were almost the same, as shown in Figure 3.4. The estimate of the object's weight went from zero (the initial estimate) to the actual value, as shown in Figure 3.5. Figure 3.6 shows that the desired internal force was maintained during the steady state, with little change during the transient period. For simplicity, Figure 3.7 only shows the line pressures in actuator 1 of the first manipulator.

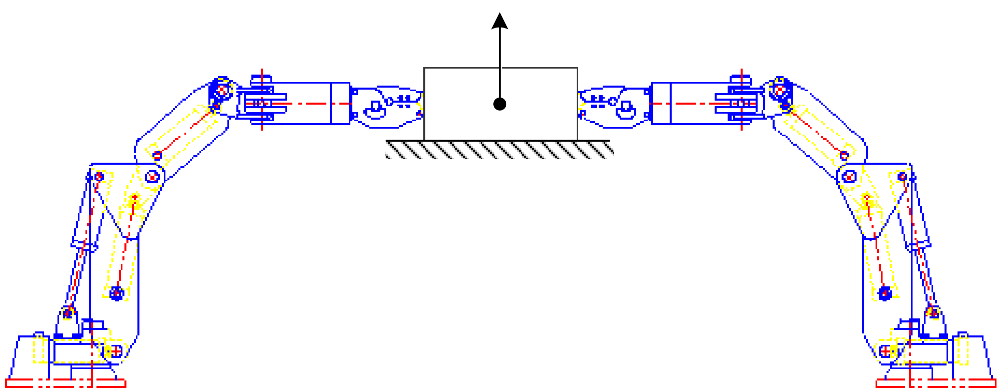

Figure 3.1: Two planar hydraulic robots co-operatively lift an object sitting on the ground.

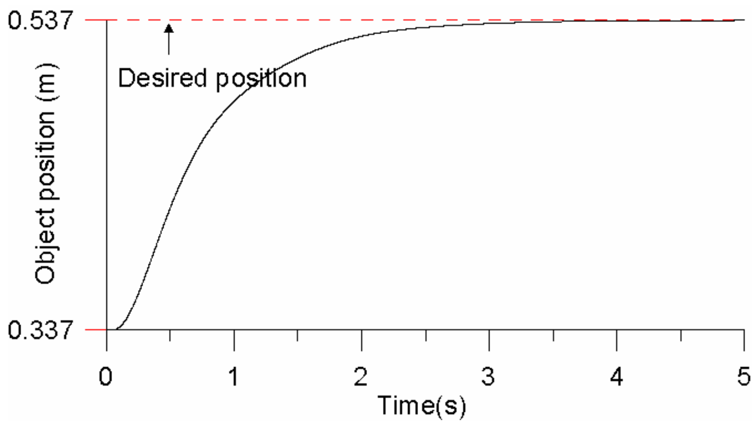

Figure 3.2: Position trajectory of the object.

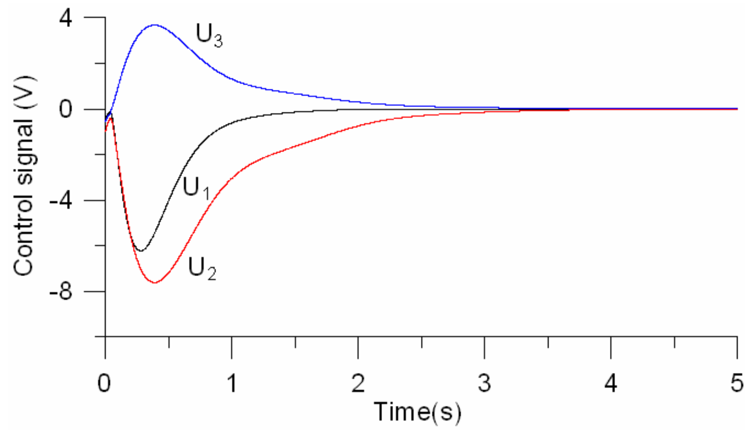

Figure 3.3: Control signals for the first manipulator.

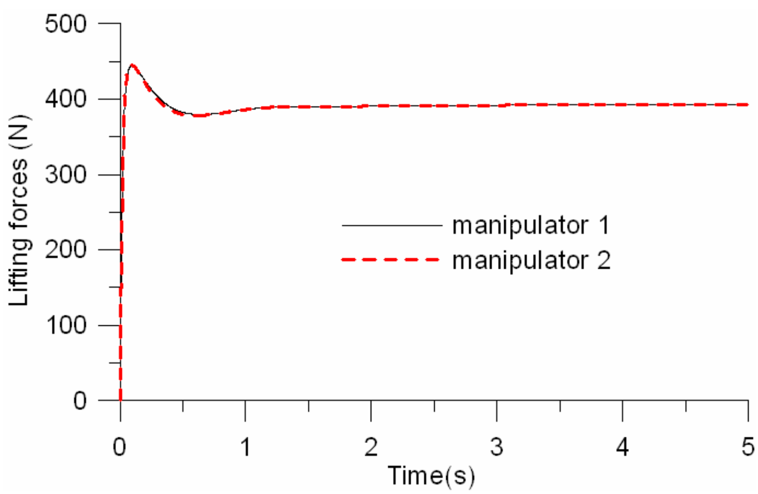

Figure 3.4: Load sharing between two manipulators.

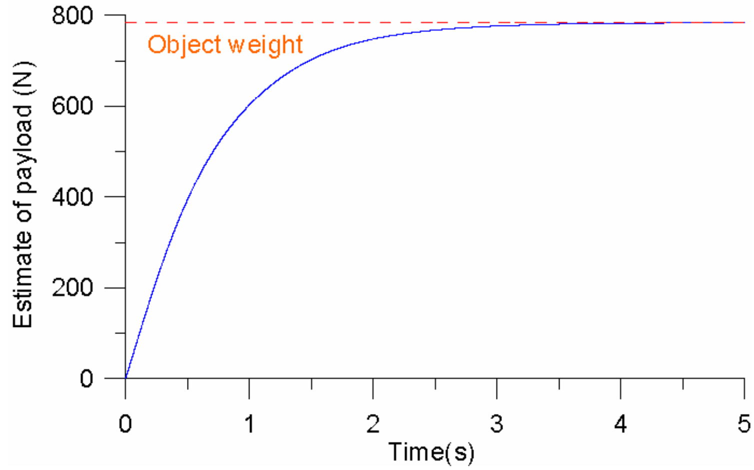

Figure 3.5: Estimation of the payload.

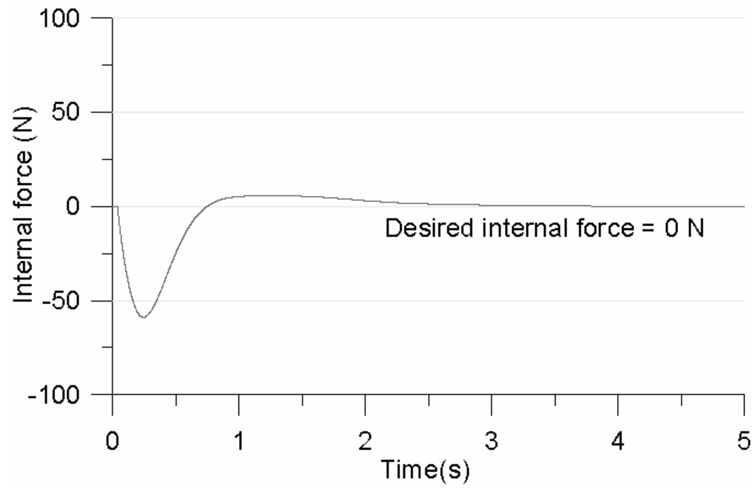

Figure 3.6: Horizontal internal force exerted on the object by two manipulators.

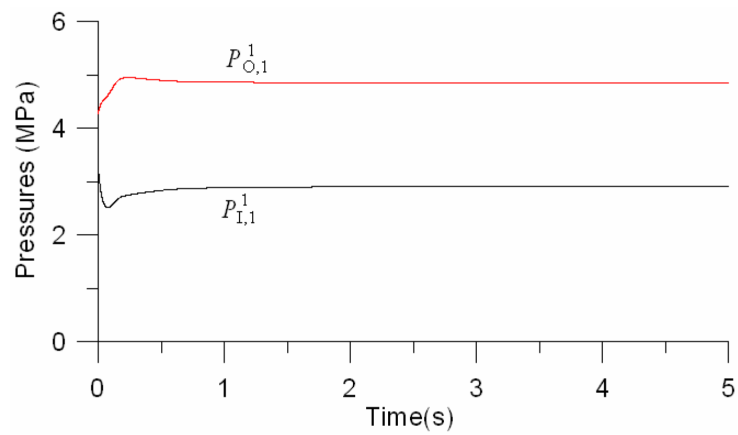

Figure 3.7: Chamber pressures in link 1 actuator of one of the manipulators.

The above simulation was repeated with an uneven load distribution, described by $\alpha^1 = 2/3$, $\alpha^2 = 1/3$. The response, such as tracking error and internal force, did not change significantly as shown in Figure 3.8 and 3.9 respectively. The control signals for the manipulators shown in Figures 3.10 and 3.11 were different from each other. Consequently, Figure 3.12 shows that lifting forces were not evenly distributed between the two manipulators; the first manipulator contributed more to the lift and hold of the object. During the steady-state phase, the lifting forces were 523N and 261N; therefore the ratio is equal to α^1/α^2. This shows that the load distribution was completely manageable by the load distribution scheme.

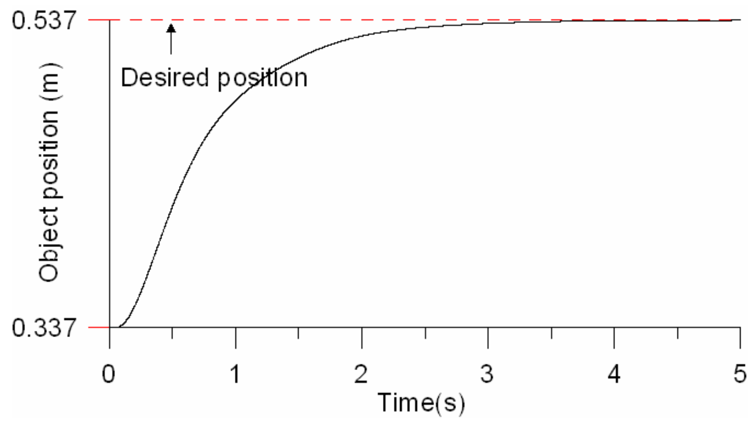

Figure 3.8: Position trajectory of the object (uneven load distribution).

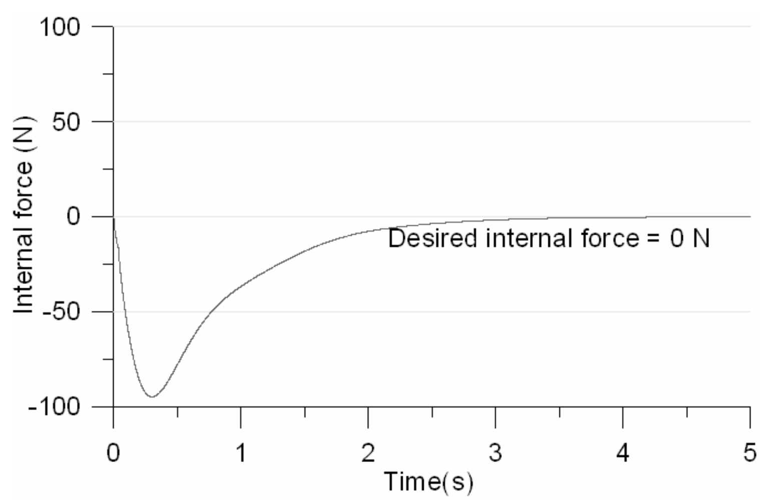

Figure 3.9: Horizontal internal force exerted on the object by two manipulators.

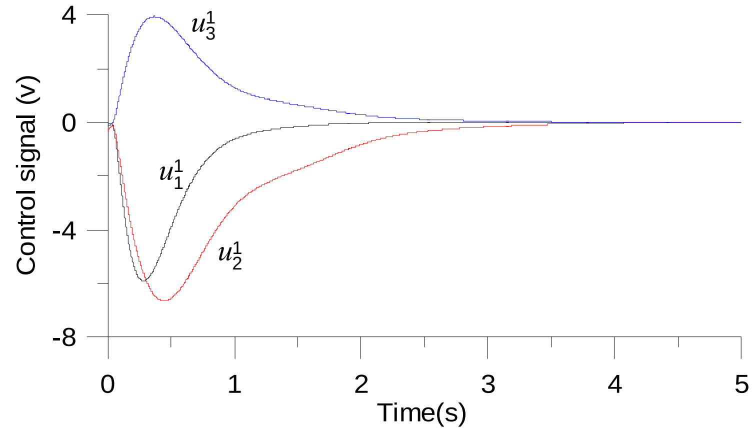

Figure 3.10: Control signals for the first manipulator.

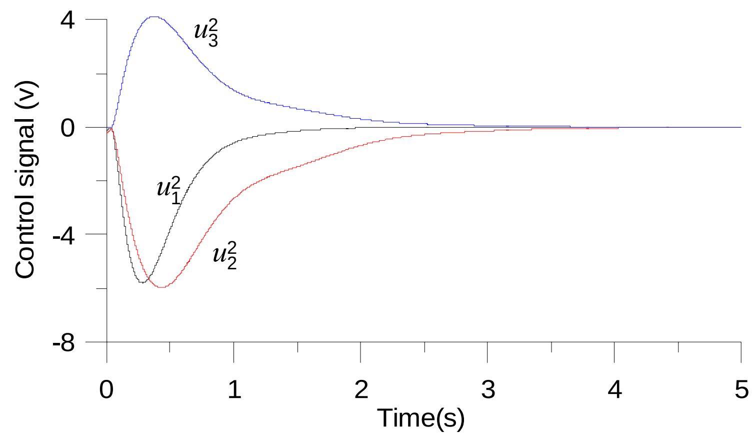

Figure 3.11: Control signals for the second manipulator.

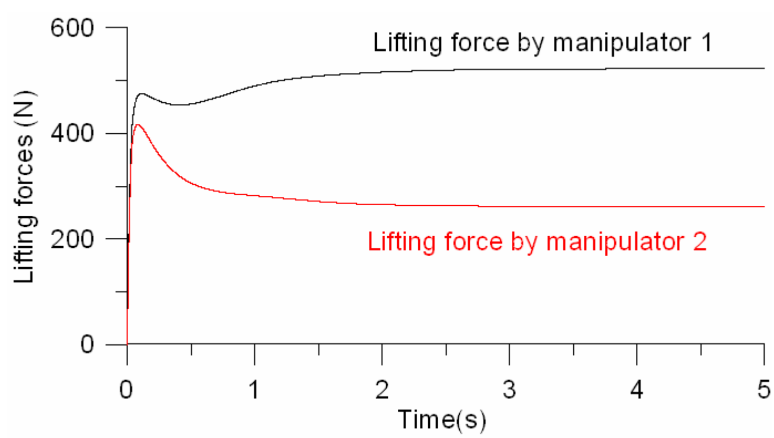

Figure 3.12: Load distribution between two manipulators.

The last simulation was about the system response over a series of step inputs as shown in Figure 3.13. The same control gains as in the first simulation study were used; and the payload was initially estimated as zero. As can be seen, the controller performed well over the entire workspace. Note that following the first step input, the object stayed at desired position and the payload was estimated properly. Thus, for the subsequent steps the gain of the adaptive scheme (3.43) was reduced to $K_{I,j}^{i} = 0.1$ s^{-1}.

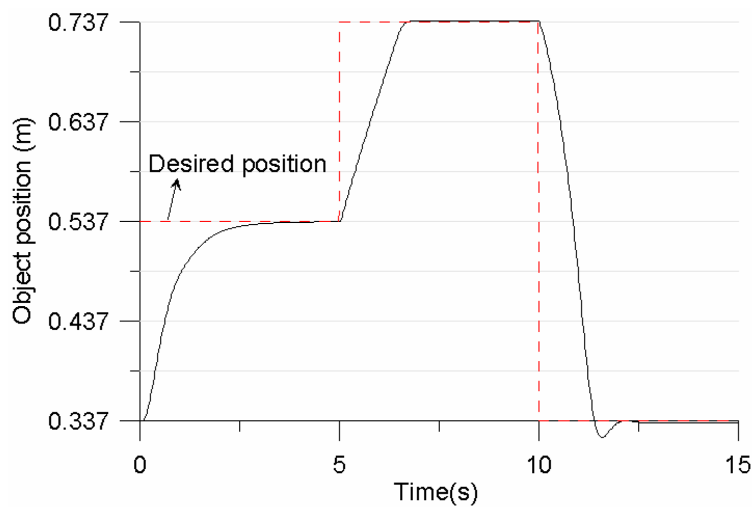

Figure 3.13: Position trajectory of the object given a series of step inputs.

3.3 Design of a General Controller to Account for the Uncertainty of Payload, Robot Dynamic Parameters and Hydraulic Functions

The controller developed in Section 3.1 is now further investigated in the case where gravity terms g_o and $\boldsymbol{G}_m(\boldsymbol{q})$ for the payload and manipulators respectively, are unknown. The desired forces needed by actuators given in equation (3.12) then become

$$\boldsymbol{F}^d = \overline{\boldsymbol{J}}^{-1}(-\boldsymbol{J}^T\boldsymbol{W}^{\dagger}\boldsymbol{W}\boldsymbol{J}^{-T}\boldsymbol{K}_p\tilde{\boldsymbol{q}} + \hat{\boldsymbol{G}}_m(\boldsymbol{q}) + \boldsymbol{J}^T\boldsymbol{W}^{\dagger}\hat{g}_o + \boldsymbol{J}^T\boldsymbol{V}F_{\text{int}}^d) \tag{3.47}$$

where, $\hat{\boldsymbol{G}}(\boldsymbol{q})$ is a rough estimate of the gravity term $\boldsymbol{G}(\boldsymbol{q})$. The equilibrium of the system under the controller (3.25) and (3.47), will then be

$$\boldsymbol{U}^{ss} = 0 \tag{3.48}$$

$$\boldsymbol{W}\boldsymbol{J}^{-T}\boldsymbol{K}_p\tilde{\boldsymbol{q}} = \hat{g}_o - g_o + \boldsymbol{W}\boldsymbol{J}^{-T}(\hat{\boldsymbol{G}}_m(\boldsymbol{q}) - \boldsymbol{G}_m(\boldsymbol{q})) \tag{3.49}$$

$$\boldsymbol{F}_c^{ss} = (I - \boldsymbol{W}^{\dagger}\boldsymbol{W})\boldsymbol{J}^{-T}(\hat{\boldsymbol{G}}_m(\boldsymbol{q}) - \boldsymbol{G}_m(\boldsymbol{q})) + \boldsymbol{W}^{\dagger} g_o + \boldsymbol{V}F_{\text{int}}^d \tag{3.50}$$

$$\boldsymbol{V}F_{\text{int}}^{ss} = \boldsymbol{F}_c^{ss} - \boldsymbol{W}^{\dagger}\boldsymbol{W}\boldsymbol{F}_c^{ss} = (I - \boldsymbol{W}^{\dagger}\boldsymbol{W})\boldsymbol{J}^{-T}(\hat{\boldsymbol{G}}_m(\boldsymbol{q}) - \boldsymbol{G}_m(\boldsymbol{q})) + \boldsymbol{V}F_{\text{int}}^d \tag{3.51}$$

Equation (3.49) shows its right-hand side becomes nonzero due to inaccurate compensation of the object gravity term or the manipulators' gravity term. This leads to a set of different equilibrium configurations from those obtained via equation (3.29) or (3.37), and the desired position can not be achieved. In the case of imperfect compensation of the manipulators' gravity term, the equilibrium does not yield desired internal force at steady state.

With respect to stability, considering a gravity energy function, $E(\boldsymbol{q})$, such that it is positive semi-definite and $\dfrac{\partial E(\boldsymbol{q})}{\partial \boldsymbol{q}} = \boldsymbol{J}^T\boldsymbol{W}^{\dagger}(g_o - \hat{g}_o) + (\boldsymbol{G}_m(\boldsymbol{q}) - \hat{\boldsymbol{G}}_m(\boldsymbol{q}))$, let the Lyapunov candidate be

$$\mathrm{V}_2 = \tfrac{1}{2}\dot{\boldsymbol{q}}^T\boldsymbol{H}_m\dot{\boldsymbol{q}} + \tfrac{1}{2}v^T\Lambda_o v + \tfrac{1}{2}\tilde{\boldsymbol{q}}^T\boldsymbol{K}_p\tilde{\boldsymbol{q}} + \tfrac{1}{2}\tilde{\boldsymbol{F}}^T\boldsymbol{\Gamma}\tilde{\boldsymbol{F}} + E(\boldsymbol{q}) \tag{3.52}$$

It can be easily shown that

$$\dot{\mathrm{V}}_2 = -\dot{\boldsymbol{q}}^T\boldsymbol{K}_{damp}\bar{\boldsymbol{J}}^2(\boldsymbol{q})\dot{\boldsymbol{q}} - \tilde{\boldsymbol{F}}^T\boldsymbol{\Gamma}\boldsymbol{K}_F\tilde{\boldsymbol{F}} \tag{3.53}$$

which is negative semi-definite. Thus, the stability is still guaranteed in spite of the imperfect gravity compensation of both the payload and the robots.

3.3.1 Controller Design

The above analysis concludes that position regulation could not be achieved if either the object's or the manipulators' gravity term is not accurately compensated. As for the regulation of internal force, it could not be achieved only because of unknown manipulators' gravity term. To avoid these undesirable performances, adaptation laws are introduced to estimate both unknown payload and manipulators' gravity term, and internal force feedback is also added to help achieve desired internal force. In addition, uncertainties from hydraulic functions are considered in this section.

To replace the terms related with parameters from hydraulic functions, manipulators, and the object required in the previous controller with their estimates, the controller is suggested to be

$$\boldsymbol{U} = \hat{\boldsymbol{A}}_{cq}^{-1}(\boldsymbol{q})(\hat{\boldsymbol{A}}_{ca}(\boldsymbol{q},\dot{\boldsymbol{q}}) - \boldsymbol{\Gamma}^{-1}\overline{\boldsymbol{J}}(\boldsymbol{q})\dot{\boldsymbol{q}} + \dot{\boldsymbol{F}}^{d} - \boldsymbol{K}_{F}\widetilde{\boldsymbol{F}}) \tag{3.54}$$

where

$$\boldsymbol{F}^{d} = \overline{\boldsymbol{J}}^{-1}(-\boldsymbol{J}^{T}\boldsymbol{W}^{\dagger}\boldsymbol{W}\boldsymbol{J}^{-T}\boldsymbol{K}_{p}\widetilde{\boldsymbol{q}} + \hat{\boldsymbol{G}}_{E} + \boldsymbol{J}^{T}\boldsymbol{V}F_{\text{int}}^{d} - \boldsymbol{J}^{T}\boldsymbol{V}K_{\text{int}}(F_{\text{int}} - F_{\text{int}}^{d})) \tag{3.55}$$

Note that vector $\hat{\boldsymbol{G}}_{E}$ is the estimate of the combined gravity term $\boldsymbol{G}_{m}(\boldsymbol{q}) + \boldsymbol{J}^{T}\boldsymbol{W}^{\dagger}g_{o}$, instead of estimation of $\boldsymbol{G}_{m}(\boldsymbol{q})$ and g_{o} separately. K_{int} is a control gain. Vector $\hat{\varphi}$ is the estimate of unknown hydraulic parameters, φ. Matrix $\hat{\boldsymbol{A}}_{cq}^{-1}(\boldsymbol{q})$ and vector $\hat{\boldsymbol{A}}_{ca}(\boldsymbol{q},\dot{\boldsymbol{q}})$ are calculated using $\hat{\varphi}$. Vectors $\hat{\boldsymbol{G}}_{E}$ and $\hat{\varphi}$ are updated by following laws

$$\dot{\hat{\boldsymbol{G}}}_{E} = -\boldsymbol{K}_{I}\boldsymbol{K}_{p}\widetilde{\boldsymbol{q}} \tag{3.56}$$

$$\dot{\hat{\varphi}} = \boldsymbol{\Gamma}_{\varphi}^{-1}\Phi^{T}(\boldsymbol{q},\dot{\boldsymbol{q}},\boldsymbol{U})\boldsymbol{\Gamma}_{F}\widetilde{\boldsymbol{F}} \tag{3.57}$$

To prove the stability of the entire system given the modified controller above, consider a gravity energy function, $E(\boldsymbol{q},\widetilde{\boldsymbol{G}}_{E})$, where $\widetilde{\boldsymbol{G}}_{E} = \hat{\boldsymbol{G}}_{E} - (\boldsymbol{G}_{m}(\boldsymbol{q}) + \boldsymbol{J}^{T}\boldsymbol{W}^{\dagger}g_{o})$, such that it is positive semi-definite, $\dfrac{\partial E(\boldsymbol{q},\widetilde{\boldsymbol{G}}_{E})}{\partial \boldsymbol{q}} = -\widetilde{\boldsymbol{G}}_{E}$, and $\dfrac{\partial E(\boldsymbol{q},\widetilde{\boldsymbol{G}}_{E})}{\partial \widetilde{\boldsymbol{G}}_{E}} = -\zeta\widetilde{\boldsymbol{G}}_{E}$, where ζ is a positive constant. Define $\widetilde{\varphi} = \hat{\varphi} - \varphi$. Let the Lyapunov candidate be

$$\mathrm{V}_{2} = \tfrac{1}{2}\dot{\boldsymbol{q}}^{T}\boldsymbol{H}_{m}\dot{\boldsymbol{q}} + \tfrac{1}{2}v^{T}\Lambda_{o}v + \tfrac{1}{2}\widetilde{\boldsymbol{q}}^{T}\boldsymbol{K}_{p}\widetilde{\boldsymbol{q}} + \tfrac{1}{2}\widetilde{\boldsymbol{F}}^{T}\boldsymbol{\Gamma}_{F}\widetilde{\boldsymbol{F}} + \tfrac{1}{2}\widetilde{\boldsymbol{G}}_{E}^{T}\zeta\widetilde{\boldsymbol{G}}_{E} + E(\boldsymbol{q},\widetilde{\boldsymbol{G}}_{E}) + \tfrac{1}{2}\widetilde{\varphi}^{T}\boldsymbol{\Gamma}_{\varphi}\widetilde{\varphi} \tag{3.58}$$

then

$$\dot{\mathrm{V}}_{2} = -\dot{\boldsymbol{q}}^{T}\boldsymbol{K}_{damp}\overline{\boldsymbol{J}}^{2}(\boldsymbol{q})\dot{\boldsymbol{q}} + \widetilde{\boldsymbol{F}}^{T}\overline{\boldsymbol{J}}(\boldsymbol{q})\dot{\boldsymbol{q}} + \widetilde{\boldsymbol{F}}^{T}\boldsymbol{\Gamma}_{F}(\dot{\boldsymbol{F}} - \dot{\boldsymbol{F}}^{d}) + \widetilde{\varphi}^{T}\boldsymbol{\Gamma}_{\varphi}\dot{\widetilde{\varphi}} \tag{3.59}$$

Since

$$\dot{\boldsymbol{F}} = \Phi(\boldsymbol{q},\dot{\boldsymbol{q}},\boldsymbol{U})(\hat{\varphi} - \widetilde{\varphi}) = \hat{\boldsymbol{A}}_{cq}(\boldsymbol{q})\boldsymbol{U} - \hat{\boldsymbol{A}}_{ca}(\boldsymbol{q},\dot{\boldsymbol{q}}) - \Phi(\boldsymbol{q},\dot{\boldsymbol{q}},\boldsymbol{U})\widetilde{\varphi} \tag{3.60}$$

with the controller (3.54) and the adaptation law (3.57), it can be easily shown that

$$\dot{\mathrm{V}}_{2} = -\dot{\boldsymbol{q}}^{T}\boldsymbol{K}_{damp}\overline{\boldsymbol{J}}^{2}(\boldsymbol{q})\dot{\boldsymbol{q}} - \widetilde{\boldsymbol{F}}^{T}\boldsymbol{\Gamma}\boldsymbol{K}_{F}\widetilde{\boldsymbol{F}} \tag{3.61}$$

which is negative semi-definite. Thus, the stability is guaranteed for the system with the controller expressed in equation (3.54).

The equilibrium of the system will then be

$$\boldsymbol{U}^{ss} = 0 \tag{3.62}$$

$$\tilde{\boldsymbol{q}} = 0 \tag{3.63}$$

$$\boldsymbol{W}\boldsymbol{J}^{-T}(\hat{\boldsymbol{G}}_E - (\boldsymbol{G}_m(\boldsymbol{q}) + \boldsymbol{J}^T\boldsymbol{W}^{\dagger}g_o)) = 0 \tag{3.64}$$

$$\boldsymbol{V}F_{\text{int}} = (\boldsymbol{I} + K_{\text{int}})^{-1}\boldsymbol{J}^{-T}(\hat{\boldsymbol{G}}_E - (\boldsymbol{G}_m(\boldsymbol{q}) + \boldsymbol{J}^T\boldsymbol{W}^{\dagger}g_o)) + \boldsymbol{V}F_{\text{int}}^d \tag{3.65}$$

Equation (3.64) implies that the external forces due to the errors of gravity compensation are zero. However, it does not guarantee $\hat{\boldsymbol{G}}_E - (\boldsymbol{G}_m(\boldsymbol{q}) + \boldsymbol{J}^T\boldsymbol{W}^{\dagger}g_o) = 0$. In other words, $\hat{\boldsymbol{G}}_E$, the estimate of the gravity term $(\boldsymbol{G}_m(\boldsymbol{q}) + \boldsymbol{J}^T\boldsymbol{W}^{\dagger}g_o)$, does not have to converge to its actual value. The desired internal force cannot be achieved at steady state by inspection of equation (3.65). Nevertheless, the internal force can be controlled through gain K_{int}. Increasing the value of K_{int} can impose the actual internal force more approximate to its desired value.

In the implementation of equation (3.55) associated with the controller (3.54), the derivative of the internal force is difficult to obtain and is calculated using numerical differentiation; or can be neglected if the variation of internal force is slow.

3.3.2 Simulation Studies

Numerical simulations on the same system that was used in Section 3.2.2 have tested the nonlinear controller presented in Section 3.3.1. The desired internal force was set to zero, i.e., $F_{\text{int}}^d = 0$. The controller gains were chosen as $K_{p,j}^i = 12\text{Nm}$, $\Gamma_j^i = 0.01\text{mN}^{-1}$, $K_{F,j}^i = 40\ \text{s}^{-1}$, $K_{I,j}^i = 2\ \text{s}^{-1}$, and $K_{\text{int}} = 0$. As shown in Figure 3.1, a payload of 80 kg sat on the ground with both robots holding it rigidly. The command was given to the robots to lift the object, 0.2-meter above the ground, while maintaining a horizontal internal force of zero on the payload. At the moment the command was issued, the combined gravity term from both the payload and the robots was unknown and estimated as zero. The vector of the unknown hydraulic function parameters $\varphi = (\beta_1^1 K_1^1 K_{sp,1}^1, \beta_1^1, \ldots, \beta_j^i K_j^i K_{sp,j}^i, \beta_j^i, \ldots)_{i=1,2;j=1,2,3}^T$, were also estimated online using half of their actual values, initially. Figure 3.14 shows that the object was moved to the desired position. The control signals to the actuators for one of the robots are shown in Figure 3.15, which is different from the one (Figure 3.3) in Section 3.2. Figure 3.16 shows that the actual internal force was not exactly the same as the desired value during the steady-state phase, as expected by the theoretical analysis in Section 3.3.1. The difference is about 10 N.

Estimates of unknown hydraulic function parameters are shown in Figure 3.17. The simulation results show that the external forces due to the errors of gravity compensation are zero i.e. $\boldsymbol{W}\boldsymbol{J}^{-T}(\hat{\boldsymbol{G}}_E - (\boldsymbol{G}_m(\boldsymbol{q}) + \boldsymbol{J}^T\boldsymbol{W}^{\dagger}g_o)) = 0$ at the steady-state phase, as can be seen in Figure 3.18 where the second component is along the gravity direction. This agrees with the theoretical analysis in Section 3.3.1.

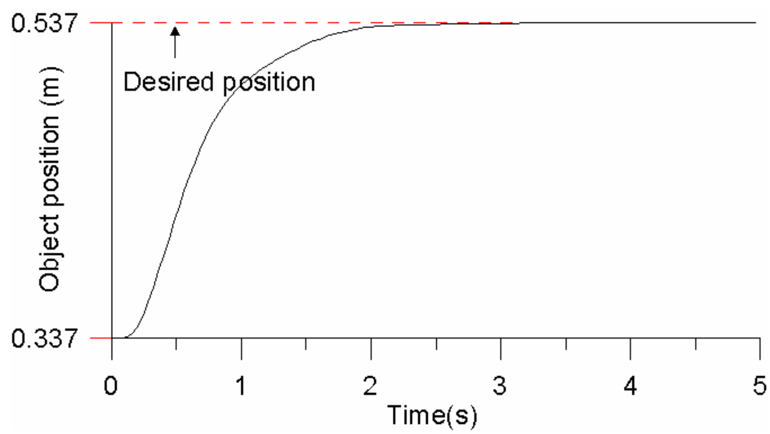

Figure 3.14: Position trajectory of the object.

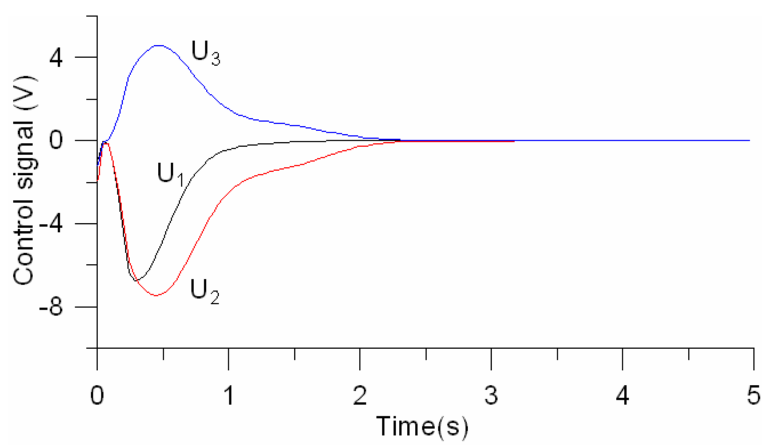

Figure 3.15: Control signals for the first manipulator.

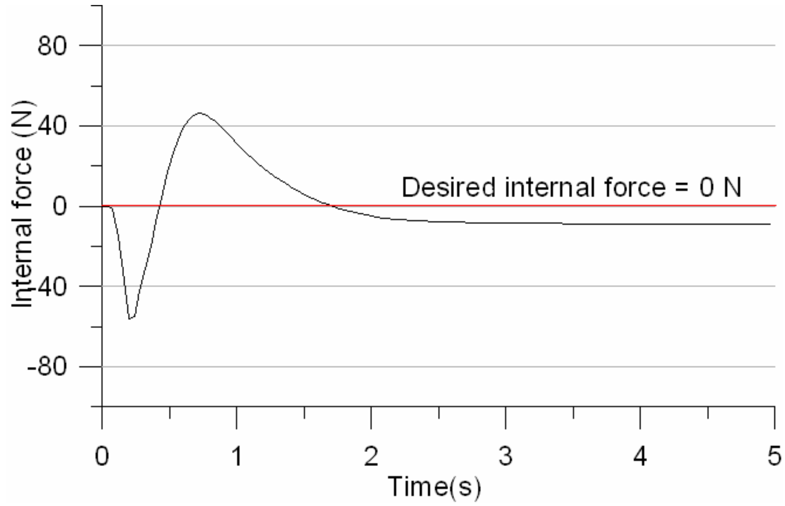

Figure 3.16: Horizontal internal force exerted on the object by two manipulators.

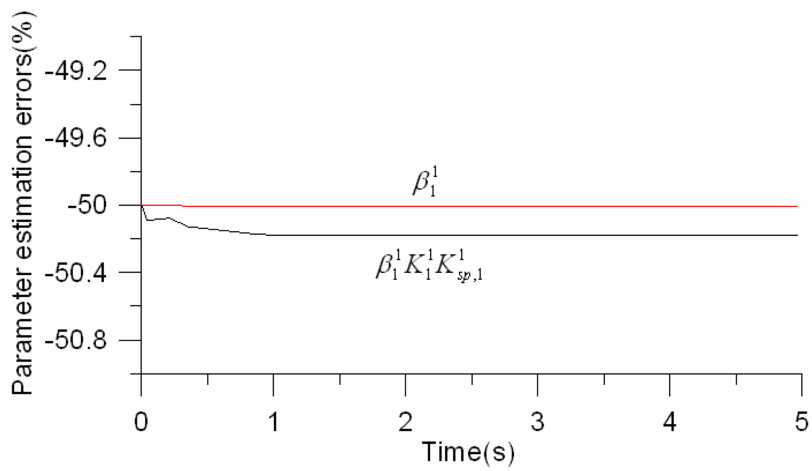

Figure 3.17: Typical hydraulic function parameter estimation errors.

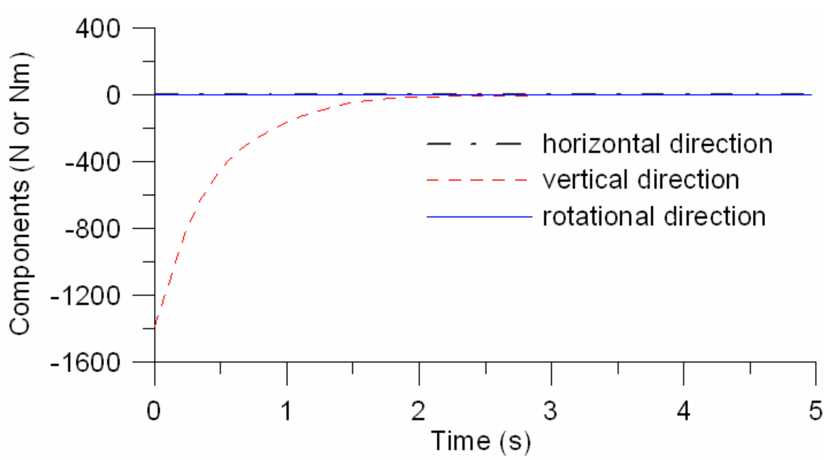

Figure 3.18: Components of the vector $WJ^{-T}(\hat{G}_E - (G_m(q) + J^T W^{\dagger} g_o))$ in Cartesian reference frame $\{X_R, Y_R, Z_R\}$.

3.4 Summary

This chapter documented design, stability analysis and numerical verification of position controllers for the problem of point-to-point regulation of a payload manipulated by several hydraulic robots. The highly nonlinear hydraulic actuator dynamics were incorporated in the Lyapunov-based controller design. Issues of motion, internal force control of the object and load sharing were addressed. The equilibrium of the system under the proposed controller was investigated leading to a set of equilibrium points corresponding to given internal forces. The issue of unknown payload was also analyzed and the controller was modified to eliminate the steady-state error due to imperfect compensation. Simulation results validated the efficacy of the proposed nonlinear controller. The controller was extended to the case where gravity terms of both the payload and the robots, as well as the parameters of hydraulic functions were unknown. Inspection of the new control system's equilibrium found that the desired internal force might not converge to the desired value. The introduction of force feedback control reduced internal force error.

The first controller is easier to implement but requires knowledge about the gravity terms for the payload and the manipulators, as well as the hydraulic function parameters. The second controller is suitable for the scenario in which only the payload is unknown. The third controller is designed for a general case where all the parameters including the gravity terms from the payload and manipulators, as well as the hydraulic function parameters are unknown.

Chapter 4 Tracking Control of Co-operating Hydraulic Manipulators

In this chapter, a scheme is developed for tracking control of multiple hydraulic manipulators handling a rigid object without relative motion between the object and the grippers. The goal is to design a controller that allows two or more hydraulic robots to coordinately track an object's position/orientation while maintaining a desired internal force on the object. The issues of load sharing between the hydraulic robots, unknown payload and uncertainty on the manipulators' dynamics as well as hydraulic functions are also addressed. Similar to the regulating controller design in the Chapter 3, friction is not yet considered for simplicity in this chapter. An on-line updating law to compensate for parametric uncertainties augments the controller.

It is assumed that the unknown parameters are constants or that they vary slowly with time due to temperature, wear, humidity etc. That is to say, their time derivatives can be treated as zero. An acceleration observer is also developed for the co-operating control system to avoid the requirement of acceleration feedback, which could be difficult to measure or determine in practice. As in Chapter 3, the backstepping technique is implemented during the adaptive controller design. The position tracking error is proven to converge to zero while internal force error is bounded and can be reduced by introducing a force feedback loop. Results from simulations, which are performed on two co-operative hydraulic manipulators, are provided to demonstrate the effectiveness of the proposed control law.

4.1 Controller Design

The following variables are defined first and used in the design of the controller.

$$e = X - X^d \tag{4.1}$$

$$\tilde{X} = X - \hat{X} \tag{4.2}$$

$$\dot{X}_r = \dot{X}^d - \lambda_1(\hat{X} - X^d) = \dot{X}^d - \lambda_1(e - \tilde{X}) \tag{4.3}$$

$$\dot{X}_o = \dot{\hat{X}} - \lambda_2(X - \hat{X}) = \dot{\hat{X}} - \lambda_2\tilde{X} \tag{4.4}$$

$$s_1 = \dot{X} - \dot{X}_r = \dot{e} + \lambda_1 (e - \widetilde{X}) \tag{4.5}$$

$$s_2 = \dot{X} - \dot{X}_o = \dot{\widetilde{X}} + \lambda_2 \widetilde{X} \tag{4.6}$$

where X^d and $\hat{X}$ are the desired and estimated values of X, respectively. λ_1 and λ_2 are diagonal positive definite matrices. It is assumed that X^d belongs to C^3 (a function with k continuous derivatives is called a C^k function (Rowland, 2006 and Husch, 2001)).

The controller is proposed as a proposition as below. That means the controller is presented first followed by stability analysis. In practice, however, the controller is obtained from constructing a Lyapunov-like scalar function and finding its time derivative. Although the backstepping technique has been implemented, trial and error method is sometime necessary to find a proper controller that theoretically guarantees the system's stability. This methodology is also applied to develop the controllers in the followed chapters.

Proposition:

Consider the system described by equations (2.39) and (2.47), without the friction term $\boldsymbol{F}_{fr}$. Given the following acceleration observer:

$$\ddot{\hat{X}} = \hat{M}^{-1}[T - \hat{D}(X,\dot{X})\dot{X}_o - \hat{G}(X) + L_p \widetilde{X} + K_d s_1 + K_d^{'} s_2] + \lambda_2 \dot{\widetilde{X}} \tag{4.7}$$

and the controller:

$$\boldsymbol{U} = \hat{\boldsymbol{A}}_{cq}^{-1}(\boldsymbol{q})\left(\hat{\boldsymbol{A}}_{ca}(\boldsymbol{q},\dot{\boldsymbol{q}}) + \dot{\boldsymbol{F}}^d - \Gamma_F^{-1} \overline{\boldsymbol{J}}^T \boldsymbol{J}^{-1} \boldsymbol{W}^T E s_1 - K_F \widetilde{\boldsymbol{F}}\right) \tag{4.8}$$

where

$$\widetilde{\boldsymbol{F}} = \boldsymbol{F} - \boldsymbol{F}^d \tag{4.9}$$

$$\boldsymbol{F}^d = \overline{\boldsymbol{J}}^{-1} \boldsymbol{J}^T (\boldsymbol{W}^{\dagger} E^{-T} T^d + \boldsymbol{V} F_{\text{int}}^d) \tag{4.10}$$

$$T^d = \hat{M}(X)\ddot{X}_r + \hat{D}(X,\dot{X}_r)\dot{X}_r + \hat{G}(X) - K_d(s_1 - s_2) - K_p e \tag{4.11}$$

with the following adaptation law for manipulators-object parameters:

$$\dot{\hat{\theta}} = -\Gamma_\theta^{-1}[\Theta_1^T(X,\dot{X}_r,\ddot{X}_r)s_1 + \Theta_2^T(X,\dot{X},\dot{X}_o,\ddot{X}_o)s_2] \tag{4.12}$$

where

$$\Theta_1(X,\dot{X}_r,\ddot{X}_r)\hat{\theta} = \hat{M}(X)\ddot{X}_r + \hat{D}(X,\dot{X}_r)\dot{X}_r + \hat{G}(X) \tag{4.13}$$

$$\Theta_2(X,\dot{X},\dot{X}_o,\ddot{X}_o)\hat{\theta} = \hat{M}(X)\ddot{X}_o + \hat{D}(X,\dot{X})\dot{X}_o + \hat{G}(X) \tag{4.14}$$

as well as the following hydraulic parameters adaptation law:

$$\dot{\hat{\varphi}} = \Gamma_{\varphi}^{-1}\boldsymbol{\Phi}^{T}(\boldsymbol{q},\dot{\boldsymbol{q}},\boldsymbol{U})\Gamma_{F}\widetilde{\boldsymbol{F}} \tag{4.15}$$

where $\hat{\theta}$ and $\hat{\varphi}$ are the estimates of θ and φ, respectively. $\hat{M},\hat{D},\hat{G}$ are estimates of the dynamic matrices M,D,G, associated with $\hat{\theta}$. $\hat{\boldsymbol{A}}_{ca}$ and $\hat{\boldsymbol{A}}_{cq}$ are the estimated vector and matrix associated with $\hat{\varphi}$. $K_p, L_p, K_d, K_d^{'}, \Gamma_F, K_F, \Gamma_{\varphi}$, and Γ_{θ} are constant positive definite diagonal matrices. F_{int}^{d} is the desired internal force.

Providing the following conditions are satisfied

$$2\sqrt{\underline{\sigma}(\lambda_1 K_p)}\sqrt{\underline{\sigma}(\lambda_2 L_p)} > \overline{\sigma}(\lambda_1 K_p) \tag{4.16}$$

$$\|r(0)\| \le \sqrt{\frac{\alpha_L}{2\alpha_U}\left[\frac{\underline{\sigma}(K_d) - D_U \dot{X}_U^d}{D_U \overline{\sigma}(\lambda_1)}\right]^2 + \frac{V_{pL} - V_{pU}}{\alpha_U}} \tag{4.17}$$

with $r(t) = (e^T \ \widetilde{X}^T \ s_1^T \ s_2^T \ \widetilde{\boldsymbol{F}}^T)^T$, then $r(t)$ is bounded and converges to zero as $t \to \infty$.

In equations (4.16) and (4.17), $\underline{\sigma}$ (.) and $\overline{\sigma}$ (.) are the minimum and maximum singular values of their matrix argument, respectively; $\dot{X}_U^d$ is the upper bound on the norm of $\dot{X}^d$; Scalars $\alpha_L, \alpha_U, V_{pL}$, and V_{pU} are positive constants defined as follows:

$$\alpha_L \|r\|^2 \le \tfrac{1}{2} s_1^T M(X) s_1 + \tfrac{1}{2} s_2^T M(x) s_2 + \tfrac{1}{2} e^T K_p e + \tfrac{1}{2} \widetilde{X}^T L_p \widetilde{X} + \tfrac{1}{2} \widetilde{\boldsymbol{F}}^T \Gamma_F \widetilde{\boldsymbol{F}} \le \alpha_U \|r\|^2 \tag{4.18}$$

$$V_{pL} \le \tfrac{1}{2} \widetilde{\theta}^T \Gamma_{\theta} \widetilde{\theta} + \tfrac{1}{2} \widetilde{\varphi}^T \Gamma_{\varphi} \widetilde{\varphi} \le V_{pU}\,. \tag{4.19}$$

where $\widetilde{\theta} = \hat{\theta} - \theta$, $\widetilde{\varphi} = \hat{\varphi} - \varphi$.

Proof:

Consider a scalar function:

$$\mathrm{V}_1 = \tfrac{1}{2} s_1^T M(X) s_1 + \tfrac{1}{2} s_2^T M(x) s_2 + \tfrac{1}{2} e^T K_p e + \tfrac{1}{2} \widetilde{X}^T L_p \widetilde{X} + \tfrac{1}{2} \widetilde{\theta}^T \Gamma_{\theta} \widetilde{\theta} \tag{4.20}$$

The following error dynamics can be obtained and will be used in $\dot{\mathrm{V}}_1$:

$$M(X)\dot{s}_1 + D(X,\dot{X})s_1 = \Theta_1(X,\dot{X}_r,\ddot{X}_r)\widetilde{\theta} - K_d(s_1 - s_2) - K_p e - D(X,s_1)\dot{X}_r + E^T \boldsymbol{W}\boldsymbol{J}^{-T}\overline{\boldsymbol{J}}\widetilde{\boldsymbol{F}} \tag{4.21}$$

$$M(X)\dot{s}_2 + D(X,\dot{X})s_2 = \Theta_2(X,\dot{X},\dot{X}_o,\ddot{X}_o)\widetilde{\theta} - K_d s_1 - K_d^{'} s_2 - L_p \widetilde{X} \tag{4.22}$$

where equations (2.39), (4.7), and (4.11) have been employed in deriving equations (4.21) and (4.22).

It can be shown that the time derivative of V_1 is given by

$$\begin{aligned}\dot{\mathrm{V}}_1 &= -s_1^T K_d s_1 - s_2^T K_d^{'} s_2 - e^T \lambda_1 K_p e - \widetilde{X}^T \lambda_2 L_p \widetilde{X} + \widetilde{X}^T \lambda_1 K_p e - s_1^T D(X, s_1)\dot{X}_r \\ &\quad + s_1^T E^T \boldsymbol{J}^{-\boldsymbol{T}} \overline{\boldsymbol{J}}\widetilde{\boldsymbol{F}} + [\dot{\widetilde{\theta}}^T \Gamma_\theta + s_2^T \Theta_1(X, \dot{X}_r, \ddot{X}_r) + s_2^T \Theta_2(X, \dot{X}, \dot{X}_o, \ddot{X}_o)]\widetilde{\theta}\end{aligned} \tag{4.23}$$

Substituting the adaptation law (4.12) leads to

$$\dot{\mathrm{V}}_1 = -s_1^T K_d s_1 - s_2^T K_d^{'} s_2 - e^T \lambda_1 K_p e - \widetilde{X}^T \lambda_2 L_p \widetilde{X} + \widetilde{X}^T \lambda_1 K_p e - s_1^T D(X, s_1)\dot{X}_r + s_1^T E^T \boldsymbol{J}^{-\boldsymbol{T}} \overline{\boldsymbol{J}}\widetilde{\boldsymbol{F}} \tag{4.24}$$

Following the backstepping approach, for the entire system, consider a scalar function:

$$\mathrm{V}_2 = \mathrm{V}_1 + \tfrac{1}{2}\widetilde{\boldsymbol{F}}^T \Gamma_F \widetilde{\boldsymbol{F}} + \tfrac{1}{2}\widetilde{\varphi}^T \Gamma_\varphi \widetilde{\varphi} \tag{4.25}$$

Since

$$\hat{\boldsymbol{A}}_{cq}(q)\boldsymbol{U} - \hat{\boldsymbol{A}}_{ca}(\boldsymbol{q}, \dot{\boldsymbol{q}}) = \Phi(\boldsymbol{q}, \dot{\boldsymbol{q}}, \boldsymbol{U})\hat{\varphi} \tag{4.26}$$

the hydraulic dynamics in equation (2.50) can be rewritten as

$$\dot{\boldsymbol{F}} = \hat{\boldsymbol{A}}_{cq}(\boldsymbol{q})\boldsymbol{U} - \hat{\boldsymbol{A}}_{ca}(\boldsymbol{q}, \dot{\boldsymbol{q}}) - \Phi(\boldsymbol{q}, \dot{\boldsymbol{q}}, \boldsymbol{U})\widetilde{\varphi} \tag{4.27}$$

With equation (4.27), the time derivative of V_2 becomes

$$\dot{\mathrm{V}}_2 = \dot{\mathrm{V}}_1 + (\hat{\boldsymbol{A}}_{cq}\boldsymbol{U} - \hat{\boldsymbol{A}}_{ca} - \dot{\boldsymbol{F}}^d)^T \Gamma_F \widetilde{\boldsymbol{F}} + \widetilde{\varphi}^T (\Gamma_\varphi \dot{\widetilde{\varphi}} - \Phi \Gamma_F \widetilde{\boldsymbol{F}}) \tag{4.28}$$

With the adaptive law (4.15) and the controller (4.18), equation (4.28) becomes

$$\begin{aligned}\dot{\mathrm{V}}_2 &= -s_1^T K_d s_1 - s_2^T K_d^{'} s_2 - e^T \lambda_1 K_p e - \widetilde{X}^T \lambda_2 L_p \widetilde{X} + \widetilde{X}^T \lambda_1 K_p e - s_1^T D(X, s_1)\dot{X}_r - \widetilde{\boldsymbol{F}}^T K_F \Gamma_F \widetilde{\boldsymbol{F}} \\ &\le -(\underline{\sigma}(K_d) - D_U(\dot{X}_U^d + \overline{\sigma}(\lambda_1)(\|e\| + \|\widetilde{X}\|)))\|s_1\|^2 - \underline{\sigma}(K_d^{'})\|s_2\|^2 - \widetilde{\boldsymbol{F}}^T K_F \Gamma_F \widetilde{\boldsymbol{F}} \\ &\quad - (\sqrt{\underline{\sigma}(\lambda_1 K_p)}\|e\| - \sqrt{\underline{\sigma}(\lambda_2 L_p)}\|\widetilde{X}\|)^2 - (2\sqrt{\underline{\sigma}(\lambda_1 K_p)}\sqrt{\underline{\sigma}(\lambda_2 L_p)} - \overline{\sigma}(\lambda_1 K_p))\|e\|\|\widetilde{X}\|\end{aligned} \tag{4.29}$$

where $D(X, s_1) \le D_U \|s_1\|$ and $\dot{X}_r = \dot{X}^d - \lambda_1(e - \widetilde{X}) \le \dot{X}_U^d + \overline{\sigma}(\lambda_1)(\|e\| + \|\widetilde{X}\|)$ have been used in deriving equation (4.29). Notice that $(\|e\| + \|\widetilde{X}\|)^2 \le 2(\|e\|^2 + \|\widetilde{X}\|^2) \le 2\|r\|^2$ and $\|r\|^2 \le (\mathrm{V}_2 - V_{pL})/\alpha_L$ resulting from equations, (4.18) and (4.19). To satisfy

$$\underline{\sigma}(K_d) - D_U(\dot{X}_U^d + \overline{\sigma}(\lambda_1)(\|e\| + \|\widetilde{X}\|)) > 0 \tag{4.30}$$

a sufficient condition is

$$\mathrm{V}_2 \le \frac{\alpha_L}{2}\left[\frac{\underline{\sigma}(K_d) - D_U \dot{X}_U^d}{D_U \overline{\sigma}(\lambda_1)}\right]^2 + V_{pL} \tag{4.31}$$

The conditions given in equations, (4.31) and (4.16) guarantee that

$$\dot{\mathrm{V}}_2 \leq -\alpha(\|e\|^2 + \|\widetilde{X}\|^2 + \|s_1\|^2 + \|s_2\|^2 + \|\widetilde{\boldsymbol{F}}\|^2) \tag{4.32}$$

with $\alpha > 0$. Inequality (4.32) guarantees $\mathrm{V}_2 \leq \mathrm{V}_2(0)$. Thus, a sufficient condition for equation (4.31) is

$$\mathrm{V}_2(0) \leq \frac{\alpha_L}{2}\left[\frac{\underline{\sigma}(K_d) - D_U \dot{X}_U^d}{D_U \overline{\sigma}(\lambda_1)}\right]^2 + V_{pL} \tag{4.33}$$

which can be satisfied by condition (4.17).

The above analysis shows that inequality (4.32) is satisfied under conditions (4.16) and (4.17). It follows that $\mathrm{V}_2(t) \leq \mathrm{V}_2(0)$ for all $t \geq 0$ and $r(t)$ is bounded.

Inspection of equations (4.25) and (4.32) further reveals that the tracking errors $e, \widetilde{X}, s_1, s_2$ and $\widetilde{\boldsymbol{F}}$ converge to zero as $\mathrm{V}_2(t)$ is lower bounded by zero. More arguments are also referred to Barbalat's lemma * and its followed theorem with examples by Khalil (2002). Since $s_1 = \dot{e} + \Lambda_1(e - \widetilde{X})$, the velocity tracking error, $\dot{e}$, also converges to zero.

4.2 Remarks

***Remarks* 1:**

The parameter convergence is not guaranteed here. In fact, the parameter estimates may not converge to their actual values, whereby the closed-loop system will have an equilibrium subspace $\{e = 0, \widetilde{X} = 0, s_1 = 0, s_2 = 0, \widetilde{\boldsymbol{F}} = 0, \widetilde{\theta} \neq 0, \widetilde{\varphi} \neq 0\}$. The estimates might converge to their actual values under the necessary condition of persistency of excitation (Slotine and Li, 1991).

***Remark* 2:**

The actual internal force is examined here for convergence to the desired value. The following can be obtained about the contact forces:

$$\boldsymbol{F}_c^{t\to\infty} = \boldsymbol{W}^{\dagger} E^{-T} T^d + \boldsymbol{V} F_{\mathrm{int}}^d - \boldsymbol{J}^{-T}(\boldsymbol{H}_m \ddot{\boldsymbol{q}}^d + \boldsymbol{C}_m \dot{\boldsymbol{q}}^d + \boldsymbol{G}_m) \tag{4.34}$$

By using equations, (2.12), (2.13) and (4.34); it can be proven that

* **Barbalat's lemma:** Let $\phi : R \to R$ be a uniformly continuous function on $[0, \infty)$. Suppose that $\lim_{t\to\infty} \int_0^t \phi(\tau) d\tau$ exists and is finite. Then, $\phi(t) \to 0$ as $t \to \infty$.

$$F_{ext}^{t\to\infty} = W\boldsymbol{F}_c^{t\to\infty} = E^{-T}T^d - W\boldsymbol{J}^{-T}(\boldsymbol{H}_m\ddot{\boldsymbol{q}}^d + \boldsymbol{C}_m\dot{\boldsymbol{q}}^d + \boldsymbol{G}_m) \tag{4.35}$$

and

$$\boldsymbol{V}F_{\text{int}}^{t\to\infty} = \boldsymbol{F}_c^{t\to\infty} - \boldsymbol{W}^{\dagger}F_{ext}^{t\to\infty} = \boldsymbol{V}F_{\text{int}}^{d} - (\boldsymbol{I} - \boldsymbol{W}^{\dagger}\boldsymbol{W})\boldsymbol{J}^{-T}(\boldsymbol{H}_m\ddot{\boldsymbol{q}}^d + \boldsymbol{C}_m\dot{\boldsymbol{q}}^d + \boldsymbol{G}_m) \tag{4.36}$$

where, $F_{ext}^{t\to\infty}$ and $F_{\text{int}}^{t\to\infty}$ are the external and internal forces when $t \to \infty$, respectively. Since $\boldsymbol{V}$ is a full-column rank matrix, it can be concluded that

$$F_{\text{int}}^{t\to\infty} = F_{\text{int}}^{d} + \boldsymbol{V}^{\dagger}(\boldsymbol{I} - \boldsymbol{W}^{\dagger}\boldsymbol{W})\boldsymbol{J}^{-T}(\boldsymbol{H}_m\ddot{\boldsymbol{q}}^d + \boldsymbol{C}_m\dot{\boldsymbol{q}}^d + \boldsymbol{G}_m) \tag{4.37}$$

Equation (4.37) shows that there exists a bounded error between the actual internal force and its desired value. By introducing a force feedback loop, the internal force can be shown to follow the desired one. Equation (4.10) is modified as

$$\boldsymbol{F}^d = \bar{\boldsymbol{J}}^{-1}\boldsymbol{J}^T(\boldsymbol{W}^{\dagger}E^{-T}T^d + \boldsymbol{V}(F_{\text{int}}^d + K_{\text{int}}(F_{\text{int}}^d - F_{\text{int}}))) \tag{4.38}$$

The actual internal force F_{int} can be extracted from contact forces, which are typically available through wrist sensors. As a result, equation (4.36) becomes

$$\boldsymbol{V}F_{\text{int}}^{t\to\infty} = \boldsymbol{V}F_{\text{int}}^{d} - (1 + K_{\text{int}})^{-1}(\boldsymbol{I} - \boldsymbol{W}^{\dagger}\boldsymbol{W})\boldsymbol{J}^{-T}(\boldsymbol{H}_m\ddot{\boldsymbol{q}}^d + \boldsymbol{C}_m\dot{\boldsymbol{q}}^d + \boldsymbol{G}_m) \tag{4.39}$$

Thus, the actual internal force can arbitrarily approximate the desired value through increasing the force feedback gain K_{int}. As for the stability, consider the same scalar function V_2 defined in (4.25). It can be recognized that the time derivative of (4.25) satisfies inequality (4.32) under the same conditions (4.16) and (4.17), since only the term related to internal force has been changed and the internal force feedback terms do not contribute to $\dot{\mathrm{V}}_2$.

In the implementation of equation (4.38) associated with the controller (4.8), the derivative of the internal force is difficult to obtain and is calculated using numerical differentiation or can be neglected if the variation of internal force is slow.

***Remark* 3:**

With respect to the controller described in equation (4.8), the only hydraulic system parameters needed by the controller are the effective piston areas $\boldsymbol{A}_I$ and $\boldsymbol{A}_O$. The effective bulk modulus of the hydraulic fluid β, the constant valve gain $\boldsymbol{K}_{sp}$, and the constant flow gain $\boldsymbol{K}$ are not required. As for the manipulators, the mass and position of the center of mass for each link is not required. Since the Jacobian matrix appears in the controller, link length is required. No knowledge about the payload is required. For the implementation of the proposed controller, only measurements of positions, velocities and hydraulic pressures are required. Force measurement is also required if a force feedback is used for the reduction of the internal force.

Note that acceleration measurements are often not available and they are replaced by numerical derivatives of the measured velocities. This may lead to chattering of the control inputs due to the combined effect of noisy measurements and un-modeled phenomena, such as joint friction and elasticity. To avoid this undesirable behavior, an acceleration observer is developed, in a way that is similar to the works by Sirouspour and Salcudean (2001) and Bu and Yao (2001), which were for a single hydraulic arm. As can be seen from equation (4.11), vector T^d does not contain any velocity terms. That is to say, $\dot{T}^d$, as well as $\dot{\boldsymbol{F}}^d$, does not contain any acceleration terms. The measurement of acceleration is not required by inspection of the controller (4.8).

4.3 Simulation Studies

The nonlinear position-tracking controller presented in Section 4.1 has been tested on the same numerical model as used in Chapter 3. With reference to Figure 4.1, two hydraulic manipulators held an object and then moved it along a desired path. Parameters of the robots were chosen to closely resemble MAGNUM 7 function hydraulic manipulators by International Submarine Engineering Ltd. of Canada. These parameters have been shown in Tables 3.1 and 3.2. The vectors of unknown parameters,

$$\theta = (\overbrace{I_1^1 + m_1^1 {a_1^1}^2, I_2^1 + m_2^1 {a_2^1}^2, I_3^1 + m_3^1 {a_3^1}^2, m_2^1, m_3^1, m_1^1 a_1^1, m_2^1 a_2^1, m_3^1 a_3^1}^{\text{Robot 1}}, \overbrace{I_1^2 + m_1^2 {a_1^2}^2, I_2^2 + m_2^2 {a_2^2}^2, \ldots,}^{\text{Robot 2}} \overbrace{m, I}^{\text{Object}})^T$$

and $\varphi = (\beta_1^1 K_1^1 K_{sp,1}^1, \beta_1^1, \ldots, \beta_j^i K_j^i K_{sp,j}^i, \beta_j^i, \ldots)_{i=1,2; j=1,2,3}^T$, were estimated online. The variables m and I are mass and inertia of the object. m_j^i, I_j^i, and $a_j^i, i = 1,2; j = 1,2,3$, are mass, inertia, and distance of center of mass to the j^{th} joint of the i^{th} robot, respectively. Each actuator has identical parameters, with the exception of a different stroke. All estimates of the unknown parameters were initially set to different values, (at least 50% off) from those used in the model; to investigate the ability of the controller to cope with parametric uncertainties. The reference internal force was set to zero and no force feedback was used. The control gains were chosen as $\lambda_1 = 50$, $\lambda_2 = 50$, $K_p = 10000$, $L_p = 3000$, $K_d = 700$ and $K_d^{'} = 700$.

Two reference trajectories along the vertical direction were chosen:

(i) point-to-point trajectory with a travel distance of 0.3m, maximum speed of 0.15m/s and maximum acceleration of 0.6m/s^2

(ii) sinusoidal trajectory consisting of one segment with an amplitude of 0.1m and frequency of 0.2Hz followed by a second segment with an amplitude of 0.02m and frequency of 1Hz.

These two reference trajectories are shown in Figure 4.2 and Figure 4.8, respectively. The controller was also required to maintain the internal force in the horizontal direction close to zero and at the same time, evenly distribute the load between the two robots.

The first set of tests was conducted using the point-to-point reference trajectory, which is shown in Figure 4.2. Figure 4.3 shows that the position error went to zero with about 1-mm error at the transient period. The control signals to the actuators for one of the robots are illustrated in Figure 4.4. Figure 4.5 shows that the internal force exists and went to a smaller value (about 40 N) at steady-state phase. Note that force feedback was not implemented in this case. The profiles of some parameter estimates are shown in Figure 4.6, in which the object, link and hydraulic parameters do not converge to their actual values. It should be stressed that the parameter convergence is not theoretically guaranteed as described in Section 4.2; therefore the results do not contradict the theoretical argument. The distribution of the lifting forces is shown in Figure 4.7, from which, it can be seen that the two robots shared the payload.

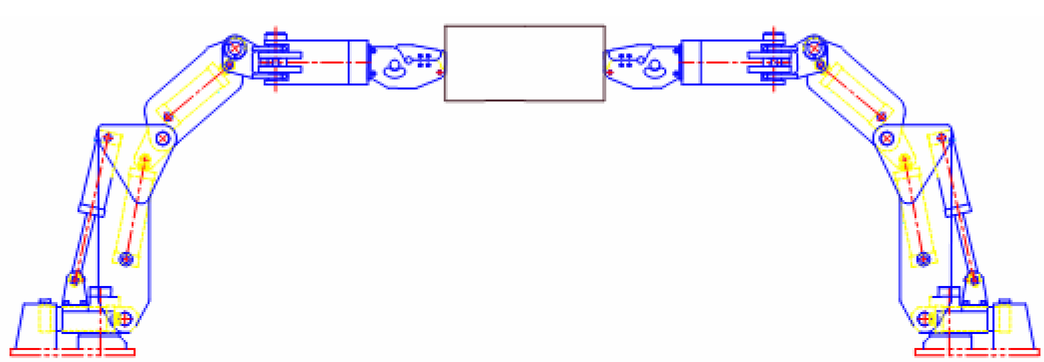

Figure 4.1: Two planar hydraulic manipulators co-operatively handle an object.

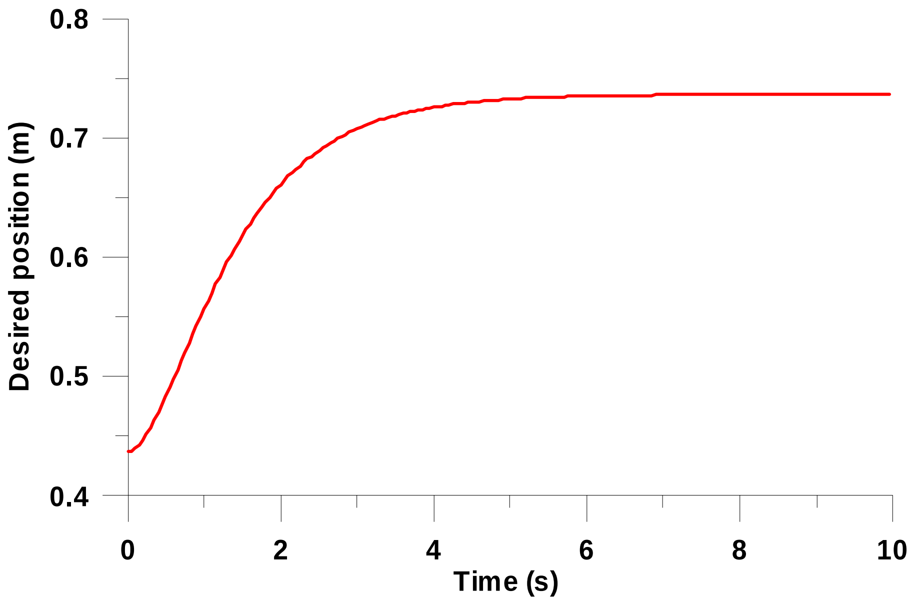

Figure 4.2: Desired position trajectory of the object in the vertical direction.

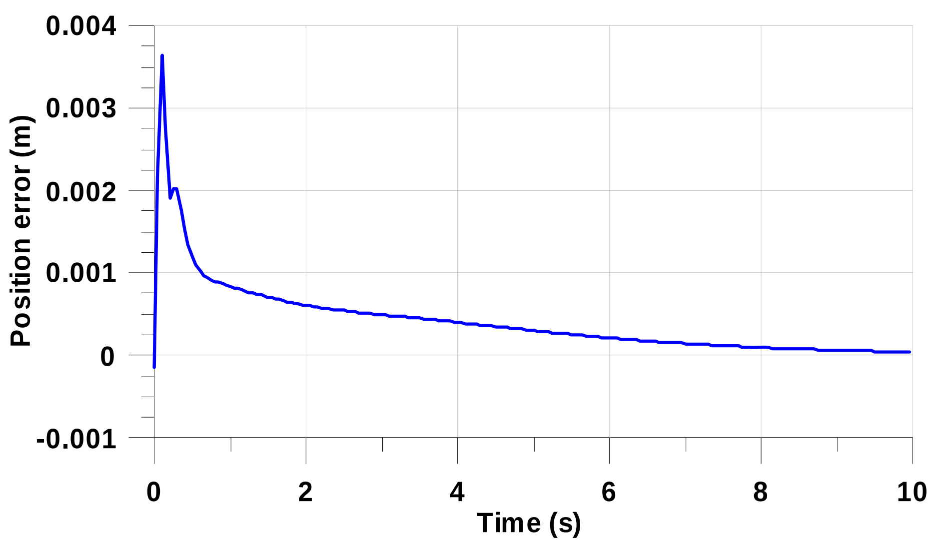

Figure 4.3: Position error of the object, when moved vertically from one point to another.

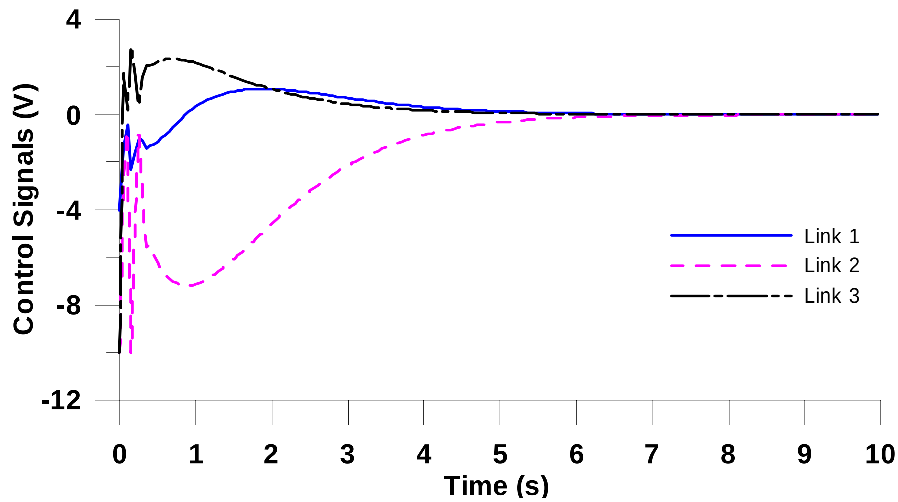

Figure 4.4: Control signals for the first manipulator.

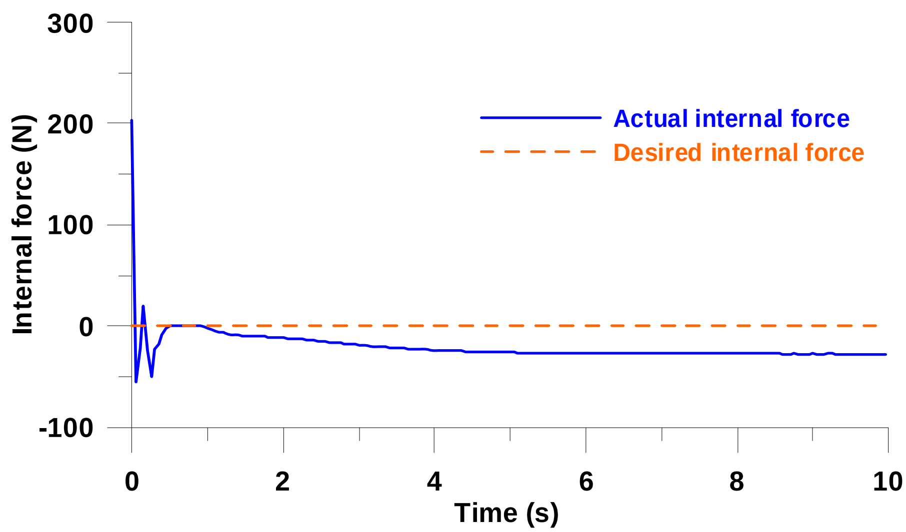

Figure 4.5: Object internal force in the horizontal direction.

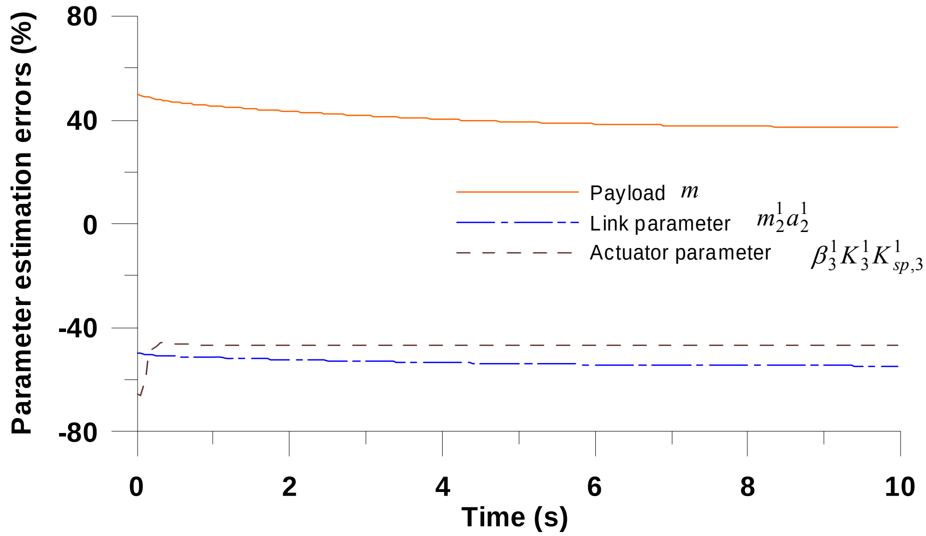

Figure 4.6: Load/parameter estimation errors.

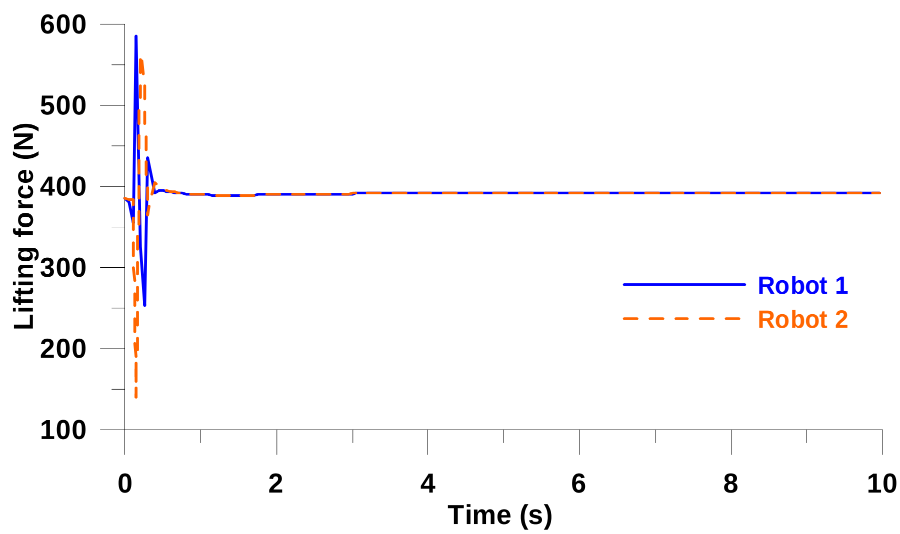

Figure 4.7: Load sharing between robots.

The next test was conducted using the sinusoidal reference trajectory. The reference trajectory is shown in Figure 4.8. Figure 4.9 shows that the position error was about 3 mm at the transient period and less than 0.2 mm thereafter. The control signals to the actuators for one of the robots are illustrated in Figure 4.10. Figure 4.11 shows that the internal force had offsets of 20 N and 10N. Amplitude changes were 10N and 5N, for the first and second half of the sinusoidal trajectory, respectively. No force feedback was implemented in this case. The profiles of some parameter estimates are shown in Figure 4.12. The object, link and hydraulic parameters did not converge to their actual values. The lifting forces were as designed, equally distributed between the two robots shown in Figure 4.13.

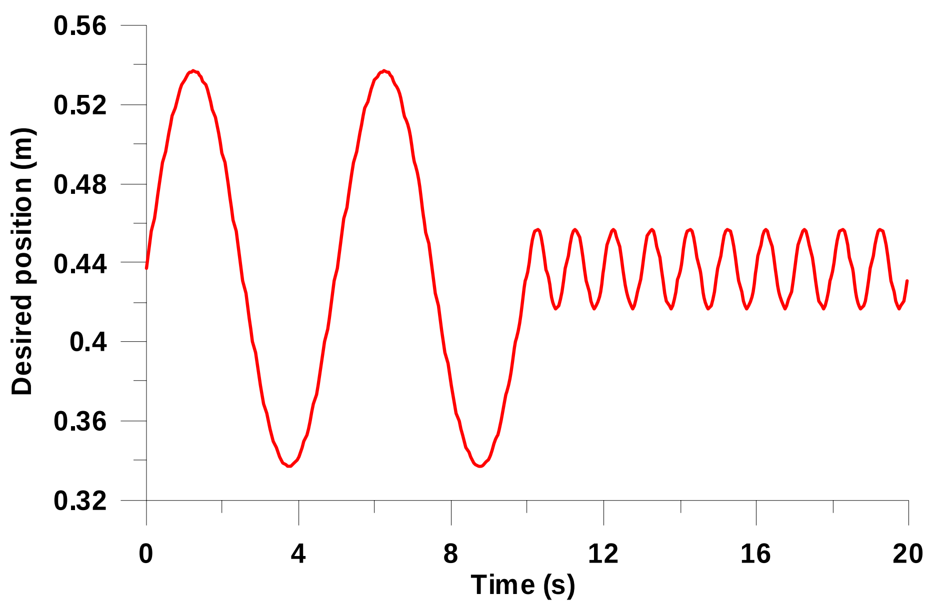

Figure 4.8: Desired position trajectory of the object in the vertical direction.

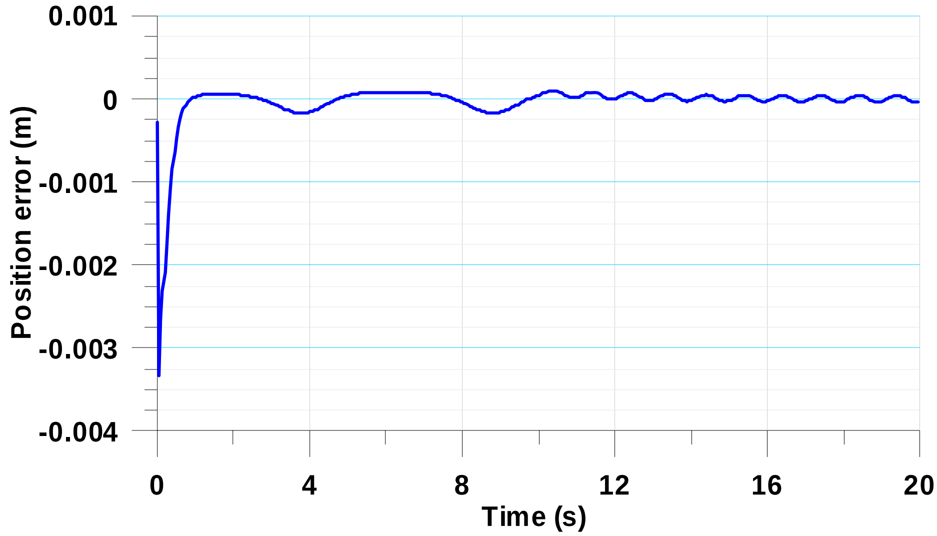

Figure 4.9: Position error of the object.

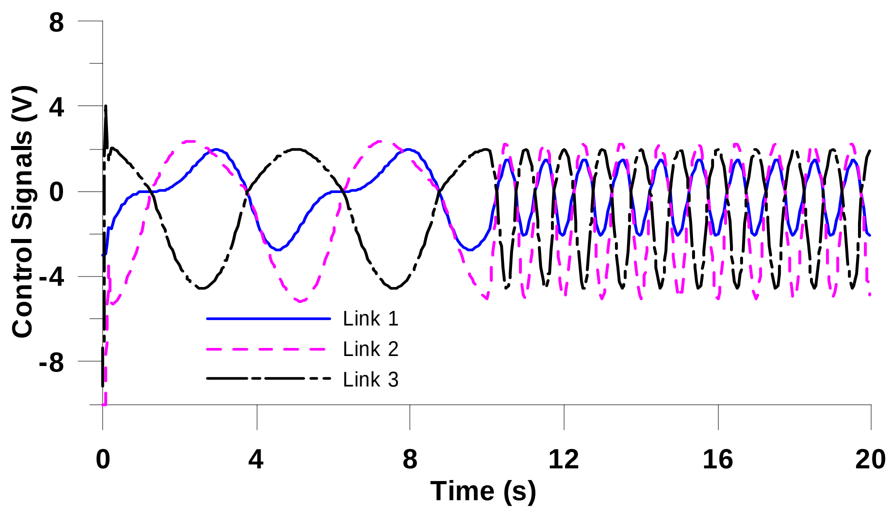

Figure 4.10: Control signals for the first manipulator.

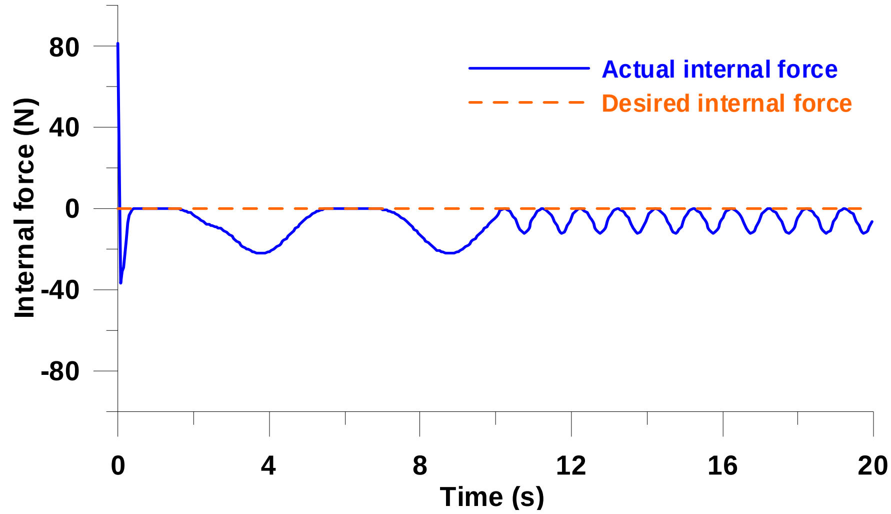

Figure 4.11: Object internal force in the horizontal direction.

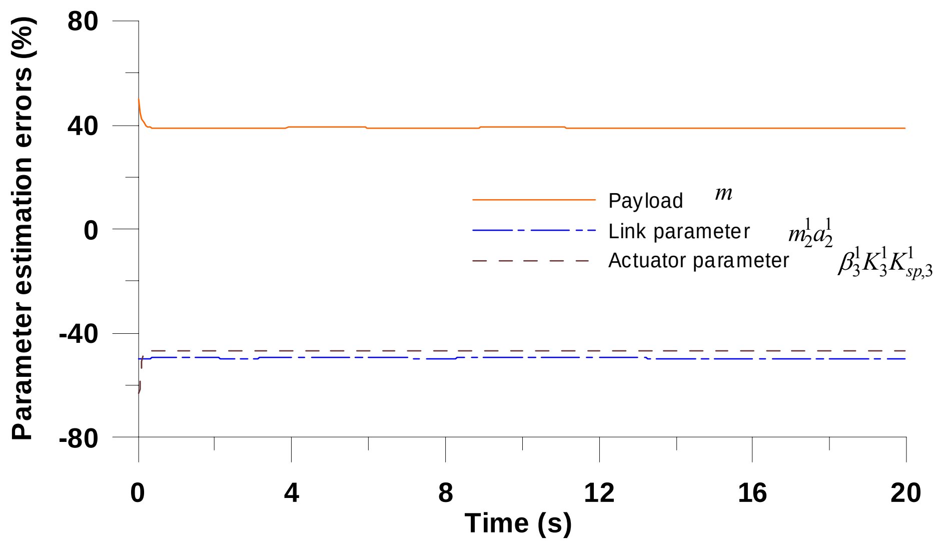

Figure 4.12: Typical load/parameter estimation errors.

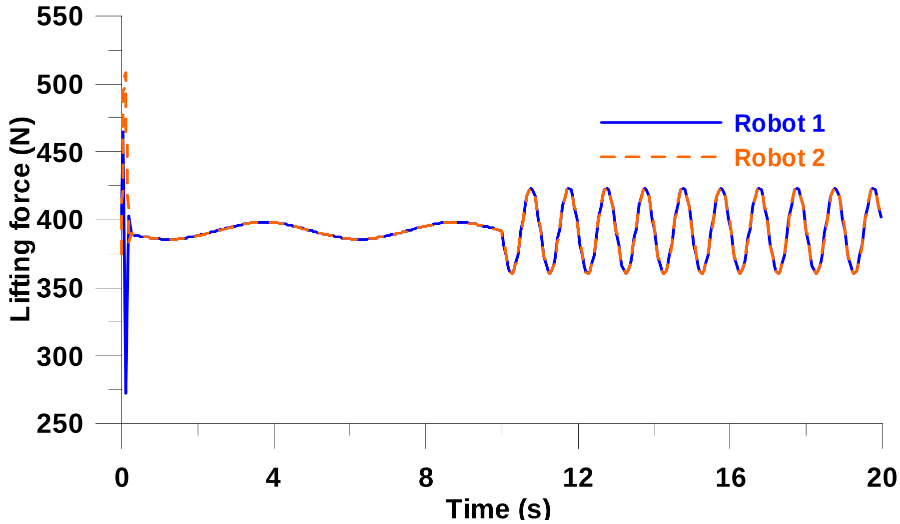

Figure 4.13: Load sharing between robots.

4.4 Summary

This chapter documented design, stability analysis and numerical verification of a tracking controller for co-operation among several hydraulic robots handling a rigid payload. The highly nonlinear hydraulic actuator dynamics were incorporated in the Lyapunov-based controller design. The issues of motion and internal force control of the object, as well as load sharing among several manipulators were addressed. To deal with parametric uncertainties, including unknown payload, robot dynamics and hydraulic functions parameters; the controller was augmented with adaptation laws. An adaptive observer was also included to avoid the need for measurement of acceleration as feedback. It was proven that the position and velocity tracking errors converged to zero, while bounded internal force errors existed. These internal force errors can be controlled with the addition of force feedback.

Simulations were performed with two manipulators resembling MAGNUM 7 hydraulic manipulators. The results demonstrated the effectiveness of the proposed nonlinear controller.

Chapter 5 Effects of Friction on the Control System

This chapter investigates the effect of friction, especially dry friction on the performance of co-operating robots. The previous control controllers are re-visited by adding a dynamic friction model (LuGre) to the actuator dynamics. Simulations are then carried out to examine the performances in the presence of friction. Three controllers, including the second and third regulating controllers developed in Chapter 3, and the tracking controller in Chapter 4; are to be studied in the following three case studies.

5.1 Regulating Controller with Unknown Payload

The controller developed in Section 3.2, which has an estimator of unknown payload and does not consider the effect of friction; is reexamined in the presence of dry friction in the hydraulic actuators. The equilibrium of the control system is first established followed by a simulation study.

5.1.1 Equilibrium of the Control System in the Presence of Friction

In the presence of dry friction, a friction term $\boldsymbol{W}\boldsymbol{J}^{-T}\bar{\boldsymbol{J}}\boldsymbol{F}_{\boldsymbol{fr}}$ is added to the left side of equation (3.9). The corresponding equilibrium of the system under the controller (3.25) associated with equations (3.34) and (3.43) will then become

$$\boldsymbol{U}^{ss} = 0 \tag{5.1}$$

$$\boldsymbol{W}\boldsymbol{J}^{-T}\boldsymbol{K}_p\tilde{\boldsymbol{q}} = 0 \tag{5.2}$$

$$\boldsymbol{F}_c^{ss} = -(I - \boldsymbol{W}^{\dagger}\boldsymbol{W})\boldsymbol{J}^{-T}\bar{\boldsymbol{J}}\boldsymbol{F}_{\boldsymbol{fr}} + \boldsymbol{W}^{\dagger}g_o + VF_{\text{int}}^d \tag{5.3}$$

$$VF_{\text{int}}^{ss} = \boldsymbol{F}_c^{ss} - \boldsymbol{W}^{\dagger}\boldsymbol{W}\boldsymbol{F}_c^{ss} = -(I - \boldsymbol{W}^{\dagger}\boldsymbol{W})\boldsymbol{J}^{-T}\bar{\boldsymbol{J}}\boldsymbol{F}_{\boldsymbol{fr}} + VF_{\text{int}}^d \tag{5.4}$$

Equation (5.4) shows that the desired internal force vector can not be achieved at steady state in the presence of friction even if the manipulators' gravity terms are known.

Note that the undesirable internal force is an additional load to the co-operating system, but makes no contribution to the motion of the object; therefore it could significantly reduce the effective lifting capacity of the system.

5.1.2 Simulation Studies

The same study as in the case study in Section 3.2.2 has been performed with the inclusion of a dry friction model in the simulation program. The LuGre friction model (Canudas de Wit et al. 1995) described in Section 2.3 was used. For simulations, the following values were used: $F_{sl,j}^{i} = 900N$, $F_{st,j}^{i} = 1100N$, $\dot{x}_s = 0.002m/s$, $\sigma_{0.j}^{i} = 2\times10^{5}\,N/m$ and $\sigma_{1.j}^{i} = 400Ns/m$, $\sigma_{2.j}^{i} = 200Ns/m$.

Figures 5.1 to 5.5 show the controller's performance, with the best performing gains (fast rise time with no overshoot); which could be compared with Figures 3.2 to 3.6. The simulation results show that, in the presence of actuator dry friction; the entire control system is still stable and the desired position is achieved (see Figure 5.1). The control signals corresponding to one of the robots are shown in Figure 5.2. They are slightly higher than the control signals when there is no actuator friction (see Figure 3.3), which is expected. The lifting forces by each robot are shown in Figure 5.3.

Based on the equilibrium of the system, it is further obtained that $\hat{g}_o = \boldsymbol{W}\boldsymbol{J}^{-T}\bar{\boldsymbol{J}}\boldsymbol{F}_{\boldsymbol{fr}} + g_o$. From the controller's point of view, the friction is taken as an extra load resulting in an increased object/load that needs to be compensated. Thus, as can be clearly seen from Figure 5.4, the object load is over-estimated. As shown by equation (5.4), the desired internal force could not be achieved in the presence of actuator friction (compare Figure 5.5 with Figure 3.6), given the controller (3.25) associated with equations (3.34) and (3.43) developed in Section 3.2.

Overall, simulation results show that the system still achieves the desired position. However, the presence of friction could make regulation longer and bring about undesirable internal forces. The transition between slip to stick friction (i.e. Stribeck effect) does not appear to affect the response in this case.

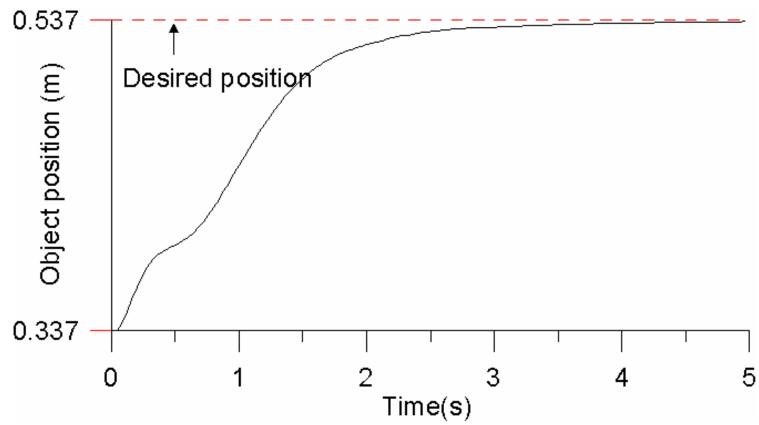

Figure 5.1: Position trajectory of the object under controller (3.25) with unknown payload and in the presence of friction.

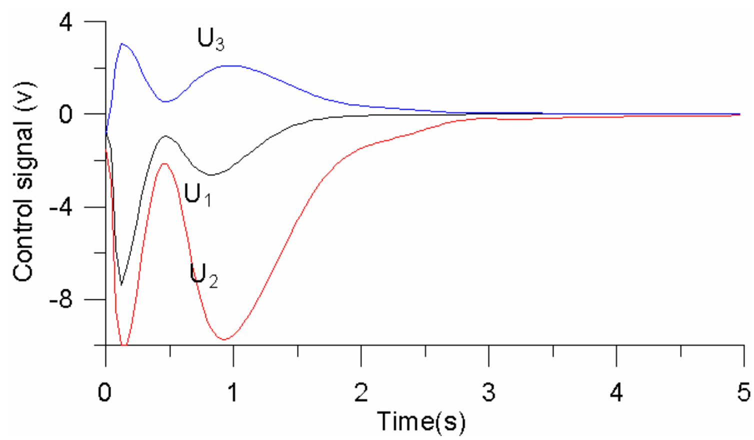

Figure 5.2: Control signals for the first manipulator.

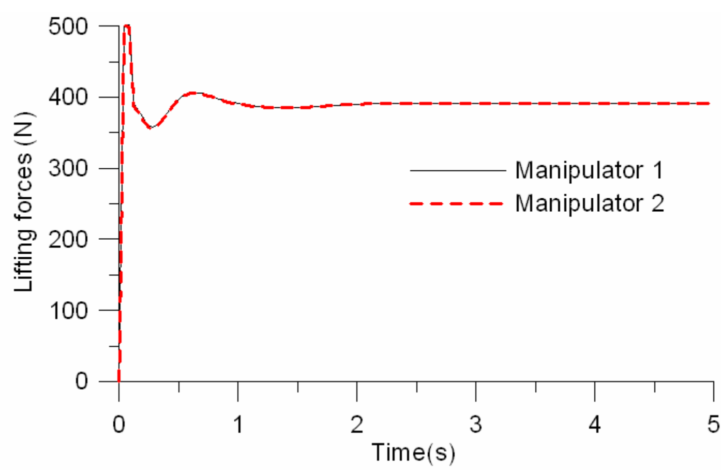

Figure 5.3: Load sharing between two manipulators.

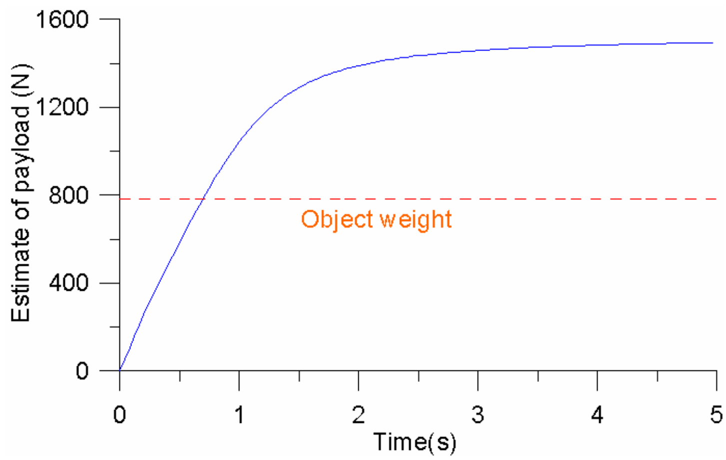

Figure 5.4: Estimation of the payload.

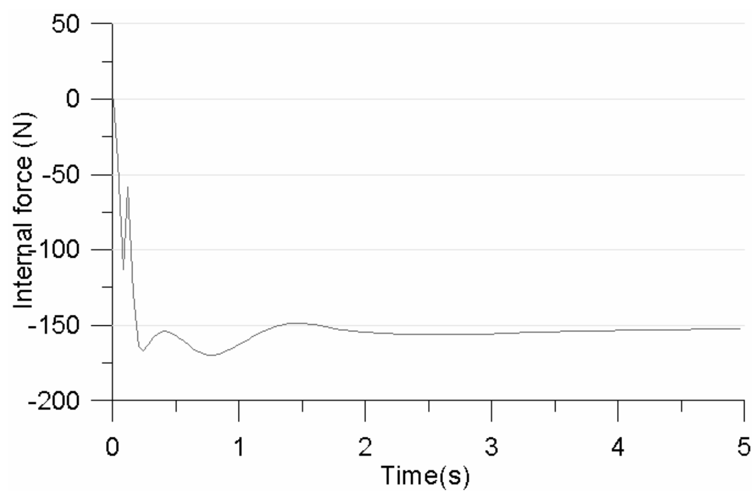

Figure 5.5: Horizontal internal force exerted on the object by two manipulators.

5.2 General Regulating Controller

The controller developed in Section 3.3, which has dealt with the uncertainty of the payload, robot dynamic parameters and hydraulic functions; is re-examined in the presence of dry friction in the hydraulic actuators. The equilibrium of the control system is first studied, followed by simulation studies.

5.2.1 Equilibrium of the Control System in the Presence of Friction

Adding a friction term $\boldsymbol{W}\boldsymbol{J}^{-T}\bar{\boldsymbol{J}}\boldsymbol{F}_{fr}$ to the left side of equation (3.9), the corresponding equilibrium of the system under the controller (3.54) becomes

$$\boldsymbol{U}^{ss} = 0 \tag{5.5}$$

$$\tilde{\boldsymbol{q}} = 0 \tag{5.6}$$

$$\boldsymbol{W}\boldsymbol{J}^{-T}(\hat{\boldsymbol{G}}_E - (\boldsymbol{G}_m(\boldsymbol{q}) + \bar{\boldsymbol{J}}\boldsymbol{F}_{fr} + \boldsymbol{J}^T\boldsymbol{W}^{\dagger}g_o)) = 0 \tag{5.7}$$

$$\boldsymbol{V}F_{\text{int}} = (\boldsymbol{I} + K_{\text{int}})^{-1}\boldsymbol{J}^{-T}(\hat{\boldsymbol{G}}_E - (\boldsymbol{G}(\boldsymbol{q}) + \bar{\boldsymbol{J}}\boldsymbol{F}_{fr} + \boldsymbol{J}^T\boldsymbol{W}^{\dagger}g_o)) + \boldsymbol{V}F_{\text{int}}^d \tag{5.8}$$

Note that if the $\boldsymbol{G}_m(\boldsymbol{q}) + \bar{\boldsymbol{J}}\boldsymbol{F}_{fr}$ is treated as an equivalent gravity term originating from the robots, the control system can be treated as the system without friction. In the presence of friction, $\hat{\boldsymbol{G}}_E$ is actually the estimate of the combined term $\boldsymbol{G}_m(\boldsymbol{q}) + \bar{\boldsymbol{J}}\boldsymbol{F}_{fr} + \boldsymbol{J}^T\boldsymbol{W}^{\dagger}g_o$.

Similarly, equation (5.7) does not guarantee $\hat{\boldsymbol{G}}_E - (\boldsymbol{G}_m(\boldsymbol{q}) + \bar{\boldsymbol{J}}\boldsymbol{F}_{fr} + \boldsymbol{J}^T\boldsymbol{W}^{\dagger}g_o) = 0$. In other words $\hat{\boldsymbol{G}}_E$, the estimate of the term $\boldsymbol{G}_m(\boldsymbol{q}) + \bar{\boldsymbol{J}}\boldsymbol{F}_{fr} + \boldsymbol{J}^T\boldsymbol{W}^{\dagger}g_o$, does not have to converge to its actual value. The desired internal force cannot be achieved by inspection of equation (5.8). Nevertheless, internal force error can be reduced by the increasing gain K_{int}.

5.2.2 Simulation Studies

The same step input response study on the same numerical model as in the previous case study in Section 3.3.2 has been performed, with the same set of gains; while the LuGre friction model is included in the hydraulic actuator dynamics. For simulations, the following values were used: $F_{sl,j}^i = 900N$, $F_{st,j}^i = 1100N$, $\dot{x}_s = 0.002m/s$, $\sigma_0 = 2\times10^5 N/m$ and $\sigma_1 = 400Ns/m$ in the LuGre friction model.

Figure 5.6 shows that the desired position is still achieved. The control signals to the actuators for one of the robots are shown in Figure 5.7, which is different from the one (Figure 3.15) in Section 3.3.2. Figure 5.8 shows that the actual internal force is different from the desired value even during the steady-state phase, which is expected in Section 5.2.1. The difference is about 240 N, much higher than the difference in the case of no dry friction (see Figure 3.16). Furthermore, the simulation results show that $\boldsymbol{W}\boldsymbol{J}^{-T}(\hat{\boldsymbol{G}}_E - (\boldsymbol{G}_m(\boldsymbol{q}) + \boldsymbol{J}^T\boldsymbol{F}_{fr} + \boldsymbol{J}^T\boldsymbol{W}^{\dagger}g_o)) = 0$ during the steady-state phase, as seen in Figure 5.9. Compared with the simulation results (Figures 3.14 to 3.18) where no dry friction was considered in the model, the inclusion of dry friction makes regulation longer and brings about more undesirable internal forces.

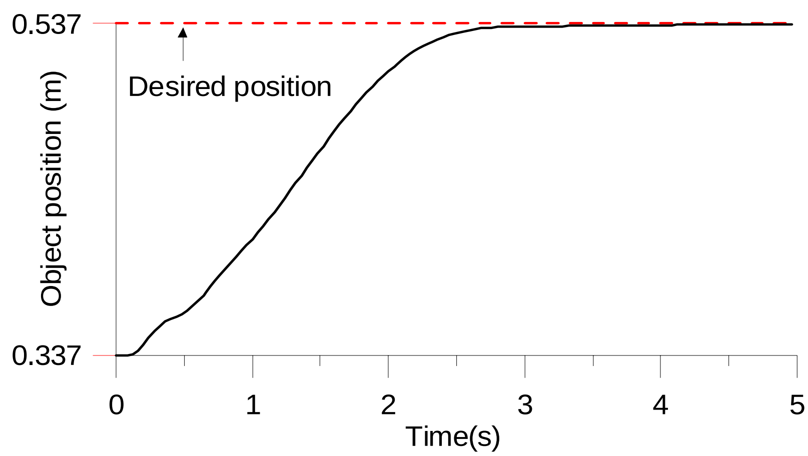

Figure 5.6: Position trajectory of the object under general regulating controller (3.54) and in the presence of friction.

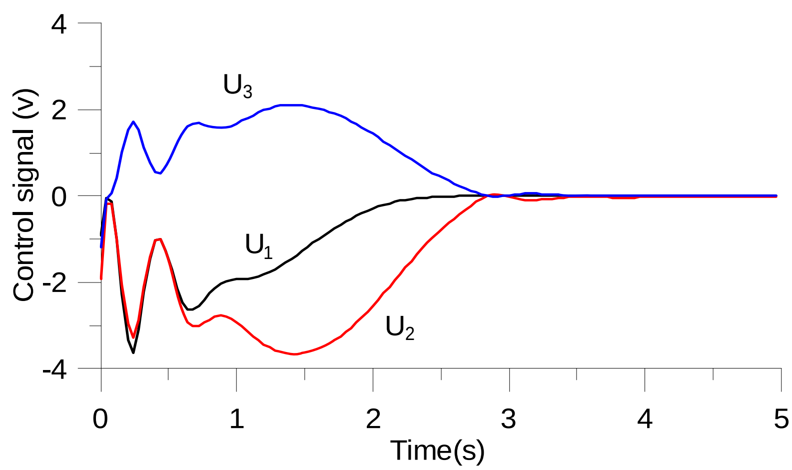

Figure 5.7: Control signals for the first manipulator.

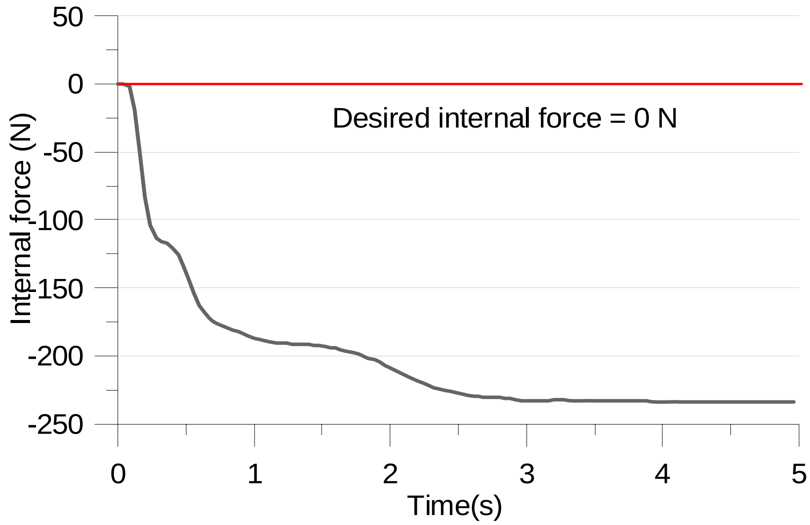

Figure 5.8: Horizontal internal force exerted on the object by two manipulators.

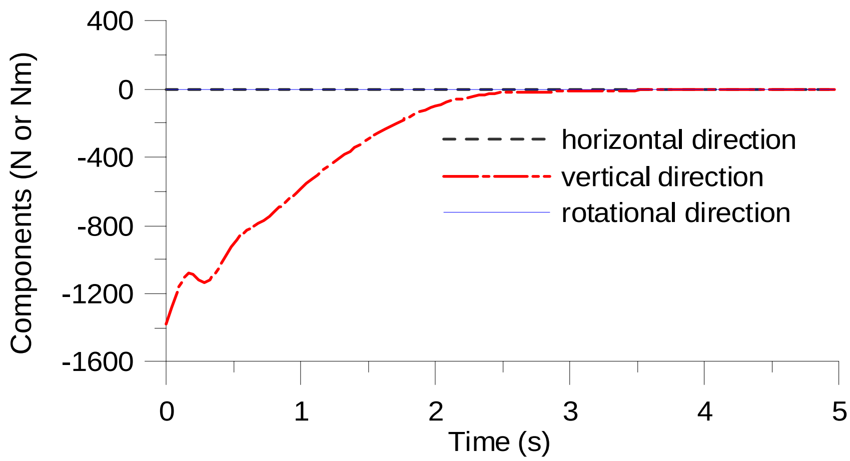

Figure 5.9: Components of the vector $\boldsymbol{W}\boldsymbol{J}^{-T}(\hat{\boldsymbol{G}}_E - (\boldsymbol{G}_m(\boldsymbol{q}) + \boldsymbol{J}^T\boldsymbol{F}_{fr} + \boldsymbol{J}^T\boldsymbol{W}^{\dagger}g_o))$ in Cartesian reference frame $\{X_R, Y_R, Z_R\}$.

The above simulation did not use force feedback. In the next simulation, set $K_{\text{int}} = 20$ and the derivative of the internal force required by the controller was neglected. The position plot remains the same and is not shown here, since only the internal force feedback gain was changed. The internal force became about 10 N, much smaller and closer to the desired internal force as shown in Figure 5.10.

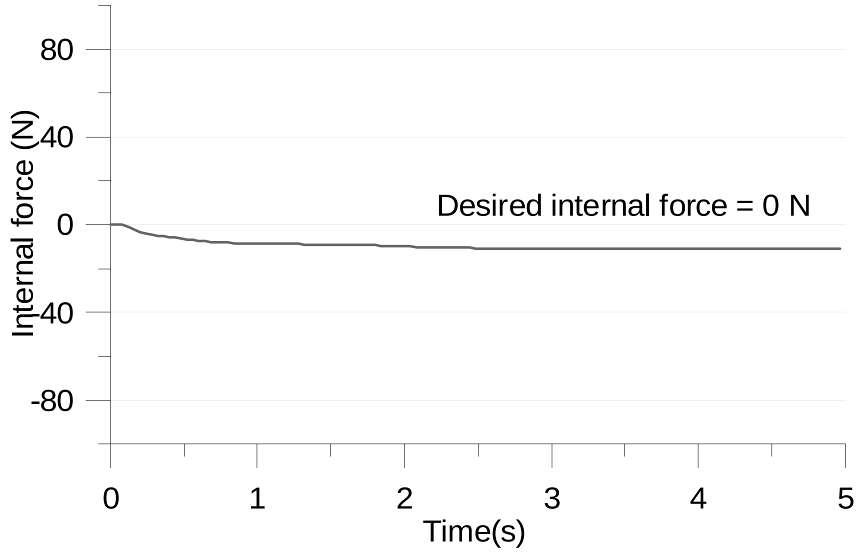

Figure 5.10: Horizontal internal force exerted on the object by two robots for the general regulating controller with force feedback and in the presence of friction.

5.3 Tracking Controller Performance in the Presence of Friction

The position tracking controller (4.8) developed in Section 4.1 is now investigated in the presence of dry friction in the hydraulic actuators.

5.3.1 Equilibrium of the Control System

In the presence of friction, equation (4.32) does not hold. Therefore, no conclusion can be drawn about the position error's convergence to zero. As for the internal force, even assuming no position error, equation (4.39) becomes

$$\boldsymbol{V}F_{\text{int}}^{t\to\infty} = \boldsymbol{V}F_{\text{int}}^{d} - (1+K_{\text{int}})^{-1}(\boldsymbol{I}-\boldsymbol{W}^{\dagger}\boldsymbol{W})\boldsymbol{J}^{-T}(\boldsymbol{H}_m(\boldsymbol{q}^d)\ddot{\boldsymbol{q}}^d + \boldsymbol{C}_m(\boldsymbol{q}^d,\dot{\boldsymbol{q}}^d)\dot{\boldsymbol{q}}^d + \boldsymbol{G}_m(\boldsymbol{q}^d) + \bar{\boldsymbol{J}}\boldsymbol{F}_{\boldsymbol{fr}}) \tag{5.9}$$

Equation (5.9) indicates that friction force will likely increase internal force.

5.3.2 Simulation Studies

The same tasks as in the previous case study in Section 4.3 have been performed with the same set of gains, with the exception of including the LuGre friction model in the hydraulic actuator dynamics. For simulations, the following values were used: $F_{sl,j}^{i} = 900N$, $F_{st,j}^{i} = 1100N$, $\dot{x}_s = 0.002m/s$, $\sigma_{0,j}^{i} = 2\times10^5 N/m$ and $\sigma_{1,j}^{i} = 400Ns/m$.

Force feedback was not used. The corresponding results are shown in Figure 5.11 and Figure 5.12. It was found out that the internal force was built so high that the robots lost their capability to do the job (reaching their limitation given certain supply pressures).

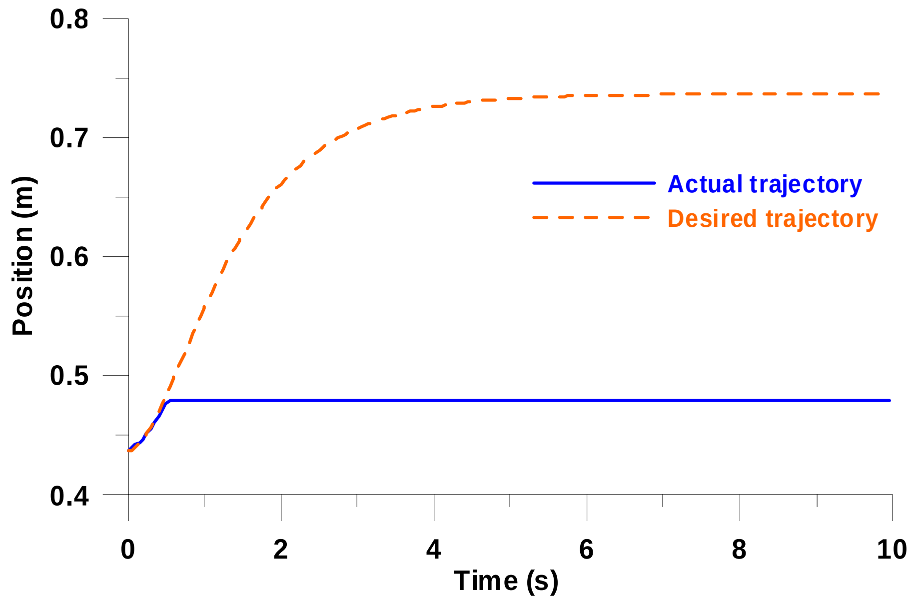

Figure 5.11: Position trajectory of the object under tracking controller (4.8) and in the presence of friction.

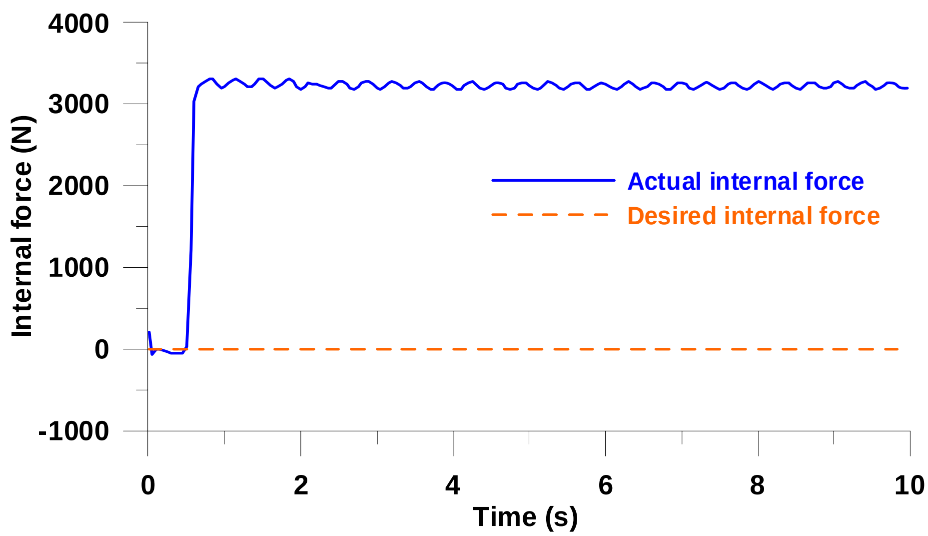

Figure 5.12: Horizontal internal force exerted on the object.

So in the following simulation, force feedback was introduced with the gain $K_{\text{int}} = 3$ and the derivative of the internal force was neglected. As shown in Figure 5.13, the internal force was reduced; however there exists a large steady-state position error which can be seen from Figure 5.14.

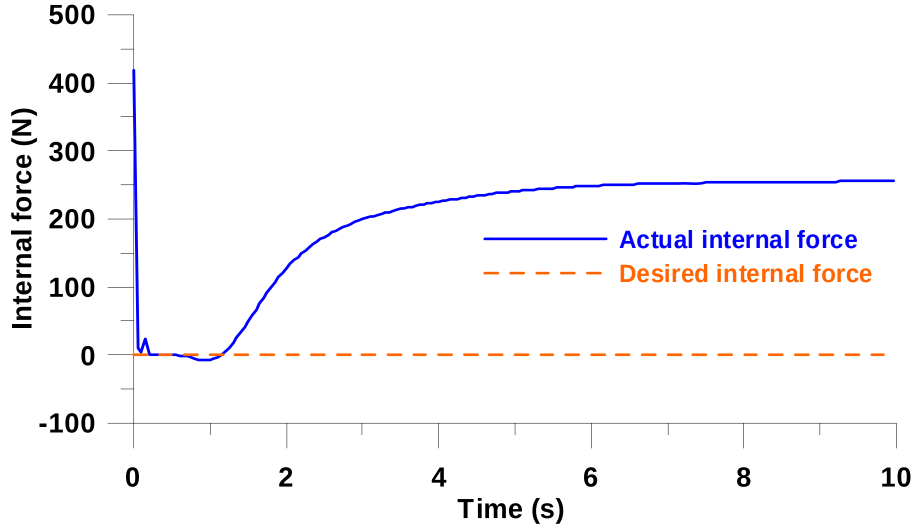

Figure 5.13: Horizontal internal force exerted on the object under controller (4.8) with force feedback and in the presence of friction.

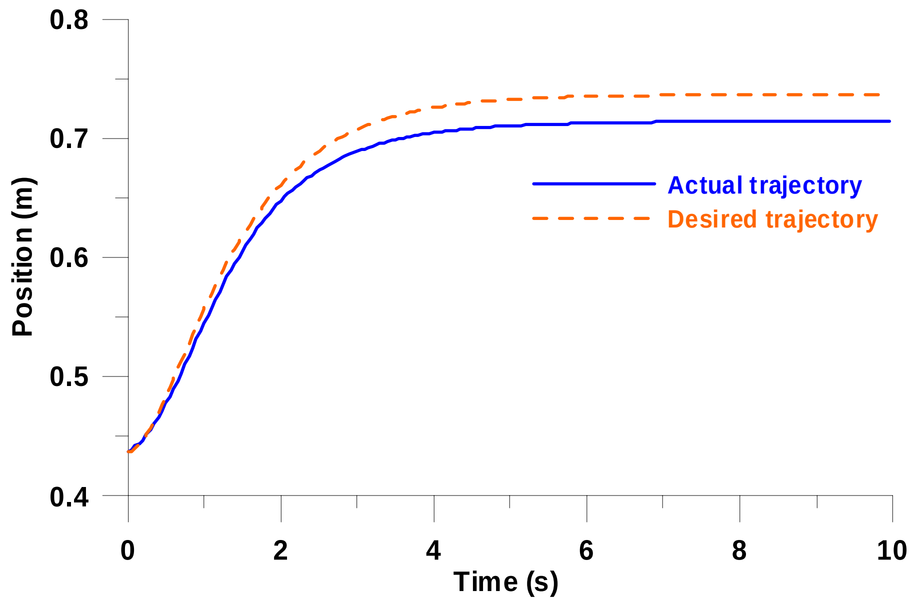

Figure 5.14: Position error of the object.

5.4 Stability Analysis in the Presence of Friction

The effect of friction on the control system has been investigated, but the stability has not been re-examined theoretically. The stability of the general regulating control system is now proven in the presence of friction. In the presence of dry friction, a friction term $\boldsymbol{WJ}^{-T}\bar{\boldsymbol{J}}\boldsymbol{F}_{fr}$ is added to the left side of equation (3.9). The time derivative of the same Lyapunov candidate as defined in equation (3.58), will have an additional term: $-\sum\sum \dot{x}_j^i F_{fr,j}^i$. If the friction model is represented by the simple static model, $F_{fr,j}^i = F_{sl,j}^i \operatorname{sgn}(\dot{x}_j^i)$, this term is then equal to $-\sum\sum \left|\dot{x}_j^i\right| F_{sl,j}^i$ which is always non-positive. It follows that the time derivative of Lyapunov candidate, remain semi negative-definite.

The following is to further prove that $-\sum\sum \dot{x}_j^i F_{fr,j}^i \le 0$ when the LuGre model represents the friction model. The following property of the friction model will be first explored.

Property: if $\left|z_j^i(0)\right| \le g(\dot{x}_j^i(0))$ then

$$\left|z_j^i(t)\right| \le g(\dot{x}_j^i) \quad \forall t \ge 0 \tag{5.10}$$

Proof: let $\mathrm{V} = {z_j^i}^2/2$, then the time derivative of V is

$$\dot{\mathrm{V}} = z_j^i(\dot{x}_j^i - \frac{\left|\dot{x}_j^i\right|}{g(\dot{x}_j^i)} z_j^i) = -\left|\dot{x}_j^i\right|\left|z_j^i\right|\left(\frac{\left|z_j^i\right|}{g(\dot{x}_j^i)} - \operatorname{sgn}(\dot{x}_j^i)\operatorname{sgn}(z_j^i)\right) \tag{5.11}$$

The derivative $\dot{\mathrm{V}}$ is negative whenever $\left|z_j^i(t)\right| > g(\dot{x}_j^i)$. Since $g(\dot{x}_j^i)$ is strictly positive and bounded by $\frac{F_{sl,j}^i}{\sigma_{0,j}^i} \le g(\dot{x}_j^i) \le \frac{F_{st,j}^i}{\sigma_{0,j}^i}$, it is seen that all the solutions of $z_j^i(t)$ starting with $\left|z_j^i(0)\right| \le g(\dot{x}_j^i(0))$ will retain this feature, i.e. $\left|z_j^i(t)\right| \le g(\dot{x}_j^i) \quad \forall t \ge 0$. If $0 \le z_j^i(0) \le g(\dot{x}_j^i(0))$ for $\dot{x}_j^i(t) > 0$, $z_j^i(t)$ will increase until it is equal to $g(\dot{x}_j^i(t))$; thus $\dot{x}_j^i(t) z_j^i(t) \ge 0$. If $0 \ge z_j^i(0) \ge -g(\dot{x}_j^i(0))$ for $\dot{x}_j^i(t) < 0$, $z_j^i(t)$ will decrease until it reaches - $g(\dot{x}_j^i(t))$; thus $\dot{x}_j^i(t) z_j^i(t) \ge 0$. If the sign of $\dot{x}_j^i(t)$ changes; it always can be broken down and falls in one or the other scenario. It is then concluded that:

$$\dot{x}_j^i(t) z_j^i(t) \geq 0 \quad \forall t \geq 0 \tag{5.12}$$

Physically, equation (5.12) means that the deflection of the bristles represented by $z_j^i(t)$ follows the direction of the relative velocity. Now using equation (2.32), the following can be obtained:

$$\dot{x}_j^i F_{fr,j}^i = \dot{x}_j^i \sigma_{0,j}^i z_j^i + \sigma_{1,j}^i \left(\left| \dot{x}_j^i \right|^2 - \frac{\left| \dot{x}_j^i \right| \dot{x}_j^i}{g(\dot{x}_j^i)} z_j^i \right) + \sigma_{2,j}^i \left| \dot{x}_j^i \right|^2 \tag{5.13}$$

Inequalities (5.10) and (5.12) are employed to arrive at

$$\dot{x}_j^i F_{fr,j}^i \geq 0 \tag{5.14}$$

which is to say, $-\sum\sum \dot{x}_j^i F_{fr,j}^i \leq 0$. Thus, the time derivative of Lyapunov candidate remains semi negative-definite with the LuGre friction model, and the regulating control system remains stable in the presence of friction.

As for the other regulating controllers previously developed in Section 3.2.1 and Section 3.1.1, proof of system stability in the presence of friction can be adopted in similar procedures and will not be repeated here. The stability of the track control system will not be analyzed here. Instead, the controller will be redesigned in the next chapters.

5.5 Summary

This chapter studied the effect of dry friction in the hydraulic actuators for the controllers developed previously for ideal robot systems with no friction. The performance of the controllers was re-examined. It was found that the regulating control system was stable and able to achieve the desired position. However, the presence of friction could make regulation longer and bring about undesirable internal forces. It was also found that the use of force feedback could bring the internal force close to the desired values in both regulating and tracking tasks.

For the position tracking control system, the stability was not proven with the same scalar function. Both position error and internal force could be significantly increased because of friction. Simulations were further carried out to verify these findings. Presented in the following chapters, friction compensation will be considered in the continued development of the controller.

Chapter 6 Tracking Control of Co-operating Hydraulic Manipulators in the Presence of Friction

This chapter describes development of a tracking controller for multiple hydraulic manipulators in the presence of substantial dry frictions at the actuators. It was previously discussed that friction could not only degrade the position tracking performance, but also bring about undesirable internal force exerted on the object. The importance of compensation for friction force was therefore established. This chapter presents a controller with friction compensation. The friction is estimated, based on the LuGre dynamic friction model. The acceleration observer is redesigned to accommodate the inclusion of the dynamic friction model in the actuator system. The issues of load sharing between the hydraulic robots, unknown payload and uncertainty on the manipulators' dynamics, as well as hydraulic parameters, are all addressed.

6.1 Controller Design with Acceleration Feedback

Using the LuGre friction model, the dynamic equation of motion for the entire robots-object system described in Chapter 2 can be further written as follows:

$$M(X)\ddot{X} + D(X,\dot{X})\dot{X} + \boldsymbol{J}_a[\boldsymbol{\sigma}_{12}]\boldsymbol{J}_a^T\dot{X} + G(X) = \boldsymbol{J}_a(\boldsymbol{F} - [\boldsymbol{\sigma}_0]\boldsymbol{z} + [\boldsymbol{\sigma}_1][\frac{|\dot{\boldsymbol{x}}|}{g(\dot{\boldsymbol{x}})}]\boldsymbol{z}) \tag{6.1}$$

$$\dot{\boldsymbol{F}} = \boldsymbol{A}_{cq}(\boldsymbol{q})\boldsymbol{U} - \boldsymbol{A}_{ca}(\boldsymbol{q},\dot{\boldsymbol{q}}) \tag{6.2}$$

$$\dot{\boldsymbol{z}} = \dot{\boldsymbol{x}} - [\frac{|\dot{\boldsymbol{x}}|}{g(\dot{\boldsymbol{x}})}]\boldsymbol{z} \tag{6.3}$$

where $[\frac{|\dot{\boldsymbol{x}}|}{g(\dot{\boldsymbol{x}})}]$ is defined as a diagonal matrix with terms $\frac{|\dot{x}_j^i|}{g(\dot{x}_j^i)}$ as its diagonal elements. $\boldsymbol{z}$ is a vector of the friction internal states z_j^i. $[\boldsymbol{\sigma}_0]$, $[\boldsymbol{\sigma}_1]$, and $[\boldsymbol{\sigma}_2]$ are diagonal matrices with $\boldsymbol{\sigma}_0$, $\boldsymbol{\sigma}_1$, and $\boldsymbol{\sigma}_2$ being vectors of diagonal elements of friction force parameters $\sigma_{0,j}^i$, $\sigma_{1,j}^i$, and $\sigma_{2,j}^i$. $[\boldsymbol{\sigma}_{12}] = [\boldsymbol{\sigma}_1] + [\boldsymbol{\sigma}_2]$ and $\boldsymbol{J}_a = E^T\boldsymbol{W}\boldsymbol{J}^{-T}\bar{\boldsymbol{J}}$. Other variables have been defined in Chapter 2.

Similar to equation (2.44), the following can be obtained

$$M(X)\ddot{X} + D(X,\dot{X})\dot{X} + \boldsymbol{J}_a[\boldsymbol{\sigma}_{12}]\boldsymbol{J}_a^T\dot{X} + G(X) = \Theta(X,\dot{X},\ddot{X})\theta \tag{6.4}$$

Equation (6.4) will be used to compensate for the unknown dynamic parameter vector, θ, which includes dynamic parameters of the manipulators and a combined parameter $\boldsymbol{\sigma}_{12}$ (equal to $\boldsymbol{\sigma}_1 + \boldsymbol{\sigma}_2$). Let $\hat{\boldsymbol{\sigma}}_0, \hat{\boldsymbol{\sigma}}_1$ and $\hat{\boldsymbol{\sigma}}_{12}$ be estimates of $\boldsymbol{\sigma}_0, \boldsymbol{\sigma}_1$ and $\boldsymbol{\sigma}_{12}$, respectively. Also, let $\hat{\boldsymbol{z}}_0$ and $\hat{\boldsymbol{z}}_1$ be two estimates of $\boldsymbol{z}$. $\tilde{\boldsymbol{\sigma}}_0 = \hat{\boldsymbol{\sigma}}_0 - \boldsymbol{\sigma}_0$, $\tilde{\boldsymbol{\sigma}}_1 = \hat{\boldsymbol{\sigma}}_1 - \boldsymbol{\sigma}_1$, $\tilde{\boldsymbol{z}}_0 = \hat{\boldsymbol{z}}_0 - \boldsymbol{z}$ and $\tilde{\boldsymbol{z}}_1 = \hat{\boldsymbol{z}}_1 - \boldsymbol{z}$ are errors between the estimates and the actual values. $\hat{\theta}, \tilde{\theta}, \hat{\varphi}$, and $\tilde{\varphi}$ have been defined earlier in Section 4.1. Additionally, the following notations are defined:

$$e = X - X^d \tag{6.5}$$

$$\dot{X}_r = \dot{X}^d - \lambda e \tag{6.6}$$

$$s = \dot{e} + \lambda e \tag{6.7}$$

where, X^d is the desired value of X and belongs to C^3. λ is a diagonal matrix.

***Proposition* 1:**

Consider the system described by equations (6.1)-(6.3). Given the following controller

$$\boldsymbol{U} = \hat{\boldsymbol{A}}_{cq}^{-1}(\boldsymbol{q})\left(\hat{\boldsymbol{A}}_{ca}(\boldsymbol{q},\dot{\boldsymbol{q}}) + \dot{\boldsymbol{F}}^d - \Gamma_F^{-1}\boldsymbol{J}_a^T s - K_F\tilde{\boldsymbol{F}}\right) \tag{6.8}$$

where

$$\tilde{\boldsymbol{F}} = \boldsymbol{F} - \boldsymbol{F}^d \tag{6.9}$$

$$\boldsymbol{F}^d = \bar{\boldsymbol{J}}^{-1}\boldsymbol{J}^T(\boldsymbol{W}^{\dagger}E^{-T}\tau^d + \boldsymbol{V}F_{\text{int}}^d) + \hat{\boldsymbol{F}}_{fc} \tag{6.10}$$

$$\hat{\boldsymbol{F}}_{fc} = [\hat{\boldsymbol{\sigma}}_0]\hat{\boldsymbol{z}}_0 - [\hat{\boldsymbol{\sigma}}_1][\frac{|\dot{\boldsymbol{x}}|}{g(\dot{\boldsymbol{x}})}]\hat{\boldsymbol{z}}_1 \tag{6.11}$$

$$\tau^d = \hat{M}(X)\ddot{X}_r + \hat{D}(X,\dot{X}_r)\dot{X}_r + \boldsymbol{J}_a[\hat{\boldsymbol{\sigma}}_{12}]\boldsymbol{J}_a^T\dot{X}_r + \hat{G}(X) - K_d s \tag{6.12}$$

and the following adaptation laws for unknown parameters pertaining to the manipulators-object dynamics, hydraulic functions and friction parameters,

$$\dot{\hat{\theta}} = -\Gamma_\theta^{-1}\Theta^T(X,\dot{X}_r,\ddot{X}_r)s \tag{6.13}$$

$$\dot{\hat{\varphi}} = \Gamma_\varphi^{-1}\Phi^T(\boldsymbol{q},\dot{\boldsymbol{q}},\boldsymbol{U})\Gamma_F\tilde{\boldsymbol{F}} \tag{6.14}$$

$$\dot{\hat{\boldsymbol{\sigma}}}_0 = -\Gamma_{\sigma_0}^{-1}[\hat{\boldsymbol{z}}_0]\boldsymbol{J}_a^T s \tag{6.15}$$

$$\dot{\hat{\boldsymbol{\sigma}}}_1 = \Gamma_{\sigma_1}^{-1}[\frac{|\dot{\boldsymbol{x}}|}{g(\dot{\boldsymbol{x}})}][\hat{\boldsymbol{z}}_1]\boldsymbol{J}_a^T s \tag{6.16}$$

and the following observers for $\boldsymbol{z}$

$$\dot{\hat{\boldsymbol{z}}}_0 = \dot{\boldsymbol{x}} - [\frac{|\dot{\boldsymbol{x}}|}{g(\dot{\boldsymbol{x}})}]\hat{\boldsymbol{z}}_0 - \Gamma_{z_0}^{-1}\boldsymbol{J}_a^T s \tag{6.17}$$

$$\dot{\hat{\boldsymbol{z}}}_1 = \dot{\boldsymbol{x}} - [\frac{|\dot{\boldsymbol{x}}|}{g(\dot{\boldsymbol{x}})}]\hat{\boldsymbol{z}}_1 + [\frac{|\dot{\boldsymbol{x}}|}{g(\dot{\boldsymbol{x}})}]\Gamma_{z_1}^{-1}\boldsymbol{J}_a^T s \tag{6.18}$$

then the position tracking error converges to zero.

Remarks 6.1.1:

(i) $\hat{M}, \hat{D}, \hat{G}$ and $[\hat{\boldsymbol{\sigma}}_{12}]$, are estimated dynamic matrices/vectors based on $\hat{\theta}$ given in equation (6.4). Similarly, matrices $\hat{\boldsymbol{A}}_{ca}$ and $\hat{\boldsymbol{A}}_{cq}$ are estimations based on parameter estimation vector $\hat{\varphi}$ from equation (2.50).

(ii) $[\hat{\boldsymbol{z}}_0]$ and $[\hat{\boldsymbol{z}}_1]$, are diagonal matrices with $\hat{\boldsymbol{z}}_0$, and $\hat{\boldsymbol{z}}_1$ as their diagonal elements, respectively.

(iii) All gains used in the controller and observers, $\Gamma_F, \mathrm{K}_F, \mathrm{K}_d, \Gamma_\theta, \Gamma_\varphi, \Gamma_{\sigma_0}, \Gamma_{\sigma 1}, \Gamma_{z0}, \Gamma_{z1}$, are constant positive definite diagonal matrices.

(iv) The friction force, appearing in equation (6.1), which can be represented by $\boldsymbol{J}_a[\boldsymbol{\sigma}_{12}]\boldsymbol{J}_a^T\dot{X} + \boldsymbol{J}_a([\boldsymbol{\sigma}_0]\boldsymbol{z} - [\boldsymbol{\sigma}_1][\frac{|\dot{\boldsymbol{x}}|}{g(\dot{\boldsymbol{x}})}]\boldsymbol{z})$, is compensated for separately. The first term $\boldsymbol{J}_a[\boldsymbol{\sigma}_{12}]\boldsymbol{J}_a^T\dot{X}$ represents the combined damping and viscous friction and does not contain any friction states. Therefore, it is combined with the manipulator dynamics and compensated for via the adaptation law for unknown manipulators-object parameters.

The second term, $\boldsymbol{J}_a([\boldsymbol{\sigma}_0]\boldsymbol{z} - [\boldsymbol{\sigma}_1][\frac{|\dot{\boldsymbol{x}}|}{g(\dot{\boldsymbol{x}})}]\boldsymbol{z})$, represents the Coulomb (dry) friction effect which is herewith termed $\boldsymbol{F}_{fc}$. It is compensated for, by the estimate $\hat{\boldsymbol{F}}_{fc}$, which requires estimates of internal friction states.

Proof:

Define a scalar function as

$$\mathrm{V}_2 = \mathrm{V}_1 + \tfrac{1}{2}\widetilde{\boldsymbol{F}}^T\Gamma_F\widetilde{\boldsymbol{F}} + \tfrac{1}{2}\widetilde{\varphi}^T\Gamma_\varphi\widetilde{\varphi} \tag{6.19}$$

and

$$\mathrm{V}_1 = \tfrac{1}{2}\{s^T M(X)s + \widetilde{\theta}^T\Gamma_\theta\widetilde{\theta} + \widetilde{\boldsymbol{\sigma}}_0^T\Gamma_{\sigma_0}\widetilde{\boldsymbol{\sigma}}_0 + \widetilde{\boldsymbol{\sigma}}_1^T\Gamma_{\sigma_1}\widetilde{\boldsymbol{\sigma}}_1 + \widetilde{z}_0^T\Gamma_{z_0}[\boldsymbol{\sigma}_0]\widetilde{z}_0 + \widetilde{z}_1^T\Gamma_{z_1}[\boldsymbol{\sigma}_1]\widetilde{z}_1\} \tag{6.20}$$

Equations (6.1) and (6.12) are employed to arrive at the following error dynamics

$$\begin{aligned} M(X)\dot{s} + D(X,\dot{X})s = \Theta(X,\dot{X}_r,\ddot{X}_r)\widetilde{\theta} - K_d s - \boldsymbol{J}_a[\boldsymbol{\sigma}_{12}]\boldsymbol{J}_a^T s + \boldsymbol{J}_a^T\widetilde{\boldsymbol{F}} \\ + \boldsymbol{J}_a^T[([\hat{\boldsymbol{\sigma}}_0]\hat{z}_0 - [\boldsymbol{\sigma}_0]z) - [\frac{|\dot{\boldsymbol{x}}|}{g(\dot{\boldsymbol{x}})}]([\hat{\boldsymbol{\sigma}}_1]\hat{z}_1 - [\boldsymbol{\sigma}_1]z)] \end{aligned} \tag{6.21}$$

It can then be shown that time derivative of V_1 is

$$\begin{aligned} \dot{\mathrm{V}}_1 = -s^T K_d s - s^T\boldsymbol{J}_a[\boldsymbol{\sigma}_{12}]\boldsymbol{J}_a^T s + s^T\boldsymbol{J}_a\widetilde{\boldsymbol{F}} + [\dot{\widetilde{\theta}}^T\Gamma_\theta + s^T\Theta(X,\dot{X}_r,\ddot{X}_r)]\widetilde{\theta} \\ + s^T\boldsymbol{J}_a^T[([\hat{\boldsymbol{\sigma}}_0]\hat{z}_0 - [\boldsymbol{\sigma}_0]z) - \frac{|\dot{\boldsymbol{x}}|}{g(\dot{\boldsymbol{x}})}([\hat{\boldsymbol{\sigma}}_1]\hat{z}_1 - [\boldsymbol{\sigma}_1]z)] + \dot{\hat{\boldsymbol{\sigma}}}_0^T\Gamma_{\sigma_0}\widetilde{\boldsymbol{\sigma}}_0 + \dot{\hat{\boldsymbol{\sigma}}}_1^T\Gamma_{\sigma_1}\widetilde{\boldsymbol{\sigma}}_1 + \dot{\widetilde{z}}_0^T\Gamma_{z_0}[\boldsymbol{\sigma}_0]\widetilde{z}_0 + \dot{\widetilde{z}}_1^T\Gamma_{z_1}[\boldsymbol{\sigma}_1]\widetilde{z}_1 \end{aligned} \tag{6.22}$$

Substituting the manipulator parameter adaptation law (6.13) and employing relations $[\hat{\boldsymbol{\sigma}}_0]\hat{z}_0 - [\boldsymbol{\sigma}_0]z = [\hat{z}_0]\widetilde{\boldsymbol{\sigma}}_0 + [\boldsymbol{\sigma}_0]\widetilde{z}_0$ and $[\hat{\boldsymbol{\sigma}}_1]\hat{z}_1 - [\boldsymbol{\sigma}_1]z = [\hat{z}_1]\widetilde{\boldsymbol{\sigma}}_1 + [\boldsymbol{\sigma}_1]\widetilde{z}_1$, lead to

$$\begin{aligned} \dot{\mathrm{V}}_1 = -s^T K_d s - s^T\boldsymbol{J}_a[\boldsymbol{\sigma}_{12}]\boldsymbol{J}_a^T s + s^T\boldsymbol{J}_a\widetilde{\boldsymbol{F}} + s^T\boldsymbol{J}_a[([\hat{z}_0]\widetilde{\boldsymbol{\sigma}}_0 + [\boldsymbol{\sigma}_0]\widetilde{z}_0) - [\frac{|\dot{\boldsymbol{x}}|}{g(\dot{\boldsymbol{x}})}]([\hat{z}_1]\widetilde{\boldsymbol{\sigma}}_1 + [\boldsymbol{\sigma}_1]\widetilde{z}_1)] \\ + \dot{\hat{\boldsymbol{\sigma}}}_0^T\Gamma_{\sigma_0}\widetilde{\boldsymbol{\sigma}}_0 + \dot{\hat{\boldsymbol{\sigma}}}_1^T\Gamma_{\sigma_1}\widetilde{\boldsymbol{\sigma}}_1 + \dot{\widetilde{z}}_0^T\Gamma_{z_0}[\boldsymbol{\sigma}_0]\widetilde{z}_0 + \dot{\widetilde{z}}_1^T\Gamma_{z_1}[\boldsymbol{\sigma}_1]\widetilde{z}_1 \end{aligned} \tag{6.23}$$

From friction state observers (6.17) and (6.18), one arrives at

$$\dot{\tilde{z}}_0 = [\frac{|\dot{x}|}{g(\dot{x})}]\tilde{z}_0 - \Gamma_{z_0}^{-1} \boldsymbol{J}_a^T s \tag{6.24}$$

$$\dot{\tilde{z}}_1 = \dot{x} - [\frac{|\dot{x}|}{g(\dot{x})}]\tilde{z}_1 + [\frac{|\dot{x}|}{g(\dot{x})}]\Gamma_{z_1}^{-1} \boldsymbol{J}_a^T s \tag{6.25}$$

Applying equations (6.24) and (6.25), and the unknown friction force parameter adaptation laws (6.15) and (6.16), results in

$$\dot{\mathrm{V}}_1 = -s^T K_d s - s^T \boldsymbol{J}_a [\boldsymbol{\sigma}_{12}] \boldsymbol{J}_a^T s + s^T \boldsymbol{J}_a \tilde{\boldsymbol{F}} - \tilde{z}_0^T [\frac{|\dot{x}|}{g(\dot{x})}][\boldsymbol{\sigma}_0]\Gamma_{z0}\tilde{z}_0 - \tilde{z}_1^T [\frac{|\dot{x}|}{g(\dot{x})}][\boldsymbol{\sigma}_1]\Gamma_{z1}\tilde{z}_1 \tag{6.26}$$

Since

$$\hat{\boldsymbol{A}}_{cq}(q)\boldsymbol{U} - \hat{\boldsymbol{A}}_{ca}(\boldsymbol{q}, \dot{\boldsymbol{q}}) = \Phi(\boldsymbol{q}, \dot{\boldsymbol{q}}, \boldsymbol{U})\hat{\varphi} \tag{6.27}$$

the hydraulic dynamics in equation (6.2) can be rewritten as

$$\dot{\boldsymbol{F}} = \hat{\boldsymbol{A}}_{cq}(\boldsymbol{q})\boldsymbol{U} - \hat{\boldsymbol{A}}_{ca}(\boldsymbol{q}, \dot{\boldsymbol{q}}) - \Phi(\boldsymbol{q}, \dot{\boldsymbol{q}}, \boldsymbol{U})\tilde{\varphi} \tag{6.28}$$

Given equation (6.28), the time derivative of the scalar function V_2, becomes

$$\dot{\mathrm{V}}_2 = \dot{\mathrm{V}}_1 + (\hat{\boldsymbol{A}}_{cq}\boldsymbol{U} - \hat{\boldsymbol{A}}_{ca} - \dot{\boldsymbol{F}}^d)^T \Gamma_F \tilde{\boldsymbol{F}} + \tilde{\varphi}^T (\Gamma_\varphi \dot{\tilde{\varphi}} - \Phi^T \Gamma_F \tilde{\boldsymbol{F}}) \tag{6.29}$$

By substituting adaptation law (6.14) of unknown hydraulic parameters and the controller (6.8) into equation (6.29), the derivative of the scalar function V_2, will be

$$\dot{\mathrm{V}}_2 = -s^T K_d s - s^T \boldsymbol{J}_a [\boldsymbol{\sigma}_{12}] \boldsymbol{J}_a^T s - \tilde{\boldsymbol{F}}^T K_F \Gamma_F \tilde{\boldsymbol{F}} - \tilde{z}_0^T [\frac{|\dot{x}|}{g(\dot{x})}][\boldsymbol{\sigma}_0]\Gamma_{z0}\tilde{z}_0 - \tilde{z}_1^T [\frac{|\dot{x}|}{g(\dot{x})}][\boldsymbol{\sigma}_1]\Gamma_{z1}\tilde{z}_1 \tag{6.30}$$

Thus, V_2 is semi negative-definite. It follows that $0 \le \mathrm{V}_2 \le \mathrm{V}_2(0)$, meaning all states are bounded. Using Barbalat's lemma arrives at $s \to 0$ which implies that the position and velocity tracking errors converge to zero as $t \to \infty$.

Remarks 6.1.2:

In realization of controller (6.8), one needs to compute $\dot{\boldsymbol{F}}^d$, which is a function of $\ddot{X}$. Accelerations then appear in the proposed control law. The requirement for measurement of accelerations as a feedback, which could be difficult in many practical situations, is removed in the following section.

6.2 Controller Design without Acceleration Feedback

The requirement for measurement of joint angular accelerations is removed by the addition of a nonlinear acceleration observer in the feedback loop. Compared with the previous observers in Chapter 4, the observers, including acceleration observer in the feedback loop, have to be redesigned to accommodate the addition of the LuGre dynamic friction model into the hydraulic actuator dynamics. The following notations are defined:

$$e = X - X^d \tag{6.31}$$

$$\widetilde{X} = X - \hat{X} \tag{6.32}$$

$$\dot{X}_r = \dot{X}^d - \lambda_1(\hat{X} - X^d) = \dot{X}^d - \lambda_1(e - \widetilde{X}) \tag{6.33}$$

$$\dot{X}_o = \dot{\hat{X}} - \lambda_2(X - \hat{X}) = \dot{\hat{X}} - \lambda_2\widetilde{X} \tag{6.34}$$

$$s_1 = \dot{X} - \dot{X}_r = \dot{e} + \lambda_1(e - \widetilde{X}) \tag{6.35}$$

$$s_2 = \dot{X} - \dot{X}_o = \dot{\widetilde{X}} + \lambda_2\widetilde{X} \tag{6.36}$$

$$\dot{\boldsymbol{x}}_r = \boldsymbol{J}_a^T \dot{X}_r \tag{6.37}$$

Vectors X^d and $\hat{X}$ are the desired and estimated values of X, respectively. λ_1 and λ_2, are positive definite diagonal matrices. X^d belongs to C^3.

Proposition:

Consider the system described by equations (6.1), (6.2), and (6.3). Given the following observers and adaptation laws:

(i) <u>Acceleration observer</u>

$$\ddot{X}_o = \hat{M}^{-1}[\boldsymbol{J}_a(\boldsymbol{F} - \hat{\boldsymbol{F}}_{fc}) - \hat{D}(X,\dot{X})\dot{X}_o - \hat{G}(X) + L_p\widetilde{X} + K_d s_1 + K_d^{'} s_2] \tag{6.38}$$

where

$$\hat{\boldsymbol{F}}_{fc} = [\hat{\boldsymbol{\sigma}}_0]\hat{\boldsymbol{z}}_0 - [\hat{\boldsymbol{\sigma}}_1][\frac{|\dot{\boldsymbol{x}}|}{g(\dot{\boldsymbol{x}})}]\hat{\boldsymbol{z}}_1 \tag{6.39}$$

(ii) <u>Unknown manipulators-object dynamic parameter adaptation law</u>

$$\dot{\hat{\theta}} = -\Gamma_\theta^{-1}[\Theta_1^T(X,\dot{X}_r,\ddot{X}_r)s_1 + \Theta_2^T(X,\dot{X},\dot{X}_o,\ddot{X}_o)s_2] \tag{6.40}$$

where

$$\Theta_1(X,\dot{X}_r,\ddot{X}_r)\hat{\theta} = \hat{M}(X)\ddot{X}_r + \hat{D}(X,\dot{X}_r)\dot{X}_r + \boldsymbol{J}_a[\hat{\boldsymbol{\sigma}}_{12}]\boldsymbol{J}_a^T\dot{X}_r + \hat{G}(X) \tag{6.41}$$

$$\Theta_2(X,\dot{X},\dot{X}_o,\ddot{X}_o)\hat{\theta} = \hat{M}(X)\ddot{X}_o + \hat{D}(X,\dot{X})\dot{X}_o + \boldsymbol{J}_a[\hat{\boldsymbol{\sigma}}_{12}]\boldsymbol{J}_a^T\dot{X}_o + \hat{G}(X) \tag{6.42}$$

(iii) <u>Unknown hydraulic function parameter adaptation law</u>

$$\dot{\hat{\varphi}} = \Gamma_\varphi^{-1}\Phi^T(\boldsymbol{q},\dot{\boldsymbol{q}},\boldsymbol{U})\Gamma_F\widetilde{\boldsymbol{F}} \tag{6.43}$$

(iv) <u>Unknown friction parameter adaptation law</u>

$$\dot{\hat{\boldsymbol{\sigma}}}_0 = -\Gamma_{\sigma_0}^{-1}[\hat{\boldsymbol{z}}_0]\boldsymbol{J}_a^T(s_1+s_2) \tag{6.44}$$

$$\dot{\hat{\boldsymbol{\sigma}}}_1 = \Gamma_{\sigma_1}^{-1}[\hat{\boldsymbol{z}}_1]([\frac{|\dot{\boldsymbol{x}}_r|}{g(\dot{\boldsymbol{x}}_r)}]\boldsymbol{J}_a^T s_1 + [\frac{|\dot{\boldsymbol{x}}|}{g(\dot{\boldsymbol{x}})}]\boldsymbol{J}_a^T s_2) \tag{6.45}$$

(v) <u>Friction internal state observers</u>

$$\dot{\hat{\boldsymbol{z}}}_0 = \dot{\boldsymbol{x}} - \frac{|\dot{\boldsymbol{x}}|}{g(\dot{\boldsymbol{x}})}\hat{\boldsymbol{z}}_0 - \Gamma_{z_0}^{-1}\boldsymbol{J}_a^T(s_1+s_2) \tag{6.46}$$

$$\dot{\hat{\boldsymbol{z}}}_1 = \dot{\boldsymbol{x}} - \frac{|\dot{\boldsymbol{x}}|}{g(\dot{\boldsymbol{x}})}\hat{\boldsymbol{z}}_1 + \Gamma_{z_1}^{-1}([\frac{|\dot{\boldsymbol{x}}_r|}{g(\dot{\boldsymbol{x}}_r)}]\boldsymbol{J}_a^T s_1 + [\frac{|\dot{\boldsymbol{x}}|}{g(\dot{\boldsymbol{x}})}]\boldsymbol{J}_a^T s_2) \tag{6.47}$$

and the following controller

$$\boldsymbol{U} = \hat{\boldsymbol{A}}_{cq}^{-1}(\boldsymbol{q})\left(\hat{\boldsymbol{A}}_{ca}(\boldsymbol{q},\dot{\boldsymbol{q}}) + \dot{\boldsymbol{F}}^d - \Gamma_F^{-1}\boldsymbol{J}_a^T s_1 - K_F\widetilde{\boldsymbol{F}}\right) \tag{6.48}$$

where

$$\widetilde{\boldsymbol{F}} = \boldsymbol{F} - \boldsymbol{F}^d \tag{6.49}$$

$$\boldsymbol{F}^d = \overline{\boldsymbol{J}}^{-1}\boldsymbol{J}^T(\boldsymbol{W}^\dagger E^{-T}\tau^d + \boldsymbol{V}F_{\text{int}}^d) + \hat{\boldsymbol{F}}_{fc}^r \tag{6.50}$$

$$\begin{aligned}\tau^d &= \hat{M}(X)\ddot{X}_r + \hat{D}(X,\dot{X}_r)\dot{X}_r + \boldsymbol{J}_a[\boldsymbol{\sigma}_{12}]\boldsymbol{J}_a^T\dot{X}_r + \hat{G}(X) - K_d(s_1-s_2) - K_p e \\ &= \Theta_1(X,\dot{X}_r,\ddot{X}_r)\hat{\theta} - K_d(s_1-s_2) - K_p e\end{aligned} \tag{6.51}$$

$$\hat{\boldsymbol{F}}_{fc}^r = [\hat{\boldsymbol{\sigma}}_0]\hat{\boldsymbol{z}}_0 - [\hat{\boldsymbol{\sigma}}_1][\frac{|\dot{\boldsymbol{x}}_r|}{g(\dot{\boldsymbol{x}}_r)}]\hat{\boldsymbol{z}}_1 \tag{6.52}$$

providing the following conditions are satisfied

$$2\sqrt{\underline{\sigma}(\lambda_1 K_p)}\sqrt{\underline{\sigma}(\lambda_2 L_p)} > \overline{\sigma}(\lambda_1 K_p) \tag{6.53}$$

$$\|r(0)\| \leq \sqrt{\frac{\alpha_L}{2\alpha_U}\left[\frac{\underline{\sigma}(K_d)+\underline{\sigma}(\boldsymbol{J}_{\boldsymbol{a}}([\boldsymbol{\sigma}_{12}])\boldsymbol{J}_{\boldsymbol{a}}^T)-D_U\dot{X}_U^d-\eta}{D_U\overline{\sigma}(\lambda_1)}\right]^2+\frac{V_{pL}-V_{pU}}{\alpha_U}} \tag{6.54}$$

where $r(0)$ is the initial value of the state vector $r(t)=[e^T\ \tilde{X}^T\ s_1^T\ s_2^T\ \tilde{\boldsymbol{F}}^T\ \tilde{\boldsymbol{z}}_0^T\ \tilde{\boldsymbol{z}}_1^T]^T$, then the position tracking error, e, converges to zero with all other states being at least bounded.

Remarks 6.2.1:

(i) Parameters $\theta,\varphi,\boldsymbol{\sigma}_0$, and $\boldsymbol{\sigma}_1$ are assumed to be slow varying. They are considered as constants by the controller. $\hat{M},\hat{D},\hat{G}$ and $[\hat{\boldsymbol{\sigma}}_{12}]$ are estimated dynamic matrices/vectors based on $\hat{\theta}$ given in equation (6.4). Similarly matrices $\hat{\boldsymbol{A}}_{ca}$ and $\hat{\boldsymbol{A}}_{cq}$ are estimations based on parameter estimation vector $\hat{\varphi}$ from equation (2.50).

(ii) $[\hat{\boldsymbol{z}}_0]$ and $[\hat{\boldsymbol{z}}_1]$ are diagonal matrices with $\hat{\boldsymbol{z}}_0$, and $\hat{\boldsymbol{z}}_1$ as their diagonal elements, respectively.

(iii) All gains used in the controller, adaptation laws and observers, ($K_p, L_p, K_d, K_d^{'}, \Gamma_F, K_F, \Gamma_\varphi, \Gamma_\theta, \Gamma_{\sigma_0}, \Gamma_{\sigma 1}, \Gamma_{z_0}$, and Γ_{z1}) are constant positive definite diagonal matrices and F_{int}^d is the desired internal force.

(iv) In equations (6.43) and (6.54), $\underline{\sigma}$ (.) and $\overline{\sigma}$ (.) are the minimum and maximum singular values of their matrix argument, respectively. $\dot{X}_U^d$ is the upper bound on the norm of $\dot{X}^d$. Finally, η is defined by

$$\eta = \frac{\overline{\sigma}(\boldsymbol{J}_a[\boldsymbol{\sigma}_1][\boldsymbol{z}]\boldsymbol{J}_a^T)}{f_{sl,L}} \tag{6.55}$$

where $f_{sl,L}$ is the lower bound of the norm of the normalized slip frictions. $\alpha_L, \alpha_U, V_{pL}$ and V_{pU}, are positive constants defined as follows:

$$\alpha_L \|r\|^2 \le \tfrac{1}{2}\{s_1^T M(X)s_1 + s_2^T M(x)s_2 + e^T K_p e + \widetilde{X}^T L_p \widetilde{X} + \widetilde{\boldsymbol{F}}^T \Gamma_F \widetilde{\boldsymbol{F}} + \widetilde{z}_0^T \Gamma_{z_0}[\boldsymbol{\sigma}_0]\widetilde{z}_0 + \widetilde{z}_1^T \Gamma_{z_1}[\boldsymbol{\sigma}_1]\widetilde{z}_1\} \le \alpha_U \|r\|^2 \tag{6.56}$$

$$V_{pL} \le \tfrac{1}{2}\{\widetilde{\theta}^T \Gamma_\theta \widetilde{\theta} + \widetilde{\varphi}^T \Gamma_\pi \widetilde{\varphi} + \widetilde{\boldsymbol{\sigma}}_0^T \Gamma_{\sigma_0} \widetilde{\boldsymbol{\sigma}}_0 + \widetilde{\boldsymbol{\sigma}}_1^T \Gamma_{\sigma_1} \widetilde{\boldsymbol{\sigma}}_1\} \le V_{pU} \tag{6.57}$$

(v) The first part of the friction force $\boldsymbol{J}_a[\boldsymbol{\sigma}_{12}]\boldsymbol{J}_a^T \dot{X}$, which does not contain any friction states; is compensated for with the manipulator adaptation law, in a similar manner as in Section 6.1 for controller (6.8). However, the compensation for the remaining part $\boldsymbol{F}_{fc} = \boldsymbol{J}_a([\boldsymbol{\sigma}_0]\boldsymbol{z} - [\boldsymbol{\sigma}_1][\frac{|\dot{\boldsymbol{x}}|}{g(\dot{\boldsymbol{x}})}]\boldsymbol{z})$, in the calculation of the desired force $\boldsymbol{F}^d$, is different. With reference to equation (6.52), velocity $\dot{\boldsymbol{x}}$ is replaced with $\dot{\boldsymbol{x}}_r$, which does not contain any velocity terms. By inspection of equation (6.50), the desired force $\boldsymbol{F}^d$, does not contain any velocity terms either. The controller does not need acceleration feedback by equation (6.48). On the other hand the compensation, for the remaining part of the friction force in acceleration observer dynamics (6.38); directly uses velocity $\dot{\boldsymbol{x}}$, since equation (6.38) is not differentiated anywhere.

Proof:

Equations describing the entire control system are expressed in a state-space form as:

$$\dot{e} = s_1 - \lambda_1(e - \widetilde{X}) \tag{6.58}$$

$$\dot{\widetilde{X}} = s_2 - \lambda_2 \widetilde{X} \tag{6.59}$$

$$\begin{aligned}\dot{s}_1 = M^{-1}(X)\{&-D(X,\dot{X})s_1 + \Theta_1(X,\dot{X}_r,\ddot{X}_r)\widetilde{\theta} - K_d(s_1 - s_2) - K_p e - D(X,s_1)\dot{X}_r \\ &- \boldsymbol{J}_a[\boldsymbol{\sigma}_{12}]\boldsymbol{J}_a^T s_1 + \boldsymbol{J}_a\widetilde{\boldsymbol{F}} + \boldsymbol{J}_a([\hat{\boldsymbol{\sigma}}_0]\hat{z}_0 - [\boldsymbol{\sigma}_0]\boldsymbol{z}) \\ &- \boldsymbol{J}_a[\frac{|\dot{\boldsymbol{x}}_r|}{g(\dot{\boldsymbol{x}}_r)}]([\hat{\boldsymbol{\sigma}}_1]\hat{z}_1 - [\boldsymbol{\sigma}_1]\boldsymbol{z}) + \boldsymbol{J}_a([\frac{|\dot{\boldsymbol{x}}|}{g(\dot{\boldsymbol{x}})}] - [\frac{|\dot{\boldsymbol{x}}_r|}{g(\dot{\boldsymbol{x}}_r)}])[\boldsymbol{\sigma}_1]\boldsymbol{z}\}\end{aligned} \tag{6.60}$$

$$\begin{aligned}\dot{s}_2 = M^{-1}(X)\{&-D(X,\dot{X})s_2 + \Theta_2(X,\dot{X},\dot{X}_o,\ddot{X}_o)\widetilde{\theta} - K_d s_1 - K_d' s_2 - L_p\widetilde{X} \\ &- \boldsymbol{J}_a[\boldsymbol{\sigma}_{12}]\boldsymbol{J}_a^T s_2 + \boldsymbol{J}_a([\hat{\boldsymbol{\sigma}}_0]\hat{z}_0 - [\boldsymbol{\sigma}_0]\boldsymbol{z}) - \boldsymbol{J}_a[\frac{|\dot{\boldsymbol{x}}|}{g(\dot{\boldsymbol{x}})}]([\hat{\boldsymbol{\sigma}}_1]\hat{z}_1 - [\boldsymbol{\sigma}_1]\boldsymbol{z})\}\end{aligned} \tag{6.61}$$

$$\dot{\widetilde{\boldsymbol{F}}} = -\Gamma_F^{-1}\boldsymbol{J}_a^T s_1 - K_F\widetilde{\boldsymbol{F}} - \Phi(\boldsymbol{q},\dot{\boldsymbol{q}},\boldsymbol{U})\widetilde{\varphi} \tag{6.62}$$

$$\dot{\tilde{\boldsymbol{z}}}_0 = -[\frac{|\dot{\boldsymbol{x}}|}{g(\dot{\boldsymbol{x}})}]\tilde{\boldsymbol{z}}_0 - \Gamma_{z_0}^{-1}\boldsymbol{J}_a^T(s_1 + s_2) \tag{6.63}$$

$$\dot{\tilde{\boldsymbol{z}}}_1 = -[\frac{|\dot{\boldsymbol{x}}|}{g(\dot{\boldsymbol{x}})}]\tilde{\boldsymbol{z}}_1 + \Gamma_{z_1}^{-1}([\frac{|\dot{\boldsymbol{x}}_r|}{g(\dot{\boldsymbol{x}}_r)}]\boldsymbol{J}_a^T s_1 + [\frac{|\dot{\boldsymbol{x}}|}{g(\dot{\boldsymbol{x}})}]\boldsymbol{J}_a^T s_2) \tag{6.64}$$

$$\dot{\tilde{\theta}} = -\Gamma_\theta^{-1}[\Theta_1^T(X, \dot{X}_r, \ddot{X}_r)s_1 + \Theta_2^T(X, \dot{X}, \dot{X}_o, \ddot{X}_o)s_2] \tag{6.65}$$

$$\dot{\tilde{\varphi}} = \Gamma_\varphi^{-1}\Phi^T(\boldsymbol{q}, \dot{\boldsymbol{q}}, \boldsymbol{U})\Gamma_F\tilde{\boldsymbol{F}} \tag{6.66}$$

$$\dot{\tilde{\boldsymbol{\sigma}}}_0 = -\Gamma_{\sigma_0}^{-1}[\hat{\boldsymbol{z}}_0]\boldsymbol{J}_a^T(s_1 + s_2) \tag{6.67}$$

$$\dot{\tilde{\boldsymbol{\sigma}}}_1 = \Gamma_{\sigma_1}^{-1}[\hat{\boldsymbol{z}}_1]([\frac{|\dot{\boldsymbol{x}}_r|}{g(\dot{\boldsymbol{x}}_r)}]\boldsymbol{J}_a^T s_1 + [\frac{|\dot{\boldsymbol{x}}|}{g(\dot{\boldsymbol{x}})}]\boldsymbol{J}_a^T s_2) \tag{6.68}$$

From the above equations it is seen that if the system is initially at the origin, it will remain there; thus the origin is an equilibrium point. We now show that the above system has a manifold of equilibrium points to which the origin belongs. Consider the case where the state vectors $e, \tilde{X}, s_1, s_2, \tilde{\boldsymbol{F}}, \tilde{z}_0, \tilde{z}_1$ and $\tilde{\varphi}$ are zero, while state vectors $\tilde{\boldsymbol{\sigma}}_0, \tilde{\boldsymbol{\sigma}}_1$ and $\tilde{\theta}$ can be set arbitrarily. Setting the right-hand side of state-space equations (6.58) to (6.68) to zero, results in the following two vector equations:

$$\Theta_1\tilde{\theta} + \boldsymbol{J}_a[\tilde{\boldsymbol{\sigma}}_0]\boldsymbol{z} - \boldsymbol{J}_a[\frac{|\dot{\boldsymbol{x}}_r|}{g(\dot{\boldsymbol{x}}_r)}][\tilde{\boldsymbol{\sigma}}_1]\boldsymbol{z} = 0 \tag{6.69}$$

$$\Theta_2\tilde{\theta} + \boldsymbol{J}_a[\tilde{\boldsymbol{\sigma}}_0]\boldsymbol{z} - \boldsymbol{J}_a[\frac{|\dot{\boldsymbol{x}}|}{g(\dot{\boldsymbol{x}})}][\tilde{\boldsymbol{\sigma}}_1]\boldsymbol{z} = 0 \tag{6.70}$$

Vector equations (6.69) and (6.70) consist of 12 linear scalar equations but with more than 12 unknowns originating from state vectors $\tilde{\boldsymbol{\sigma}}_0$, $\tilde{\boldsymbol{\sigma}}_1$ and $\tilde{\theta}$. There are infinite solutions for the unknowns, indicating a manifold containing infinite non-isolated equilibrium points. Therefore, we can only resort to constructing a Lyapunov-like scalar function to show that all the states of the system under the proposed controller are bounded. Further, following Barbalat's lemma, we prove that the position tracking error converges to zero.

Consider a continuous positive-definite scalar function:

$$\mathrm{V}_2 = \mathrm{V}_1 + \tfrac{1}{2}\{\widetilde{\boldsymbol{F}}^T \Gamma_F \widetilde{\boldsymbol{F}} + \widetilde{\varphi}^T \Gamma_\varphi \widetilde{\varphi} + \widetilde{\boldsymbol{\sigma}}_0^T \Gamma_{\sigma_0} \widetilde{\boldsymbol{\sigma}}_0 + \widetilde{\boldsymbol{\sigma}}_1^T \Gamma_{\sigma_1} \widetilde{\boldsymbol{\sigma}}_1 + \widetilde{\boldsymbol{z}}_0^T \Gamma_{z_0} [\boldsymbol{\sigma}_0] \widetilde{\boldsymbol{z}}_0 + \widetilde{\boldsymbol{z}}_1^T \Gamma_{z_1} [\boldsymbol{\sigma}_1] \widetilde{\boldsymbol{z}}_1\} \quad (6.71)$$

where

$$\mathrm{V}_1 = \tfrac{1}{2}\{s_1^T M(X) s_1 + s_2^T M(x) s_2 + e^T K_p e + \widetilde{X}^T L_p \widetilde{X} + \widetilde{\theta}^T \Gamma \widetilde{\theta}\} \quad (6.72)$$

The time derivative of V_2 is

$$\begin{aligned}\dot{\mathrm{V}}_2 = & -s_1^T \boldsymbol{J_a}[\boldsymbol{\sigma}_{12}]\boldsymbol{J_a}^T s_1 - s_1^T K_d s_1 - s_1^T D(X, s_1)\dot{X}_r + s_1^T \boldsymbol{J_a}([\frac{|\dot{\boldsymbol{x}}|}{g(\dot{\boldsymbol{x}})}] - [\frac{|\dot{\boldsymbol{x}}_r|}{g(\dot{\boldsymbol{x}}_r)}])[\boldsymbol{\sigma}_1]\boldsymbol{z} \\ & - s_2^T \boldsymbol{J_a}[\boldsymbol{\sigma}_{12}]\boldsymbol{J_a}^T s_2 - \tfrac{1}{2} s_2^T K_d^{'} s_2 - e^T \lambda_1 K_p e - \widetilde{X}^T \lambda_2 L_p \widetilde{X} + \widetilde{X}^T \lambda_1 K_p e \\ & - \widetilde{\boldsymbol{z}}_0^T [\frac{|\dot{\boldsymbol{x}}|}{g(\dot{\boldsymbol{x}})}][\boldsymbol{\sigma}_0]\Gamma_{z0}\widetilde{\boldsymbol{z}}_0 - \widetilde{\boldsymbol{z}}_1^T [\frac{|\dot{\boldsymbol{x}}|}{g(\dot{\boldsymbol{x}})}][\boldsymbol{\sigma}_1]\Gamma_{z1}\widetilde{\boldsymbol{z}}_1 - \widetilde{\boldsymbol{F}}^T K_F \Gamma_F \widetilde{\boldsymbol{F}}\end{aligned} \quad (6.73)$$

Since $\left\| [\frac{|\dot{\boldsymbol{x}}|}{g(\dot{\boldsymbol{x}})}] - [\frac{|\dot{\boldsymbol{x}}_r|}{g(\dot{\boldsymbol{x}}_r)}] \right\| \le \frac{\|\dot{\boldsymbol{x}} - \dot{\boldsymbol{x}}_r\|}{F_{sl,L}} = \frac{\|\boldsymbol{J}_a^T s_1\|}{F_{sl,L}}$, one arrives at

$$s_1^T \boldsymbol{J_a}([\frac{|\dot{\boldsymbol{x}}|}{g(\dot{\boldsymbol{x}})}] - [\frac{|\dot{\boldsymbol{x}}_r|}{g(\dot{\boldsymbol{x}}_r)}])[\boldsymbol{\sigma}_1]\boldsymbol{z} \le \frac{\overline{\sigma}(\boldsymbol{J}_a[\boldsymbol{\sigma}_1][z]\boldsymbol{J}_a^T)\|s_1\|^2}{F_{sl,L}} = \eta \|s_1\|^2 \quad (6.74)$$

Thus,

$$\begin{aligned}\dot{\mathrm{V}}_2 \le & -(\underline{\sigma}(K_d) + \underline{\sigma}(\boldsymbol{J_a}[\boldsymbol{\sigma}_{12}]\boldsymbol{J_a}^T) - D_U(\dot{X}_U^d + \overline{\sigma}(\lambda_1)(\|e\| + \|\widetilde{X}\|)) - \eta)\|s_1\|^2 \\ & - (\underline{\sigma}(K_d^{'}) + \underline{\sigma}(\boldsymbol{J_a}[\boldsymbol{\sigma}_{12}]\boldsymbol{J_a}^T))\|s_2\|^2 \\ & - (\sqrt{\underline{\sigma}(\lambda_1 K_p)}\|e\| - \sqrt{\underline{\sigma}(\lambda_2 L_p)}\|\widetilde{X}\|)^2 - (2\sqrt{\underline{\sigma}(\lambda_1 K_p)}\sqrt{\underline{\sigma}(\lambda_2 L_p)} - \overline{\sigma}(\lambda_1 K_p))\|e\|\|\widetilde{X}\| \\ & - \widetilde{\boldsymbol{z}}_0^T [\frac{|\dot{\boldsymbol{x}}|}{g(\dot{\boldsymbol{x}})}][\boldsymbol{\sigma}_0]\Gamma_{z0}\widetilde{\boldsymbol{z}}_0 - \widetilde{\boldsymbol{z}}_1^T [\frac{|\dot{\boldsymbol{x}}|}{g(\dot{\boldsymbol{x}})}][\boldsymbol{\sigma}_1]\Gamma_{z1}\widetilde{\boldsymbol{z}}_1 - \widetilde{\boldsymbol{F}}^T K_F \Gamma_F \widetilde{\boldsymbol{F}}\end{aligned}$$

(6.75)

Note that $(\|e\| + \|\widetilde{X}\|)^2 \le 2(\|e\|^2 + \|\widetilde{X}\|^2) \le 2\|r\|^2$ and $\|r\|^2 \le (\mathrm{V}_2 - \mathrm{V}_{pL})/\alpha_L$ which are arrived at from equations (6.56) and (6.57). To satisfy

$$\underline{\sigma}(K_d) + \underline{\sigma}(\boldsymbol{J_a}[\boldsymbol{\sigma}_{12}]\boldsymbol{J_a}^T) - D_M(\dot{X}_M^d + \overline{\sigma}(\lambda_1)(\|e\| + \|\widetilde{X}\|)) - \eta > 0 \quad (6.76)$$

a sufficient condition is

$$\mathrm{V}_2 \le \frac{\alpha_L}{2}\left[\frac{\underline{\sigma}(K_d)+\underline{\sigma}(\boldsymbol{J_a}[\boldsymbol{\sigma}_{12}]\boldsymbol{J_a}^T)-D_U\dot{X}_U^d-\eta}{D_U\overline{\sigma}(\lambda_1)}\right]^2+V_{pL} \tag{6.77}$$

From equation (6.75), the conditions (6.53) and (6.77) guarantee that (note that $\alpha > 0$)

$$\dot{\mathrm{V}}_2 \le -\alpha(\|e\|^2+\|\widetilde{X}\|^2+\|s_1\|^2+\|s_2\|^2+\|\widetilde{\boldsymbol{F}}\|^2)-\widetilde{\boldsymbol{z}}_0^T[\frac{|\dot{\boldsymbol{x}}|}{g(\dot{\boldsymbol{x}})}][\boldsymbol{\sigma}_0]\Gamma_{z0}\widetilde{\boldsymbol{z}}_0-\widetilde{\boldsymbol{z}}_1^T[\frac{|\dot{\boldsymbol{x}}|}{g(\dot{\boldsymbol{x}})}][\boldsymbol{\sigma}_1]\Gamma_{z1}\widetilde{\boldsymbol{z}}_1 \tag{6.78}$$

Inequality (6.78) guarantees $\mathrm{V}_2 \le \mathrm{V}_2(0)$. Thus, a sufficient condition for (6.77) is

$$\mathrm{V}_2(0) \le \frac{\alpha_L}{2}\left[\frac{\underline{\sigma}(K_d)+\underline{\sigma}(\boldsymbol{J_a}[\boldsymbol{\sigma}_{12}]\boldsymbol{J_a}^T)-D_U\dot{X}_U^d-\eta}{D_U\overline{\sigma}(\lambda_1)}\right]^2+V_{pL} \tag{6.79}$$

which can be satisfied following inequality (6.54) and $\mathrm{V}_2 \le \alpha_U\|r\|^2+V_{pU}$ that can be derived from inequalities (6.56) and 6.57).

The above analysis shows that (6.78) is satisfied under conditions (6.53) and (6.54). The right hand side of (6.78) is also semi-negative. Thus, $\mathrm{V}_2 \le \mathrm{V}_2(0)$, meaning states in $r(t)$ are bounded. Using Barbalat's lemma, inspection of (6.71) and (6.78) reveals that the tracking errors $e, \widetilde{X}, s_1, s_2$ and $\widetilde{\boldsymbol{F}}$ approach zero as $t \to \infty$. Furthermore, since $s_1 = \dot{e}+\lambda_1(e-\widetilde{X})$, the velocity tracking error $\dot{e}$, also converges to zero. Additionally, inspection of term $-\widetilde{\boldsymbol{z}}_0^T[\frac{|\dot{\boldsymbol{x}}|}{g(\dot{\boldsymbol{x}})}][\boldsymbol{\sigma}_0]\Gamma_{z0}\widetilde{\boldsymbol{z}}_0-\widetilde{\boldsymbol{z}}_1^T[\frac{|\dot{\boldsymbol{x}}|}{g(\dot{\boldsymbol{x}})}][\boldsymbol{\sigma}_1]\Gamma_{z1}\widetilde{\boldsymbol{z}}_1$ shows that this term is negative definite everywhere, except for instances in which $\dot{x}=0$. Thus, for tracking tasks with non-zero velocity trajectories, inequality (6.78) can be written as

$$\dot{\mathrm{V}}_2 \le -\alpha\|r\|^2 \tag{6.80}$$

and it can be further concluded that $\widetilde{\boldsymbol{z}}_0, \widetilde{\boldsymbol{z}}_1 \to 0$ as $t \to \infty$. Finally, from equation (6.75), inequality (6.78) shows that a local negative semi-definite upper bound on $\dot{\mathrm{V}}_2$ can be obtained. The size of the bounded region can be expanded by changing the values of control gains $\underline{\sigma}(K_d^{'})$, $\underline{\sigma}(K_d^{'})$ and $\underline{\sigma}(\lambda_2 L_p)$.

Remarks 6.2.2:

(i) The parameter estimates, however, do not necessarily converge to their exact values. In general, parameter convergence to true values can be potentially achieved if the desired trajectory is "sufficiently rich" (Slotine and Li, 1991). Additionally, it is desirable to keep parameter estimates within bounded sets. This is particularly important since if the estimates of some parameters, such as $\beta_j^i k_j^i k_{sp,j}^i$, approach zero, the inverse of the estimated matrix $\hat{A}_{cq}(q)$ in (6.48) becomes very large and the control signal saturates. An intuitively motivated procedure (Slotine and Li, 1991) is to stop updating parameter estimates when they reach their assigned upper or lower bounds. Updating, resumes as soon as the corresponding derivatives change signs. The inclusion of this procedure, also termed discontinuous projection (Goodwin and Mayne, 1987), does not affect the stability proof presented above. The remarks presented here are also applicable for previously developed controllers that involve adaptation laws for unknown parameters. The inclusion of the discontinuous projection with the adaptation law is demonstrated in the next chapter.

(ii) With respect to controller (6.48), the only hydraulic parameters needed by the controller are the effective piston areas $\boldsymbol{A}_I$ and $\boldsymbol{A}_O$. Other hydraulic function parameters such as effective bulk modulus β or control valve gain K_{sp}, are all considered in the adaptation laws described in the proposed control strategy. Similarly, the control law requires no knowledge about mass or inertia of the manipulators' links or payload. The controller only needs knowledge about the length of the manipulators' links, since the Jacobian matrix appears in the control law.

(iii) The internal force is examined here for convergence to the desired value. The following can be obtained about the contact forces:

$$\boldsymbol{F}_c^{t\to\infty} = \boldsymbol{W}^{\dagger} E^{-T}\tau^d + VF_{\text{int}}^d - \boldsymbol{J}^{-T}[\boldsymbol{H}_m\ddot{\boldsymbol{q}}^d + \boldsymbol{C}_m\dot{\boldsymbol{q}}^d + \boldsymbol{G}_m + \bar{\boldsymbol{J}}(\boldsymbol{F}_{fc} - \hat{\boldsymbol{F}}_{fc}^r)] \qquad (6.81)$$

From equations (2.12), (2.13) and (6.81), it can then be proven that

$$F_{ext}^{t\to\infty} = W\boldsymbol{F}_c^{t\to\infty} = E^{-T}\tau^d - W\boldsymbol{J}^{-T}[\boldsymbol{H}_m\ddot{\boldsymbol{q}}^d + \boldsymbol{C}_m\dot{\boldsymbol{q}}^d + \boldsymbol{G}_m + \bar{\boldsymbol{J}}(\boldsymbol{F}_{fc} - \hat{\boldsymbol{F}}_{fc}^r)] \qquad (6.82)$$

and

$$\begin{aligned} \boldsymbol{V}F_{\mathrm{int}}^{t\to\infty} &= \boldsymbol{F}_c^{t\to\infty} - \boldsymbol{W}^{\dagger}F_{ext}^{t\to\infty} \\ &= \boldsymbol{V}F_{\mathrm{int}}^{d} - (\boldsymbol{I} - \boldsymbol{W}^{\dagger}\boldsymbol{W})\boldsymbol{J}^{-T}[\boldsymbol{H}_m\ddot{\boldsymbol{q}}^d + \boldsymbol{C}_m\dot{\boldsymbol{q}}^d + \boldsymbol{G}_m + \bar{\boldsymbol{J}}(\boldsymbol{F}_{fc} - \hat{\boldsymbol{F}}_{fc}^r)] \end{aligned} \tag{6.83}$$

where $F_{ext}^{t\to\infty}$ and $F_{\mathrm{int}}^{t\to\infty}$ are the external and internal forces as $t \to \infty$, respectively. Since $\boldsymbol{V}$ is a full-column-rank matrix, it can be concluded that

$$F_{\mathrm{int}}^{t\to\infty} = F_{\mathrm{int}}^{d} + \boldsymbol{V}^{\dagger}(\boldsymbol{I} - \boldsymbol{W}^{\dagger}\boldsymbol{W})\boldsymbol{J}^{-T}[\boldsymbol{H}_m\ddot{\boldsymbol{q}}^d + \boldsymbol{C}_m\dot{\boldsymbol{q}}^d + \boldsymbol{G}_m + \bar{\boldsymbol{J}}(\boldsymbol{F}_{fc} - \hat{\boldsymbol{F}}_{fc}^r)] \tag{6.84}$$

Equation (6.84) indicates that the actual internal force is bounded, but does not converge to the desired value. In order to enhance the regulation of the internal force, a force feedback loop in the control law (6.48) is further introduced by replacing $\boldsymbol{V}F_{\mathrm{int}}^{d}$ with $\boldsymbol{V}(F_{\mathrm{int}}^{d} + K_{\mathrm{int}}(F_{\mathrm{int}}^{d} - F_{\mathrm{int}}))$ in equation (6.50) that describes the desired force $\boldsymbol{F}^d$:

$$\boldsymbol{F}^d = \bar{\boldsymbol{J}}^{-1}\boldsymbol{J}^T(\boldsymbol{W}^{\dagger}E^{-T}\tau^d + \boldsymbol{V}(F_{\mathrm{int}}^{d} + K_{\mathrm{int}}(F_{\mathrm{int}}^{d} - F_{\mathrm{int}}))) + \hat{\boldsymbol{F}}_{fc}^r \tag{6.85}$$

The internal force F_{int}, can be extracted from contact forces, which are typically available through wrist force sensors. As a result, equation (6.84) becomes

$$F_{\mathrm{int}}^{t\to\infty} = F_{\mathrm{int}}^{d} - (1 + K_{\mathrm{int}})^{-1}\boldsymbol{V}^{\dagger}(\boldsymbol{I} - \boldsymbol{W}^{\dagger}\boldsymbol{W})\boldsymbol{J}^{-T}[\boldsymbol{H}_m\ddot{\boldsymbol{q}}^d + \boldsymbol{C}_m\dot{\boldsymbol{q}}^d + \boldsymbol{G}_m + \bar{\boldsymbol{J}}(\boldsymbol{F}_{fc} - \hat{\boldsymbol{F}}_{fc}^r)] \tag{6.86}$$

Theoretically, the actual internal force can be arbitrarily set as close as possible to the desired value through adjusting the force feedback gain K_{int}. With respect to stability, the format of the Lyapunov-like scalar function remains the same, since only the term related to internal force has been changed.

(v) The time derivative of the virtual force $\boldsymbol{F}^d$ is required by the controller (6.48). But the virtual force contains term $|\dot{\boldsymbol{x}}_r|$ in its friction compensation part, which is not differentiable at $\dot{\boldsymbol{x}}_r = 0$. Fortunately, $\boldsymbol{F}^d$ is continuous everywhere, differentiable anywhere except at the point of $\dot{\boldsymbol{x}}_r = 0$, and its left and right derivatives at $\dot{\boldsymbol{x}}_r = 0$ exist and finite. Actual control input can still be synthesized to accomplish the job. Another way to deal with this problem is to replace $|\dot{\boldsymbol{x}}_r|$ with $\dot{\boldsymbol{x}}_r \tanh(\dot{\boldsymbol{x}}_r / \varepsilon)$ in the friction compensation part of $\boldsymbol{F}^d$. Replacing the control gain K_d, used in equations (6.38) and (6.51), with $K_d + K_{ds}$, equation (6.80) becomes

$$\dot{V}_2 \le -\alpha\|r\|^2 - K_{ds}\|s_1\|^2 + s_1^T \boldsymbol{J_a}[\frac{|\dot{\boldsymbol{x}}_r| - \dot{\boldsymbol{x}}_r \tanh(\dot{\boldsymbol{x}}_r/\varepsilon)}{g(\dot{\boldsymbol{x}}_r)}][\hat{\boldsymbol{\sigma}}_1]\hat{\boldsymbol{z}}_1 \tag{6.87}$$

Define $\eta' = \dfrac{\overline{\sigma}(\boldsymbol{J}_a[\hat{\boldsymbol{\sigma}}_1][\hat{z}_1])}{f_{sl,L}}$. Using the following property (Polycarpou and Ioannou, 1993):

$$0 < |\dot{\boldsymbol{x}}_r| - \dot{\boldsymbol{x}}_r \tanh(\dot{\boldsymbol{x}}_r/\varepsilon) < 0.2785\varepsilon, \forall\varepsilon > 0 \tag{6.88}$$

One can arrive at

$$\dot{V}_2 \le -\alpha\|r\|^2 - K_{ds}\|s_1\|^2 + 0.2785\varepsilon\eta'\|s_1\| \tag{6.89}$$

Since $0.2785\varepsilon\eta'\|s_1\| \le K_{ds}\|s_1\|^2 + (0.2785\varepsilon\eta')^2/(4K_{ds})$, one further obtains

$$\dot{V}_2 \le -\alpha\|r\|^2 + (0.2785\varepsilon\eta')^2/(4K_{ds}) \tag{6.90}$$

$\dot{V}_2 \le 0$ whenever r is outside the compact set $\{r \mid \|r\|^2 < (0.2785\varepsilon\eta')^2/(4K_{ds}\alpha)\}$. Thus, it can be concluded that the tracking error is bounded and converges to a small neighbourhood of zero, whose size is adjustable by design parameters ε and K_{ds}.

6.3 Simulation Results

The nonlinear controller derived in Section 6.2, has been examined by numerical simulations, using the same model as in the previous chapters. The task was to have two identical planar three degree-of-freedom hydraulic manipulators hold a rigid object and move it along a desired path (see Figure 6.1). The stick and slip frictions were chosen as 2200N and 1500N respectively. The values of other friction parameters used in the simulation model were $\sigma_{0,j}^i = 2\times10^5$ N/m, $\sigma_{1,j}^i = 400$Ns/m, $\sigma_{2,j}^i = 200$Ns/m, and $\dot{x}_{s,j}^i = 0.002$m/s.

The vectors of unknown parameters θ and φ, for the above system are given below:

$$\theta = \{\overbrace{I_1^1 + m_1^1 a_1^{1\,2}, I_2^1 + m_2^1 a_2^{1\,2}, I_3^1 + m_3^1 a_3^{1\,2}, m_2^1, m_3^1, m_1^1 a_1^1, m_2^1 a_2^1, m_3^1 a_3^1}^{\text{Robot 1}}, \overbrace{I_1^2 + m_1^2 a_1^{2\,2}, \ldots,}^{\text{Robot 2}} \overbrace{m, I}^{\text{Object}},$$
$$\overbrace{\sigma_{12,1}^1, \sigma_{12,2}^1 \sigma_{12,3}^1, \sigma_{12,1}^2, \sigma_{12,2}^2 \sigma_{12,3}^2}^{\sigma_{12}}\}^T \tag{6.91}$$

$$\varphi = \{\beta_1^1 K_1^1 K_{sp,1}^1, \beta_1^1, \ldots, \beta_j^i K_j^i K_{sp,j}^i, \beta_j^i, \ldots\}_{i=1,2;\, j=1,2,3}^T \tag{6.92}$$

In equation (6.91), m and I are mass and inertia of the object, respectively. m_j^i, I_j^i and a_j^i (i=1,2; j=1,2,3) are mass, inertia and distance of center of mass to the j^{th} joint of the i^{th} manipulator, respectively. For the controller, the values of these unknown parameters were initially set to values different from those used in the model to investigate the ability of the controller to cope with parametric uncertainties. The controller gains were chosen as

$\lambda_1^{(6\times6)} = diag(50,...,50)$, $\lambda_2^{(6\times6)} = diag(50,...,50)$, $K_p^{(6\times6)} = diag(1000,...,1000)$,

$L_p^{(6\times6)} = diag(300,...,300)$, $K_d^{(6\times6)} = diag(700,...,700)$, $K_d^{'\,(6\times6)} = diag(700,...,700)$,

$K_F^{(6\times6)} = diag(200,...,200)$, $\Gamma_F^{(6\times6)} = diag(0.05,...,0.05)$,

$\Gamma_\theta = diag(1, 1, 1, 1, 1, 1, 5, 1, 1, 1, 1, 1, 1, 1, 5, 1, 0.02, 1,\ 10^{-4},\ 10^{-4},\ 10^{-4}, 10^{-4},\ 10^{-4},\ 10^{-4})$,

$\Gamma_\varphi^{(12\times12)} = diag(4.2\times10^8,\ 5\times10^{-7},\ ..., 4.2\times10^8,\ 5\times10^{-7})$,

$\Gamma_{\sigma_0}^{(6\times6)} = diag(5\times10^{-10},\ ..., 5\times10^{-10})$, $\Gamma_{\sigma_1}^{(6\times6)} = diag(10^{-5},\ ..., 10^{-5})$,

$\Gamma_{z_0}^{(6\times6)} = diag(10,\ ..., 10)$, $\Gamma_{z_1}^{(6\times6)} = diag(10,\ ..., 10)$.

Two reference trajectories along the vertical direction were simulated:

(i) point-to-point trajectory with a travel distance of 0.3m, maximum speed of 0.15m/s and maximum acceleration of 0.6m/s^2 and,

(ii) sinusoidal trajectory consisting of one segment with an amplitude of 0.1m and frequency of 0.2Hz, followed by a second segment with an amplitude of 0.02m and frequency of 1Hz.

These two reference trajectories are shown in Figures 6.1 and 6.11, respectively. The controller was also required to maintain the internal object force in the horizontal direction close to zero and at the same time, evenly distribute the load between the two robots.

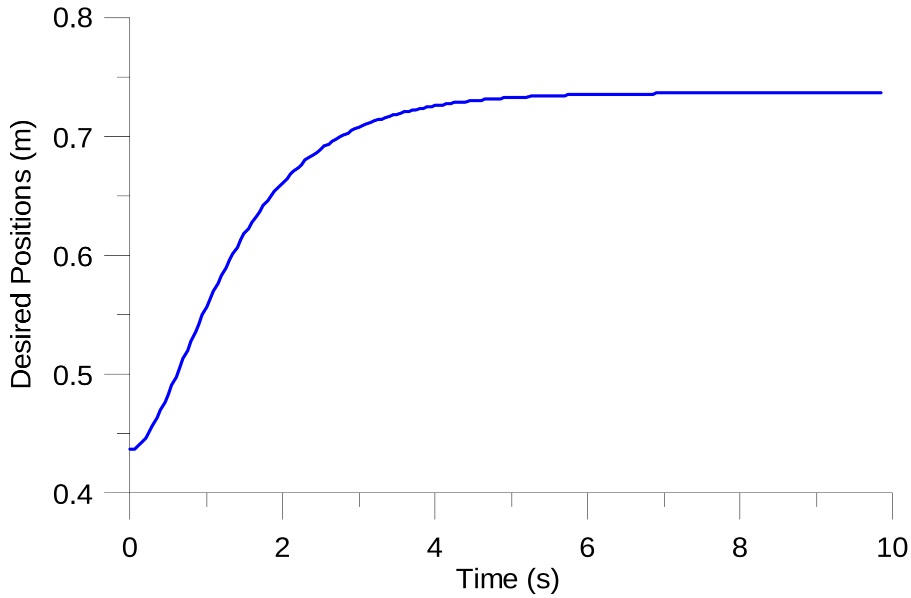

Figure 6.1: Point-to-point vertical reference trajectory.

The first set of tests was conducted using the point-to-point reference trajectory shown in Figure 6.1. Simulations were first conducted with controller (6.48) and no force feedback. Figure 6.2 shows the tracking error. As can be seen, the object follows the desired path closely. In the calculation of the control signals, the derivative of $|\dot{x}_r|$ was set to zero at $\dot{x}_r = 0$.

Additional simulations, where term $|\dot{x}_r|$ was replaced with $\dot{x}_r \tanh(\dot{x}_r / \varepsilon)$ in their controllers were also carried out, with no significant differences apparent. The control signals shown in Figure 6.3 are all reasonable and smooth. With reference to Figure 6.4, the internal force acting on the object is different from the desired level of zero. This was expected since the internal force is theoretically not guaranteed to converge to the desired level, given the controller (6.48) with no force sensed at each of the manipulators' end-effectors. Estimates of typical parameters are shown in Figure 6.5. Note that the estimated values of the parameters do not converge to the actual. Such results do not contradict the theoretical argument, since the parameter convergence is not theoretically guaranteed as discussed in Section 6.2. The distribution of the payload between the two manipulators was fairly even as seen from Figure 6.6 where two manipulators' lifting forces are very close to each other. Figure 6.7 shows the friction estimation for the second link of one manipulator calculated from equation (6.39), which follows the actual value reasonably well.

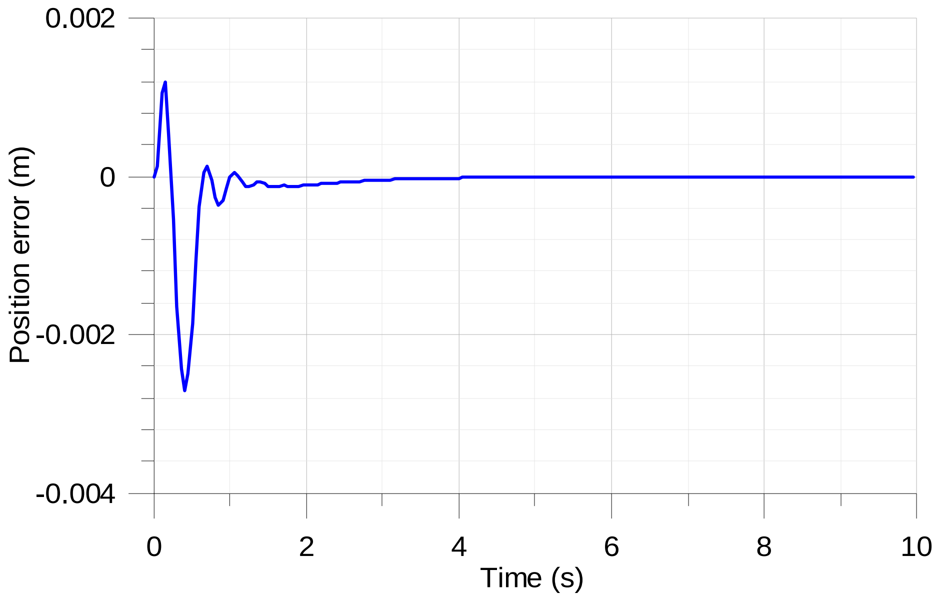

Figure 6.2: Tracking error in the vertical direction under controller (6.48) with no force feedback.

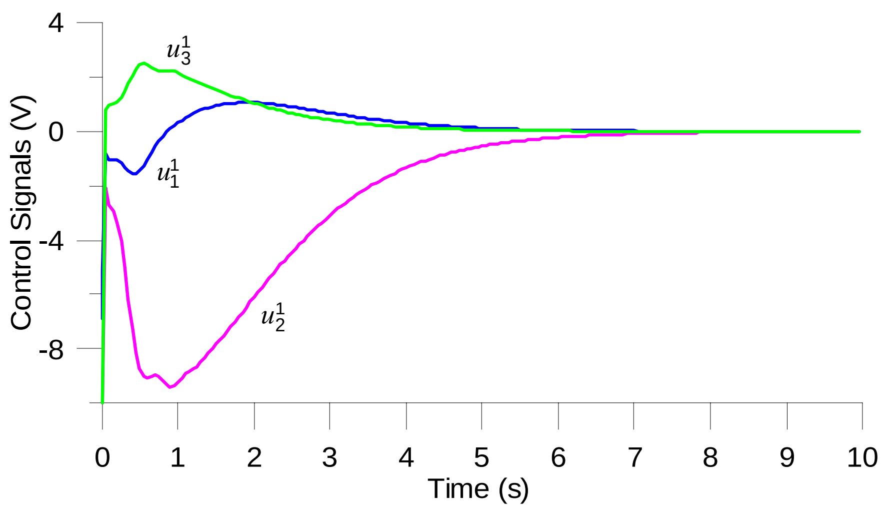

Figure 6.3: Control signals for one of the manipulators.

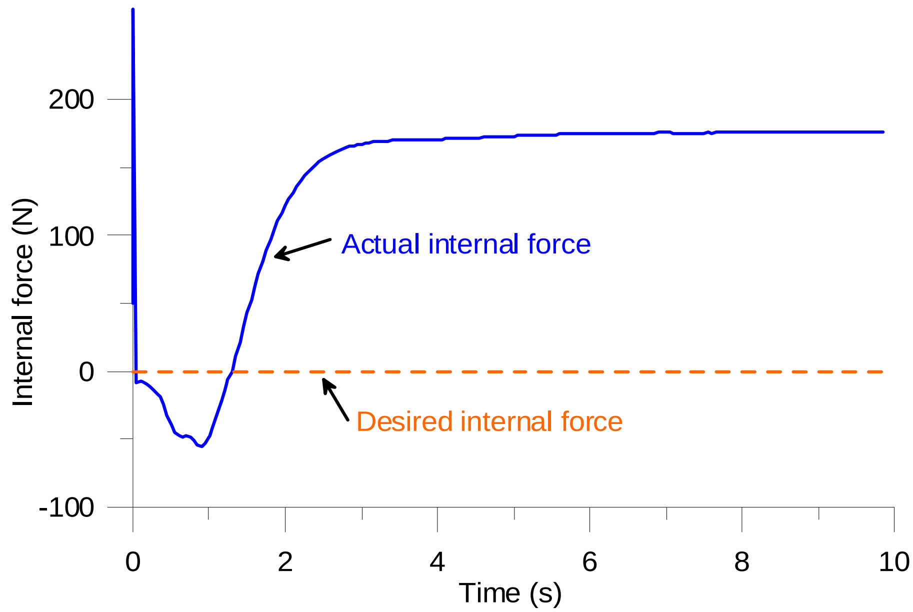

Figure 6.4: Internal force on the object in the horizontal direction.

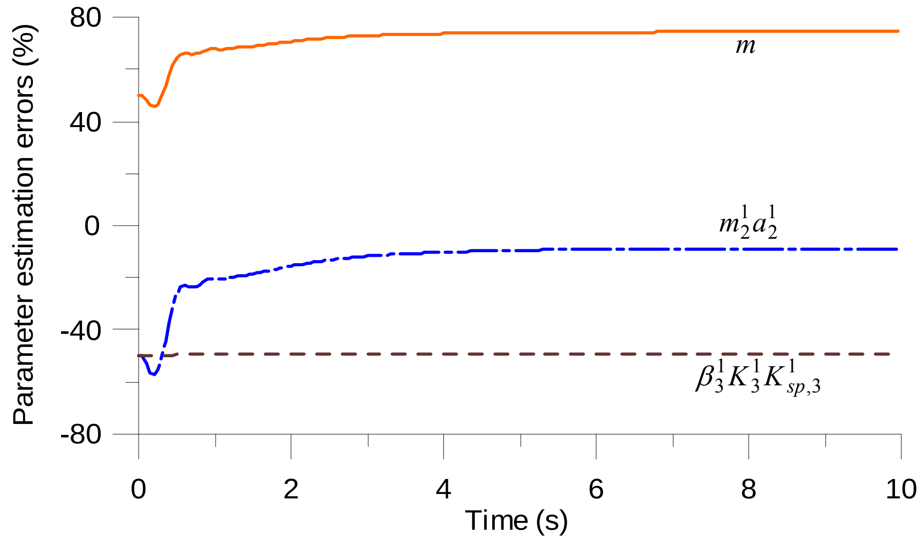

Figure 6.5: Typical parameter estimation relative errors.

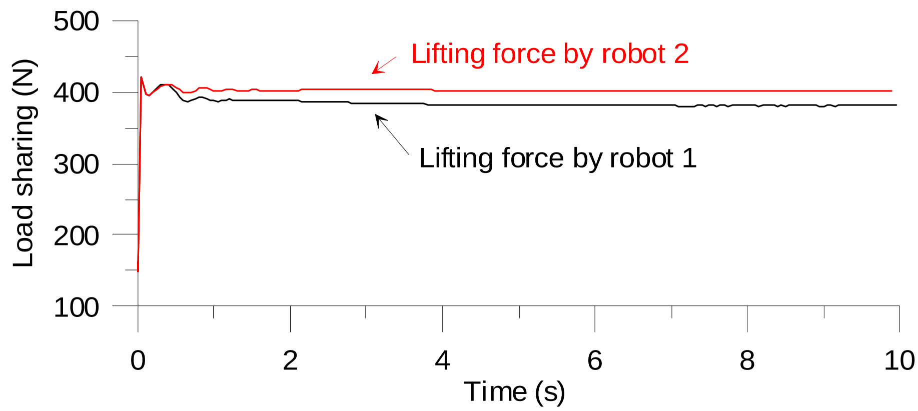

Figure 6.6: Lifting forces by two manipulators.

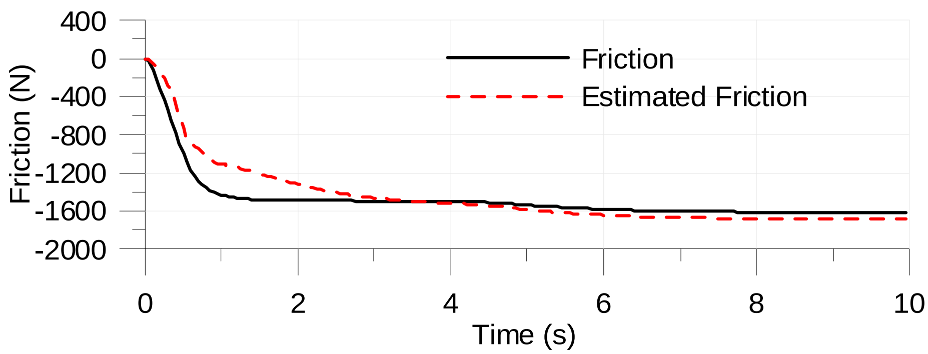

Figure 6.7: Friction and its estimate (link two of the first manipulator).

In order to bring the internal force closer to the desired level, the controller (6.48) incorporating the force feedback signal given in equation (6.85), was applied to the same point-to-point-tracking trajectory shown in Figure 6.1. The same control gains as before were used with the addition of force feedback gain, which was set to $K_{\text{int}} = 3$. The derivative of the internal force was neglected in the calculation of the control signals. The position tracking error shown in Figure 6.8 is very similar to the one in the tracking control with no force feedback (see Figure 6.2). The control signals (see Figure 6.9) exhibit less effort (i.e. peak control signals are less) than the previous case (compare Figures 6.9 and 6.3). Figure 6.10 shows a great improvement in the internal force response as a result from adding a force feedback in the loop. The internal force is noticeably reduced to 40N. This also explains why less control efforts (smaller control signals) are needed for the controller with force feedback.

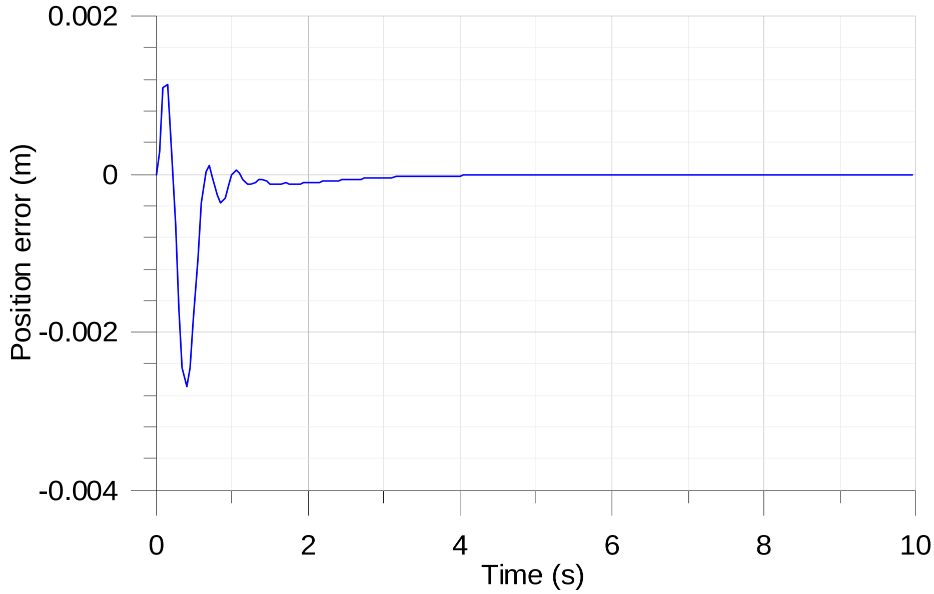

Figure 6.8: Tracking error in the vertical direction (controller with force feedback).

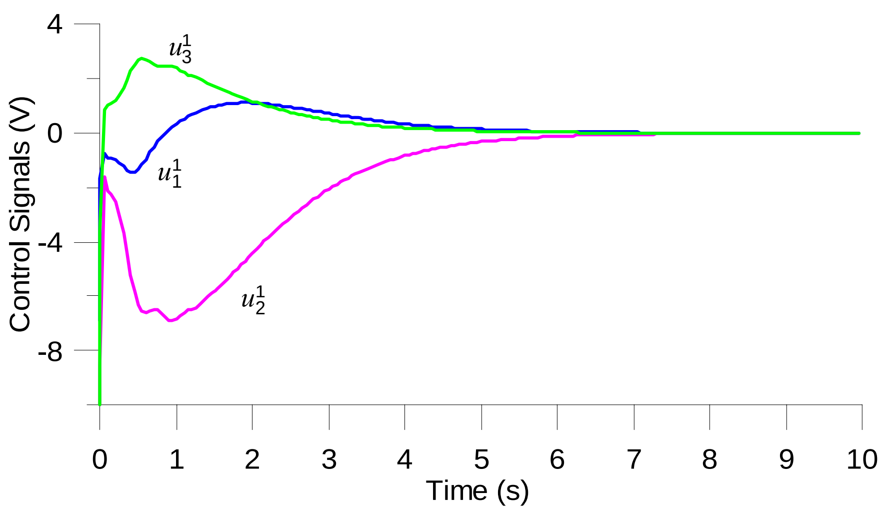

Figure 6.9: Control signals for the first manipulator pertaining to Figure 6.8.

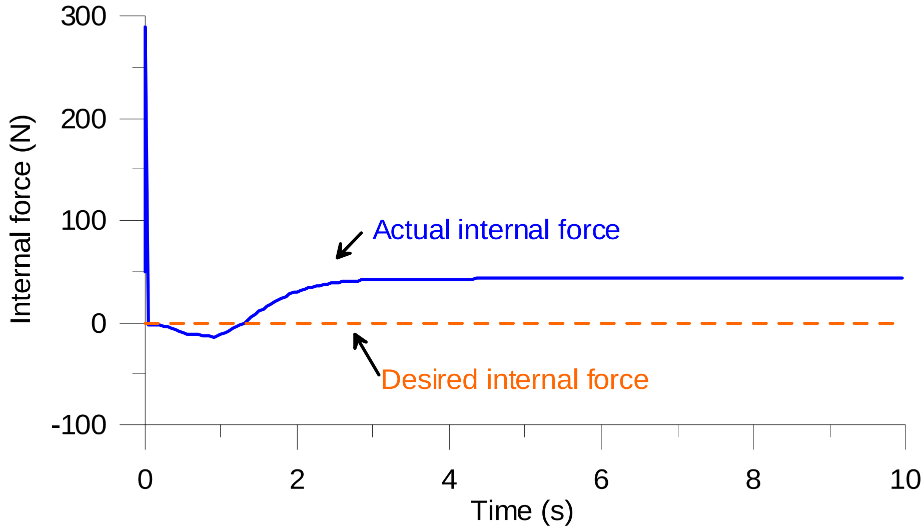

Figure 6.10: Object internal force in the horizontal direction.

The next test was conducted using sinusoidal trajectory tracking shown in Figure 6.11. Controller (6.48), with the addition of force feedback and having same gains as in the previous set of tests; was used and the derivative of the internal force was neglected again. Figures 6.12 to 6.15 show the simulation results. As can be seen in Figure 6.12, the control system shows excellent performance. The amplitude of the tracking error, corresponding to the trajectory with higher frequency and lower amplitude, is about 4×10^{-4} m. The control signals to the actuators are reasonable and not saturated (see Figure 6.13 for a plot of a typical signal). Figure 6.14 shows that the internal force on the object changes slightly with the response. The distribution of the lifting forces was quite even, as shown in Figure 6.15.

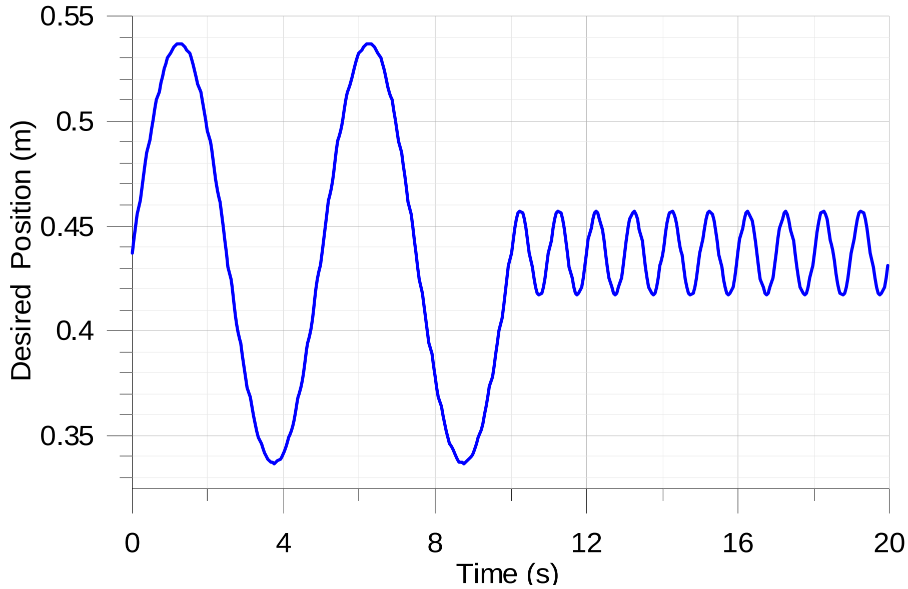

Figure 6.11: Sinusoidal reference trajectory used for further controller evaluation.

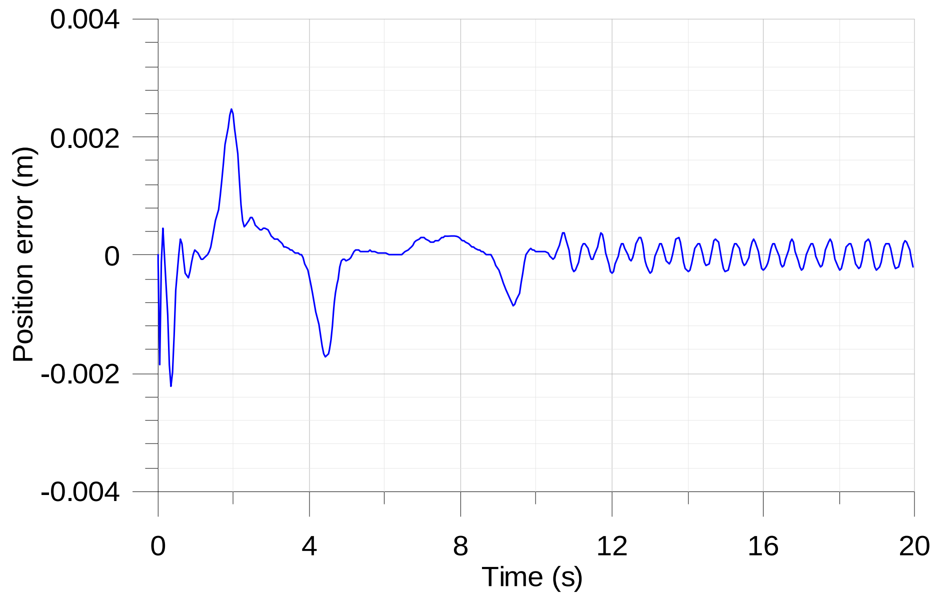

Figure 6.12: Tracking error in the vertical direction.

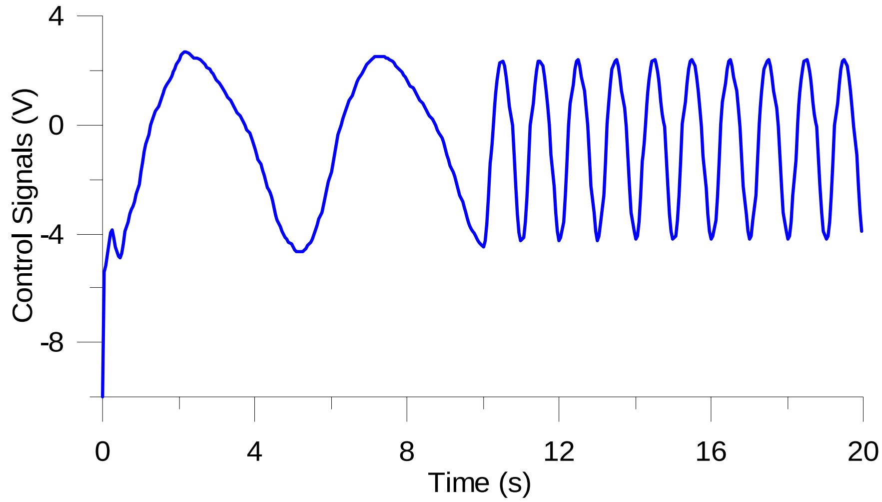

Figure 6.13: Control signals for link two of the first manipulator.

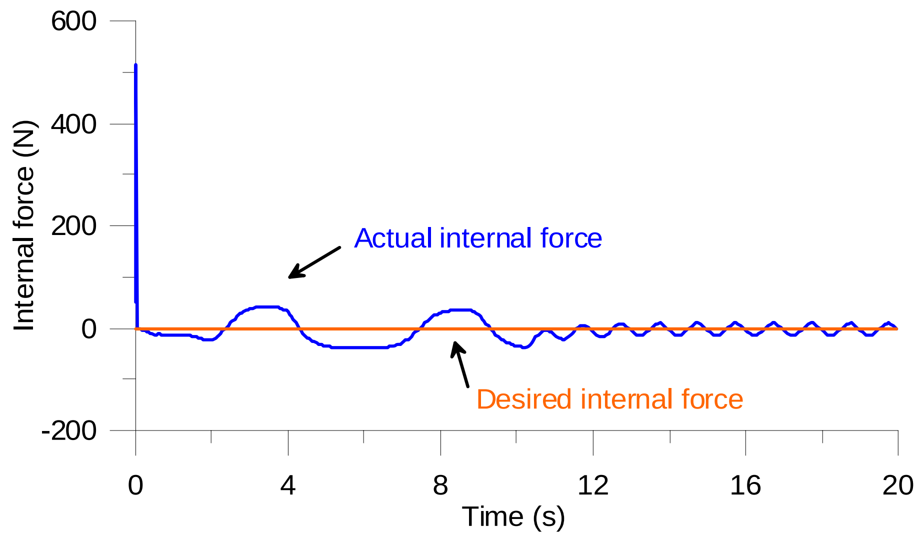

Figure 6.14: Internal force on the object in the horizontal direction.

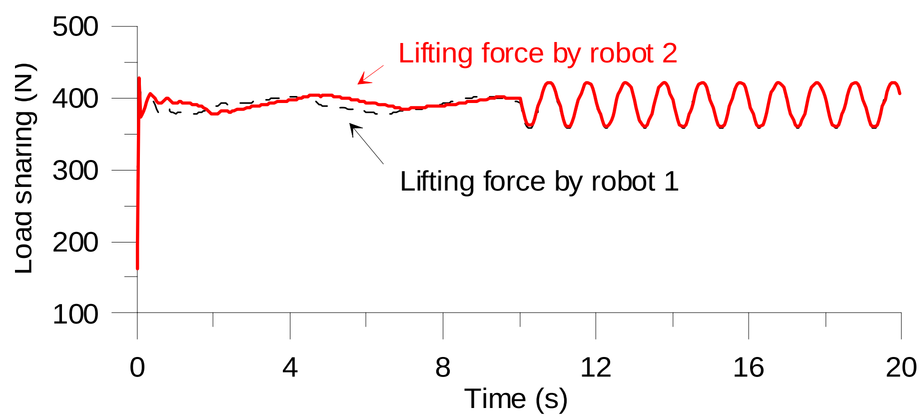

Figure 6.15: Load sharing between manipulators.

6.4 Summary

This chapter documented the design, stability analysis and numerical verification of a tracking controller for co-operation among several hydraulic manipulators handling a rigid payload. The highly nonlinear dynamic behavior of hydraulic actuation, manipulators and dry friction were incorporated in the controller design. The issues of internal force control on the object, as well as load sharing among several manipulators were also addressed. To deal with parametric uncertainties in the payload, manipulators, hydraulic functions as well as friction, the controller was augmented with various adaptation laws. An appropriate observer was included to avoid the need for measurement of acceleration as feedback. Thus, the proposed tracking controller does not need exact knowledge of the payload, manipulators' dynamic parameters, or hydraulic function parameters. With respect to the implementation, the controller only requires measurements of robots' joint angular positions and velocities as well as hydraulic line pressures. In the case force feedback is implemented to impose desired internal forces, the contact forces need to be measured as well.

The equilibrium of the entire system under the proposed controller was theoretically investigated, and the stability of the position tracking system was ensured with final zero position tracking error while the internal force on the object was maintained arbitrarily close to the desired level. Simulations were performed with two manipulators resembling MAGNUM hydraulic manipulators. The results demonstrated the effectiveness of the proposed nonlinear controller.

Chapter 7 Dynamic Surface Control of Co-operating Hydraulic Manipulators in the Presence of Friction

The previous chapter used the backstepping method to develop a Lyapuov-based nonlinear controller for co-operating hydraulic manipulators. The method however, suffers from the problem of "explosion of terms" (Swaroop, et al., 1997). This can be seen, for example, by an inspection of the controller (6.48), which requires the calculation of the derivative of $\boldsymbol{F}^d$ that creates many terms. To overcome the problem of "explosion of terms" associated with the backstepping method and the problem of finding derivatives, dynamic surface control technique by Swaroop et. al. (2000), which is a dynamic extension to multiple surface sliding (MSS) control by Won and Hedrick (1996); is introduced in this chapter. By incorporating a low pass filter in the controller design within the framework of the backstepping method, the control law does not involve model differentiation. Thus the problem of "explosion of terms" is avoided. Another benefit is that no acceleration observer is required, in order to avoid the requirement of acceleration feedback.

7.1 Controller Design

Let $\hat{\theta}, \hat{\varphi}, \hat{\boldsymbol{\sigma}}_0, \hat{\boldsymbol{\sigma}}_1$ and $\hat{\boldsymbol{\sigma}}_{12}$ be estimates of $\theta, \varphi, \boldsymbol{\sigma}_0, \boldsymbol{\sigma}_1$ and $\boldsymbol{\sigma}_{12}$, respectively. Also, let $\hat{\boldsymbol{z}}_0$ and $\hat{\boldsymbol{z}}_1$ be two estimates of $\boldsymbol{z}$. $\tilde{\theta} = \hat{\theta} - \theta$, $\tilde{\varphi} = \hat{\varphi} - \varphi$, $\tilde{\boldsymbol{\sigma}}_0 = \hat{\boldsymbol{\sigma}}_0 - \boldsymbol{\sigma}_0$, $\tilde{\boldsymbol{\sigma}}_1 = \hat{\boldsymbol{\sigma}}_1 - \boldsymbol{\sigma}_1$, $\tilde{\boldsymbol{z}}_0 = \hat{\boldsymbol{z}}_0 - \boldsymbol{z}$ and $\tilde{\boldsymbol{z}}_1 = \hat{\boldsymbol{z}}_1 - \boldsymbol{z}$ are errors between the estimates and the actual values. Additionally, the following notations are defined:

$$e = X - X^d \tag{7.1}$$

$$\dot{X}_r = \dot{X}^d - \lambda e \tag{7.2}$$

$$s = \dot{e} + \lambda e \tag{7.3}$$

X^d is the desired value of X and belongs to C^2. It is assumed that X, $\dot{X}^d, \ddot{X}^d$ are all bounded. Matrix λ is diagonal and positive definite. The unknown parameters satisfy:

$\mu_L \le \|\mu\| \le \mu_U$ where $\mu = \theta, \varphi, \boldsymbol{\sigma}_0, \boldsymbol{\sigma}_1$.

***Proposition*:**

Consider the system described by equations (6.1), (6.2) and (6.3). Given the following control law, updating laws and observers:

(i) Controller

$$\boldsymbol{U} = \hat{\boldsymbol{A}}_{cq}^{-1}(\boldsymbol{q})\left(\hat{\boldsymbol{A}}_{ca}(\boldsymbol{q},\dot{\boldsymbol{q}}) + \dot{\boldsymbol{F}}^d - \boldsymbol{\Gamma}_F^{-1}\boldsymbol{J}_a^T s - K_F \widetilde{\boldsymbol{F}}\right) \tag{7.4}$$

where

$$\widetilde{\boldsymbol{F}} = \boldsymbol{F} - \boldsymbol{F}^d \tag{7.5}$$

$$\dot{\boldsymbol{F}}^d = -\widetilde{\boldsymbol{F}}^d / \tau_0; \quad \widetilde{\boldsymbol{F}}^d = \boldsymbol{F}^d - \overline{\boldsymbol{F}}; \quad \boldsymbol{F}^d(0) = \overline{\boldsymbol{F}}(0) \tag{7.6}$$

$$\overline{\boldsymbol{F}} = \overline{\boldsymbol{J}}^{-1}\boldsymbol{J}^T(\boldsymbol{W}^{\dagger}E^{-T}\tau^d + \boldsymbol{V}F_{\text{int}}^d) + \hat{\boldsymbol{F}}_{fc} \tag{7.7}$$

$$\hat{\boldsymbol{F}}_{fc} = [\hat{\boldsymbol{\sigma}}_0]\hat{\boldsymbol{z}}_0 - [\hat{\boldsymbol{\sigma}}_1][\frac{|\dot{\boldsymbol{x}}|}{g(\dot{\boldsymbol{x}})}]\hat{\boldsymbol{z}}_1 \tag{7.8}$$

$$\tau^d = \hat{M}(X)\ddot{X}_r + \hat{D}(X,\dot{X}_r)\dot{X}_r + \boldsymbol{J}_a[\hat{\sigma}_{12}]\boldsymbol{J}_a^T\dot{X}_r + \hat{G}(X) - K_d s \tag{7.9}$$

(ii) Discontinuous projection-based adaptation laws for unknown parameters pertaining to the manipulators-object dynamics, hydraulic functions and friction parameters,

$$\dot{\hat{\mu}} = \text{Proj}_{\mu}(w_\mu Y_\mu) = \begin{cases} 0 \quad \forall \ \hat{\mu} = \mu_L \ \text{ and } \ w_\mu Y_\mu < 0 \\ 0 \quad \forall \ \hat{\mu} = \mu_U \ \text{ and } \ w_\mu Y_\mu > 0 \\ w_\mu Y_\mu \qquad \text{otherwise} \end{cases} \tag{7.10}$$

where $\mu = \theta, \varphi, \boldsymbol{\sigma}_0, \boldsymbol{\sigma}_1$. μ_L and μ_U are lower and upper bounds of μ. Scalar $w_\mu > 0$ represents the adaptation rate, and Y_μ is an adaptation function to be synthesized later.

(iii) Observers for friction state $\boldsymbol{z}$

$$\dot{\hat{\boldsymbol{z}}}_0 = \dot{\boldsymbol{x}} - [\frac{|\dot{\boldsymbol{x}}|}{g(\dot{\boldsymbol{x}})}]\hat{\boldsymbol{z}}_0 - \Gamma_{z_0}^{-1}\boldsymbol{J}_a^T s \tag{7.11}$$

$$\dot{\hat{\boldsymbol{z}}}_1 = \dot{\boldsymbol{x}} - [\frac{|\dot{\boldsymbol{x}}|}{g(\dot{\boldsymbol{x}})}]\hat{\boldsymbol{z}}_1 + [\frac{|\dot{\boldsymbol{x}}|}{g(\dot{\boldsymbol{x}})}]\Gamma_{z_1}^{-1}\boldsymbol{J}_a^T s \tag{7.12}$$

then, there exists a set of control gains and a filter time constant such that, the closed-loop control system is stable and achieves arbitrarily small bounded tracking error.

Remarks 7.1.1

(i) The desired force $\boldsymbol{F}^d$ is obtained by filtering $\overline{\boldsymbol{F}}$ through the first order filter (7.6), which also provides $\dot{\boldsymbol{F}}^d$ for the controller. With this filter, one does not need explicit differentiation of $\overline{\boldsymbol{F}}$. τ_0, is a positive design parameter constant.

(ii) For a discontinuous projection-based adaptation law, it has been shown (Kristic et. al., 1995) that for any adaptation function Y_μ, if $\mu_L \le \|\hat{\mu}(0)\| \le \mu_U$, the adaptation law given by equation (7.10) guarantees

$$\mu_L \le \|\hat{\mu}\| \le \mu_U, \quad \forall \quad \hat{\mu} \tag{7.13}$$

$$\tilde{\mu}^T(\dot{\hat{\mu}} - w_\mu Y_\mu) \le 0, \quad \forall \quad Y_\mu \tag{7.14}$$

(iii) $\hat{M}, \hat{D}, \hat{G}$ and $[\hat{\boldsymbol{\sigma}}_{12}]$ are estimated dynamic matrices or vectors corresponding to the parametric estimation vector $\hat{\theta}$. Similarly, matrices $\hat{\boldsymbol{A}}_{ca}$ and vector $\hat{\boldsymbol{A}}_{cq}$ are the estimates of $\boldsymbol{A}_{ca}$ and $\boldsymbol{A}_{cq}$, corresponding to parameter estimation vector $\hat{\varphi}$. Vector $\hat{\boldsymbol{F}}_{fc}$ is the estimate of $\boldsymbol{F}_{fc} = \boldsymbol{J}_a([\boldsymbol{\sigma}_0]\boldsymbol{z} - [\boldsymbol{\sigma}_1][\dfrac{|\dot{\boldsymbol{x}}|}{g(\dot{\boldsymbol{x}})}]\boldsymbol{z})$, based on the estimates of internal friction states and friction force parameters.

(iv) $[\hat{\boldsymbol{z}}_0]$ and $[\hat{\boldsymbol{z}}_1]$ are diagonal matrices with $\hat{\boldsymbol{z}}_0$, and $\hat{\boldsymbol{z}}_1$ as their diagonal elements, respectively.

(v) All gains used in the controller and observers, Γ_F, K_F, K_d, Γ_{z0}, Γ_{z1}, are constant positive definite diagonal matrices.

Proof:

Define a Lyapunov-like scalar function as:

$$\mathrm{V}_2 = \mathrm{V}_1 + \tfrac{1}{2}\tilde{\boldsymbol{F}}^T \Gamma_F \tilde{\boldsymbol{F}} + \tfrac{1}{2}\tilde{\boldsymbol{F}}^{d^T} \Gamma_F \tilde{\boldsymbol{F}}^d \tag{7.15}$$

where

$$\mathrm{V}_1 = \tfrac{1}{2}\{s^T M(X)s + \tilde{\boldsymbol{z}}_0^T \Gamma_{z_0}[\boldsymbol{\sigma}_0]\tilde{\boldsymbol{z}}_0 + \tilde{\boldsymbol{z}}_1^T \Gamma_{z_1}[\boldsymbol{\sigma}_1]\tilde{\boldsymbol{z}}_1\} \tag{7.16}$$

Equations (6.1) and (7.9) are employed to arrive at the following error dynamics

$$\begin{aligned} M(X)\dot{s}+D(X,\dot{X})s &= \Theta(X,\dot{X}_r,\ddot{X}_r)\widetilde{\theta}-K_d s-\boldsymbol{J}_a[\boldsymbol{\sigma}_{12}]\boldsymbol{J}_a^T s+\boldsymbol{J}_a^T(\boldsymbol{F}-\overline{\boldsymbol{F}}) \\ &+\boldsymbol{J}_a^T[([\hat{\boldsymbol{\sigma}}_0]\hat{z}_0-[\boldsymbol{\sigma}_0]z)-[\frac{|\dot{\boldsymbol{x}}|}{g(\dot{\boldsymbol{x}})}]([\hat{\boldsymbol{\sigma}}_1]\hat{z}_1-[\boldsymbol{\sigma}_1]z)] \end{aligned} \tag{7.17}$$

where matrix Θ is defined by equation (6.4). It can then be shown that time derivative of V_1 is

$$\begin{aligned} \dot{\mathrm{V}}_1 &= -s^T K_d s - s^T\boldsymbol{J}_a[\boldsymbol{\sigma}_{12}]\boldsymbol{J}_a^T s + s^T\boldsymbol{J}_a(\boldsymbol{F}-\overline{\boldsymbol{F}})-\widetilde{\theta}^T Y_\theta + s^T\boldsymbol{J}_a^T[([\hat{\boldsymbol{\sigma}}_0]\hat{z}_0-[\boldsymbol{\sigma}_0]z) \\ &-[\frac{|\dot{\boldsymbol{x}}|}{g(\dot{\boldsymbol{x}})}]([\hat{\boldsymbol{\sigma}}_1]\hat{z}_1-[\boldsymbol{\sigma}_1]z)]+\dot{\tilde{z}}_0^T\Gamma_{z_0}[\boldsymbol{\sigma}_0]\widetilde{z}_0+\dot{\tilde{z}}_1^T\Gamma_{z_1}[\boldsymbol{\sigma}_1]\widetilde{z}_1 \end{aligned} \tag{7.18}$$

where $Y_\theta = -\Theta^T(X,\dot{X}_r,\ddot{X}_r)s$ is the adaptation function for $\hat{\theta}$. According to equations (7.1) to (7.3), variables $X,\dot{X}_r,\ddot{X}_r$ can be defined by state variables *e*, *s*, and desired values X^d, $\dot{X}^d,\ddot{X}^d$. There exists a positive continuous function γ_θ given by

$$\|Y_\theta\| \le \gamma_\theta(e,s,X^d,\dot{X}^d,\ddot{X}^d)\|s\| \tag{7.19}$$

Employing relations $[\hat{\boldsymbol{\sigma}}_0]\hat{z}_0-[\boldsymbol{\sigma}_0]\boldsymbol{z}=[\hat{z}_0]\widetilde{\boldsymbol{\sigma}}_0+[\boldsymbol{\sigma}_0]\widetilde{z}_0$ and $[\hat{\boldsymbol{\sigma}}_1]\hat{z}_1-[\boldsymbol{\sigma}_1]\boldsymbol{z}=[\hat{z}_1]\widetilde{\boldsymbol{\sigma}}_1+[\boldsymbol{\sigma}_1]\widetilde{z}_1$, leads to

$$\begin{aligned} \dot{\mathrm{V}}_1 &= -s^T K_d s - s^T\boldsymbol{J}_a[\boldsymbol{\sigma}_{12}]\boldsymbol{J}_a^T s + s^T\boldsymbol{J}_a(\boldsymbol{F}-\overline{\boldsymbol{F}})-\widetilde{\theta}^T Y_\theta-\widetilde{\boldsymbol{\sigma}}_0^T Y_{\sigma_0}-\widetilde{\boldsymbol{\sigma}}_1^T Y_{\sigma_1} \\ &+s^T\boldsymbol{J}_a([\boldsymbol{\sigma}_0]\widetilde{z}_0-[\frac{|\dot{\boldsymbol{x}}|}{g(\dot{\boldsymbol{x}})}][\boldsymbol{\sigma}_1]\widetilde{z}_1)+\dot{\tilde{z}}_0^T\Gamma_{z_0}[\boldsymbol{\sigma}_0]\widetilde{z}_0+\dot{\tilde{z}}_1^T\Gamma_{z_1}[\boldsymbol{\sigma}_1]\widetilde{z}_1 \end{aligned} \tag{7.20}$$

where $Y_{\sigma_0}=-[\hat{z}_0]\boldsymbol{J}_a^T s$, $Y_{\sigma_1}=[\frac{|\dot{\boldsymbol{x}}|}{g(\dot{\boldsymbol{x}})}][\hat{z}_1]\boldsymbol{J}_a^T s$. There exist two continuous functions γ_{σ_0} and γ_{σ_1} given by

$$\|Y_{\sigma_0}\| \le \gamma_{\sigma_0}(e,\widetilde{z}_0,X^d)\|s\| \tag{7.21}$$

$$\|Y_{\sigma_1}\| \le \gamma_{\sigma_1}(e,s,\widetilde{z}_1,X^d,\dot{X}^d)\|s\| \tag{7.22}$$

From equations (7.11) and (7.12), one arrives at

$$\dot{\tilde{\boldsymbol{z}}}_0 = [\frac{|\dot{\boldsymbol{x}}|}{g(\dot{\boldsymbol{x}})}]\widetilde{z}_0-\Gamma_{z_0}^{-1}\boldsymbol{J}_a^T s \tag{7.23}$$

$$\dot{\tilde{z}}_1 = [\frac{|\dot{\boldsymbol{x}}|}{g(\dot{\boldsymbol{x}})}]\tilde{z}_1 + [\frac{|\dot{\boldsymbol{x}}|}{g(\dot{\boldsymbol{x}})}]\Gamma_{z_1}^{-1}\boldsymbol{J}_a^T s \tag{7.24}$$

Applying equations (7.23) and (7.24) results in

$$\begin{aligned}\dot{\mathrm{V}}_1 &= -s^T K_d s - s^T \boldsymbol{J}_a[\boldsymbol{\sigma}_{12}]\boldsymbol{J}_a^T s + s^T \boldsymbol{J}_a(\tilde{\boldsymbol{F}} + \tilde{\boldsymbol{F}}^d) - \tilde{\theta}^T Y_\theta \\ &\quad - \tilde{\boldsymbol{\sigma}}_0^T Y_{\sigma_0} - \tilde{\boldsymbol{\sigma}}_1^T Y_{\sigma_1} - \tilde{z}_0^T[\frac{|\dot{\boldsymbol{x}}|}{g(\dot{\boldsymbol{x}})}][\boldsymbol{\sigma}_0]\Gamma_{z0}\tilde{z}_0 - \tilde{z}_1^T[\frac{|\dot{\boldsymbol{x}}|}{g(\dot{\boldsymbol{x}})}][\boldsymbol{\sigma}_1]\Gamma_{z1}\tilde{z}_1\end{aligned} \tag{7.25}$$

Since

$$\hat{\boldsymbol{A}}_{cq}(q)\boldsymbol{U} - \hat{\boldsymbol{A}}_{ca}(\boldsymbol{q},\dot{\boldsymbol{q}}) = \Phi(\boldsymbol{q},\dot{\boldsymbol{q}},\boldsymbol{U})\hat{\varphi} \tag{7.26}$$

the hydraulic dynamics in equation (2.50) can be rewritten as

$$\dot{\boldsymbol{F}} = \hat{\boldsymbol{A}}_{cq}(\boldsymbol{q})\boldsymbol{U} - \hat{\boldsymbol{A}}_{ca}(\boldsymbol{q},\dot{\boldsymbol{q}}) - \Phi(\boldsymbol{q},\dot{\boldsymbol{q}},\boldsymbol{U})\tilde{\varphi} \tag{7.27}$$

Given equation (7.27), the time derivative of the Lyapunov-like scalar function becomes

$$\dot{\mathrm{V}}_2 = \dot{\mathrm{V}}_1 + (\hat{\boldsymbol{A}}_{cq}\boldsymbol{U} - \hat{\boldsymbol{A}}_{ca} - \dot{\boldsymbol{F}}^d)^T \Gamma_F \tilde{\boldsymbol{F}} - \tilde{\varphi}^T Y_\varphi + (\dot{\boldsymbol{F}}^d - \dot{\bar{\boldsymbol{F}}})^T \Gamma_F \tilde{\boldsymbol{F}}^d \tag{7.28}$$

where $Y_\varphi = \Phi^T(\boldsymbol{q},\dot{\boldsymbol{q}},\boldsymbol{U})\Gamma_F \tilde{\boldsymbol{F}}$. There exists a continuous positive function γ_φ, given by

$$\|Y_\varphi\| \le \gamma_\varphi(e, s, \tilde{\boldsymbol{F}}, \tilde{\boldsymbol{F}}^d, X^d, \dot{X}^d, \ddot{X}^d, \tau_0)\|\tilde{\boldsymbol{F}}\| \tag{7.29}$$

Substituting controller (7.4) into equation (7.28), the derivative of V_2 will be

$$\dot{\mathrm{V}}_2 = \dot{\mathrm{V}}_1 - s^T \boldsymbol{J}_a \tilde{\boldsymbol{F}} - \tilde{\boldsymbol{F}}^T K_F \Gamma_F \tilde{\boldsymbol{F}} - \tilde{\varphi}^T Y_\varphi + (\dot{\boldsymbol{F}}^d - \dot{\bar{\boldsymbol{F}}})^T \Gamma_F \tilde{\boldsymbol{F}}^d \tag{7.30}$$

Employing filter (7.6), the last term in equation (7.30) arrives at

$$(\dot{\boldsymbol{F}}^d - \dot{\bar{\boldsymbol{F}}})^T \Gamma_F \tilde{\boldsymbol{F}}^d = -\tau_0^{-1}\tilde{\boldsymbol{F}}^{dT}\Gamma_F \tilde{\boldsymbol{F}}^d - \dot{\bar{\boldsymbol{F}}}^T \Gamma_F \tilde{\boldsymbol{F}}^d \tag{7.31}$$

Two issues have to be taken care of here, with respect to $\dot{\bar{\boldsymbol{F}}}$ that appears in equation (7.31). First, term $\dot{\bar{\boldsymbol{F}}}$ will include $\dot{s}$. Following the DSC method, $\dot{s}$ is shown bounded as follows. Equation (7.17) shows that

$$\dot{s} = M^{-1}(X)\{\Theta(X, \dot{X}_r, \ddot{X}_r)\tilde{\theta} - K_d s - \boldsymbol{J}_a[\boldsymbol{\sigma}_{12}]\boldsymbol{J}_a^T s + \boldsymbol{J}_a^T(\tilde{\boldsymbol{F}} + \tilde{\boldsymbol{F}}^d) - D(X, \dot{X})s$$
$$+ \boldsymbol{J}_a^T[([\hat{\boldsymbol{\sigma}}_0]\hat{z}_0 - [\boldsymbol{\sigma}_0]\boldsymbol{z}) - [\frac{|\dot{\boldsymbol{x}}|}{g(\dot{\boldsymbol{x}})}]([\hat{\boldsymbol{\sigma}}_1]\hat{z}_1 - [\boldsymbol{\sigma}_1]\boldsymbol{z})]\} \tag{7.32}$$

All the estimates $\hat{\theta}$, $\hat{\boldsymbol{\sigma}}_0$ and $\hat{\boldsymbol{\sigma}}_1$ in equation (7.32) are bounded according to equation (7.13); so is $\tilde{\theta}$. Therefore, there exists a positive continuous function γ_s, such that

$$\|\dot{s}\| \le \gamma_s(e, s, \tilde{\boldsymbol{F}}, \tilde{\boldsymbol{F}}^d, \tilde{\boldsymbol{z}}_0, \tilde{\boldsymbol{z}}_1, X^d, \dot{X}^d, \ddot{X}^d, K_d) \tag{7.33}$$

Second, vector $\overline{\boldsymbol{F}}$ includes friction compensation $\hat{\boldsymbol{F}}_{fc}$, which has a term containing $|\dot{x}_j^i|$. The gradient of $|\dot{x}_j^i|$ is undetermined when $\dot{x}_j^i = 0$. However, the generalized gradient (Clark, 1983)

$$\partial|\dot{x}_j^i| = SGN(\dot{x}_j^i) = \begin{cases} 1 & \dot{x}_j^i \in R^+ \\ [-1,+1] & \dot{x}_j^i = 0 \\ -1 & \dot{x}_j^i \in R^- \end{cases} \tag{7.34}$$

is bounded anywhere, including $\dot{x}_j^i = 0$. Based on equation (7.7) and the above analysis, there exists a continuous positive function γ_F, such that

$$-\dot{\overline{\boldsymbol{F}}}^T \Gamma_F \tilde{\boldsymbol{F}}^d \le \gamma_F(e, s, \tilde{\boldsymbol{F}}, \tilde{\boldsymbol{F}}^d, \tilde{\boldsymbol{z}}_0, \tilde{\boldsymbol{z}}_1, X^d, \dot{X}^d, \ddot{X}^d, K_d)\tilde{\boldsymbol{F}}^d \tag{7.35}$$

The generalized gradient at a point $\dot{x}_j^i$ can be viewed as a set valued map equal to the convex closure of the limiting gradient near $\dot{x}_j^i$ [for a similar argument, see references by Maciuca and Hedrick (1997) and Duraiswamy and Chiu (2003)]. Now from equation (7.30), one arrives at

$$\dot{\mathrm{V}}_2 \le \dot{\mathrm{V}}_1 - s^T \boldsymbol{J}_a \tilde{\boldsymbol{F}} - \tilde{\boldsymbol{F}}^T K_F \Gamma_F \tilde{\boldsymbol{F}} + \|\tilde{\varphi}\|\gamma_\varphi \|\tilde{\boldsymbol{F}}\| - \tau_0^{-1}\Gamma_F \|\tilde{\boldsymbol{F}}^d\|^2 + \gamma_F \|\tilde{\boldsymbol{F}}^d\| \tag{7.36}$$

Replacing $\dot{\mathrm{V}}_1$ in equation (7.36) with equation (7.25) gives

$$\begin{aligned}\dot{\mathrm{V}}_2 \le & -s^T K_d s - s^T \boldsymbol{J}_a[\boldsymbol{\sigma}_{12}]\boldsymbol{J}_a^T s + s^T \boldsymbol{J}_a \widetilde{\boldsymbol{F}}^d + \|\widetilde{\theta}\|\gamma_\theta\|s\| + \|\widetilde{\boldsymbol{\sigma}}_0\|\gamma_{\sigma_0}\|s\| \\ & + \|\widetilde{\boldsymbol{\sigma}}_1\|\gamma_{\sigma_1}\|s\| - \widetilde{\boldsymbol{z}}_0^T[\frac{|\dot{\boldsymbol{x}}|}{g(\dot{\boldsymbol{x}})}][\boldsymbol{\sigma}_0]\Gamma_{z0}\widetilde{\boldsymbol{z}}_0 - \widetilde{\boldsymbol{z}}_1^T[\frac{|\dot{\boldsymbol{x}}|}{g(\dot{\boldsymbol{x}})}][\boldsymbol{\sigma}_1]\Gamma_{z1}\widetilde{\boldsymbol{z}}_1 \\ & - \widetilde{\boldsymbol{F}}^T K_F \Gamma_F \widetilde{\boldsymbol{F}} + \|\widetilde{\varphi}\|\gamma_\varphi\|\widetilde{\boldsymbol{F}}\| - \tau_0^{-1}\Gamma_F\|\widetilde{\boldsymbol{F}}^d\|^2 + \gamma_F\|\widetilde{\boldsymbol{F}}^d\|\end{aligned} \tag{7.37}$$

For any $r_\varepsilon > 0$ and $\forall\{\mathrm{V}_2 \le r_\varepsilon\}$, define constants C_1, C_2, C_3

$$C_1 = \max(\theta_M \gamma_\theta) + \max(\boldsymbol{\sigma}_{0,M}\gamma_{\sigma_0}) + \max(\boldsymbol{\sigma}_{1,M}\gamma_{\sigma_1}) \tag{7.38a}$$

$$C_2 = \max(\varphi_M \gamma_\varphi) \tag{7.38b}$$

$$C_3 = \max(\gamma_F) \tag{7.38c}$$

where $\mu_M = \|\mu_U - \mu_L\|$, $\mu = \theta, \varphi, \boldsymbol{\sigma}_0, \boldsymbol{\sigma}_1$.

Since $C_1\|s\| \le \frac{C_1^2}{4\varepsilon_1}\|s\|^2 + \varepsilon_1$, $C_2\|\widetilde{\boldsymbol{F}}\| \le \frac{C_2^2}{4\varepsilon_2}\|\widetilde{\boldsymbol{F}}\|^2 + \varepsilon_2$, $C_3\|\widetilde{\boldsymbol{F}}^d\| \le \frac{C_3^2}{4\varepsilon_3}\|\widetilde{\boldsymbol{F}}^d\|^2 + \varepsilon_3$, for any $\varepsilon_i > 0, i = 1, 2, 3;$ the following is obtained

$$\begin{aligned}\dot{\mathrm{V}}_2 \le & (-K_d + \frac{\overline{\sigma}(\boldsymbol{J}_a)}{2} + \frac{C_1^2}{4\varepsilon_1})\|s\|^2 + (-K_F\Gamma_F + \frac{C_2^2}{4\varepsilon_2})\|\widetilde{\boldsymbol{F}}\|^2 - \widetilde{\boldsymbol{z}}_0^T[\frac{|\dot{\boldsymbol{x}}|}{g(\dot{\boldsymbol{x}})}][\boldsymbol{\sigma}_0]\Gamma_{z0}\widetilde{\boldsymbol{z}}_0 \\ & - \widetilde{\boldsymbol{z}}_1^T[\frac{|\dot{\boldsymbol{x}}|}{g(\dot{\boldsymbol{x}})}][\boldsymbol{\sigma}_1]\Gamma_{z1}\widetilde{\boldsymbol{z}}_1 + (-\frac{1}{\tau_0}\Gamma_F + \frac{\overline{\sigma}(\boldsymbol{J}_a)}{2} + \frac{C_3^2}{4\varepsilon_3})\|\widetilde{\boldsymbol{F}}^d\|^2 + \varepsilon\end{aligned} \tag{7.39}$$

where $\varepsilon = \varepsilon_1 + \varepsilon_2 + \varepsilon_3$. Noting the semi-negative terms $-\widetilde{\boldsymbol{z}}_0^T\frac{|\dot{\boldsymbol{x}}|}{g(\dot{\boldsymbol{x}})}[\boldsymbol{\sigma}_0]\Gamma_{z0}\widetilde{\boldsymbol{z}}_0 - \widetilde{\boldsymbol{z}}_1^T\frac{|\dot{\boldsymbol{x}}|}{g(\dot{\boldsymbol{x}})}[\boldsymbol{\sigma}_1]\Gamma_{z1}\widetilde{\boldsymbol{z}}_1$ in equation (7.39), there exist appropriate gains K_d and K_F, and a filter time constant τ_0, such that

$$\dot{\mathrm{V}}_2 \le -\eta(\|s\|^2 + \|\widetilde{\boldsymbol{F}}\|^2 + \|\widetilde{\boldsymbol{F}}^d\|^2) + \varepsilon \tag{7.40}$$

and

$$\eta = \min\{(K_d - \frac{\overline{\sigma}(\boldsymbol{J}_a)}{2} - \frac{C_1^2}{4\varepsilon_1}), (K_F\Gamma_F - \frac{C_2^2}{4\varepsilon_2}), (\frac{1}{\tau_0}\Gamma_F - \frac{\overline{\sigma}(\boldsymbol{J}_a)}{2} - \frac{C_3^2}{4\varepsilon_3})\} > 0 \tag{7.41}$$

which is to say

$$K_d > \frac{\bar{\sigma}(\boldsymbol{J}_a)}{2} + \frac{C_1^2}{4\varepsilon_1} \tag{7.42}$$

$$K_F \Gamma_F > \frac{C_2^2}{4\varepsilon_2} \tag{7.43}$$

$$\tau_0 < \Gamma_F \left(\frac{\bar{\sigma}(\boldsymbol{J}_a)}{2} + \frac{C_3^2}{4\varepsilon_3} \right)^{-1} \tag{7.44}$$

$\dot{\mathrm{V}}_2 \le 0$, whenever vector $r(s, \tilde{\boldsymbol{F}}, \tilde{\boldsymbol{F}}^d) = (s^T, \tilde{\boldsymbol{F}}^T, \tilde{\boldsymbol{F}}^{d^T})^T$ is outside the compact set $\{r(s, \tilde{\boldsymbol{F}}, \tilde{\boldsymbol{F}}^d) \,|\, (\|s\|^2 + \|\tilde{\boldsymbol{F}}\|^2 + \|\tilde{\boldsymbol{F}}^d\|^2) < \varepsilon / \eta\}$. Thus, it is concluded that the closed–loop system is stable and eventually the tracking error converges to a small neighborhood of zero, whose size is adjustable by the design parameters ε, K_d, K_F and τ_0. Moreover, for most of the time during the tracking task, velocity is nonzero, i.e. $|\dot{\boldsymbol{x}}| \neq 0$. Therefore, excluding the zero velocity, equation (7.39) becomes

$$\dot{\mathrm{V}}_2 \le -\xi \mathrm{V}_2 + \varepsilon \tag{7.45}$$

and

$$\xi = \min\{\eta, [\frac{|\dot{\boldsymbol{x}}|}{g(\dot{\boldsymbol{x}})}][\boldsymbol{\sigma}_0]\Gamma_{z0}, [\frac{|\dot{\boldsymbol{x}}|}{g(\dot{\boldsymbol{x}})}][\boldsymbol{\sigma}_1]\Gamma_{z1}\} / \alpha_U > 0 \tag{7.46}$$

where α_U >0, and is defined by

$$\mathrm{V}_2 \le \alpha_U (\|s\|^2 + \|\tilde{\boldsymbol{F}}\|^2 + \|\tilde{\boldsymbol{F}}^d\|^2 + \|\tilde{\boldsymbol{z}}_0\| + \|\tilde{\boldsymbol{z}}_1\|) \tag{7.47}$$

Inequality (7.45) gives

$$\mathrm{V}_2(t) \le \exp(-\xi\, t)\mathrm{V}_2(0) + [1 - \exp(-\xi\, t)]\varepsilon / \xi \tag{7.48}$$

This further indicates that an exponentially converging transient performance is achieved with the exponentially converging rate ξ and the final tracking error can be adjusted via controller parameters freely, in a known form. It is seen from equation (7.46) that the convergence rate can be made arbitrarily large, and final tracking errors ε / ξ, can be made arbitrarily small by increasing the control gains K_d, K_F, Γ_{z0}, Γ_{z1}; or decreasing the design parameter ε and the filter time constant τ_0. A small or appropriate time constant plays a role to ensure that $\boldsymbol{F}^d$ follows $\overline{\boldsymbol{F}}$ timely without affecting the system's stability.

Finally, since $s = \dot{e} + \lambda e \ (\lambda > 0)$, the position tracking error is bounded and reaches an arbitrarily small value. This completes the proof of the proposition.

Remarks 7.1.2:

(i) The proposed controller is also robust against un-modeled nonlinearities. Let term $\widetilde{\delta}$ be an uncertain and nonlinear function in the dynamics of the system under investigation, and practically $|\widetilde{\delta}| < \widetilde{\delta}_U$. Accordingly, the term in equation (7.38a) is adjusted as

$$C_1 = \max(\theta_M |\gamma_\theta|) + \max(\boldsymbol{\sigma}_{0,M} |\gamma_{\sigma_0}|) + \max(\boldsymbol{\sigma}_{1,M} |\gamma_{\sigma_1}| + \widetilde{\delta}_U) \tag{7.49}$$

which, shows that the inclusion of an uncertain non-linearity increases C_1 and thus may require a higher gain K_d to meet equation (7.41). In other words, without any other efforts, simply increasing the control gain K_d can improve the control system's robustness against un-modeled nonlinearities.

(ii) The contact force of the entire control system can be shown to be

$$\boldsymbol{F}_c^{t\to\infty} = \boldsymbol{W}^\dagger E^{-T}\tau^d + \boldsymbol{V}F_{\text{int}}^d - \boldsymbol{J}^{-T}[\boldsymbol{H}_m\ddot{\boldsymbol{q}}^d + \boldsymbol{C}_m\dot{\boldsymbol{q}}^d + \boldsymbol{G}_m + \overline{\boldsymbol{J}}(\boldsymbol{F}_{fc} - \hat{\boldsymbol{F}}_{fc}) + \widetilde{\varepsilon}] \tag{7.50}$$

where $\widetilde{\varepsilon}$ is a bounded function of the bounded state errors. From equations (2.12), (2.13) and (7.50), it can then be proven that

$$F_{ext}^{t\to\infty} = \boldsymbol{W}\boldsymbol{F}_c^{t\to\infty} = E^{-T}\tau^d - \boldsymbol{W}\boldsymbol{J}^{-T}[\boldsymbol{H}_m\ddot{\boldsymbol{q}}^d + \boldsymbol{C}_m\dot{\boldsymbol{q}}^d + \boldsymbol{G}_m + \overline{\boldsymbol{J}}(\boldsymbol{F}_{fc} - \hat{\boldsymbol{F}}_{fc}) + \widetilde{\varepsilon}] \tag{7.51}$$

and

$$\boldsymbol{V}F_{\text{int}}^{t\to\infty} = \boldsymbol{F}_c^{t\to\infty} - \boldsymbol{W}^\dagger F_{ext}^{t\to\infty} = \boldsymbol{V}F_{\text{int}}^d - (\boldsymbol{I} - \boldsymbol{W}^\dagger\boldsymbol{W})\boldsymbol{J}^{-T}[\boldsymbol{H}_m\ddot{\boldsymbol{q}}^d + \boldsymbol{C}_m\dot{\boldsymbol{q}}^d + \boldsymbol{G}_m + \overline{\boldsymbol{J}}(\boldsymbol{F}_{fc} - \hat{\boldsymbol{F}}_{fc}) + \widetilde{\varepsilon}] \tag{7.52}$$

where, $F_{ext}^{t\to\infty}$ and $F_{\text{int}}^{t\to\infty}$ are the external and internal forces as $t \to \infty$, respectively. Since $\boldsymbol{V}$ is a full-column-rank matrix, it can be concluded that

$$F_{\text{int}}^{t\to\infty} = F_{\text{int}}^d - \boldsymbol{V}^\dagger(\boldsymbol{I} - \boldsymbol{W}^\dagger\boldsymbol{W})\boldsymbol{J}^{-T}[\boldsymbol{H}_m\ddot{\boldsymbol{q}}^d + \boldsymbol{C}_m\dot{\boldsymbol{q}}^d + \boldsymbol{G}_m + \overline{\boldsymbol{J}}(\boldsymbol{F}_{fc} - \hat{\boldsymbol{F}}_{fc}) + \widetilde{\varepsilon}] \tag{7.53}$$

Equation (7.53) indicates that the actual internal force is bounded, but does not converge to the desired value. In order to enhance the regulation of the internal force, a force feedback loop in the control law (7.4) is further introduced by replacing $\boldsymbol{V}F_{\text{int}}^{d}$ with $\boldsymbol{V}(F_{\text{int}}^{d} + K_{\text{int}}(F_{\text{int}}^{d} - F_{\text{int}}))$ in equation (7.7):

$$\overline{\boldsymbol{F}} = \overline{\boldsymbol{J}}^{-1}\boldsymbol{J}^{T}(\boldsymbol{W}^{\dagger}E^{-T}\tau^{d} + \boldsymbol{V}(F_{\text{int}}^{d} + K_{\text{int}}(F_{\text{int}}^{d} - F_{\text{int}}))) + \hat{\boldsymbol{F}}_{fc} \tag{7.54}$$

The internal force, F_{int}, can be extracted from contact forces, which are typically available through wrist force sensors. As a result, equation (7.53) becomes

$$F_{\text{int}}^{t\to\infty} = F_{\text{int}}^{d} - (1+K_{\text{int}})^{-1}\boldsymbol{V}^{\dagger}(\boldsymbol{I} - \boldsymbol{W}^{\dagger}\boldsymbol{W})\boldsymbol{J}^{-T}[\boldsymbol{H}_{m}\ddot{\boldsymbol{q}}^{d} + \boldsymbol{C}_{m}\dot{\boldsymbol{q}}^{d} + \boldsymbol{G}_{m} + \overline{\boldsymbol{J}}(\boldsymbol{F}_{fc} - \hat{\boldsymbol{F}}_{fc}) + \widetilde{\varepsilon}] \tag{7.55}$$

Theoretically, the actual internal force can be arbitrarily set as close as possible to the desired value through adjusting the force feedback gain K_{int}. With respect to stability, the same Lyapunov-like scalar function will result in the same conclusion, since only the term related to internal force has been changed.

Regarding the load distribution, it is noticed that the contact force in equation (7.50) has an extra term $-\boldsymbol{J}^{-T}[\boldsymbol{H}_{m}\ddot{\boldsymbol{q}}^{d} + \boldsymbol{C}_{m}\dot{\boldsymbol{q}}^{d} + \boldsymbol{G}_{m} + \overline{\boldsymbol{J}}(\boldsymbol{F}_{fc} - \hat{\boldsymbol{F}}_{fc}) + \widetilde{\varepsilon}]$, when compared with the reverse mapping $\boldsymbol{F}_{c} = \boldsymbol{W}^{\dagger}F_{ext} + \boldsymbol{V}F_{\text{int}}$ as stated in equation (2.13). Therefore, the load distribution scheme described in $\boldsymbol{W}^{\dagger}$ can be dynamically changed because of this extra term, especially when uneven load distribution is scheduled.

(iii) With respect to the controller (7.4), the only hydraulic parameters needed by the controller are the effective piston areas $\boldsymbol{A}_{I}$ and $\boldsymbol{A}_{O}$. Other hydraulic function parameters such as effective bulk modulus β or control valve gain K_{sp}; are all considered in the adaptation laws described in the proposed control strategy. Similarly, the control law requires no knowledge about mass or inertia of the manipulators' links or payload. The controller only needs knowledge about the length of the manipulators' links, since the Jacobian matrix appears in the control law. Only measurements of manipulators' joint angular positions and velocities as well as hydraulic line pressures are required for feedback.

(iv) Construct the following Lyapunov-like scalar function for the same control system:

$$\mathrm{V}_2 = \mathrm{V}_1 + \tfrac{1}{2}\widetilde{\boldsymbol{F}}^T \mathit{\Gamma}_F \widetilde{\boldsymbol{F}} + \tfrac{1}{2}\widetilde{\boldsymbol{F}}^{d^T} \mathit{\Gamma}_F \widetilde{\boldsymbol{F}}^d + \tfrac{1}{2}(\widetilde{\theta}^T w_\theta^{-1}\widetilde{\theta} + \widetilde{\boldsymbol{\sigma}}_0^T w_{\sigma_0}^{-1}\widetilde{\boldsymbol{\sigma}}_0 + \widetilde{\boldsymbol{\sigma}}_1^T w_{\sigma_1}^{-1}\widetilde{\boldsymbol{\sigma}}_1 + \widetilde{\varphi}^T w_\varphi^{-1}\widetilde{\varphi}) \quad (7.56)$$

where term V_1 is given by equation (7.16). Given the above Lyapunov-like scalar candidate, instead of arriving at equation (7.37), one obtains

$$\begin{aligned}\dot{\mathrm{V}}_2 \le & -s^T K_d s - s^T \boldsymbol{J}_a[\boldsymbol{\sigma}_{12}]\boldsymbol{J}_a^T s + s^T \boldsymbol{J}_a \widetilde{\boldsymbol{F}}^d - \widetilde{\boldsymbol{F}}^T K_F \mathit{\Gamma}_F \widetilde{\boldsymbol{F}} - \tau_0^{-1}\Gamma_F \left\|\widetilde{\boldsymbol{F}}^d\right\|^2 + \gamma_F \left\|\widetilde{\boldsymbol{F}}^d\right\| \\ & - \widetilde{\boldsymbol{z}}_0^T[\frac{|\dot{\boldsymbol{x}}|}{g(\dot{\boldsymbol{x}})}][\boldsymbol{\sigma}_0]\mathit{\Gamma}_{z0}\widetilde{\boldsymbol{z}}_0 - \widetilde{\boldsymbol{z}}_1^T[\frac{|\dot{\boldsymbol{x}}|}{g(\dot{\boldsymbol{x}})}][\boldsymbol{\sigma}_1]\mathit{\Gamma}_{z1}\widetilde{\boldsymbol{z}}_1 \\ & + \widetilde{\theta}^T(w_\theta^{-1}\dot{\hat{\theta}} - Y_\theta) + \widetilde{\boldsymbol{\sigma}}_0^T(w_{\sigma_0}^{-1}\dot{\hat{\boldsymbol{\sigma}}}_0 - Y_{\sigma_0}) + \widetilde{\boldsymbol{\sigma}}_1^T(w_{\sigma_1}^{-1}\dot{\hat{\boldsymbol{\sigma}}}_1 - Y_{\sigma_1}) + \widetilde{\varphi}^T(w_\varphi^{-1}\dot{\hat{\varphi}} - Y_\varphi)\end{aligned} \quad (7.57)$$

Using inequality (7.14), one further arrives at

$$\begin{aligned}\dot{\mathrm{V}}_2 \le & -s^T K_d s - s^T \boldsymbol{J}_a[\boldsymbol{\sigma}_{12}]\boldsymbol{J}_a^T s + s^T \boldsymbol{J}_a \widetilde{\boldsymbol{F}}^d - \widetilde{\boldsymbol{F}}^T K_F \mathit{\Gamma}_F \widetilde{\boldsymbol{F}} - \tau_0^{-1}\Gamma_F \left\|\widetilde{\boldsymbol{F}}^d\right\|^2 + \gamma_F \left\|\widetilde{\boldsymbol{F}}^d\right\| \\ & - \widetilde{\boldsymbol{z}}_0^T[\frac{|\dot{\boldsymbol{x}}|}{g(\dot{\boldsymbol{x}})}][\boldsymbol{\sigma}_0]\mathit{\Gamma}_{z0}\widetilde{\boldsymbol{z}}_0 - \widetilde{\boldsymbol{z}}_1^T[\frac{|\dot{\boldsymbol{x}}|}{g(\dot{\boldsymbol{x}})}][\boldsymbol{\sigma}_1]\mathit{\Gamma}_{z1}\widetilde{\boldsymbol{z}}_1\end{aligned} \quad (7.58)$$

Similar to inequality (7.39), one obtains

$$\begin{aligned}\dot{\mathrm{V}}_2 \le & (-K_d + \frac{\overline{\sigma}(\boldsymbol{J}_a)}{2})\|s\|^2 - K_F \mathit{\Gamma}_F \left\|\widetilde{\boldsymbol{F}}\right\|^2 - \widetilde{\boldsymbol{z}}_0^T[\frac{|\dot{\boldsymbol{x}}|}{g(\dot{\boldsymbol{x}})}][\boldsymbol{\sigma}_0]\mathit{\Gamma}_{z0}\widetilde{\boldsymbol{z}}_0 \\ & - \widetilde{\boldsymbol{z}}_1^T[\frac{|\dot{\boldsymbol{x}}|}{g(\dot{\boldsymbol{x}})}][\boldsymbol{\sigma}_1]\mathit{\Gamma}_{z1}\widetilde{\boldsymbol{z}}_1 + (-\frac{1}{\tau_0}\mathit{\Gamma}_F + \frac{\overline{\sigma}(\boldsymbol{J}_a)}{2} + \frac{C_3^2}{4\varepsilon_3})\left\|\widetilde{\boldsymbol{F}}^d\right\|^2 + \varepsilon\end{aligned} \quad (7.59)$$

From inequality (7.59), the same conclusions can be made as from inequality (7.39), except that exponentially converging transient performance is not shown. Compared with equation (7.41), the ranges for K_d and $K_F \mathit{\Gamma}_F$ are wider, which can be obtained from equation (7.59) as below:

$$K_d > \frac{\overline{\sigma}(\boldsymbol{J}_a)}{2} \quad (7.60)$$

$$K_F \mathit{\Gamma}_F > 0 \quad (7.61)$$

It follows, that to achieve exponentially converging transient performance, gains K_d, $K_F \mathit{\Gamma}_F$ are expected to be higher, to account for the parameter uncertainties represented by C_1 and C_2.

7.2 Simulation Results

The nonlinear controller derived in Section 7.1 has been examined by numerical simulations using the same simulation model presented in the previous Chapter. The same two reference trajectories as used in Chapter 6 were used again:

(i) point-to-point trajectory with a travel distance of 0.3m, maximum speed of 0.15m/s and maximum acceleration of 0.6m/s^2 and

(ii) sinusoidal trajectory consisting of one segment with an amplitude of 0.1m and frequency of 0.2Hz followed by a second segment with an amplitude of 0.02m and frequency of 1Hz.

These two reference trajectories are shown in Figures 7.1 and Figure 7.13, respectively. The controller was also required to maintain the internal force on the object in the horizontal direction close to zero and at the same time, evenly distribute the load between the two robots, i.e. $\alpha^1 = \alpha^2 = 0.5$. The control gains were chosen as follows:

$\lambda = diag(200,...,200)$, $\tau_0 = diag(0.01,...,0.01)$, $K_{\text{int}} = diag(3,...,3)$,

$K_d = diag(2000,...,2000)$, $K_F = diag(2,...,2)$, $\Gamma_F = diag(0.05,...,0.05)$,

$w_\theta = diag(1,1,1,1,1,1,0.2,1,1,1,1,1,1,1,0.25,1,50,1,\ 10^7,\ 10^7,\ 10^7,10^7,\ 10^7,\ 10^7)$,

$w_\varphi^{(12\times12)} = diag(2.4\times10^{-9},\ 2\times10^6,\ ...,2.4\times10^{-9},\ 2\times10^6)$,

$w_{\sigma_0}^{(6\times6)} = diag(2\times10^9,\ ...,2\times10^9)$, $w_{\sigma_1}^{(6\times6)} = diag(5\times10^6,\ ...,5\times10^6)$,

$\Gamma_{z_0}^{(6\times6)} = diag(10,\ ...,10)$, $\Gamma_{z_1}^{(6\times6)} = diag(10,\ ...,10)$.

The first set of tests was conducted using the point-to-point trajectory tracking shown in Figure 7.1. Figure 7.2 shows the tracking error. As can be seen, the object follows the desired path closely with almost zero steady state error of position. The control signals shown in Figure 7.3 are all reasonable and smooth. The internal force is theoretically not guaranteed to converge to the desired level. With force feedback ($K_{\text{int}} = diag(3,...,3)$), the internal force has a small value of 40N (shown in Figure 7.4), which is the same magnitude as the simulation in last chapter. Estimations of typical parameters are shown in Figure 7.5. Note that the estimated values of the parameters do not converge to the actual. Such results, however, do not contradict the theoretical argument, since the parameter convergence is not theoretically guaranteed in Section 7.1. The distribution of the payload between the two manipulators was fairly even as shown in Figure 7.6. Finally, Figure 7.7 shows the friction estimation $\hat{F}_{fc}$, for the second link of one manipulator during the tracking control, which follows the actual (F_{fc}) reasonably well.

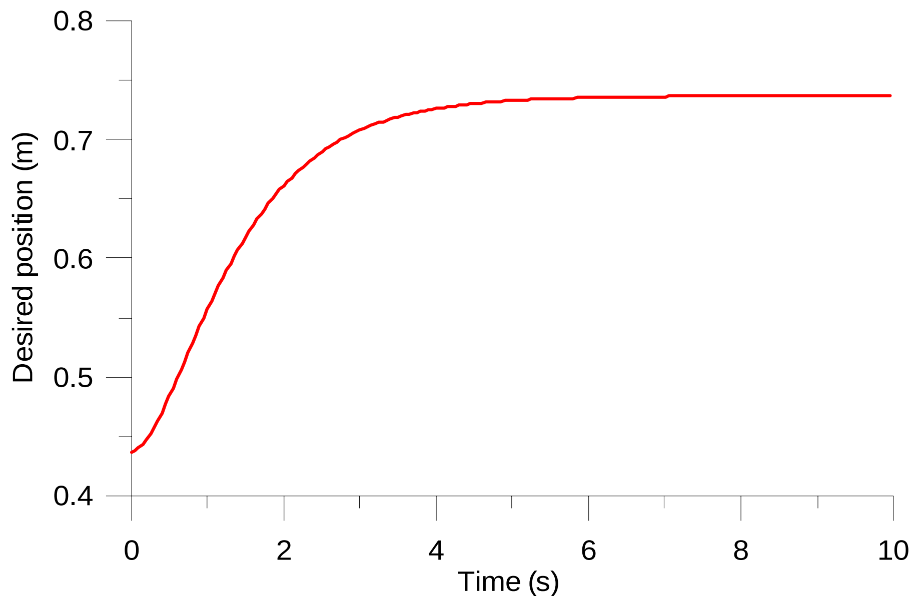

Figure 7.1: Point-to-point reference trajectory.

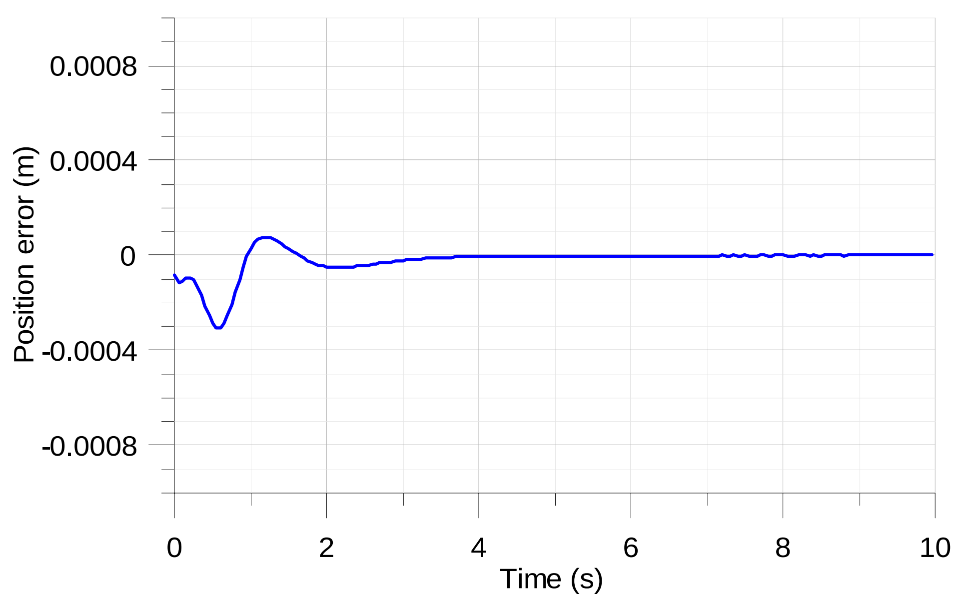

Figure 7.2: Position tracking error.

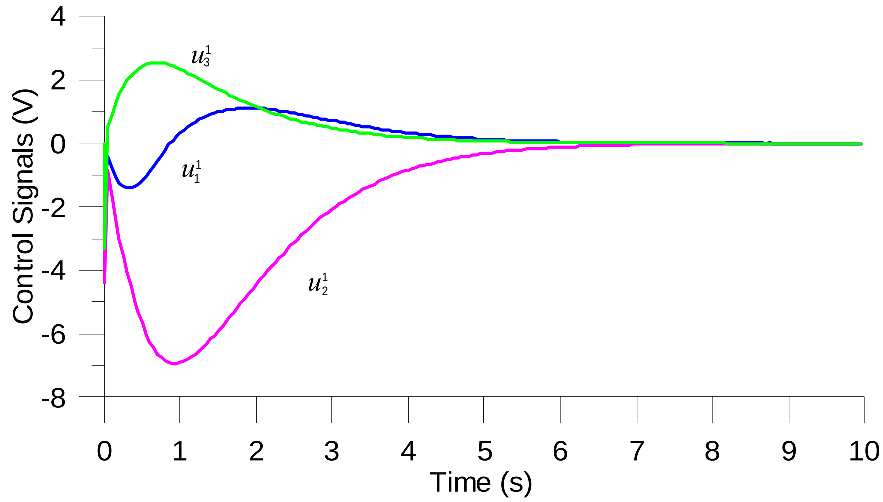

Figure 7.3: Control signals for one of the manipulators.

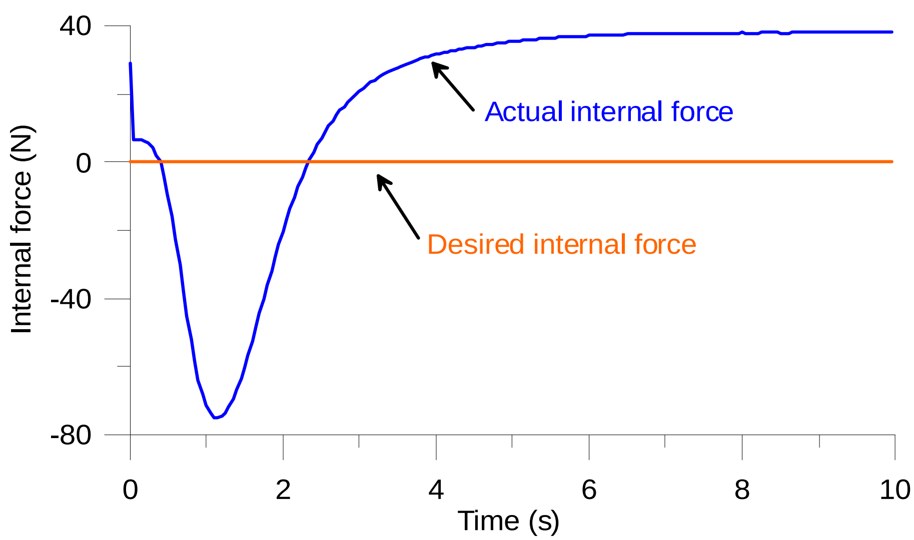

Figure 7.4: Internal force on the object in the horizontal direction.

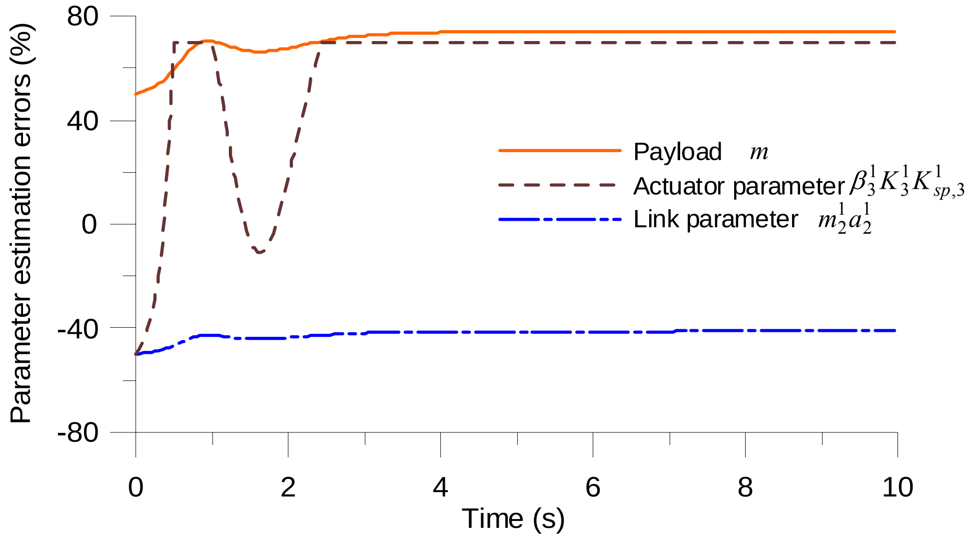

Figure 7.5: Typical parameter estimation errors.

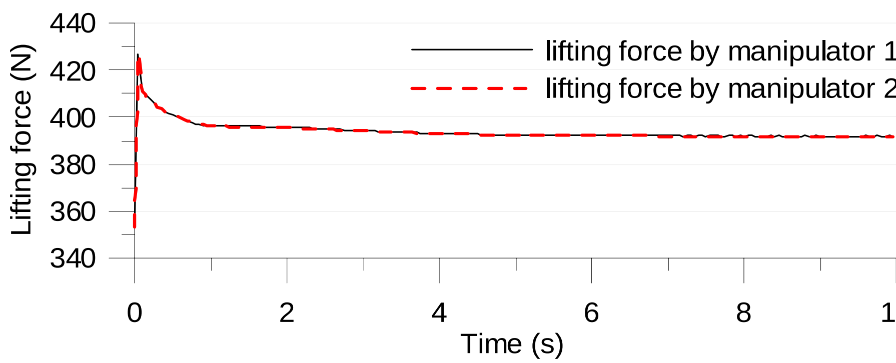

Figure 7.6: Load sharing between manipulators.

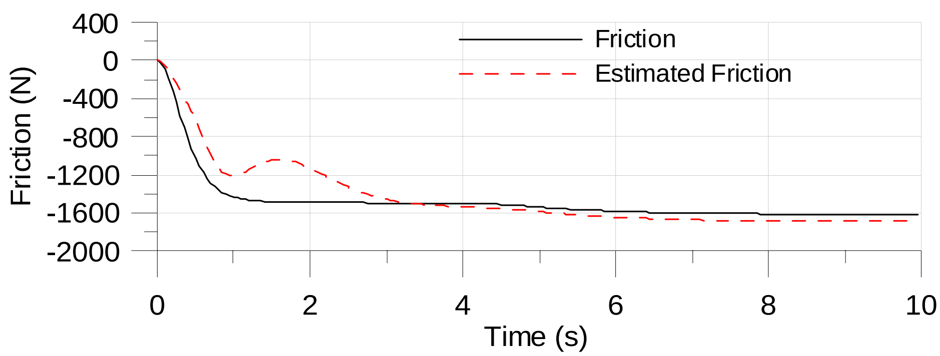

Figure 7.7: Friction and its estimate (link two of one of the manipulators).

The above simulation was repeated with uneven load distribution described by $\alpha^1 = 0.6$ and $\alpha^2 = 0.4$ that required the first manipulator to contribute more to carry the payload. Tracking errors and the internal force did not change much as shown in Figure 7.8 and 7.9 respectively. The control signals for the manipulators, shown in Figures 7.10 and 7.11, were quite different from each other. Consequently, Figure 7.12 shows that the lifting forces were not evenly distributed between the two manipulators. The first manipulator contributed more to the lift and hold of the object. Quantitatively, the distribution was not exactly the same as expected by the values of $\alpha^1 = 0.6$ and $\alpha^2 = 0.4$ due to the extra term in (7.50) that has been discussed in Section 7.1. Nevertheless, it is shown that the load distribution is still adjustable in the presence of significant friction in the actuators.

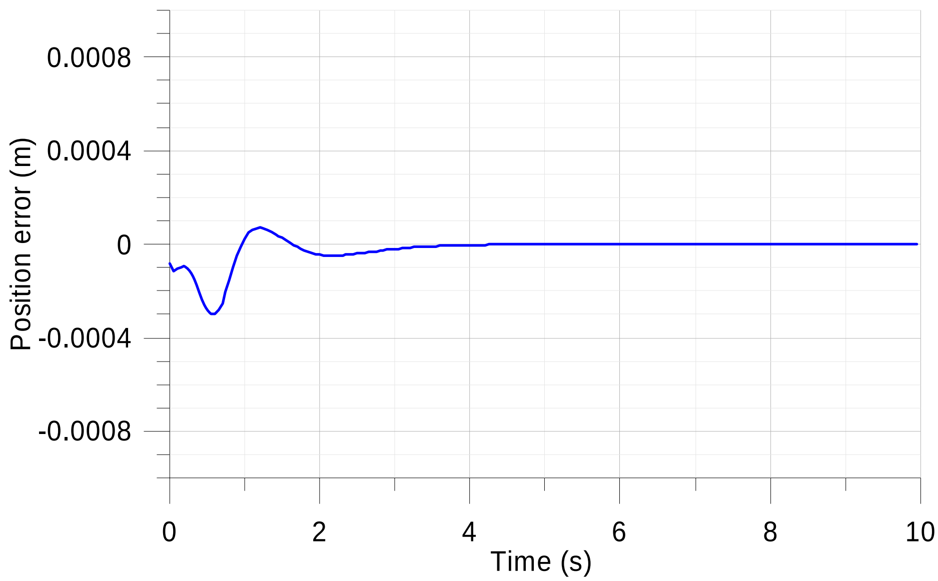

Figure 7.8: Position tracking error (uneven load distribution).

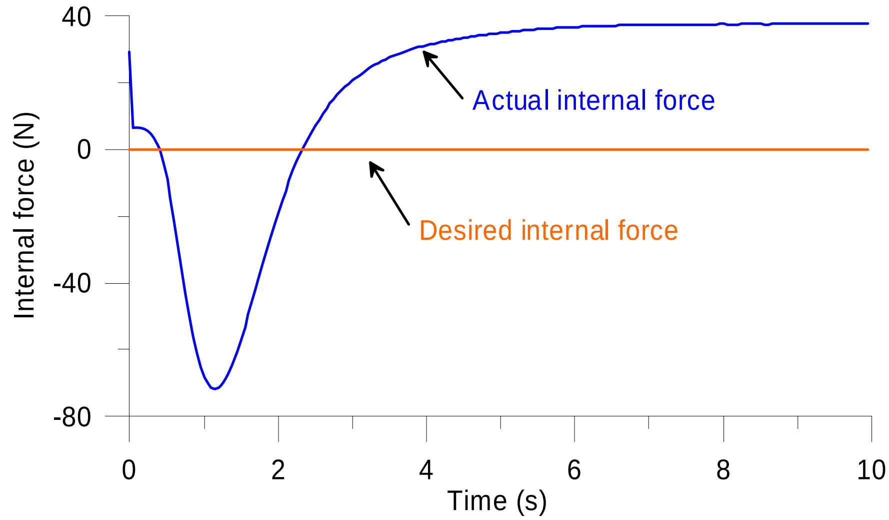

Figure 7.9: Internal force on the object in the horizontal direction.

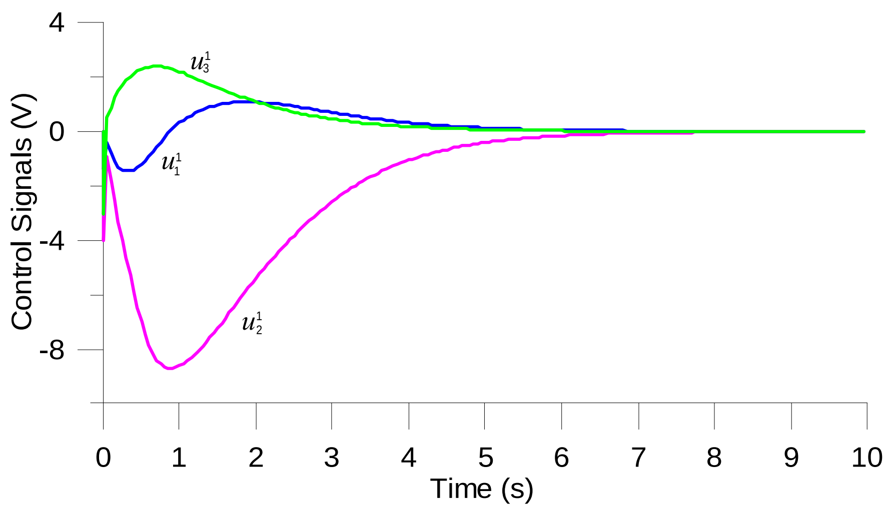

Figure 7.10: Control signals for the first manipulator.

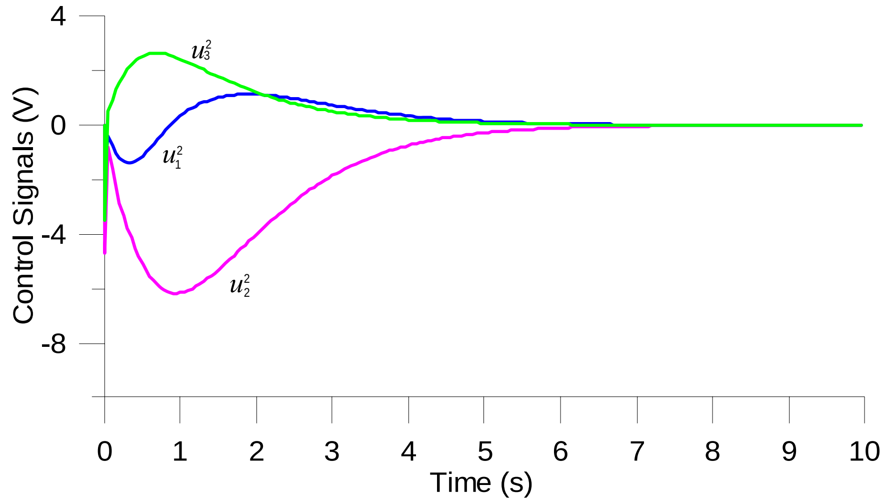

Figure 7.11: Control signals for the second manipulator.

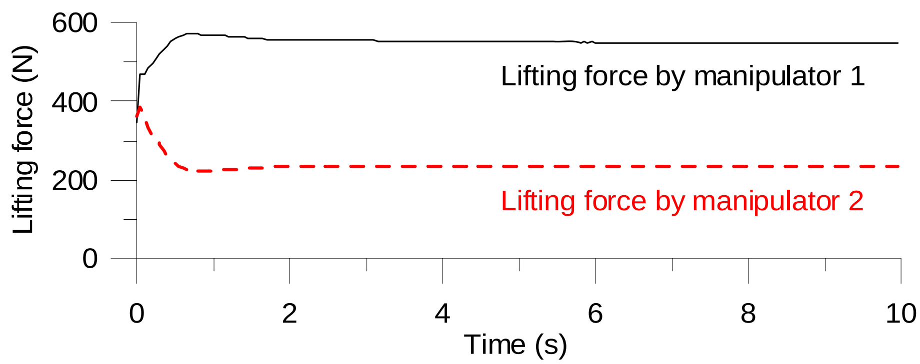

Figure 7.12: Load sharing between manipulators.

The next set of tests was conducted using even load distribution and sinusoidal trajectory tracking shown in Figure 7.13. All the gains were kept without changes. Figures 7.14 to 7.18 show the simulation results. As seen in Figure 7.14, the control system had excellent performances. The amplitudes of the position tracking errors, corresponding to the trajectory with lower frequency and higher amplitude, and the one with higher frequency and lower amplitude, are about 1 mm and 0.2 mm, respectively. The control signals to the actuators are reasonable and not saturated (see Figure 7.15). Figure 7.16 shows that the internal force on the object changes less and is closer to zero during the tracking of the low-amplitude reference. Estimations of parameters are shown in Figure 7.17. Again, they do not converge to their actual values as discussed before. The distribution of the lifting forces from the robots was quite even, as shown in Figure 7.18.

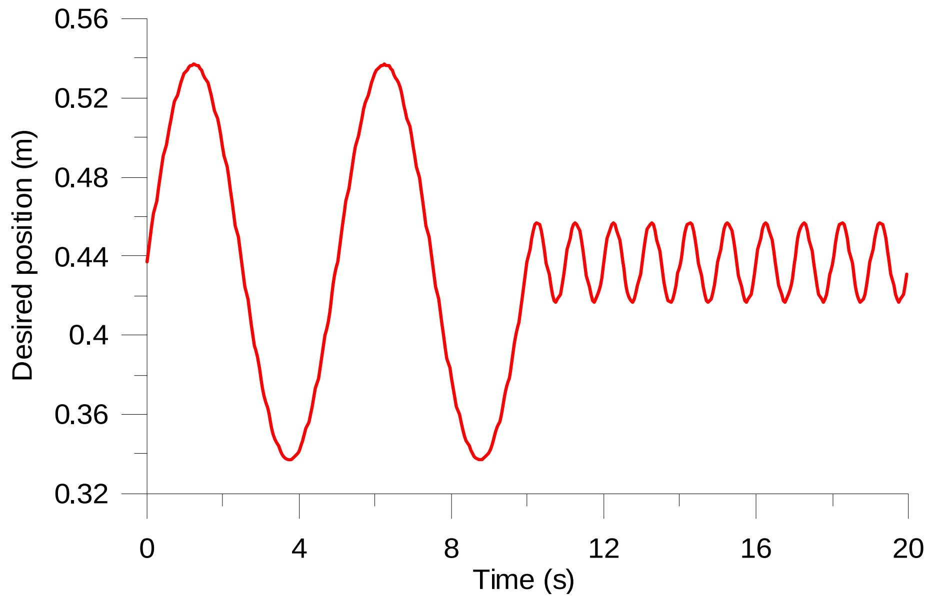

Figure 7.13: Sinusoidal reference trajectory.

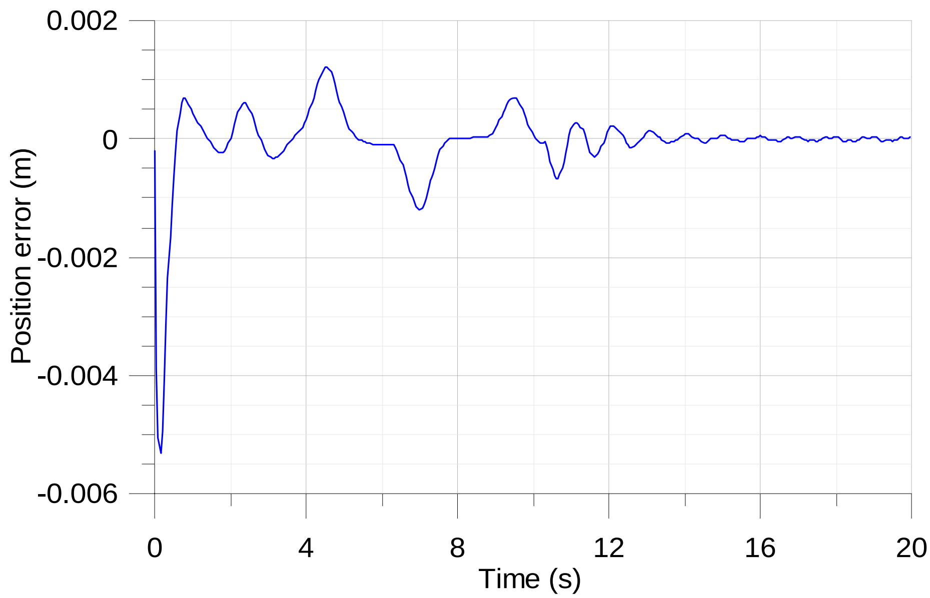

Figure 7.14: Position tracking error of the object.

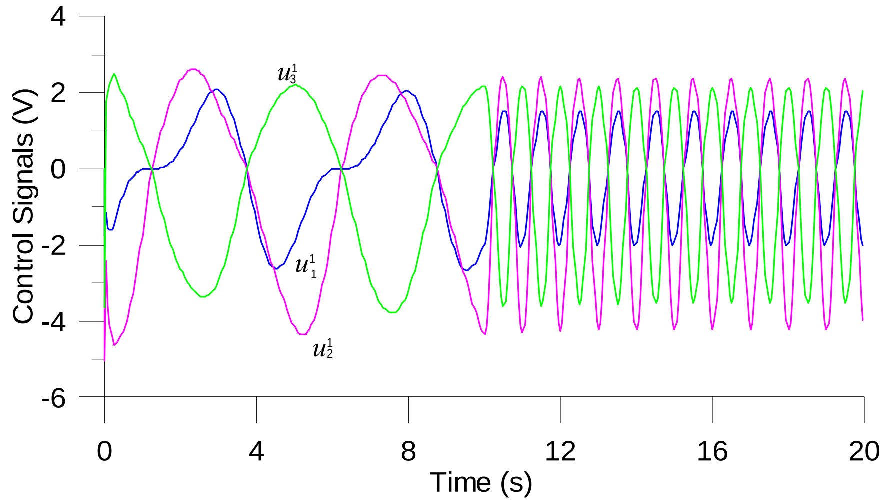

Figure 7.15: Control signals for the first manipulator.

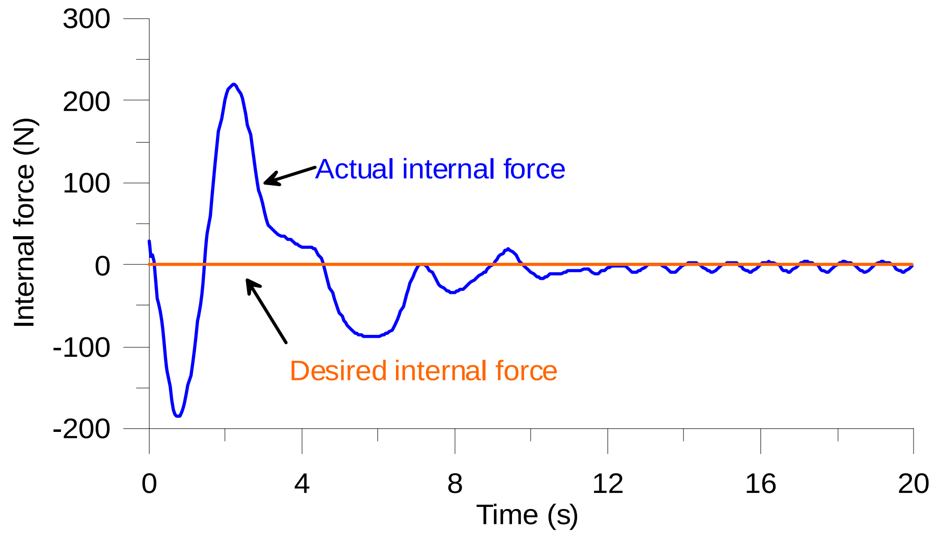

Figure 7.16: Internal force on the object in the horizontal direction.

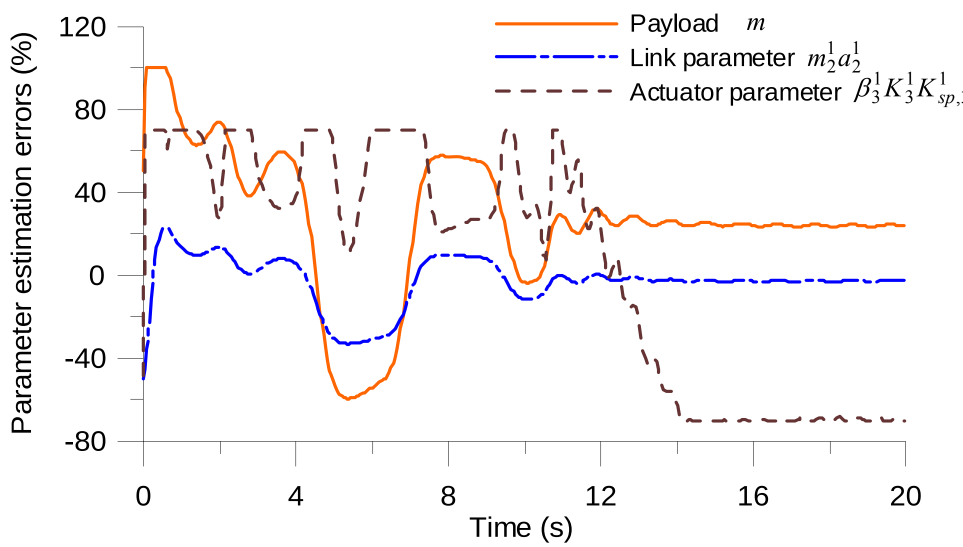

Figure 7.17: Typical parameter estimation errors

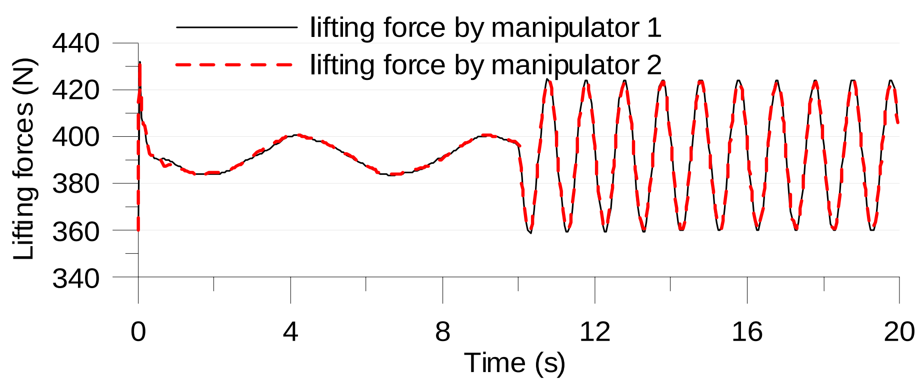

Figure 7.18: Load sharing between manipulators.

7.3 Summary

This chapter documented design, stability analysis and numerical verification of a tracking controller for co-operation among several hydraulic manipulators handling a rigid payload. Different from the controller developed in last chapter, this controller used the concept of dynamic surface control. A low pass filter was integrated in the controller design, eliminating model differentiation. Thus, complex calculation arising from "explosion of terms", as well as the requirement of acceleration feedback and the derivative of F_{int} in the case that force feedback is implemented, was avoided.

The controller design also addressed all the other issues listed in Chapter 6. The highly nonlinear dynamic behavior of hydraulic actuation, manipulators and dry friction were incorporated in the controller design. The issues of internal force control on the object, as well as load sharing among several manipulators were also addressed. To deal with parametric uncertainties in the payload, manipulators, hydraulic functions as well as friction, the controller was augmented with various adaptation laws. The proposed tracking controller does not need exact knowledge of the payload, manipulators' dynamic parameters, or hydraulic function parameters. With respect to the implementation, the controller only requires measurements of robots' joint angular positions and velocities, and hydraulic line pressures. The measurements of contact forces are needed when force feedback is implemented.

The equilibrium of the entire system under the proposed controller was theoretically investigated. Although final zero error of the object position tracking was not ensured, which was achieved by the controller previously developed in Chapter 6; position errors were proven bounded in a ball which could be made arbitrarily small by adjusting control gains, design parameters and filter time constant. In addition, the closed-loop system was robust against un-modeled nonlinearities. The internal force on the object could be made arbitrarily close to the desired level.

Simulations were performed with two manipulators resembling MAGNUM hydraulic manipulators. The results demonstrated the effectiveness of the proposed nonlinear controller.

Chapter 8 Experimental Studies

The controller developed in Chapter 7 has been implemented on an available fully instrumented system, including two single-axis electro-hydraulic actuators. The goal is to further show that the proposed control scheme can effectively cope with parametric uncertainties, counteract friction effects and achieve desired position tracking and internal force adjustment on a real system.

8.1 Description of the Test Rig

The test rig shown in Figure 8.1 includes two hydraulic actuators. Each of them is treated as a single-axis hydraulic robot. The system is originally constructed for experimentation on fault tolerant control and condition monitoring algorithms in fluid power systems, in which one actuator acts as a fault simulator and the other as a load simulator (Sepehri, et. al, 2005).

With reference to Figure 8.1, Actuator 1 on the left side is controlled by a high performance, closed-center nozzle-flapper servovalve. It is a double rod type with a 610 mm (24 in.) stroke, a 38.1 mm (1.5 in.) bore and 25.4 mm (1 in.) diameter rods. A Moog D765 servovalve modulates the flow in the circuit. The D765 is a modern servovalve that utilizes a linear variable differential transformer (LVDT) to measure the position of the spool. The spool position loop is closed, via integrated electronics that allow the spool to be positioned proportionally to an electrical command signal. The D765 flows 34 L/min (9 GRM) at 21 MPa (3000 psi) and has a nominal 2 ms rise time (Moog Inc., form no. 500-300 601).

Actuator 2 on the right side in Figure 8.1 is controlled by a Moog 31 series servovalve, an aerospace grade, closed-center nozzle-flapper type. The Moog 31 is capable of delivering fluid at a rate of 26 L/min (7 GPM) when operated at 21 MPa (3000 psi) and has a nominal 1.5 ms rise time (Thayer, 1965). With the exception of a shorter 203-mm (8 in) stroke, Actuator 1 is identical to Actuator 2.

Figure 8.1: Test rig on which all experiments are performed.

Both actuators are mounted on a reinforced steel table. The fluid pressures at the actuator chambers, as well as the pressures of fluid supplied to the valves, can be measured by six pressure transducers. An S-beam type load cell measures the contact force between Actuator 1 and the load, named $F_{c,1}^{1}$. There is no force sensor between Actuator 2 and the load. Two rotary encoders with a resolution of 1024 counts/revolution (linear resolution of 0.038mm) established the relative position of the actuators. Each encoder works with a steel cable which is tightly in contact with the encoder. When the actuator moves, the cable synchronically moves and causes the encoder to rotate. End-to-end round trips are carried out to find the accuracy of the position measurement. Their relative errors are about 0.5% and 0.2%, for Actuators 1 and 2 respectively. Actuator velocities are obtained by numerical differentiation with filtration since differentiation process amplifies the noise.

The structure of the object (payload) shown in Figure 8.2, was designed to protect the system from damage in the case that high internal force is built up. The object consists of three plates and in-between springs that can compromise the two actuators' motions. Actuator 2 is firmly connected to plate B through a hole in plate C. Actuator 1 is fixed to Plate A which is connected with Plate C by bolts that go through holes in Plate B. When the object is compressed, springs between Plates A and B will be compressed. Conversely when the object is stretched, springs between Plate B and C will be compressed standing for the internal stretching force inside the object. In other words, springs on the left-side can comprise compression and springs on the right comprises tension. At the same time, the springs have to be stiff to meet the realistic assumption that the grasped object is rigid. The overall stiffness of the object is 602.54N/mm which results in a 0.33 mm incremental displacement in compression or stretching when there is a 200 N change of internal force on the object.

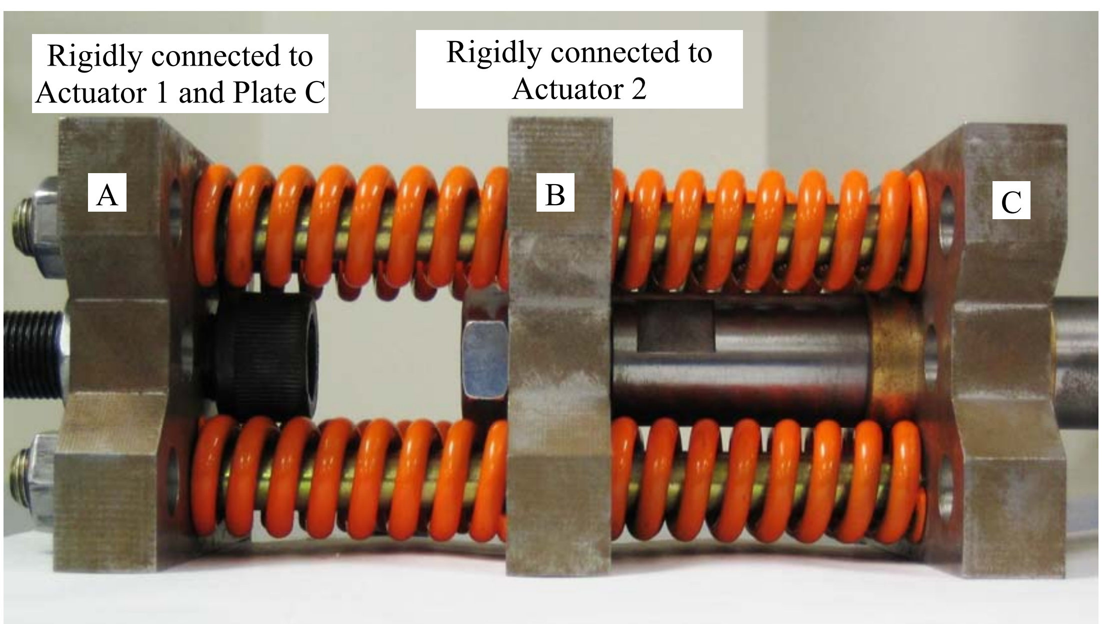

Figure 8.2: Close-up view of the object.

The data acquisition system is comprised of two Pentium II personal computers, operating at 866 MHz. They are configured such that each actuator has a dedicated processor. A DAS-16F input /output (I/O) board is installed in each PC and each board is capable of monitoring 16 single-ended analog to digital input channels while supporting 2 channels of digital to analog output. All sensors are directed to the DAS-16F I/O boards with the exception of the optical rotary position encoders, which are supported by independent Keithley M5312 quadrature incremental encoder cards installed in each PC. Since the output of the DAS-16F is unipolar, both output channels are required to generate bipolar servovalve command signals. Each servovalve is controlled by the appropriate PC. A local area network (LAN) is configured to establish a connection between the PCs so that both actuator circuits can be synchronized.

8.2 Controller Implements

8.2.1 Controller Layout

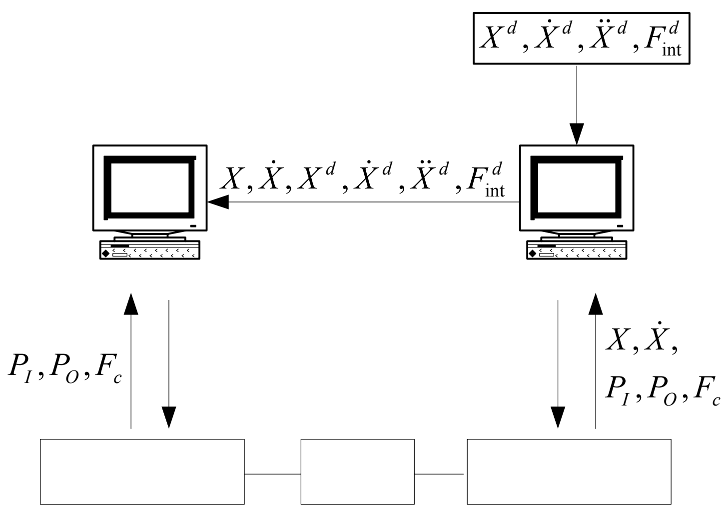

Figure 8.3: Controller layout.

The system consists of two actuators. Each is independently wired, with its own PC and dedicated processor. Without rewiring the system, a distributed control scheme is designed such that experiments on co-operating hydraulic manipulators can be conducted on the available system.

The layout is shown in Figure 8.3. There are two levels of information exchange between the physical structures. The information exchanged between the actuators and their associated computers includes measurement of line pressures to the chambers, and sending control signals (voltages) to the valves. The control signals are directly sent to the valves by the dedicated local computers. The computer dedicated to Actuator 2 also has the object position and velocity. The information related to desired and actual positions and velocities, and desired accelerations, is sent from Workstation 2 to Workstation 1 using UDP protocol.

8.2.2 Selection of Supply Pressure

Both actuators share one common pump. The maximum supply pressure is 21MPa (3000 psi). All the pressure gauges can only read up to 21MPa beyond which the sensors could be destroyed. There are relief valves built in this experimental system to protect it from becoming overloaded. However, the response of these valves may not be fast enough to protect the pressure sensors. For unforeseen pressure spikes, the final supply pressure used in the experiments was chosen as around 8 MPa (1150 psi).

8.2.3 Measurement of Object Position, Contact Forces and Calculation of Internal Force

The object's position can be obtained from Actuator 1 or Actuator 2. The position measurement of Actuator 1 is chosen to represent the object's position in the experiments because of better accuracy than in Actuator 2. At this time, there is no force sensor between the object and Actuator 2 to measure the contact force applied by Actuator 2. It is possible to calculate this contact force (named $F_{c,1}^{2}$) using

$$F_{c,1}^{1} + F_{c,1}^{2} = ma \tag{8.1}$$

i.e.

$$F_{c,1}^{2} = ma - F_{c,1}^{1} \tag{8.2}$$

In the experiments, the object mass is about 4.5 kg and the maximum acceleration for the desired sinusoidal trajectory is about 0.1 m/s^2. Therefore, the maximum value for the inertia force will theoretically be about 0.45 N. The real value might be higher than this value, but it is still small and negligible compared to the contact force (above 100N).

The contact force, $F_{c,1}^2$, is obtained by

$$F_{c,1}^2 = -F_{c,1}^1 \tag{8.3}$$

that is to say, $F_{c,1}^2$ is just opposed to $F_{c,1}^1$, meaning that the internal force could be represented by one of the contact forces as follows:

$$F_{\text{int}} \approx F_{c,1}^2 \tag{8.4}$$

8.3 Experimental Results

A sinusoidal desired trajectory with a travel distance of 0.12m and frequency of 0.2Hz was used as reference. The desired internal force was set to zero, i.e., $F_{\text{int}}^d = 0$. The values of stick and slip frictions were chosen as 1300N and 1100N, respectively. The controller gains were chosen as shown in Table 8.1.

Table 8.1: Control gains.

Control gains	Value	Control gains	Value
λ	100	$w_\theta^{2\times2}$	$diag(1,\ 10^5)$
$\tau_0^{(2\times2)}$	$diag(0.005,0.005)$	$w_\varphi^{(4\times4)}$	$diag(8\times10^{-12},\ \ 2\times10^6, 8\times10^{-12},\ \ 2\times10^6)$
$K_d^{(2\times2)}$	$diag(200,200)$	$w_{\sigma_0}^{(2\times2)}$	$diag(10^9, 10^9)$
$K_F^{(2\times2)}$	$diag(100,200)$	$w_{\sigma_1}^{(2\times2)}$	$diag(10^4,\ 10^4)$
$\Gamma_F^{(2\times2)}$	$diag(0.01,.0.01)$	$\Gamma_{z_0}^{(2\times2)}$	$diag(1,\ 1)$
$K_{\text{int}}^{(2\times2)}$	$diag(2.25,2.25)$	$\Gamma_{z_1}^{(2\times2)}$	$diag(1,\ 1)$

The experimental results are shown in Figures 8.4 to 8.12. Figure 8.4 shows the desired position trajectory of the object. The position tracking error of the object, shown in Figure 8.5, is less than 1 mm. The internal force is between ± 200 N as shown in Figure 8.6. Control signals to the two actuator valves are shown in Figures 8.7 and 8.8, respectively. Figure 8.9 shows the chamber pressures in Actuator 1 and the supply pressure, which presented variations of $\pm 10\%$ of its nominal value. Estimations of typical parameters are shown in Figure 8.10. Note that the parameter convergence is not theoretically guaranteed. Estimates of friction states are shown in Figure 8.11. Based on the estimated friction parameters and friction states, the friction is estimated and compensated for as shown in Figure 8.12.

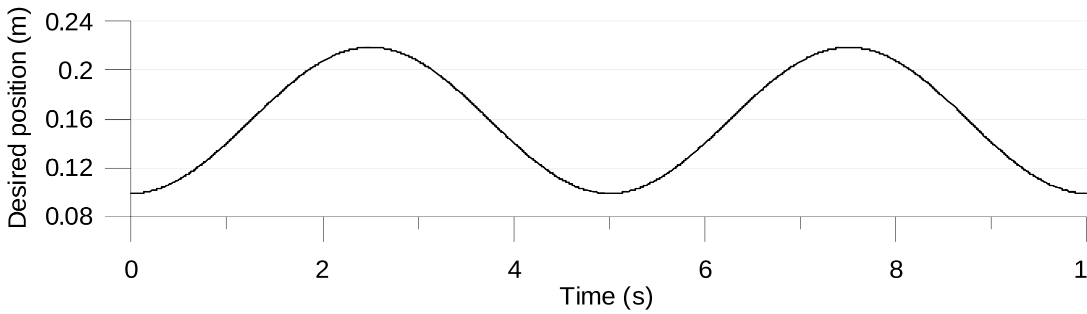

Figure 8.4: Reference trajectory.

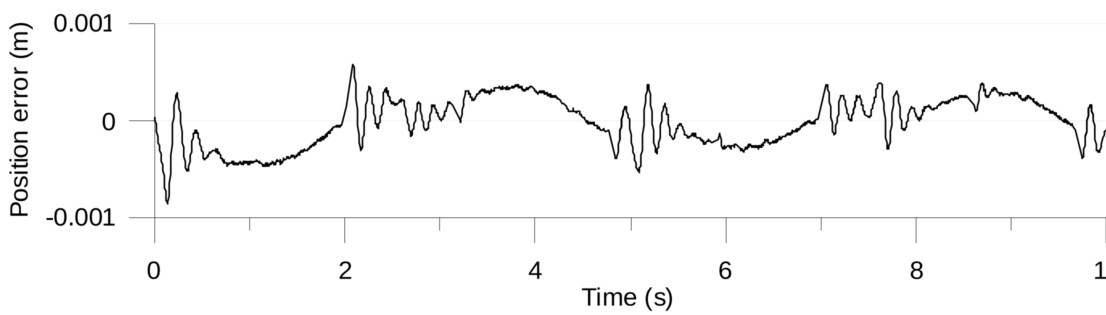

Figure 8.5: Position tracking error (Experiment 1).

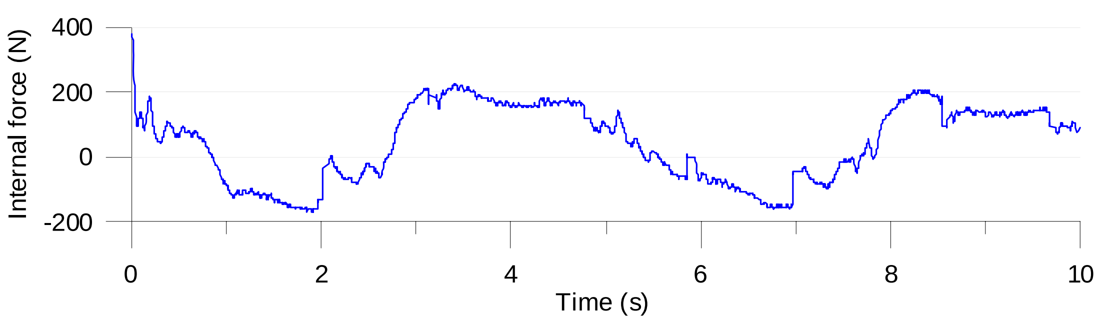

Figure 8.6: Internal force acting on the object (Experiment 1).

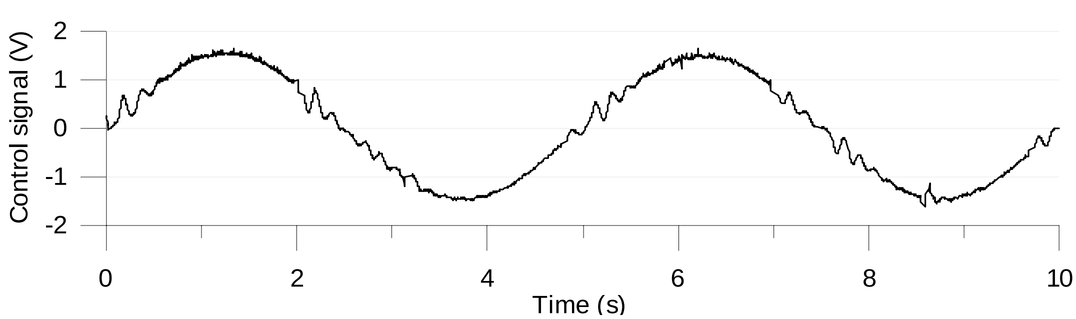

Figure 8.7: Control signal to Actuator 1 (Experiment 1).

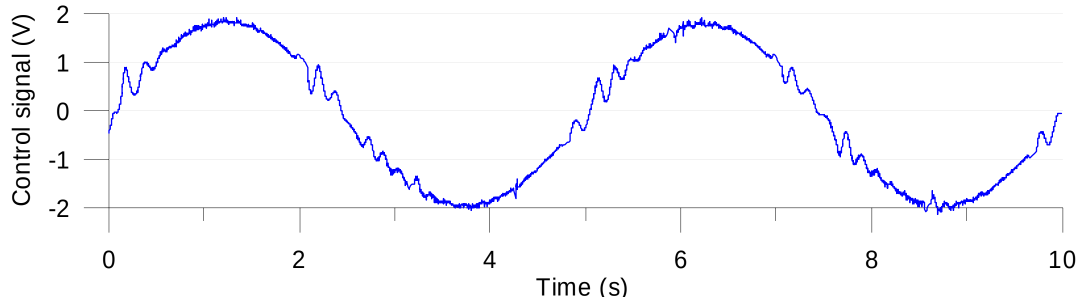

Figure 8.8: Control signal to Actuator 2 (Experiment 1).

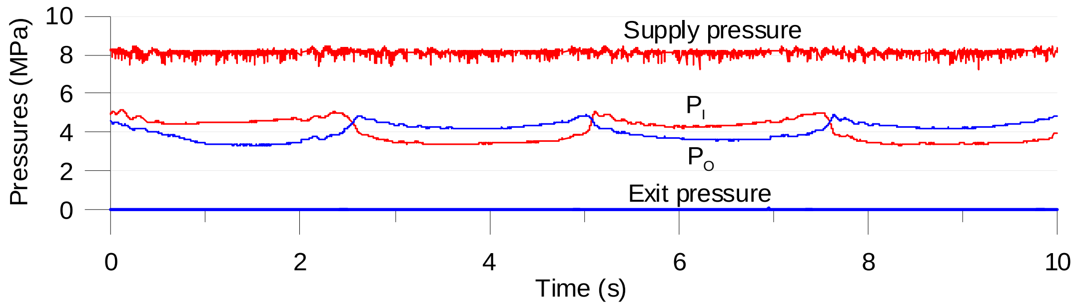

Figure 8.9: Supply and Actuator 1 line pressures (Experiment 1).

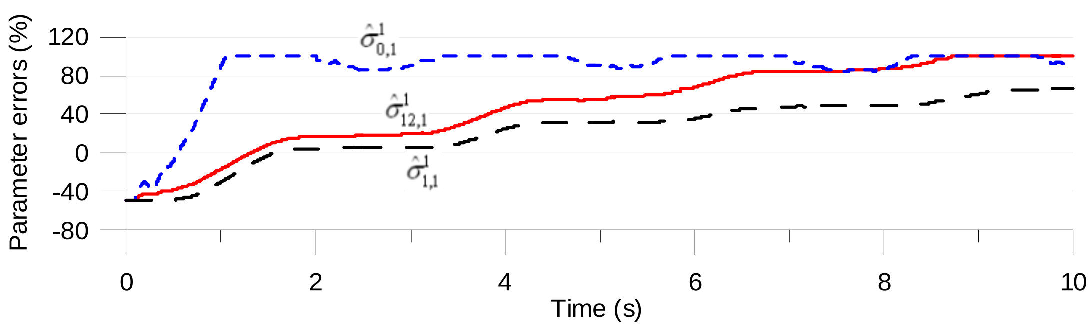

Figure 8.10: Parameter estimates pertaining to Actuator 1 (Experiment 1).

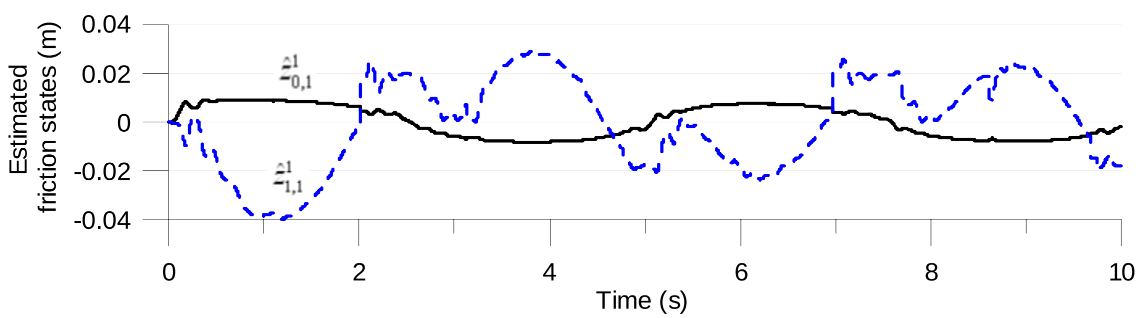

Figure 8.11: Friction state estimates in Actuator 1 (Experiment 1).

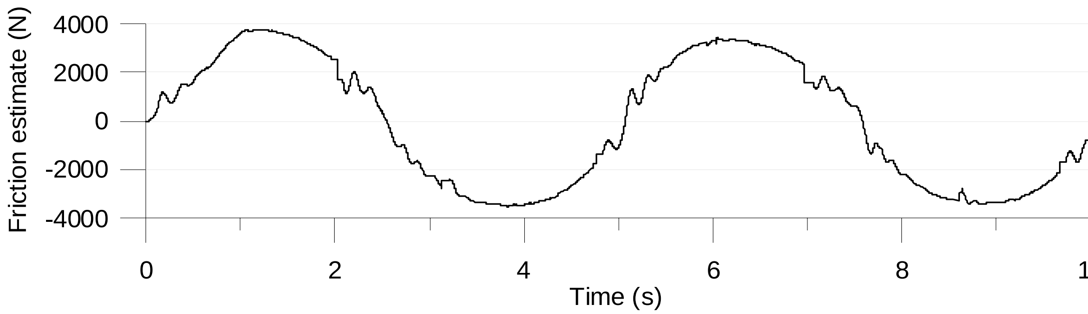

Figure 8.12: Friction estimate in Actuator 1 (Experiment 1).

To compare the performance of the developed controller with that of a simple proportional controller, two experiments were conducted with the same position tracking reference as in the previous experiment. The proportional gain is 2000 V/m. No force feedback was used for both experiments; thus, the developed controller used $K_{\text{int}} = 0$. Control signals are shown in Figures 8.14, 8.16 and 8.17. Figures 8.13 and 8.15 show the position errors and internal forces obtained from the experiments that used the proportional controller and the developed nonlinear controller, respectively. Both the position errors are smaller than 1 mm. However, the developed controller resulted in much smaller internal force. It was also observed during the experiments that the increasing of proportional gain did not change much of the internal force. The experiments conducted here involved two single-axis actuators only. In the case of multi-axis robot manipulators, the internal force could be significantly larger because of the coupling dynamics among the links.

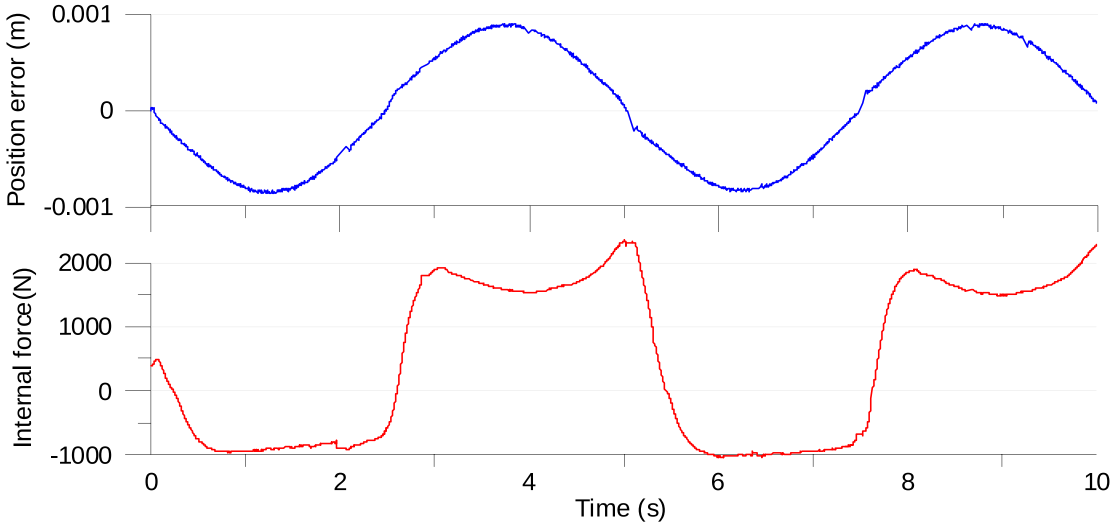

Figure 8.13: Response of a proportional position controller (Experiment 2).

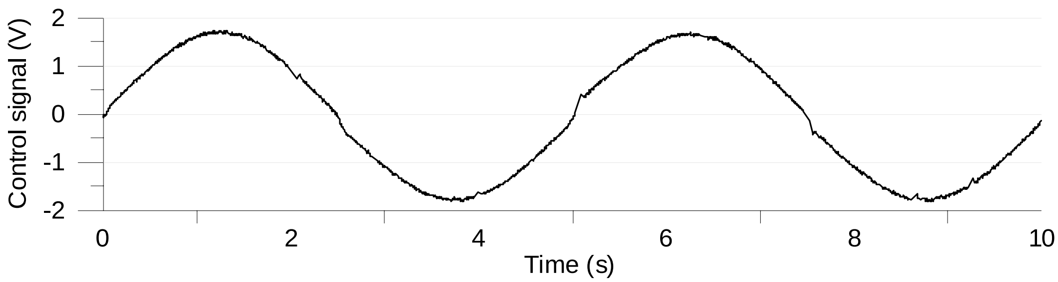

Figure 8.14: Control signal to each of the Actuators 1 and 2 (Experiment 2).

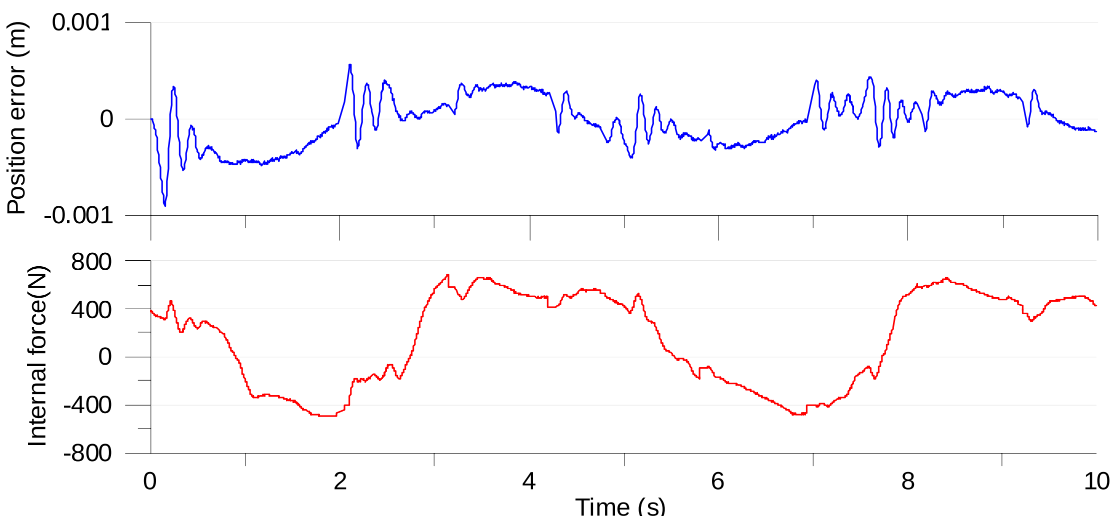

Figure 8.15: Response of the developed controller (desired internal force was set to zero, no force feedback, with adaptation of dynamic parameters) (Experiment 3).

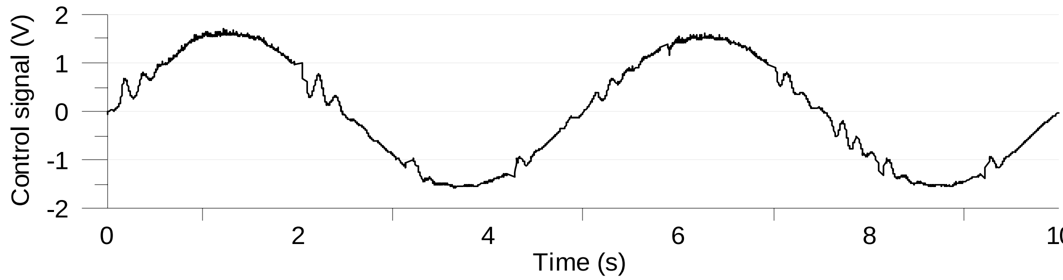

Figure 8.16: Control signal to Actuator 1 (Experiment 3).

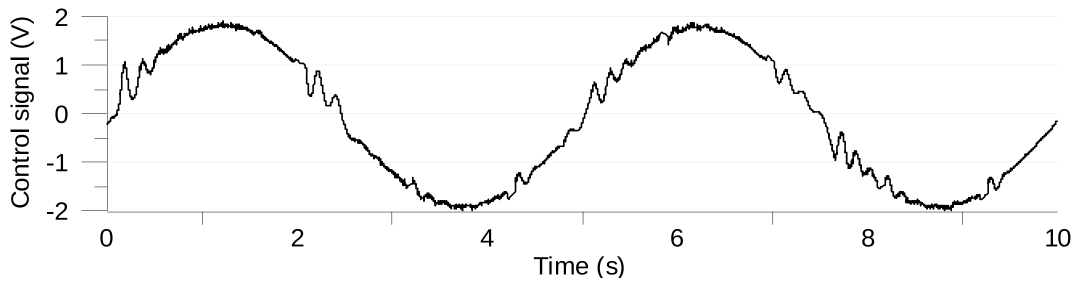

Figure 8.17: Control signal to Actuator 2 (Experiment 3).

The next experiment was conducted with no online adaptations of the unknown parameters. The results are shown in Figure 8.18 and indicate that the maximum position tracking error is much larger, close to 3 mm. The internal force seems not to change significantly. Figures 8.19 and 8.20 show the control signals to Actuator 1 and 2 respectively. Estimated friction state and friction force in Actuator 1 are provided in Figures 8.21 and 8.22.

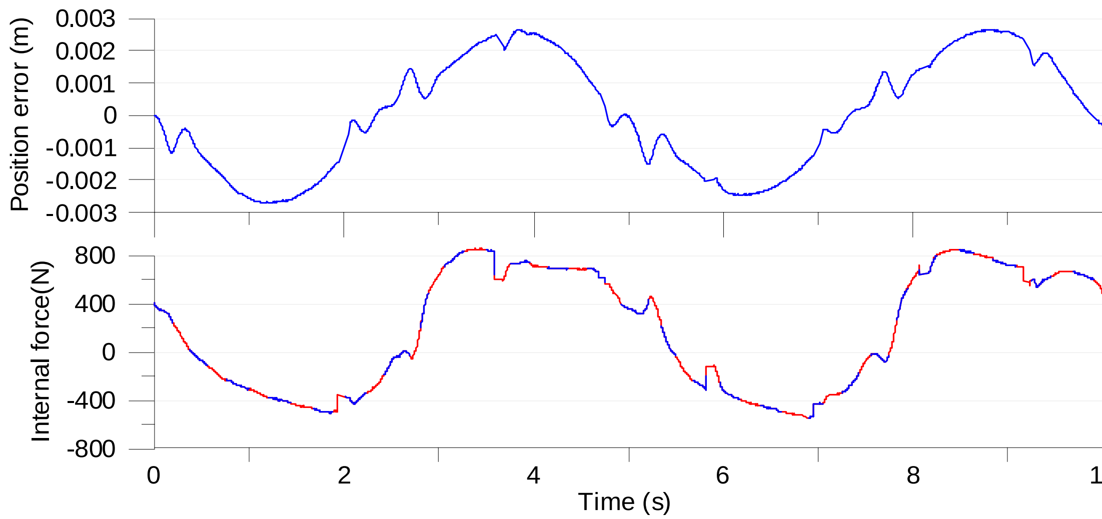

Figure 8.18: Response of the developed controller (desired internal force was set to zero, no force feedback, no adaptation of dynamic parameters) (Experiment 4).

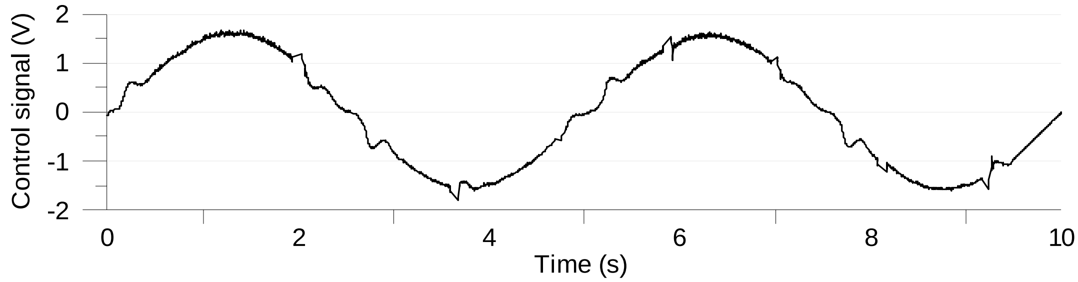

Figure 8.19: Control signal to Actuator 1 (Experiment 4).

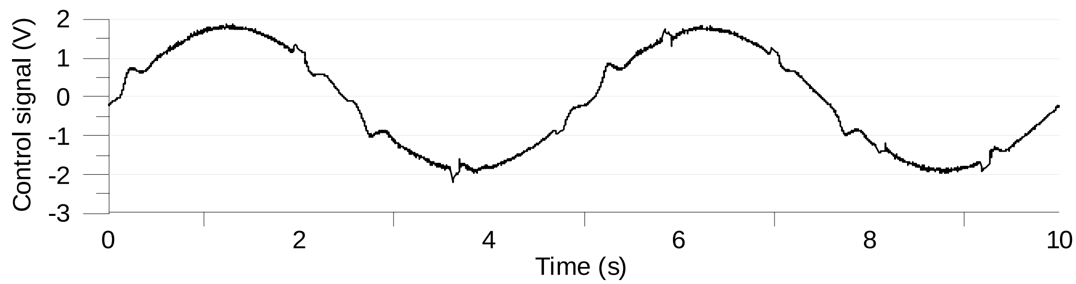

Figure 8.20: Control signal to Actuator 2 (Experiment 4).

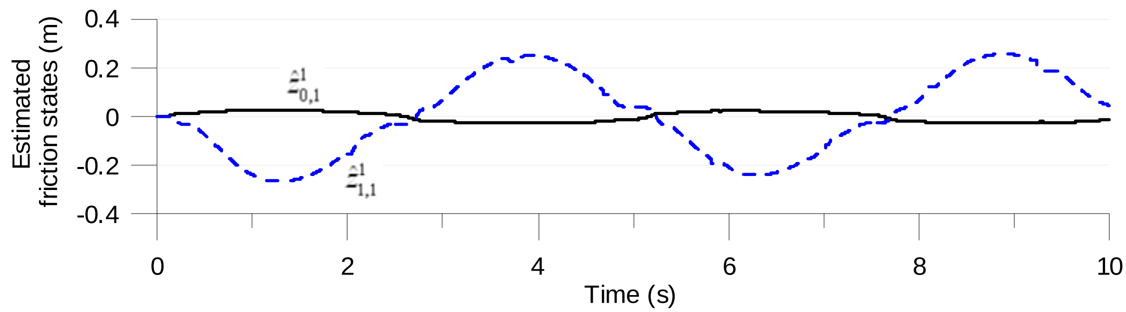

Figure 8.21: Friction state estimates in Actuator 1 (Experiment 4).

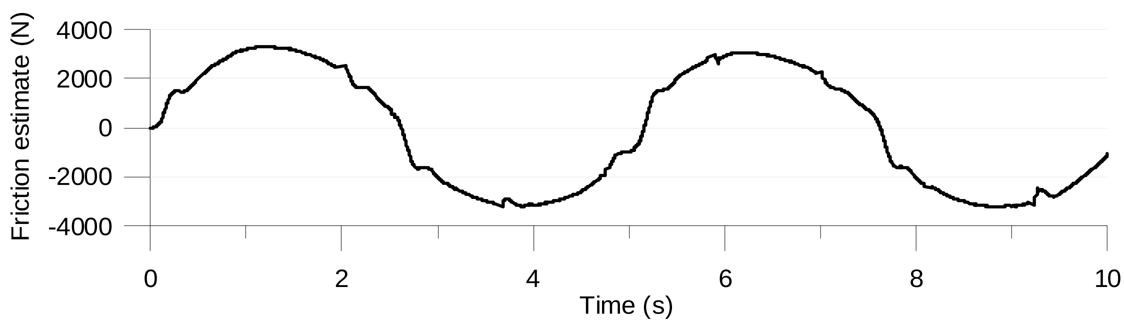

Figure 8.22: Friction estimate in Actuator 1 (Experiment 4).

The last experiment was done in comparison with the first experiment, with the exception that the desired internal force F_{int}^{d} was set to -444.8N (-100lb), instead of zero. The results shown in Figure 8.23 indicate that the internal force had shifted down about

400N, yet the position tracking error did not change much. This demonstrates that the internal force is adjustable by the controller. The control signals to Actuator 1 and 2 are presented in Figures 8.24 and 8.25 respectively.

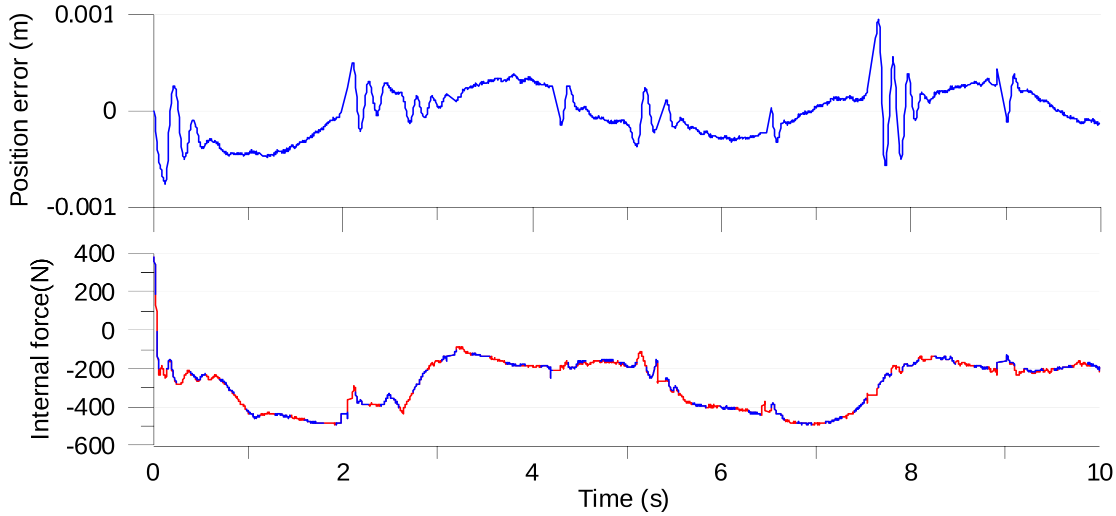

Figure 8.23: Response of the developed controller (desired internal force was set to -444.8N, force feedback gain was 2.25) (Experiment 5).

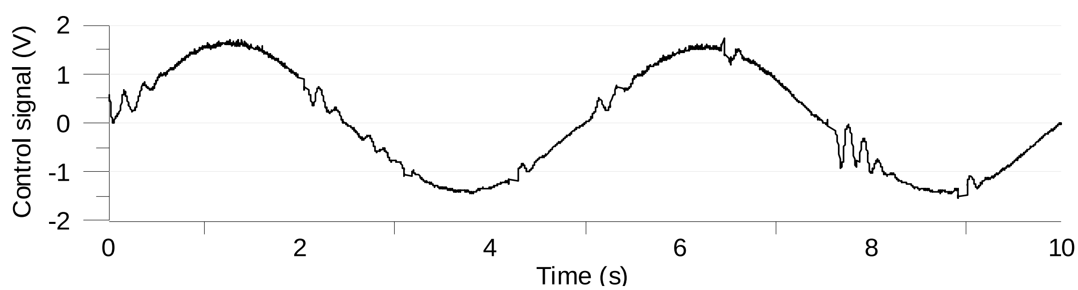

Figure 8.24: Control signal to Actuator 1 (Experiment 5).

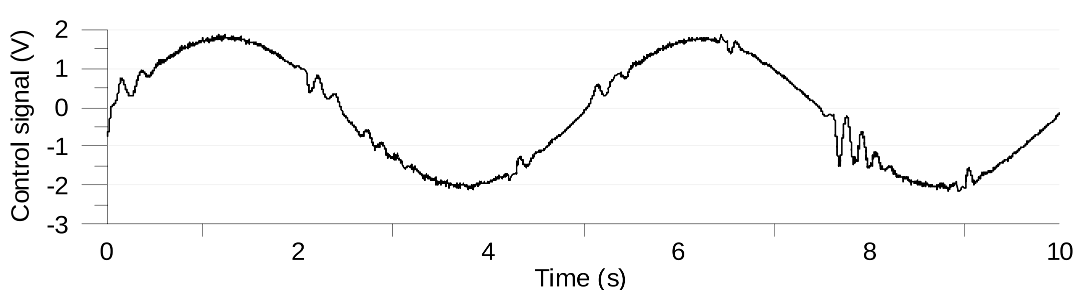

Figure 8.25: Control signal to Actuator 2 (Experiment 5).

Summary:

In this chapter, the tracking controller for co-operation among several hydraulic manipulators handling a rigid payload developed in Chapter 7, was tested on a two-single-axis hydraulic actuator system. A sinusoidal desired trajectory with travel distance of 0.12m and frequency of 0.2Hz was used. The experimental results further validated the developed controller which:

(i) is capable of tracking a reference position of the common object and regulating a reference internal force

(ii) is robust against uncertainties and nonlinearities presented in hydraulic power systems

(iii) does not require measurement of acceleration, only needs to measure line pressures, position and velocity

(iv) guarantees stability.

Chapter 9 Summary and Conclusions

This thesis has made important contributions to the development, implementation, and experimental evaluation of stable and robust control laws, for co-operating hydraulic manipulators handling a common rigid object. In spite of existence of many references regarding multi-robot systems, the literature in the area of co-operating hydraulic manipulators is sparse. Especially, prior to this work there was no publication on coordinated control of multi-axis hydraulic manipulators handling a common object. The detailed contributions made in this thesis are listed below.

A complete general model of co-operating hydraulic manipulators including object and manipulator dynamics and hydraulic functions was developed. This was under the assumption that there was no relative motion among the object and the manipulators' end-effectors. Plant nonlinearities including servovalve flow-pressure characteristics, unequal piston cross sectional areas and variations of fluid volume under compression. As well, plant uncertainties such as bulk modulus were included in the model.

First, a position-regulating controller was developed under the assumption that the system's physical parameters were fully known and that there was no friction. The highly nonlinear hydraulic actuator dynamics were incorporated in the Lyapunov-based controller design. The issues of motion and internal force control of the object, and load sharing were addressed. The equilibrium of the system under the proposed controller was investigated, leading to a set of equilibrium points corresponding to the desired position and internal forces. Further, the issue of unknown payload was analyzed and the controller was modified to eliminate the steady-state error due to imperfect compensation. Next, the controller was modified to account for the uncertain parameters in both robot dynamics and hydraulic functions.

The adaptive approach within the framework of backstepping controller design technique was employed next to design a tracking controller in the presence of uncertainties as a natural direction for control of co-operating hydraulic robots. The design methodology proceeded with the construction of on-line updating laws and observers. The controller features updating laws to consider parametric uncertainties (unknown dynamic parameters of the payload, robots, and hydraulic functions), and observers to avoid the requirement of acceleration feedback.

Many researchers have shown that friction plays an important albeit damaging role in control systems. The above controllers were investigated for hydraulic manipulators having substantial friction. Theoretical analysis showed that the regulating control system was stable and could achieve the desired position. However, the existing friction could make regulation longer, when compared with the case having no friction, and bring about undesirable internal forces. It was discovered that the use of force feedback could bring the internal force closer to the desired value. For the position tracking control system, both position and internal force errors could be significantly increased with the presence of friction and the stability could not be guaranteed given the existing Lyapunov-like scalar function. Simulations were further carried out to verify the theoretical findings.

Built upon the above studies, a new Lyapunov-based controller was developed for co-operating hydraulic manipulators handling a common rigid object in the presence of friction. The well known LuGre friction model was introduced in the actuator dynamics and was considered when designing the controller. Main parameters in the friction model were assumed to be unknown and were estimated by an adaptive control scheme. Adaptive observers were used to identify friction internal states that were not measurable. Utilizing the online estimated friction parameters and observed friction states, a novel friction compensator was designed. Additionally, in an effort to avoid the need for measuring acceleration, an acceleration observer was introduced. Using the new controller, the states of the control system were proven bounded. The Lyapunov-like analysis showed that the position tracking error moved to zero as time went to infinity. The internal force error could theoretically be made arbitrarily small, when using an additional force feedback.

Inspired by the concept of dynamic surface control, the above controller was redesigned. The problem of “explosion of terms” was solved while the need for measuring acceleration was avoided without having to design an observer. Other features remained, except for the position tracking error which was made arbitrarily small rather than zero.

The above tracking controllers were tested in simulations using two 3-DoF hydraulic manipulators. The kinematic and dynamic model of robot manipulators in the simulations was built to resemble a Magnum robot, manufactured by the International Submarine Engineering, Canada. A number of simulations were carried out on the developed simulation model. Simulation results validated the effectiveness of the developed controllers.

The dynamic surface controller was further tested experimentally on an available hydraulic system consisting of two single-axis actuators. A hierarchical distributed control scheme built on local network and using UDP protocol, was designed to carry out the experiments. The experimental results further validated the effectiveness of the controller.

Future work should focus on experiments on multi-axis hydraulic robot manipulators, as well as on the following issues. Firstly, in this study the valve dynamics were neglected by assuming a small rise time. Incorporating a general model of the valve with the controller design could accurately represent the valve dynamics. Secondly, to eliminate the internal force error, an integral-like term, $\int_0^t (F_{\text{int}}^d - F_{\text{int}})d\tau$, could be considered to add in the force feedback loop. Finally, one feature of the LuGre friction model is, that it is continuous compared to other friction models. However, it is not differentiable at some isolated points while the backstepping controller design technique requires a differentiable model. It is, therefore, worthwhile to investigate the possibility of modifying the LuGre model such that it becomes differentiable.

References

Alford, C.O. and Belyeu, S.M., 1984, “Coordinated Control of Two R obot Arms,” Proceedings of the IEEE International Conference on Robotics and Automation, pp. 468–473.

Alleyne A., 1996, “Nonlinear Force Control of an Electro-Hydraulic Actuator,” Proc. Japan/USA Symposium on Flexible Automation, Boston, MA, pp.193-200.

Amin, J., Friedland, B., and Harnoy, A., 1997, “Implementation of a Friction Estimation and Compensation Technique,” *IEEE Contr. Syst. Mag*., **17**(4), 71–76.

Armstrong-H´elouvry, B., 1991, Control of Machines with Friction. Boston, MA: Kluwer.

Armstrong-H´elouvry, B., Dupont, P., and Canudas de Wit, C., 1994, “A Survey of Models, Analysis Tools and Compensation Methods for the Control of Machines with Friction,” *Automatica*, **30**(7), 1083–1138.

Bonchis, A., Corke, P.I., and Rye, D.C., 2002, “Experimental Evaluation of Position Control Methods for Hydraulic Systems,” *IEEE Transactions on Control Systems Technology*, **10**, 876-882.

Bu, F. and Yao, B., 2000, “Observer Based Coordinated Adaptive Robust Control of Robot Manipulators Driven by Single-Rod Hydraulic Actuators,” Proc. IEEE Int. Conf. Robotics and Automation, pp. 3034–3039.

Bu, F. and Yao, B., 2001, “Nonlinear Model Based Coordinated Adaptive Robust Control of Electro-Hydraulic Robotic Arms via Overparametrizing Method,” Proceedings of the 2001 IEEE International Conference on Robotics and Automation, pp. 3459–3464.

Caccavale, F., Chiacchio, P., and Chiaverini, S., 1999, “Task-space Tracking Control without Velocity Measurements,” Proceedings of the IEEE International Conference on Robotics and Automation, pp. 512 - 517.

Caccavale, F., Chiacchio, P., and Chiaverini, S., 1999, “Stability Analysis of a Joint Space Control Law for a Two-Manipulator System,” *IEEE Transactions on Automatic Control*, **44**, 85–88.

Canudas de Wit, C., Olsson, H., Åström, K.J., and Lischinsky, P., 1995, “A new model for control of systems with friction,” *IEEE Trans. Automat. Contr*., **40**, 419–425.

Chaimowicz, L., Sugar, T., Kumar, V., and Campos, M.F.M., 2001, “An Architecture for Tightly Coupled Multi-robot Co-operation,” Proceedings of IEEE International Conference on Robotics and Automation, Seoul, Korea, pp. 2992–2997.

Clarke, F. H., 1983, “Optimization and Nonsmooth Analysis,” John Wiley and Sons, NY.

d'Andrea-Novel, B., Garnero, M.A., and Abichou, A., 1994, Nonlinear control of a hydraulic robot using singular perturbations, Systems, Man, and Cybernetics, 'Humans, Information and Technology'., IEEE International Conference on, pp. 1932–1937.

Duraiswamy, S. and Chiu, G.T.-C, 2003, “Nonlinear Adaptive Nonsmooth Dynamic Surface Control of Electro-Hydraulic Systems,” Proceedings of the American Control Conference, pp.3287-3291.

Friedland, B. and Mentzelopoulou, S., 1992, “On Adaptive Friction Compensation without Velocity Measurement,” Proc. IEEE Conf. Contr. Applicat., vol. 2, pp. 1076–1081.

Friedland, B. and Park, Y.J., 1992, “On Adaptive Friction Compensation,” *IEEE Trans. Automat. Contr.*, **37**, 1609–1612.

Gafvert, M., 1999, “Dynamic Model Based Friction Compensation on the Furuta Pendulum,” Proceedings of the 1999 IEEE International Conference on Control Applications, pp. 1260 - 1265

Gerdes, J. and Hedrick, J.K, 1999, “Loop-at-a-time Design of Dynamic Surface Control for Nonlinear Systems,” Proceedings of American Control Conferenc, pp. 3574–3578.

Goodwin, G.C. and Mayne D.Q., 1987, “A Parameter Estimation Perspective of Continuous Time Model Reference Adaptive Control,” *Automatica*, **23**, 57–70.

Haessig, D.A. and Friedland, B., 1991, “On the Modelling and Simulation of Friction.,” *J. of Dynamic Systems, Measurement and Control,* **113**(3), 354–362.

Hu, Y.-R. and Goldenberg, A.A., 1989, “An Adaptive Approach to Motion and Force Control of Multiple Coordinated Robot Arms,” Proceedings of the IEEE International Conference on Robotics and Automation, pp.1091–1096.

Husch, L.S., 2001, “Visual Calculus”, University of Tennessee.

Isidori, A., 1995, “Nonlinear Control Systems,” Springer-Verlag.

Karpenko, M., Anderson, J., and Sepehri, N., 2006, "Coordination of Hydraulic Manipulators by Reinforcement Learning," Proceedings of American Control Conference, pp. 3221–3226.

Khalil, H.K., 2002, "Nonlinear Systems," 3nd edtion, Prentice-Hall.

Khatib, O., 1988, "Object Manipulation in a Multi-effector Robot System," *Robotics Research, the Fourth International Symposium*, 137–144.

Kristic, M., Kanellakopoulos, I., and Kokotovic, P.V., 1995, "Nonlinear and Adaptive Control Design," John Wiley &Sons.

Lin, J. and Chen, C.H., 2006, "A Novel Fuzzy Friction Compensation Approach for Tracking of a Linear Motion Stage," Proceedings of American Control Conference, pp. 3188–3193.

Lischinsky, P., Canudas-de-Wit, C., and Morel, G., 1999, "Friction Compensation of an Industrial Hydraulic Robot," *IEEE Control Sytems Magazine*, **19**(1): 25-32.

Liu, Y.H. and Arimoto, S., 1996, "Distributively Controlling Two Robots Handling an Object in the Task Space without any Communication," *IEEE Transactions on Automatic Control*, **41**, 1193–1198.

Maciuca, D.B. and Hedrick, J.K., 1997, "Nonsmooth Dynamic Surface Control of Non-Lipschitz Nonlinear Systems with Application to Brake Control," Proceedings of IEEE International Conference on Control Applications, pp. 711-716.

Mentzelopoulou, S. and Friedland, B., 1994, "Experimental Evaluation of Friction Estimation and Compensation Techniques," Proc. Amer. Contr. Conf., Baltimore, MD, pp. 3132–3136.

Merritt, H.E., 1967, "Hydraulic Control Systems," New York: John Wiley & Sons.

Niksefat, N., Wu, Q., and Sepehri, N., 2000, "Stable Control of an Electro-Hydraulic Actuator During Contact Tasks: Theory and Experiments," Proceedings of the American Control Conference, pp. 4114-4118.

Niksefat, N. and Sepehri, N., 2000, "Design and Experimental Evaluation of a Robust Force Controller for an Electro-hydraulic Actuator via Quantitative Feedback Theory," *Control Engineering Practice*, **8**, 1335–1345.

Noble, B. and Daniel, J.W., 1977, "Applied Linear Algebra", Englewood Cliffs, N.J.: Prentice-Hall.

Pan, Z. and Basar, T., 1998, “Adaptive Controller Design for Tracking and Disturbance Attenuation in Parametric Strict-feedback Nonlinear Systems,” *IEEE Transactions on Automatic Control*, **43**, 1066–1083.

Paul, R., 1981, “Robot Manipulators: Mathematics, Programming, and Control,” Cambridge, Massachusetts and London, England: MIT.

Polycarpou, M.M. and Ioannou, P.A., 1993, “A Robust Adaptive Nonlinear Control Design,” Proceedings of the American Control Conference, pp.1365–1369.

Rowland, Todd. "Ck Function." From *MathWorld*--A Wolfram Web Resource, created by Eric W. Weisstein. http://mathworld.wolfram.com/C-kFunction.html

Shieh, H.J. and Shyu, K.K., 1999, “Nonlinear Sliding-mode Torque Control with Adaptive Backstepping Approach for Induction Motor Drive,” *IEEE Transactions on Industrial Electronics*, **46**, 380–389.

Sirouspour, M.R. and Salcudean, S.E., 2001, “Nonlinear Control of Hydraulic Robots,” *IEEE Transactions on Robotics and Automation*, **17**, 173–182.

Slotine, J.-J.E. and Li, W., 1991, “Applied Nonlinear Control,” Engliwood Cliffs, NJ: Prentice-Hall.

Sugar, T. and Kumar, V., 1999, “Multiple Co-operating Mobile Manipulators,” Proceedings of the IEEE International Conference on Robotics and Automation, pp. 1538–1543.

Sun, H. and Chiu, G.T.-C., 2002, “Motion Synchronization for Dual-cylinder Electrohydraulic Lift Systems,” *IEEE/ASME Transactions on Mechatronics*, **7**, 171-181.

Sun, D. and Mills, J.K., 2002, “Manipulating Rigid Payloads with Multiple Robots Using Compliant Grippers,” *IEEE Transactions on Mechatronics*, **7**(1), 23-33.

Swaroop, D., Gerdes, J.C., Yip, P.P., and Hedrick, J.K, 1997, “Dynamic Surface Control of Nonlinear Systems,” Proceedings of American Control Conferenc, pp. 3028–3034.

Swaroop, D., Hedrick, J.K., Yip, P.P., and Gerdes, J.C., 2000, “Dynamic Surface Control for a Class of Nonlinear Systems,” *IEEE Transactions on Automatic Control*, **45**(10), 1893-1899.

Tafazoli, S., de Silva, C.W., Lawrence, P.D., 1998, “Tracking Control of an Electrohydraulic Manipulator in the Presence of Friction,” *Control Systems Technology, IEEE Transactions on*, **6**(3), 401-411.

Tan, Y., Chang, J., and Tan, H., 2003, “Adaptive Backstepping Control and Friction Compensation for AC Servo with Inertia and Load Uncertainties,” *IEEE Transactions on Industrial Electronics*, **50**, 944-952.

Tarn, T.J., Bejczy, A.K., and Yun, X., 1987, “Design of Dynamic Control of Two Co-operating Robot Arms: Closed Chain Formulation,” Proceedings of IEEE International Conference on Robotics and Automation, pp. 7–13.

Thayer, W.J., 1965, “Transfer Functions for Moog Servovalvles,” Moog Technical Bulletin #103, Moog Inc., New York.

Thornton, S.T. and Marion, J.B., 2004, “Classical Dynamics of Particles and Systems”, 5th edition, Belmont, CA, USA: Brooks Cole.

Tomei, P., 1991, “Adaptive Controller for Robot Manipulators,” *IEEE Transaction on Robotics Automation*, **7**, 565–570.

Uchiyama, M. and Dauchez, P., 1988, “A Symmetric Hybrid Position/force Control Scheme for the Coordination of Two Robots,” Proceedings of IEEE International Conference on Robotics and Automation, pp. 350–356.

Uzmay, I., Burkan, R., and Sarikaya, H., 2004, “Application of Robust and Adaptive Control Techniques to Co-operative Manipulation,” *Control Engineering Practice*, **12**, 139-148.

Vedagarbha, P., Dawson, D.M., Feemster, M., 1999, “Tracking Control of Mechanical Systems in the Presence of Nonlinear Dynamic Friction Effects,” *IEEE Trans Control System Technology*, **7**, 446–56.

Vukbrotovic, M. and Tuneski, A.I., 1998, “Mathematical Model of Multiple Manipulators: Co-operative Compliant Manipulation on Dynamical Environments,” *Mechanism and Machine Theory*, **33**, 1211–1239.

Walker, I.D., Freeman, R.A., and Marcus, S.I., 1991, “Analysis of Motion and Internal Loading of Objects Grasped by Multiple Co-operating Manipulators,” *International Journal of Robotics Research,* **10**, 396–409.

Walker, M.W., Kim, D., and Dionise, J., 1989, "Adaptive Coordinated Motion Control of Two Manipulator Arms," Proceedings of IEEE International Conference on Robotics and Automation, pp. 1084–1090.

Watton, J., 1989, "Fluid Power Systems," Englewood Cliffs, NJ: Prentice- Hall.

Won, M.C. and Hedrick, J.K., 1996, "Multiple surface sliding control of a class of uncertain nonlinear systems," *International Journal of Control*, **64**(4), 693–706.

Wu, Q., Zeng, H., and Sepehri, N., "On Uniqueness of Filippov's Solutions for Non-Smooth Systems Having Multiple Discontinuity Surfaces with Applications to Control Engineering", 2004 ASME International Mechanical Engineering Congress, paper#: IMECE2004-59824.

Yao, B., Bu, F., Reedy, J., and Chiu, G.T.-C., 2000, "Adaptive Robust Motion Control of Single-Rod Hydraulic Actuators: Theory and Experiments," *IEEE/ASME Transactions On Mechatronics*, **5**, 79-91.

Yip, P.P., Hedrick, J.K., and Swaroop, D., 1996, "The Use of Linear Filter to Simplify Integrator Backstepping Control of Nonlinear Systems," IEEE workshop on Variable structure systems, pp. 211-215.

Yu, J., Chen, Z., and Lu, Y., 1994, "The Variation of Oil Effective Bulk Modulus with Pressure in Hydraulic Systems," *Journal of Dynamic Systems, Measurement, and Control*, **116**, 146-150.

Zeng, H. and Sepehri, N., "Tracking Control of Hydraulic Robot Manipulators with Friction Compensation," *Journal of Dynamic Systems, Measurement, and Control*, (in press).

Zeng, H. and Sepehri, N., 2007, "On Tracking Control of Co-operative Hydraulic Manipulators," *International Journal of Control*, **80**, 454–469.

Zeng, H. and Sepehri, N., 2005, "Nonlinear Position Control of Co-operative Hydraulic Manipulators Handling Unknown Payloads," *International Journal of Control*, **78**, 196–207.

Zeng, H. and Sepehri, N., 2006, "Dynamic Surface Control of Co-operating Hydraulic Manipulators in the Presence of Friction," 2007 American Control Conference, pp. 94–99.

Zeng, H. and Sepehri, N., 2006, “Adaptive Backsteping Control of Hydraulic Manipulators with Friction Compensation Using LuGre Model,” 2006 American Control Conference, pp. 3164-3169.

Zeng, H. and Sepehri, N., 2006, “Design of a Tracking Controller for Co-operating Hydraulic Manipulators Handling a Rigid Object”, 2006 American Control Conference, pp. 4639-4644.

Zeng, H. and Sepehri, N., 2004, “Design of a Nonlinear Controller for Co-operating Hydraulic Manipulators Handling a Rigid Object,” 2004 ASME International Mechanical Engineering Congress, paper#: IMECE2004-61241.

Zheng, Y.F. and Luh, J.Y.S., 1986, “Joint Torques for Control of Two Coordinated Moving Robots,” Proceedings of IEEE International Conference on Robotics and Automation, pp. 1375–1380.

Zribi, M. and Ahmad S., 1992, “Adaptive Controller for Multiple Co-operative Robot Arms,” Proceedings of the 31st Conference on Decision and Control, pp. 1392–1398.

Appendix A
Degree of Freedom of the Co-operating System

Katib (1988) has discussed the issue of degree of freedom of a multi-end effector/object system. The following is a review with more details.

The system considered in this thesis results from rigidly connecting an object to the end-effectors of n N-degree-of-freedom manipulators. One way to see this system's structure is that it is formed by $n(N$-1) links, one object link and one ground link connected through nN one-degree-of-freedom joints. The number of total degrees of freedom of these links obtained before the connection is $n_0(n_{\text{link}} - 1)$, where the numbers of total links n_{link}, is $n(N$-1)+2, and n_0 is the number of degrees of freedom of an unconnected link (3 in the planar case and 6 in the spatial case). The number of total degrees of freedom lost by the joint constraints after the connection is $(n_0 - 1)n_{\text{joint}}$, where n_{joint} is the number of total joints. Thus, the number n_s of degrees of freedom of this system is given by the difference between $n_0(n_{\text{link}} - 1)$ and $(n_0 - 1)n_{\text{joint}}$. This number is given by the Grubler formula (Hartenberg and Denavit, 1964),

$$n_s = n_0(n_{\text{link}} - 1) - (n_0 - 1)n_{\text{joint}} \tag{A.1}$$

For the system of n N degree-of-freedom manipulators and the object considered here,

$$n_s = n_0(n(N-1)+1) - (n_0 - 1)nN = n_0 + n(N - n_0) \tag{A.2}$$

With the assumption of non redundancy, the number of degrees of freedom in the planar case (n_0 =N=3) is n_s=3. This number is n_s =6 in the spatial case (n_0 =N=6).

Appendix B

Properties of Matrices M and D

Given

$$\Lambda = E^T \boldsymbol{W}\boldsymbol{J}^{-T}\boldsymbol{H}\boldsymbol{J}^{-1}\boldsymbol{W}^T E \tag{B.1}$$

$$B = E^T \boldsymbol{W}\boldsymbol{J}^{-T}[\boldsymbol{C}\boldsymbol{J}^{-1}\boldsymbol{W}^T E + \boldsymbol{H}\boldsymbol{J}^{-1}(\dot{\boldsymbol{W}}^T E + \boldsymbol{W}^T \dot{E} - \dot{\boldsymbol{J}}\boldsymbol{J}^{-1}\boldsymbol{W}^T E)] \tag{B.2}$$

$$M = \Lambda + M_o \tag{B.3}$$

$$D = B + D_o \tag{B.4}$$

and the following properties:

Property B.1: $\boldsymbol{H}$ is a symmetric positive definite matrix,

Property B.2: $(\dot{\boldsymbol{H}} - 2\boldsymbol{C})$ is a skew-symmetric matrix, i.e., $x^T(\dot{\boldsymbol{H}} - 2\boldsymbol{C})x = 0; \forall x \in R^{6n\times 1}$,

Property B.3: $\boldsymbol{C}(\boldsymbol{q}, x)y = \boldsymbol{C}(\boldsymbol{q}, y)x \quad \forall \boldsymbol{q}, x, y \in R^{6n\times 1}$ and,

Property B.4: $\boldsymbol{H}(\boldsymbol{q})$ and $\boldsymbol{C}(\boldsymbol{q}, \dot{\boldsymbol{q}})$ are bounded, i.e., $0 < \boldsymbol{H}_L \le \|\boldsymbol{H}(\boldsymbol{q})\| \le \boldsymbol{H}_U \quad \forall \boldsymbol{q} \in R^{6n\times 1}$

and $\|\boldsymbol{C}(\boldsymbol{q}, x)\| \le \boldsymbol{C}_M \|x\| \quad \forall \boldsymbol{q}, x \in R^{6n\times 1}$.

Property B.5: M_o is a symmetric positive definite matrix,

Property B.6: $(\dot{M}_o - 2D_o)$ is a skew-symmetric matrix, i.e., $x^T(\dot{M}_o - 2D_o)x = 0; \forall x \in R^{6n\times 1}$

Property B.7: $D_o(x, y)z = D_o(x, z)y \quad \forall x, y, z \in R^{6n\times 1}$ and,

Property B.8: $M_o(x)$ and $D_o(x, y)$ are bounded, i.e., $0 < M_{o,L} \le \|M_o(x)\| \le M_{o,U}$

$\forall x \in R^{6n\times 1}$ and $\|D_o(x, y)\| \le D_{o,U}\|y\| \qquad \forall x, y \in R^{6n\times 1}$.

Matrices M and D have the same properties, i.e.,

Property B.9: M is a symmetric positive definite matrix,

Property B.10: $\dot{M} - 2D$ is a skew-symmetric matrix, i.e., $x^T(\dot{M} - 2D)x = 0; \forall x \in R^{6n\times 1}$,

Property B.11: $D(x, y)z = D(x, z)y \quad \forall x, y, z \in R^{6n\times 1}$, and

Property B.12: $M(x)$ and $D(x, y)$ are bounded as follows:

$$0 < M_L \le \|M(x)\| \le M_U \quad \forall x \in R^{6n\times 1}$$

$$\|D(x, y)\| \le D_U \|y\| \qquad \forall x, y \in R^{6n\times 1}$$

Proof:

i) It is easy to see that $\Lambda(X)$ is a symmetric positive definite matrix in observation of *Property* B.1. Thus, *Property* B.9 is true.

ii) Equations (B.3) and (B.4) show that

$$\dot{X}^T(\dot{M}-2D)\dot{X} = \dot{X}^T(\Lambda - 2B)\dot{X} + \dot{X}^T(M_o - 2D_o)\dot{X} \tag{B.5}$$

Using *Property* B.6, one arrives at

$$\begin{aligned}\dot{X}^T(\dot{M}-2D)\dot{X} &= \dot{X}^T(\dot{\Lambda}-2B)\dot{X} = \dot{X}^T E^T \boldsymbol{W}\boldsymbol{J}^{-T}(\dot{\boldsymbol{H}}-2\boldsymbol{C})\boldsymbol{J}^{-1}\boldsymbol{W}^T E\dot{X} \\ &+ \dot{X}^T\Big(\frac{d(E^T\boldsymbol{W}\boldsymbol{J}^{-T})}{dt}\boldsymbol{H}\boldsymbol{J}^{-1}\boldsymbol{W}^T E + E^T\boldsymbol{W}\boldsymbol{J}^{-T}\boldsymbol{H}\frac{d(\boldsymbol{J}^{-1}\boldsymbol{W}^T E)}{dt} \\ &- 2E^T\boldsymbol{W}\boldsymbol{J}^{-T}\boldsymbol{H}\boldsymbol{J}^{-1}(\dot{\boldsymbol{W}}^T E + \boldsymbol{W}^T\dot{E} - \dot{\boldsymbol{J}}\boldsymbol{J}^{-1}\boldsymbol{W}^T E)\Big)\dot{X}\end{aligned} \tag{B.6}$$

Using *Property* B.2 and that $\frac{d(\boldsymbol{J}^{-1}\boldsymbol{W}^T E)}{dt} = \boldsymbol{J}^{-1}(\dot{\boldsymbol{W}}^T E + \boldsymbol{W}^T\dot{E} - \dot{\boldsymbol{J}}\boldsymbol{J}^{-1}\boldsymbol{W}^T E)$, one arrives at

$$\dot{X}^T(\dot{M}-2D)\dot{X} = \dot{X}^T\Big(\frac{d(E^T\boldsymbol{W}\boldsymbol{J}^{-T})}{dt}\boldsymbol{H}\boldsymbol{J}^{-1}\boldsymbol{W}^T E - E^T\boldsymbol{W}\boldsymbol{J}^{-T}\boldsymbol{H}\frac{d(\boldsymbol{J}^{-1}\boldsymbol{W}^T E)}{dt}\Big)\dot{X} \tag{B.7}$$

Because $\dot{X}^T\frac{d(E^T\boldsymbol{W}\boldsymbol{J}^{-T})}{dt}\boldsymbol{H}\boldsymbol{J}^{-1}\boldsymbol{W}^T E\dot{X}$ is a scalar (hence equal to its transpose) and $\boldsymbol{H}^T = \boldsymbol{H}$, the following is obtained,

$$\dot{X}^T\frac{d(E^T\boldsymbol{W}\boldsymbol{J}^{-T})}{dt}\boldsymbol{H}\boldsymbol{J}^{-1}\boldsymbol{W}^T E\dot{X} = \dot{X}^T E^T\boldsymbol{W}\boldsymbol{J}^{-T}\boldsymbol{H}\frac{d(\boldsymbol{J}^{-1}\boldsymbol{W}^T E)}{dt}\dot{X} \tag{B.8}$$

This results in *Property* B.10

$$\dot{X}^T(\dot{M}-2D)\dot{X} = 0 \tag{B.9}$$

iii) Equation (B.2) and *Property* B.7 show that

$$D(x,y)z = B(x,y)z + D_o(x,y)z = E^T\boldsymbol{W}\boldsymbol{J}^{-T}[\boldsymbol{C}\boldsymbol{J}^{-1}\boldsymbol{W}^T E + \boldsymbol{H}\frac{d(\boldsymbol{J}^{-1}\boldsymbol{W}^T E)}{dt}]z + D_o(x,z)y \tag{B.10}$$

where

$$B(x,y)z = E^T\boldsymbol{W}\boldsymbol{J}^{-T}[\boldsymbol{C}\boldsymbol{J}^{-1}\boldsymbol{W}^T E + \boldsymbol{H}\frac{d(\boldsymbol{J}^{-1}\boldsymbol{W}^T E)}{dt}]z \tag{B.11}$$

$$D_o(x,y)z = D_o(x,z)y \tag{B.12}$$

Noting that $\boldsymbol{J}^{-1}\boldsymbol{W}^{T}E$ is a function of position only, and using *Property* B.3, it is concluded that

$$B(x, y)z = B(x, z)y \tag{B.13}$$

thus *Property* B.11 is proven.

iv) $\boldsymbol{J}^{-1}$ is bounded since $\boldsymbol{J}$ is assumed to be nonsingular. Thus, *Property* B.12 is true.

Appendix C

Review of Backstepping Controller Design Technique

A third order system of co-operating hydraulic manipulators is presented in Chapter 2. To design appropriate controllers for the system under investigation, the backstepping technique is utilized.

Backstepping is a recursive procedure that interlaces the choice of a Lyapunov function with the design of feedback control. It breaks a design problem for the full system into a sequence of design problems for lower order subsystems. Thus backstepping is suitable for high-order systems. By exploiting the extra flexibility that exists with lower order subsystems, backstepping can often solve stabilization, tracking, and robust control problems under certain conditions. The following is a brief introduction of backstepping adopted from the work by Khalil (2002).

***Proposition*:**

Consider the system

$$\dot{\eta} = f(\eta) + G(\eta)\xi \tag{C.1a}$$

$$\dot{\xi} = f_a(\eta,\xi) + G_a(\eta,\xi)u \tag{C.1b}$$

where, $\eta \in R^n, \xi \in R^m$ and $u \in R^m$, in which m could be greater than one. Suppose f, f_a, G, and G_a are known smooth functions over the domain of interest, $f(0) = 0$ and $f_a(0,0) = 0$, and the $m \times m$ matrix G_a is nonsingular. Suppose further that the component (C.1a) can be stabilized by a smooth feedback control law $\xi = \phi(\eta)$ (also called virtual controller) with $\phi(0) = 0$, and a known Lyapunov function $\mathrm{V}_1(\eta)$ satisfies the following inequality

$$\frac{\partial \mathrm{V}_1(\eta)}{\partial \eta}[f(\eta) + G(\eta)\phi(\eta)] \le -W(\eta) \tag{C.2}$$

where function $W(\eta)$ is positive definite. Then the following control law asymptotically stabilizes the whole system described by equations (C.1a) and (C.1b)

$$u = G_a^{-1}(\eta,\xi)[\dot{\phi}(\eta) - (\frac{\partial \mathrm{V}_1(\eta)}{\partial \eta} G(\eta))^T - f_a - k(\xi - \phi(\eta))], \quad k > 0 \tag{C.3}$$

Proof:

The proof is adopted from the framework by Khalil (2002). Using

$$\mathrm{V}_2 = \mathrm{V}_1(\eta) + \tfrac{1}{2}[\xi - \phi(\eta)]^T [\xi - \phi(\eta)] \tag{C.4}$$

as a Lyapunov function candidate for the overall system, one arrives at

$$\dot{\mathrm{V}}_2 = \frac{\partial \mathrm{V}_1}{\partial \eta}(f + G\phi) + \frac{\partial \mathrm{V}_1}{\partial \eta} G(\xi - \phi) + [\xi - \phi]^T [f_a + G_a u - \frac{\partial \phi}{\partial \eta}(f + G\xi)] \tag{C.5}$$

Note that the variables' names in bracket parts following the function names are not presented for the sake of simplicity. Taking the law (C.3) results in

$$\dot{\mathrm{V}}_2 = \frac{\partial \mathrm{V}_1}{\partial \eta}(f + G\phi) - k[\xi - \phi]^T [\xi - \phi] \le -W(\eta) - k[\xi - \phi]^T [\xi - \phi] \tag{C.6}$$

which shows that the origin $(\eta = 0, \xi - \phi = 0)$ is asymptotically stable.

Remark:

The above design does not address parametric system uncertainties. By inspection equation (C.3), the controller for the overall system needs the time derivative of the virtual control law $\phi(\eta)$ for the component system (C.1a). This requires more measurements as feedback to the controller for the overall system. To avoid the requirement, observers should be developed. Thus, the above controller has to be redesigned with the observer dynamics and parametric updating law included.

The differentiation of the virtual control law might bring about the issue of "explosion of terms" (Swaroop, et al., 1997) that introduces many more terms to measure or calculate.

Appendix D

Dynamics of a Three-link Robot

The physical parameters of the i^{th} robot manipulator are as follows:

Link length: l_1^i, l_2^i, l_3^i

Center of mass: a_1^i, a_2^i, a_3^i

Mass: m_1^i, m_2^i, m_3^i

Inertia: I_1^i, I_2^i, I_3^i

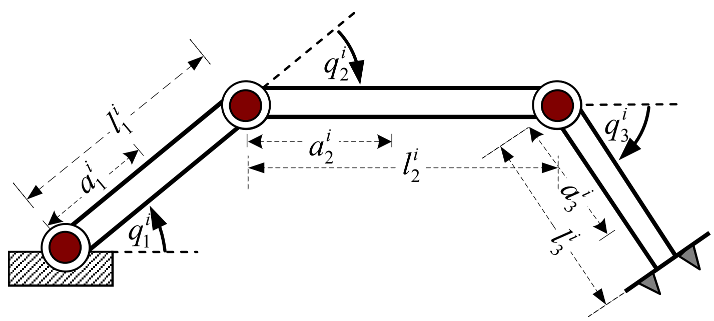

Figure D.1: Three-link planar robot.

While other approaches are available to formulate robotic arm dynamics, such as the Newton-Euler and the generalized d'Alembert principle formulations, the Lagrange-Euler method is used to obtain the following dynamic equations that are used for simulations in the studies.

$$H^i(q^i)\ddot{q}^i + C^i(q^i,\dot{q}^i)\dot{q}^i + G^i(q^i) = T^i - J^{i^T} F_c^i \tag{D.1}$$

where $H^i \in R^{3\times3}, C^i \in R^{3\times3}, G^i \in R^{3\times1}$. The details of these matrices or the vector are given as follows:

$$\begin{aligned} H_{11}^i &= I_1^i + I_2^i + I_3^i + m_1^i(a_1^i)^2 + m_2^i[(l_1^i)^2 + (a_2^i)^2 + 2l_1^i a_2^i \cos q_2^i] \\ &\quad + m_3^i[(l_1^i)^2 + (l_2^i)^2 + (a_3^i)^2 + 2l_1^i l_2^i \cos q_2^i + 2l_2^i a_3^i \cos q_3^i + 2l_1^i a_3^i \cos(q_2^i + q_3^i)] \end{aligned} \tag{D.2}$$

$$\begin{aligned} H_{12}^i &= I_2^i + I_3^i + m_2^i[(a_2^i)^2 + l_1^i a_2^i \cos q_2^i] + m_3^i[(l_2^i)^2 + (a_3^i)^2 \\ &\quad + l_1^i l_2^i \cos q_2^i + 2l_2^i a_3^i \cos q_3^i + l_1^i a_3^i \cos(q_2^i + q_3^i)] \end{aligned} \tag{D.3}$$

$$H_{13}^i = I_3^i + m_3^i[(a_3^i)^2 + l_2^i a_3^i \cos q_3^i + l_1^i a_3^i \cos(q_2^i + q_3^i)] \tag{D.4}$$

$$H_{21}^{i} = H_{12}^{i} \tag{D.5}$$

$$H_{22}^{i} = I_{2}^{i} + I_{3}^{i} + m_{2}^{i}(a_{2}^{i})^{2} + m_{3}^{i}[(l_{2}^{i})^{2} + (a_{3}^{i})^{2} + 2l_{2}^{i}a_{3}^{i}\cos q_{3}^{i}]; \tag{D.6}$$

$$H_{23}^{i} = I_{3}^{i} + m_{3}^{i}[(a_{3}^{i})^{2} + l_{2}^{i}a_{3}^{i}\cos q_{3}^{i}] \tag{D.7}$$

$$H_{31}^{i} = H_{13}^{i} \tag{D.8}$$

$$H_{32}^{i} = H_{23}^{i} \tag{D.9}$$

$$H_{33}^{i} = I_{3}^{i} + m_{3}^{i}(a_{3}^{i})^{2} \tag{D.10}$$

$$\begin{aligned} C_{11}^{i} = & -m_{2}^{i}l_{1}^{i}a_{2}^{i}\dot{q}_{2}^{i}\sin q_{2}^{i} - m_{3}^{i}l_{1}^{i}l_{2}^{i}\dot{q}_{2}^{i}\sin q_{2}^{i} - m_{3}^{i}l_{1}^{i}a_{3}^{i}(\dot{q}_{2}^{i} + \dot{q}_{3}^{i})\sin(q_{2}^{i} + q_{3}^{i}) \\ & - m_{3}^{i}l_{2}^{i}a_{3}^{i}\dot{q}_{3}^{i}\sin q_{3}^{i} \end{aligned} \tag{D.11}$$

$$\begin{aligned} C_{12}^{i} = & -m_{2}^{i}l_{1}^{i}a_{2}^{i}(\dot{q}_{1}^{i} + \dot{q}_{2}^{i})\sin q_{2}^{i} - m_{3}^{i}l_{1}^{i}l_{2}^{i}(\dot{q}_{1}^{i} + \dot{q}_{2}^{i})\sin q_{2}^{i} \\ & - m_{3}^{i}l_{1}^{i}a_{3}^{i}(\dot{q}_{1}^{i} + \dot{q}_{2}^{i} + \dot{q}_{3}^{i})\sin(q_{2}^{i} + q_{3}^{i}) - m_{3}^{i}l_{2}^{i}a_{3}^{i}\dot{q}_{3}^{i}\sin q_{3}^{i} \end{aligned} \tag{D.12}$$

$$C_{13}^{i} = -m_{3}^{i}l_{1}^{i}a_{3}^{i}(\dot{q}_{1}^{i} + \dot{q}_{2}^{i} + \dot{q}_{3}^{i})\sin(q_{2}^{i} + q_{3}^{i}) - m_{3}^{i}l_{2}^{i}a_{3}^{i}(\dot{q}_{1}^{i} + \dot{q}_{2}^{i} + \dot{q}_{3}^{i})\sin q_{3}^{i} \tag{D.13}$$

$$C_{21}^{i} = m_{2}^{i}l_{1}^{i}a_{2}^{i}\dot{q}_{1}^{i}\sin q_{2}^{i} + m_{3}^{i}l_{1}^{i}l_{2}^{i}\dot{q}_{1}^{i}\sin q_{2}^{i} - m_{3}^{i}l_{2}^{i}a_{3}^{i}\dot{q}_{3}^{i}\sin q_{3}^{i} + m_{3}^{i}l_{1}^{i}a_{3}^{i}\dot{q}_{1}^{i}\sin(q_{2}^{i} + q_{3}^{i}) \tag{D.14}$$

$$C_{22}^{i} = -m_{3}^{i}l_{2}^{i}a_{3}^{i}\dot{q}_{3}^{i}\sin q_{3}^{i} \tag{D.15}$$

$$C_{23}^{i} = -m_{3}^{i}l_{2}^{i}a_{3}^{i}(\dot{q}_{1}^{i} + \dot{q}_{2}^{i} + \dot{q}_{3}^{i})\sin q_{3}^{i} \tag{D.16}$$

$$C_{31}^{i} = m_{3}^{i}l_{2}^{i}a_{3}^{i}(\dot{q}_{1}^{i} + \dot{q}_{2}^{i})\sin q_{3}^{i} + m_{3}^{i}l_{1}^{i}a_{3}^{i}\dot{q}_{1}^{i}\sin(q_{2}^{i} + q_{3}^{i}) \tag{D.17}$$

$$C_{32}^{i} = m_{3}^{i}l_{2}^{i}a_{3}^{i}(\dot{q}_{1}^{i} + \dot{q}_{2}^{i})\sin q_{3}^{i} \tag{D.18}$$

$$C_{33}^{i} = 0 \tag{D.19}$$

$$\begin{aligned} G_{1}^{i} = & \, m_{1}^{i}a_{1}^{i}g\cos q_{1}^{i} + m_{2}^{i}l_{1}^{i}g\cos q_{1}^{i} + m_{2}^{i}a_{2}^{i}g\cos(q_{1}^{i} + q_{2}^{i}) + m_{3}^{i}l_{1}^{i}g\cos q_{1}^{i} \\ & + m_{3}^{i}l_{2}^{i}g\cos(q_{1}^{i} + q_{2}^{i}) + m_{3}^{i}a_{3}^{i}g\cos(q_{1}^{i} + q_{2}^{i} + q_{3}^{i}) \end{aligned} \tag{D.20}$$

$$G_{2}^{i} = m_{2}^{i}a_{2}^{i}g\cos(q_{1}^{i} + q_{2}^{i}) + m_{3}^{i}l_{2}^{i}g\cos(q_{1}^{i} + q_{2}^{i}) + m_{3}^{i}a_{3}^{i}g\cos(q_{1}^{i} + q_{2}^{i} + q_{3}^{i}) \tag{D.21}$$

$$G_{3}^{i} = m_{3}^{i}a_{3}^{i}g\cos(q_{1}^{i} + q_{2}^{i} + q_{3}^{i}) \tag{D.22}$$

Note: it is easy to verify that $x^{T}(\dot{H}^{i} - 2C^{i})x = 0; \forall x \in R^{3\times1}$.